Using biogeochemical tracers and sclerochronologies derived from fish otoliths to detect environmental change

Gretchen L. Grammer

Presented for the degree of Doctor of Philosophy
School of Biological Sciences
The University of Adelaide

July 2015

THE UNIVERSITY of ADELAIDE

Declaration

I, Gretchen L. Grammer, certify that this work contains no material which has been accepted for the award of any other degree or diploma in my name, in any university or other tertiary institution and, to the best of my knowledge and belief, contains no material previously published or written by another person, except where due reference has been made in the text. In addition, I certify that no part of this work will, in the future, be used in a submission in my name, for any other degree or diploma in any university or other tertiary institution without the prior approval of the University of Adelaide and where applicable, any partner institution responsible for the joint-award of this degree.

I give consent to this copy of my thesis when deposited in the University Library, being made available for loan and photocopying, subject to the provisions of the Copyright Act 1968.

The author acknowledges that copyright of published works contained within this thesis resides with the copyright holder(s) of those works.

I also give permission for the digital version of my thesis to be made available on the web, via the University's digital research repository, the Library Search and also through web search engines, unless permission has been granted by the University to restrict access for a period of time.

Gretchen L. Grammer

1 July 2015

Cover Image: *Helicolenus percoides* (NZ): Perch, 1867, by Frank Edward Clarke. Purchased 1921. Te Papa (1992-0035-2278/65) No known copyright restrictions

Table of Contents

Abstract

Biogeochemical tracers and sclerochronologies are used to answer many ecological questions that require linking organisms with the environment. Calcified hard parts of organisms that remain chemically inert after formation are particularly advantageous for extracting information (e.g. otoliths, shells, coral) on both the organism and the environment. These structures have growth increments enabling time-resolved information to be extracted on a range of time-scales (sub-daily to centennial). For my research, otoliths (fish earstones) were chosen as an environmental proxy, as they contain both biogeochemical (i.e. radiocarbon and trace elements) and sclerochronological (i.e. growth) signals that reflect environmental change in marine systems. My overarching aim is to use otolith-based proxy records to provide new data describing environmental change in marine systems of southern Australia and New Zealand. More specifically, I employ biogeochemical tracers and sclerochronologies to: (1) detect changes in radiocarbon transport through time in marine waters; (2) establish a radiocarbon record for upwelled waters in the southeastern Indian Ocean; (3) examine local and regional effects of climate forcing on fish growth, and (4) determine the physiological controls acting upon trace element assimilation into otoliths and the differences in chemical constituents of an upwelled water mass. Otoliths of deep water fish – ocean perch from the genus *Helicolenus* – are used in all applications and originate from areas along southern Australia and New Zealand. Thus, the biogeochemical and sclerochronological data derived from these fish describe changes occurring in the marine environments of the southwest Pacific and southeastern Indian Oceans.

Radiocarbon records from the otoliths of *H. barathri,* combined with published records of other fish species in the southwest Pacific Ocean, show transport of the bomb radiocarbon signal from marine surface waters to depths approaching 1000 m. Transports lags ranging from 5 to 20 years are documented, and radiocarbon reservoir ages are calculated for water masses associated with the Tasman Sea.

Radiocarbon measurements from *H. percoides,* in an upwelling area along the southern coast of Australian (southeastern Indian Ocean), are the very first radiocarbon time series

documented for the region and reflect the lower radiocarbon values expected for seasonally upwelled water.

Long term growth responses resulting from sclerochronologies from a *Helicolenus* species complex from southern Australia to New Zealand are compared across regions and species with broad- and local-scale climatic/oceanographic variables using univariate mixed effects models. These data demonstrate how broad scale climate patterns and weather can have additive or synergistic effects on the local environment, which are reflected in the growth of the fish.

Biogeochemical tracers (Na, Sr, Mg, Ba, Li) and sclerochronologies (growth) are also extracted from otoliths of the same fish in this upwelling region. These data are used simultaneously in combination with univariate and multivariate mixed effects modelling to describe physiological and environmental controls on otolith chemistry. Temporal signals within these data are correlated with seasonal upwelling events. Ba:Ca and Li:Ca are more influenced by the environment, while Sr:Ca and Na:Ca are controlled by physiological processes. Ba:Ca negatively tracks upwelling events, suggesting an upwelled water mass not enriched in Ba. Li:Ca correlates positively with chlorophyll-a, indicating a possible proxy for marine productivity.

Thus, the overarching aim of this research has been achieved: biogeochemical tracers and sclerochronologies derived from *Helicolenus* otoliths have provided new data describing environmental change in marine systems of southern Australia and New Zealand.

Acknowledgements

What an adventure this has been!

I was lucky enough to work under the outstanding supervision of Bronwyn Gillanders. Bronwyn is not only an excellent scientist, she is very compassionate and willing to lend an ear and give guidance on many fronts (usually when I was in angst about something or other). I also had the good fortune of being Chris Izzo's very first PhD student, and have greatly benefited from his quick wit and pep-talks. There were many times when I ran into Bronwyn's and Chris's offices with excitement about some discovery I just made, and being able to share and have the enthusiasm returned was quite inspiring.

My network of friends and colleagues made this work possible, and I am indebted to each of them. Thanks especially to Zoe Doubleday, Chloe McSkimming (my long-time officemate), and Jennifer Young for helping me celebrate the good stuff and being supportive through the not so good stuff. I thank Pete Hawthorne for making otolith samples magically appear, for teaching me that the Hawks were the 'right' AFL team to cheer for, and for camaraderie. Thanks to Chris Fulton and Mae Noble for making me welcome in their home during my stints at the Australian National University. Special thanks to Kevin Rowling for his mentorship and sight-seeing excursions whenever we are able to catch up. I extend all around thanks to Stephen Ryan and his family - just because. Thanks to my friends and family in North America who have supported me from afar. It's made the distance much less…distant.

To Mom and Dad, thanks so very much for your love, support, guidance and inspiration. You are truly great parents. And to Gary, I thank you for your unwavering support, keeping me well-balanced, and reminding me there are still many adventures to come in our future!

CHAPTER 1

General Introduction

Where the ocean perch live: Heading out of Vivonne Bay, Kangaroo Island, South Australia to find the elusive ocean perch *Helicolenus percoides*.

General Introduction:

Biological archives and proxy records

The magnitude and temporal scales of change within environments are of interest to many disciplines, and a myriad of approaches have been used to gather relevant data. Ice cores are used to track changes in the chemical constituents of the atmosphere (including dust) over hundreds of thousands of years (Jouzel et al. 2007, Lambert et al. 2008), whilst varves (paired sediment layers) provide clues to sedimentation processes and biological productivity in modern or past aquatic environments (Hughen 2014). Speleothems, mineral deposits formed in caves, are excellent archives of proxies for climate, atmospheric moisture, soils and vegetation (Fairchild and Baker 2012). The aforementioned are examples of geoarchives, but biological material can also be an informational trove. Some organisms produce permanent hard structures through periodic accretion of biogenic material. These structures, called bioarchives, can be used to produce high-resolution records of past environments akin to those of geoarchives (Schöne and Gillikin 2013). Trees are well-known bioarchives with the tree rings providing temporally resolved information (the science of dendrochronology). Other bioarchives produced by both terrestrial and aquatic organisms may be either calcareous (e.g. bones, teeth, shells, earstones) or keratinous (e.g. hair, baleen, whiskers, nails and feathers). In aquatic systems, calcium-carbonate structures are the most commonly used types of bioarchive and include hard parts from molluscs, fish, and coral. Similar to dendrochronology, the science of sclerochronology concentrates on the physical and chemical variations in organismal accretionary hard tissues through time (Oschmann 2009).

A key property required for an archive, that both geo- and bioarchives provide, is time-resolved records of growth and biogeochemistry. Growth chronologies – continuous temporal records of organismal growth – can provide proxy information on both the environment and ecology of the organism through growth increment counts and width measurements (Morrongiello et al. 2012). Biogeochemical tracers, chemicals incorporated into organismal tissue from the environment, are used to examine feeding habits, track migratory patterns, and understand physiological responses to the environment, as well as reconstruct past environmental histories (Morrongiello et al. 2012, Ramos and González-Solís 2012). Examples of biochemical tracers include stable isotopes, radiocarbon,

persistent organic pollutants (e.g. dichlorodiphenyltrichloroethane, polychlorinated biphenyl), and trace elements. When these tracers are extracted, time-resolved, and coupled with growth records, they become a powerful tool for providing data about ecosystems and responses to climatic changes and pollution in areas where there is a paucity of instrumental information (Ramos and González-Solís 2012). This is particularly applicable to aquatic ecosystems in the Southern Hemisphere where there is a dearth of long-term data (Nielsen et al. 2004, Moros et al. 2009).

Southern Hemisphere palaeoclimate research has become a high priority for many entities concerned with global climate change (e.g. Intergovernmental Panel on Climate Change, International Geosphere-Biosphere Programme, International Union for Quaternary Research, National Oceanic and Atmospheric Administration), as dramatic differences in the way that the two hemispheres respond to climate variability have become evident (Jones and Mann 2004, IPCC 2007). To study these differing hemispheric responses more closely, high-resolution proxy records are desirable to validate climate model simulations, particularly for examining El Niño - Southern Oscillation variability (Moros et al. 2009).

Long-term datasets that form the basis for palaeoclimate reconstructions are also very useful for understanding the ecological responses of organisms to natural and anthropogenic environmental change. However, these data sets are expensive and logistically difficult to acquire using traditional observational approaches and are, therefore, largely absent in aquatic environments (Richardson and Poloczanska 2008). Bioarchives are frequently more accessible and cost effective than geoarchives, particularly for deep aquatic environments, and thus can help fill gaps in environments where instrumental records may not be forthcoming. Fish accrete otoliths (earstones), which are typically aragonite-based and used to maintain balance and facilitate hearing (Secor et al. 1995, Campana 1999). Since fish occur globally, these biogenic structures are available in almost every aquatic environment, and fishery records and otolith archives provide an avenue to easily procure large amounts of long-term data (Richardson and Poloczanska 2008, Morrongiello et al. 2012).

Otoliths as bioarchives: applications, assumptions, limitations

Otoliths contain growth increments that can be time resolved, making them one of the most extensively studied calcified structures of a higher organism. The microstructural formation of growth increments in otoliths allows the individual age and growth rate of a fish to be examined (Campana and Thorrold 2001). Similarly, as otoliths are acellular and metabolically inert, changes in the chemical composition of the fish's environment are permanently retained on the otolith's growing surface (Campana and Neilson 1985).

Annually-resolved growth increment chronologies can be produced from otoliths and offer a metric to examine synchrony in growth and possible environmental drivers within or across regions (Black et al. 2008, Gillanders et al. 2012, Morrongiello et al. 2012). Otolith growth chronologies are similar to coral or tree-ring chronologies in their ability to provide indirect records of the environment. Fish growth records gleaned from otoliths, particularly in the Northern Hemisphere, have shown some of the interconnections existing with both large-scale climate phenomenon and localised oceanographic variables (e.g. Matta et al. 2010, Black et al. 2015). Additionally, otolith biogeochemical profiles are widely used as natural tags to examine stock structures, population connectivity, and movement patterns through different aquatic environments (e.g. Gillanders 2002, Elsdon and Gillanders 2003, Elsdon et al. 2008). They are also used as proxies to infer past environments (Disspain et al. 2011, Disspain et al. 2015).

Trace elements and stable isotopes are two of the most frequently applied biogeochemical tracers in otoliths (Campana 1999, Elsdon et al. 2008, Gao and Noakes 2012). Trace elements in otoliths, such as Sr, Mg and Ba ratioed to calcium (element:Ca), are generally used as natural tags for movement patterns or stock structure (Gillanders 2002, Elsdon and Gillanders 2003). Stable isotopes are usually used for dietary comparisons and estimates of metabolic rates ($\delta^{15}N$, $\delta^{13}C$; (Kalish 1991, Rowell et al. 2010) or for environmental temperature reconstructions ($\delta^{18}O$; Elsdon and Gillanders 2002, Gao and Beamish 2003). Radiocarbon (^{14}C) is another type of isotope used in otolith research, but its application is more frequently seen in relation to coral carbonate and within the geosciences. Otolith carbonate provides a complementary archive to coral with respect to ^{14}C, particularly the contemporary distribution of bomb ^{14}C (natural ^{14}C levels augmented by thermonuclear

weapons in the 1950s and 1960s), and can be a valuable record of changes in ^{14}C over both time and space (Kalish 1993, Campana et al. 2008). The 'bomb ^{14}C chronometer' is also extensively used as a precision tool for validating ages in hard-to-age fish species to improve fish resource management and stock assessments (Campana 2001, Haltuch et al. 2013, Morin et al. 2013).

Often, biogeochemical tracers in otoliths are targeted to answer questions about the biology or the ecology of the fish, i.e. ontogenetic changes in habitat use or diet (Gao and Noakes 2012). They have been less frequently used to address geophysical questions than similar biogeochemical tracers in molluscs or coral. This is, perhaps, for two reasons: 1) fish are motile and 2) otoliths are not in direct contact with the environment – they are encapsulated in the fish's head surrounded by endolymph. Physiological processes make the biogeochemical relationship between the environment and the otolith less predictable then in lower organisms (Weiner and Dove 2003, Stanley 2006, Cusack and Freer 2008). Understanding and accounting for these processes allow biological and environmental influences on element assimilation to be disentangled. Experimental work relating water chemistry and environmental conditions to otolith elemental composition has provided evidence for changes in the environment being reflected in the otolith (e.g. Elsdon and Gillanders 2002, de Vries et al. 2005, Walther and Thorrold 2006). More recently, further testing of physiological regulation on elements within the otolith has revealed certain elements may be less physiologically regulated than others. Barium, Mg, and Li in blood plasma of fish show less biological fractionation compared to Sr (Sturrock et al. 2014). An additional consideration when using otolith biogeochemical tracers is any type of movement undertaken by the fish will influence the element composition (Elsdon et al. 2008). Depending on the question, this may or may not be beneficial, e.g. beneficial: assessing ontogenetic habitat shifts; not beneficial: temporal reconstruction of parameters in a specific environment.

Relating otolith growth increment patterns to the corresponding biogeochemical tracers can produce a complete record of the environment that the fish has been exposed to over the course of its lifetime. The first step requires high quality growth increment sclerochronologies to be produced. This can be done by using sclerochronological

techniques (crossdating) or mixed-effects modelling. Crossdating is a dendrochronological technique that cross-matches synchronous growth increment width patterns among multiple samples at a given time and place (Douglass 1941, Yamaguchi 1991, Black et al. 2005). After individual sclerochronologies have been combined through crossdating, they are compared with instrumental climatic records for a given area, potentially creating a long-term record of seasonality in climate-growth relationships to better understand the effects of environmental variability (Black et al. 2005, Black 2009, Helama et al. 2009). Alternatively, hierarchical mixed-effects models are used to first partition intrinsic effects (such as age, sex, spawning season), and then apply an optimal model to predict fish growth relative to environmental parameters (Weisberg et al. 2010, Morrongiello and Thresher 2015). Mixed-effects models also allow differences in growth between and among individuals and populations to be compared. These models can be tailored to use available biological information to explore ecological, physiological and evolutionary responses to changing environmental conditions (Morrongiello et al. 2012, Morrongiello and Thresher 2015). Linked biogeochemical data can be resolved and compared using the same techniques. To date, the integration of otolith chemical chronologies and growth increment chronologies has not been extensively explored, particularly in a direct context with environmental variability.

When developing proxy records of biogeochemical tracers or growth for a region, it is imperative to understand the species's life history, specifically patterns of movement, diet and habitat. This will help to qualify or negate variability within the proxy data. It is also necessary to understand regional circulation patterns to give context to the data. An 'ideal' candidate species for environmental reconstructions within a specific location would possess a number of characteristics that include:

1. site attached (non-migratory at all - vertical or otherwise);
2. produces readable growth rings that can be validated/verified to some time scale;
3. longevity (max age >10 yrs);
4. known larval/juvenile life history and modes of reproduction (priority with biogeochemical data);
5. known diet (priority with biogeochemical data);

6. archives (samples readily available and collected over a temporal span);

Ocean perches of the genus *Helicolenus* represent suitable candidate species for growth and environmental reconstructions. Further information is provided below.

Study species

Ocean perches (*Helicolenus* spp., Family: Sebastidae) are demersal fishes that occur in continental waters, offshore ridges and seamounts of the Atlantic, Pacific and Indian Oceans. In the southwest Pacific, *H. percoides* and *H. barathri* are distributed in southeast Australian and New Zealand waters, with a third undescribed *Helicolenus* species found on the Chatham Rise, east of New Zealand (Fig. 1a and c) (Smith et al. 2009). I focused primarily on reef ocean perch (*Helicolenus percoides*; Fig. 1b) which live in depths of < 350 m (Chapters 2 to 5) and big-eye ocean perch (*Helicolenus barathri*) that inhabits depths > 350 m (Chapters 2 and 4) (Park 1993, Smith et al. 2009), but also included *Helicolenus* spp. collected off the Chatham Rise for comparison (Chapter 4). All *Helicolenus* species are fished commercially in New South Wales (NSW), Australia as well as New Zealand (Park 1993, Paul and Horn 2009); they are also frequently captured as bycatch in the southern rock lobster fishery in southeast Australia (Brock et al. 2007). *Helicolenus* can reach lengths of > 40 cm and attain ages > 50 years (Bentley et al. 2014).

Ocean perches are highly evolved in their reproductive strategies and display a transition from oviparity to viviparity within the genus (Pavlov and Emel'yanova 2013). *Helicolenus percoides* is lecithotrophic viviparous (live-bearing; Pavlov and Emel'yanova 2013), whilst the specific reproductive strategy (either embryoparity or lecithotrophic viviparity) of *H. barathri* has yet to be confirmed (Park 1993). These species of ocean perch mature around 5 years of age and spawn in the austral winter/spring and summer, depending on latitude (July to January; Park 1993, Paul and Horn 2009). Ocean perches are benthopelagic omnivores (Bulman et al. 2001) and demersal as both juveniles and adults (Park 1993).

The *Helicolenus* genus ticks all six of the 'ideal' candidate species criteria (references in text above):

1. site attached: benthic and non-migratory
2. growth increments: produces annual, validated/verified growth increments
3. longevity: > 50 years

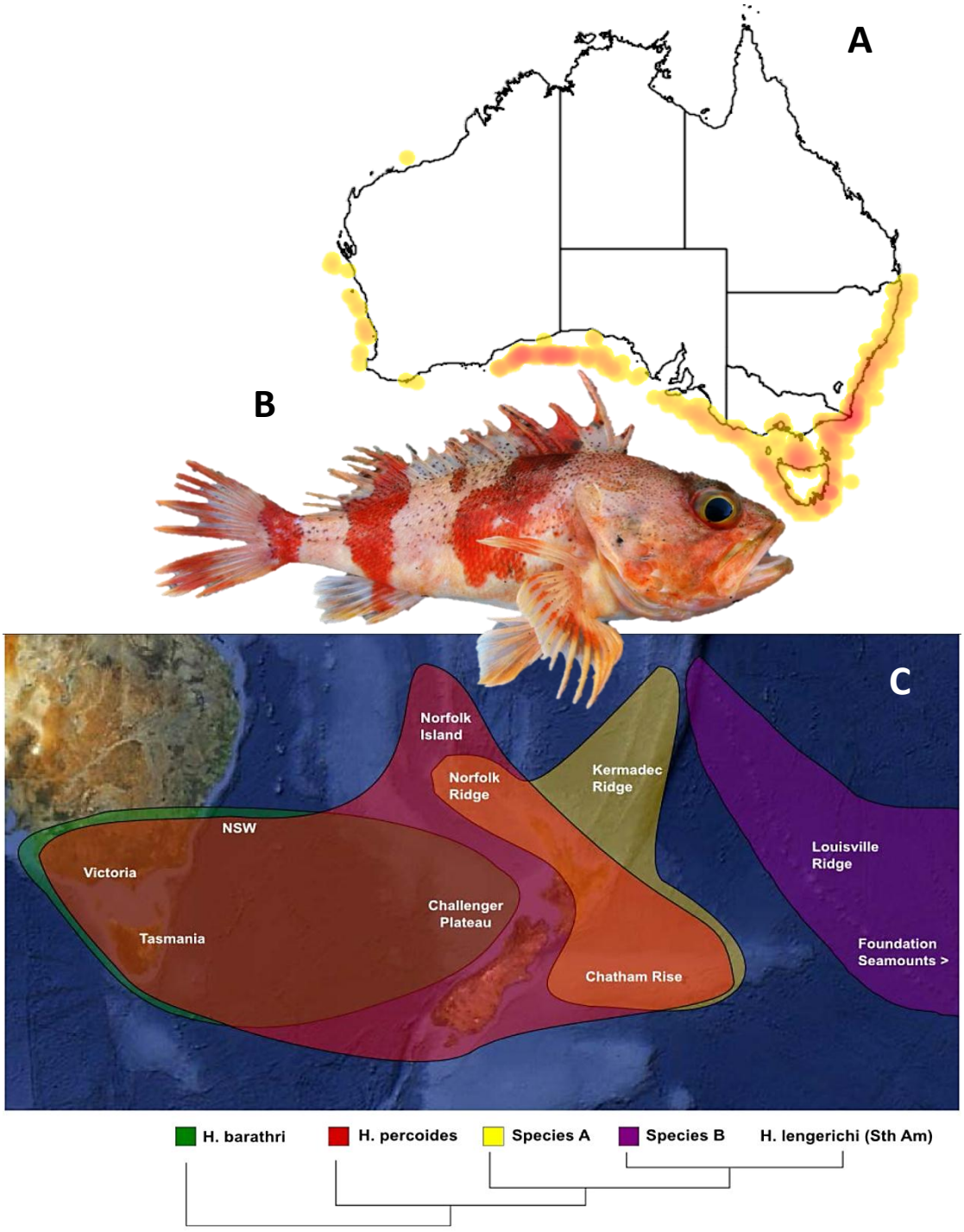

Fig. 1. A) Distribution of *Helicolenus percoides* along the continental shelf of Australia at depths of ≤ 350 m. B) Reef ocean perch *Helicolenus percoides*. C) Distribution of the ocean perches in in southeastern Australian (Victoria, New South Wales, Tasmania) and New Zealand: *H. percoides* (red), *Helicolenus barathri* (green) and an unknown *Helicolenus* spp. (Species A; yellow) from New Zealand (Norfolk Ridge, Kermadec Ridge, Chatham Rise). Distribution map based on genetics and fishery data (Smith et al. 2009, Bentley et al. 2014). [Image Credits: A) © Australian Museum, http://australianmuseum.net.au; B) G. L. Grammer; C) Reproduced from Bentley et al. 2014]

4. known life history: demersal as both juveniles and adults; benthic live bearing
5. known diet: benthopelagic omnivores
6. archives: commercial fisheries species with otolith archives in both Australia and New Zealand

Therefore, biogeochemical tracers and sclerochronologies derived from the otoliths of *Helicolenus percoides* and *H. barathri* have the potential to act as proxies for ocean-atmospheric processes in southeast Australian and New Zealand.

Oceanographic setting of study area

A brief summary of the regional oceanography (≤ 2000 m of the water column) in the southwest Pacific is necessary to give context to the *Helicolenus* growth chronologies and biogeochemical tracers presented in this thesis; the following is based on Sokolov and Rintoul (2000), Ridgway and Dunn (2003) and Ganachaud et al. (2014) unless otherwise noted (see Chapter 2, Fig. 1a and Chapter 3, Fig. 1a-b for schematic depictions). The Australia/New Zealand region of the southern Pacific Ocean is primarily influenced by the South Equatorial Current (SEC) of the South Pacific Gyre (SPG) transporting three main water masses: Upper Thermocline Waters (origin: subducted centre of SPG), Lower Thermocline Waters (origin: subducted in part northeast of New Zealand) and Southeast Pacific Antarctic Intermediate Water (AAIW) (origin: subducted ~ 50°S, 170W - 65W) (see Qu et al. 2009, Bostock et al. 2013). The SEC turns south as it nears Australia and becomes the East Australian Current (EAC), the highly variable, western boundary current of the SPG. The EAC continues south along the Australian coast where it bifurcates into the Tasman Front (flowing eastward around northern New Zealand) and the EAC Extension (flowing southward towards Tasmania). Lower Thermocline Waters and Southeast Pacific AAIW are transported south by the EAC to the Tasman Front and EAC Extension. The EAC Extension is dominated by very intense, warm-core anticyclonic eddies that can reach from the surface to abyssal depths. Around New Zealand, the Tasman Front becomes the southeast flowing East Auckland Current that eventually forms the East Cape Current, feeding back into the main SPG gyre after flowing east along the Chatham Rise. Anticyclonic eddies, similar to the vigorous EAC Extension warm core eddies, are associated with the flows along the north and eastern coasts of New Zealand and can extend to depths of at least 1500 m.

Three different types of AAIW are found within the Tasman Sea and along the east coast of New Zealand (refer to Chapter 2, Fig. 1a and Fig. 2): (1) Southeast Pacific AAIW (origin: main SPG), (2) Tasman AAIW (origin: Tasman Sea), and (3) Southern Ocean AAIW (origin: Southern Ocean 150°E - 120°W) (Bostock et al. 2013). The Antarctic intermediate waters of the South Pacific are identified by the distinct salinity minimum typically found near depths of 600 to 1200 m (Chapter 2, Fig. 2; Bostock et al. 2010, Bostock et al. 2013). The saltier Tasman Sea AAIW is thought to form by mixing of older Southeast Pacific AAIW, that has travelled around the STG, with higher salinity thermocline waters (possibly Lower Thermocline Waters) within the recirculating central Tasman Sea (Bostock et al. 2013). Some of the Tasman AAIW flows out of the Tasman Sea eastward around the northern coast of New Zealand and east along the Chatham Rise (Chapter 2, Fig. 2b; Bostock et al. 2013).

In the southeast Indian Ocean, upwelling occurs along the Bonney Coast of southern Australia in the austral summer, each event lasting three to ten days in duration, interspersed by episodes of weak downwelling and surface water mixing (Kämpf et al. 2004, Middleton and Bye 2007). These upwelling areas are wind-forced and influenced by the Flinders Current flowing westward along the shelf-slope of southern Australia (Chapter 3, Fig. 1a-b) (Middleton and Bye 2007). The Flinders Current results from wind curl stress and the equatorward Sverdrup transport of water in the Southern Ocean; it is similar to the larger continental western boundary currents but is actually part of a northern boundary current system that produces upwelling areas (Middleton and Cirano 2002, Middleton and Bye 2007). The Flinders Current flows west at depths of 400 to 800 m and transports Tasmanian Subantarctic Mode Water (TSAMW) and Tasmanian Intermediate Water (TIW) to the northwest (Barker 2004, Middleton and Bye 2007). TSAMW is formed in surface waters off the southwest coast of Tasmania (47°S) and is subducted to 500 m, and TIW is formed at depths of ~ 1000 m in the same region (Barker 2004). The Flinders Current also transports remnants of the East Australian Current from the Pacific Ocean via the Tasman Outflow (Middleton and Bye 2007). A reversal in current strength ensues in the winter months of southern Australia where an eastward flowing current, the Leeuwin Current, becomes dominant, producing downwelling. The Leeuwin Current system (depths < 200 m) has its origins in the tropical east Indian Ocean and advects water from both the Indonesian

Flowthrough and East Gyral Current into the Great Australian Bight (Feng et al. 2003, James and Bone 2011). The main Leeuwin Current becomes weaker as it flows westward, joining with the South Australian current in the central Great Australian Bight and the Zeehan Current off western Tasmania (James and Bone 2011). Both the Flinders and Leeuwin Current systems are wind-dominated, which causes the seasonal strengthening or weakening of either current system (Middleton and Bye 2007, James and Bone 2011).

Thesis scope:

The southwest Pacific Ocean and southeast Indian Ocean, described above, is a dynamic oceanographic region of the Southern Hemisphere; however, there is still a paucity of instrumental records relating to the ocean and climate. Changes in climate drivers, such as ENSO, will likely alter oceanographic processes (e.g. current strength, mixing, seasonality), which will have cascading effects on the marine biota. Otolith carbonate records are an accessible mechanism that gives us the capacity to examine magnitude and direction of environmental change in this region in both a spatial and temporal context.

The overarching aim of this thesis is to use biogeochemical tracers and sclerochronologies derived from *Helicolenus* otoliths as proxies to provide new data describing environmental change in marine systems of southern Australia and New Zealand.

The main objectives are to:

(i) Identify changes to the distribution of radiocarbon ($\Delta^{14}C$) that has entered and mixed within the ocean from thermonuclear bomb testing by using the ^{14}C signatures found in otoliths. (Chapters 2 and 3)

(ii) Relate otolith-based growth increment chronologies from ocean perches to broad-scale climate processes as well as localised oceanographic variables across the southwest Pacific and southeast Indian Ocean region with mixed effects models to examine growth responses. (Chapter 4)

(iii) Use biogeochemical tracers and fish growth concurrently with mixed effects models to explore synergistic effects of physiology and the environment on chemical assimilation into otoliths. (Chapter 5)

Thesis structure and a note on chapter styles:

Each data chapter (2 to 5) is written in the form of a stand-alone scientific paper suitable for publication in a peer-reviewed journal and therefore includes separate introductions, methods, results, discussion and references. All chapters are co-authored with acknowledgement made at the start of each chapter hence the use of plural throughout. All tables and figures are embedded within the text and the numbering of figures and tables begins at one for each chapter. However, all chapters are tied to the overarching aim of my PhD research, and I present them as a cohesive flow of work reflecting my research philosophies as they have developed in the General Discussion (Chapter 6). The following is a brief synopsis of each chapter:

Chapter 2

Otoliths from long-lived fish provide an indirect method to examine the 'bomb pulse' of radiocarbon that originated in the 1950s and 1960s, allowing identification of changes to distributions of $\Delta^{14}C$ that has entered and mixed within the ocean. I use carbonate from the otoliths of ocean perch (*H. barathri*) to produce a mid-water $\Delta^{14}C$ reference record in depths > 350 m for the mid-latitudes of the southwest Pacific Ocean. Next, I compare the linear increase of multiple otolith-based $\Delta^{14}C$ curves for the southwest Pacific Ocean to examine temporal ^{14}C transport through the water column. Finally, I present a compilation of regional otolith, coral and atmospheric $\Delta^{14}C$ curves for the southwest Pacific Ocean to examine temporal trends in ^{14}C transport.

Chapter 3

Biogenic carbonates are successfully used to track radiocarbon ($\Delta^{14}C$) evolution through time, and we use otoliths of fish to establish a new record of the bomb $\Delta^{14}C$ decline (since ~ 1980 to the present) in an upwelling area of the southeast Indian Ocean. Marine surface waters were enriched with ^{14}C during the 1950-60s when thermonuclear weapons testing was at its zenith (bomb $\Delta^{14}C$). Upwelling events ventilate ocean surface waters with subsurface water lower in radiocarbon $\Delta^{14}C$ through a wind-driven, oceanographic process. In this chapter, I aim to examine the range of $\Delta^{14}C$ values measured in otolith carbonate by depth and through time in the upwelling region; compare otolith ^{14}C values to seawater

$\Delta^{14}C$ values measured in adjacent non-upwelling areas; and compare this record with coral $\Delta^{14}C$ records from the eastern Indian Ocean and Pacific Ocean.

Chapter 4

Broad scale climate patterns are modulated through ocean-atmosphere coupling and complex interactions with surrounding landmasses. Weather and climate dynamics cause ecosystem forcing at various time scales, which is thought to synchronize geographically separate populations of fish. Annually-resolved growth chronologies can be produced from otoliths and offer a metric to further examine synchrony in growth and possible climatic drivers across regions. I compare chronologies of growth derived from the otoliths of ocean perches from southern Australia and New Zealand across multiple regions spanning 3000 km with broad- and local-scale climatic/oceanographic variables. I partition age-dependent drivers of growth through time to allow other sources of variability to be extracted from the growth record.

Chapter 5

Biogeochemical tracers found in the hard parts of organisms are frequently used to answer key ecological questions by linking the organism with the environment. However, as physiological processes become more complex in higher organisms, the biogeochemical relationship between the environment and the biogenic structure becomes less predictable. Therefore, I use the simultaneous combination of biogeochemical tracers and fish growth with univariate and multivariate mixed effects modelling to describe physiological and environmental controls on otolith chemistry over multiple years. I also explore synergistic effects of age and the environment on chemical assimilation into the otolith and growth by using a strong, local upwelling signal as an extrinsic cue.

Chapter 6

In this chapter, I provide a general discussion on the key findings of the previous data chapters and suggest directions for future research.

References

Barker, P. M. 2004. The circulation and formation of water masses south of Australia and the inter-annual wind variability along the southern Australian coast. PhD Thesis. The University of Melbourne, Victoria, Australia.

Bentley, N., T. H. Kendrick, and D. J. MacGibbon. 2014. Fishery characterisation and catch-per-unit-effort analyses for sea perch (*Helicolenus* spp.) in New Zealand, 1989–90 to 2009–10. New Zealand Fisheries Assessment Report 2014/27. 181 p.

Black, B. A. 2009. Climate-driven synchrony across tree, bivalve, and rockfish growth-increment chronologies of the northeast Pacific. Marine Ecology Progress Series **378**:37-46.

Black, B. A., G. W. Boehlert, and M. M. Yoklavich. 2005. Using tree-ring crossdating techniques to validate annual growth increments in long-lived fishes. Canadian Journal of Fisheries and Aquatic Sciences **62**:2277-2284.

Bostock, H. C., B. N. Opdyke, and M. J. M. Williams. 2010. Characterising the intermediate depth waters of the Pacific Ocean using δ13C and other geochemical tracers. Deep Sea Research Part I: Oceanographic Research Papers **57**:847-859.

Bostock, H. C., P. J. Sutton, M. J. M. Williams, and B. N. Opdyke. 2013. Reviewing the circulation and mixing of Antarctic Intermediate Water in the South Pacific using evidence from geochemical tracers and Argo float trajectories. Deep Sea Research Part I: Oceanographic Research Papers **73**:84-98.

Brock, D. J., P. J. Hawthorne, T. M. Ward, and A. J. Linnane. 2007. Two monitoring methods that assess species composition and spatio-temporal trends in bycatch from an important temperate rock lobster (*Jasus edwardsii*) fishery. Marine and Freshwater Research **58**:273-285.

Bulman, C., F. Althaus, X. He, N. Bax, and A. Williams. 2001. Diets and trophic guilds of demersal fishes of the south-eastern Australian shelf. Marine and Freshwater Research **52**:537-548.

Campana, S. E. 1999. Chemistry and composition of fish otoliths: pathways, mechanisms and applications. Marine Ecology Progress Series **188**:263-297.

Campana, S. E. 2001. Accuracy, precision and quality control in age determination, including a review of the use and abuse of age validation methods. Journal of Fish Biology **59**:197-242.

Campana, S. E., J. M. Casselman, and C. M. Jones. 2008. Bomb radiocarbon chronologies in the Arctic, with implications for the age validation of lake trout (*Salvelinus namaycush*) and other Arctic species. Canadian Journal of Fisheries and Aquatic Sciences **65**:733-743.

Campana, S. E. and J. D. Neilson. 1985. Microstructure of fish otoliths. Canadian Journal of Fisheries and Aquatic Sciences **42**:1014-1032.

Campana, S. E. and S. R. Thorrold. 2001. Otoliths, increments, and elements: keys to a comprehensive understanding of fish populations? Canadian Journal of Fisheries and Aquatic Sciences **58**:30-38.

Cusack, M. and A. Freer. 2008. Biomineralization: elemental and organic influence in carbonate systems. Chemical Reviews **108**:4433-4454.

de Vries, M. C., B. M. Gillanders, and T. S. Elsdon. 2005. Facilitation of barium uptake into fish otoliths: Influence of strontium concentration and salinity. Geochimica et Cosmochimica Acta **69**:4061-4072.

Disspain, M., L. A. Wallis, and B. M. Gillanders. 2011. Developing baseline data to understand environmental change: a geochemical study of archaeological otoliths from the Coorong, South Australia. Journal of Archaeological Science **38**:1842-1857.

Disspain, M. C. F., S. Ulm, and B. M. Gillanders. 2015. Otoliths in archaeology: methods, applications and future prospects. Journal of Archaeological Science: Reports: http://dx.doi.org/10.1016/j.jasrep.2015.1005.1012.

Douglass, A. E. 1941. Crossdating in dendrochronology. Journal of Forestry **39**:825-831.

Elsdon, T. S. and B. M. Gillanders. 2002. Interactive effects of temperature and salinity on otolith chemistry: challenges for determining environmental histories of fish. Canadian Journal of Fisheries and Aquatic Sciences **59**:1796-1808.

Elsdon, T. S. and B. M. Gillanders. 2003. Reconstructing migratory patterns of fish based on environmental influences on otolith chemistry. Reviews in Fish Biology and Fisheries **13**:217-235.

Elsdon, T. S., B. K. Wells, S. E. Campana, B. M. Gillanders, C. M. Jones, K. E. Limburg, D. H. Secor, S. R. Thorrold, and B. D. Walther. 2008. Otolith chemistry to describe movements and life-history parameters of fishes: Hypotheses, assumptions, limitations and inferences. Pages 297-330 *in* R. N. Gibson, R. J. A. Atkinson, and J. D. M. Gordon, editors. Oceanography and Marine Biology: An Annual Review, Vol 46. Crc Press-Taylor & Francis Group, Boca Raton.

Fairchild, I. J. and A. Baker. 2012. Introduction to Speleothems and Systems. Pages 1-27 Speleothem Science. John Wiley & Sons, Ltd.

Feng, M., G. Meyers, A. Pearce, and S. Wijffels. 2003. Annual and interannual variations of the Leeuwin Current at 32°S. Journal of Geophysical Research **108**:1-20.

Ganachaud, A., S. Cravatte, A. Melet, A. Schiller, N. J. Holbrook, B. M. Sloyan, M. J. Widlansky, M. Bowen, J. Verron, P. Wiles, K. Ridgway, P. Sutton, J. Sprintall, C. Steinberg, G. Brassington, W. Cai, R. Davis, F. Gasparin, L. Gourdeau, T. Hasegawa, W. Kessler, C. Maes, K. Takahashi, K. J. Richards, and U. Send. 2014. The Southwest Pacific Ocean circulation and climate experiment (SPICE). Journal of Geophysical Research: Oceans **119**:7660-7686.

Gao, Y. and R. J. Beamish. 2003. Stable isotope variations in otoliths of Pacific halibut (*Hippoglossus stenolepis*) and indications of the possible 1990 regime shift. Fisheries Research **60**:393-404.

Gao, Y. and D. G. Noakes. 2012. Chemical signatures of otoliths and application in fisheries. Environmental Biology of Fishes **95**:415-418.

Gillanders, B. M. 2002. Temporal and spatial variability in elemental composition of otoliths: Implications for determining stock identity and connectivity of populations. Canadian Journal of Fisheries and Aquatic Sciences **59**:669-679.

Haltuch, M. A., O. S. Hamel, K. R. Piner, P. McDonald, C. R. Kastelle, and J. C. Field. 2013. A California Current bomb radiocarbon reference chronology and petrale sole (*Eopsetta jordani*) age validation. Canadian Journal of Fisheries and Aquatic Sciences **70**:22-31.

Helama, S., J. K. Nielsen, M. Macias Fauria, and I. Valovirta. 2009. A fistful of shells: amplifying sclerochronological and palaeoclimate signals from molluscan death assemblages. Geological Magazine **146**:917-930.

Hughen, K. 2014. Marine Varves. *in* J. Rink and J. Thompson, editors. Encyclopedia of Scientific Dating Methods. Springer.

IPCC. 2007. Climate Change 2007: Synthesis Report. Contribution of Working Groups I, II and III to the Fourth Assessment Report of the Intergovernmental Panel on Climate Change. *in* R. K. Pachauri, A. Reisinger, and Core Writing Team, editors. Intergovernmental Panel on Climate Change, Geneva.

James, N. P. and Y. Bone. 2011. Neritic Carbonate Sediments in a Temperate Realm: Southern Australia. Springer, London.

Jones, P. D. and M. E. Mann. 2004. Climate over past millennia. Reviews of Geophysics **42**:1-42.

Jouzel, J., V. Masson-Delmotte, O. Cattani, G. Dreyfus, S. Falourd, G. Hoffmann, B. Minster, J. Nouet, J. M. Barnola, J. Chappellaz, H. Fischer, J. C. Gallet, S. Johnsen, M. Leuenberger, L. Loulergue, D. Luethi, H. Oerter, F. Parrenin, G. Raisbeck, D. Raynaud, A. Schilt, J. Schwander, E. Selmo, R. Souchez, R. Spahni, B. Stauffer, J. P. Steffensen, B. Stenni, T. F. Stocker, J. L. Tison, M. Werner, and E. W. Wolff. 2007. Orbital and millennial Antarctic climate variability over the past 800,000 years. Science **317**:793-796.

Kalish, J. M. 1991. Oxygen and carbon stable isotopes in the otoliths of wild and laboratory-reared Australian salmon (*Arripis trutta*). Marine Biology **110**:37-47.

Kalish, J. M. 1993. Pre- and post-bomb radiocarbon in fish otoliths. Earth and Planetary Science Letters **114**:549-554.

Kämpf, J., M. Doubell, D. Griffin, R. L. Matthews, and T. M. Ward. 2004. Evidence of a large seasonal coastal upwelling system along the southern shelf of Australia. Geophysical Research Letters **31**:1-4.

Lambert, F., B. Delmonte, J. R. Petit, M. Bigler, P. R. Kaufmann, M. A. Hutterli, T. F. Stocker, U. Ruth, J. P. Steffensen, and V. Maggi. 2008. Dust-climate couplings over the past 800,000 years from the EPICA Dome C ice core. Nature **452**:616-619.

Middleton, J. F. and J. A. T. Bye. 2007. A review of the shelf-slope circulation along Australia's southern shelves: Cape Leeuwin to Portland. Progress in Oceanography **75**:1-41.

Middleton, J. F. and M. Cirano. 2002. A northern boundary current along Australia's southern shelves: The Flinders Current. Journal of Geophysical Research. C. Oceans **107**:1-11.

Morin, R., S. G. LeBlanc, and S. E. Campana. 2013. Bomb radiocarbon validates age and long-term growth declines in American plaice in the southern Gulf of St. Lawrence. Transactions of the American Fisheries Society **142**:458-470.

Moros, M., P. De Deckker, E. Jansen, K. Perner, and R. J. Telford. 2009. Holocene climate variability in the Southern Ocean recorded in a deep-sea sediment core off South Australia. Quaternary Science Reviews **28**:1932-1940.

Morrongiello, J. R. and R. E. Thresher. 2015. A statistical framework to explore ontogenetic growth variation among individuals and populations: a marine fish example. Ecological Monographs **85**:93-115.

Morrongiello, J. R., R. E. Thresher, and D. C. Smith. 2012. Aquatic biochronologies and climate change. Nature Climate Change **2**:849-857.

Nielsen, S. H. H., N. Koc, and X. Crosta. 2004. Holocene climate in the Atlantic sector of the Southern Ocean: Controlled by insolation or oceanic circulation? Geology **32**:317-320.

Oschmann, W. 2009. Sclerochronology: editorial. International Journal of Earth Sciences **98**:1-2.

Park, T. J. 1993. A comparison of the morphology, growth and reproductive biology of two colour forms of ocean perch (*Helicoleus percoides*), NSW, Australia. Masters. University of Sydney, Sydney, Australia.

Paul, L. J. and P. L. Horn. 2009. Age and growth of sea perch (*Helicolenus percoides*) from two adjacent areas off the east coast of South Island, New Zealand. Fisheries Research **95**:169-180.

Pavlov, D. A. and N. G. Emel'yanova. 2013. Transition to viviparity in the order Scorpaeniformes: Brief review. Journal of Ichthyology **53**:52-69.

Qu, T., S. Gao, I. Fukumori, R. A. Fine, and E. J. Lindstrom. 2009. Origin and pathway of equatorial 13°C water in the Pacific identified by a simulated passive tracer and its adjoint. Journal of Physical Oceanography **39**:1836-1853.

Ramos, R. and J. González-Solís. 2012. Trace me if you can: the use of intrinsic biogeochemical markers in marine top predators. Frontiers in Ecology and the Environment **10**:258-266.

Richardson, A. J. and E. S. Poloczanska. 2008. Under-resourced, under threat. Science **320**:1294-1295.

Ridgway, K. R. and J. R. Dunn. 2003. Mesoscale structure of the mean East Australian Current System and its relationship with topography. Progress in Oceanography **56**:189-222.

Rowell, K., D. Dettman, and R. Dietz. 2010. Nitrogen isotopes in otoliths reconstruct ancient trophic position. Environmental Biology of Fishes **89**:415-425.

Schöne, B. R. and D. P. Gillikin. 2013. Unraveling environmental histories from skeletal diaries - advances in sclerochronology. Palaeogeography, Palaeoclimatology, Palaeoecology **373**:1-5.

Secor, D. H., J. M. Dean, and S. E. Campana. 1995. Recent Developments in Fish Otolith Research. University of South Carolina Press, Columbia, SC, USA.

Smith, P. J., C. D. Struthers, C. D. Paulin, S. M. McVeagh, and R. K. Daley. 2009. Shallow genetic and morphological divergence among seaperches in the South Pacific (family Scorpaenidae; genus *Helicolenus*). Journal of Fish Biology **74**:1104-1128.

Sokolov, S. and S. Rintoul. 2000. Circulation and water masses of the southwest Pacific: WOCE section P11, Papua New Guinea to Tasmania. Journal of Marine Research **58**:223-268.

Stanley, S. M. 2006. Influence of seawater chemistry on biomineralization throughout phanerozoic time: Paleontological and experimental evidence. Palaeogeography, Palaeoclimatology, Palaeoecology **232**:214-236.

Sturrock, A. M., C. N. Trueman, J. A. Milton, C. P. Waring, M. J. Cooper, and E. Hunter. 2014. Physiological influences can outweigh environmental signals in otolith microchemistry research. Marine Ecology Progress Series **500**:245-264.

Walther, B. D. and S. R. Thorrold. 2006. Water, not food, contributes the majority of strontium and barium deposited in the otoliths of a marine fish. Marine Ecology Progress Series **311**:125-130.

Weiner, S. and P. M. Dove. 2003. An overview of biomineralization processes and the problem of the vital effect. Reviews in Mineralogy and Geochemistry **54**:1-29.

Weisberg, S., G. Spangler, and L. S. Richmond. 2010. Mixed effects models for fish growth. Canadian Journal of Fisheries and Aquatic Sciences **67**:269-277.

Yamaguchi, D. K. 1991. A simple method for cross-dating increment cores from living trees. Canadian Journal of Forest Research **21**:414-416.

CHAPTER 2: Investigating bomb radiocarbon transport in the southern Pacific Ocean with otolith radiocarbon

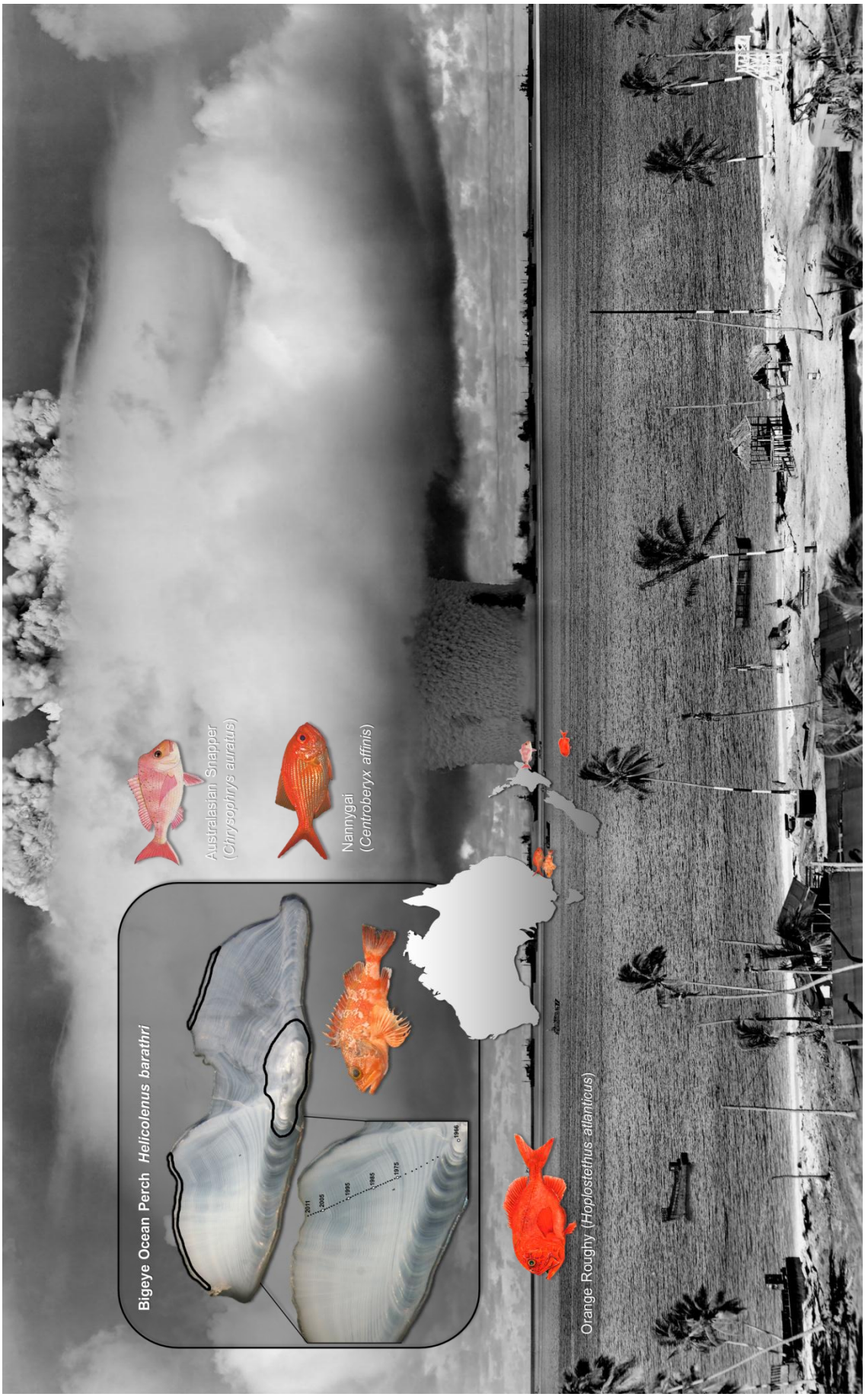

Operation Crossroads 'Baker Shot', a United States thermonuclear test in 1946 at Bikini Atoll, Pacific Ocean. Otolith radiocarbon levels in ocean perch, Australasian snapper, nannygai and orange roughy are used to track bomb ^{14}C transport in the ocean

Statement of Authorship

Title of Paper	Investigating bomb radiocarbon transport in the southern Pacific Ocean with otolith radiocarbon
Publication Status	☑ Published ☐ Accepted for Publication ☐ Submitted for Publication ☐ Publication Style
Publication Details	This chapter is a co-authored manuscript and has been published in Earth and Planetary Science Letters. This chapter can be cited as: Grammer, G. L., S. J. Fallon, C. Izzo, R. Wood, and B. M. Gillanders. 2015. Investigating bomb radiocarbon transport in the southern Pacific Ocean with otolith radiocarbon. Earth and Planetary Science Letters 424:59-68.

Principal Author

Name of Principal Author (Candidate)	Gretchen L. Grammer		
Contribution to the Paper	Collected specimens, extracted otolith carbonate samples, graphitised samples for AMS analyses, preformed statistical analyses, wrote the manuscript and acted as corresponding author.		
Overall percentage (%)	90		
Signature		Date	17 June 2015

Co-Author Contributions

By signing the Statement of Authorship, each author certifies that:

i. the candidate's stated contribution to the publication is accurate (as detailed above);

ii. permission is granted for the candidate in include the publication in the thesis; and

iii. the sum of all co-author contributions is equal to 100% less the candidate's stated contribution.

Name of Co-Author	Stewart Fallon		
Contribution to the Paper	Assisted with intellectual development and AMS analyses, and provided suggestions, comments and feedback on manuscript drafts		
Signature		Date	17 June 2015

Name of Co-Author	Christopher Izzo		
Contribution to the Paper	Assisted with intellectual development, and provided suggestions, comments and feedback on manuscript drafts		
Signature		Date	17 June 2015

Name of Co-Author	Rachel Wood		
Contribution to the Paper	Assisted with AMS analyses, and provided suggestions, comments, and feedback on manuscript drafts		
Signature		Date	17 June 2015

Name of Co-Author	Bronwyn Gillanders		
Contribution to the Paper	Assisted with intellectual development, supplied funding, and provided suggestions, comments and feedback on manuscript drafts		
Signature		Date	17 June 2015

Earth and Planetary Science Letters 424 (2015) 59–68

Contents lists available at ScienceDirect

Earth and Planetary Science Letters

www.elsevier.com/locate/epsl

Investigating bomb radiocarbon transport in the southern Pacific Ocean with otolith radiocarbon

G.L. Grammer [a,*], S.J. Fallon [b], C. Izzo [a], R. Wood [b], B.M. Gillanders [a]

[a] Southern Seas Ecology Laboratories, School of Biological Sciences, The University of Adelaide, SA 5005, Australia
[b] Radiocarbon Facility, Research School of Earth Sciences, The Australian National University, Canberra, ACT 0200, Australia

ARTICLE INFO

Article history:
Received 6 October 2014
Received in revised form 4 May 2015
Accepted 5 May 2015
Available online xxxx
Editor: J. Lynch-Stieglitz

Keywords:
Antarctic intermediate water
southwest Pacific
lower thermocline water
East Australian Current
Tasman Sea
Helicolenus

ABSTRACT

To explore the transport of carbon into water masses from the surface ocean to depths of ~1000 m in the southwest Pacific Ocean, we generated time series of radiocarbon ($\Delta^{14}C$) from fish otoliths. Otoliths (carbonate earstones) from long-lived fish provide an indirect method to examine the "bomb pulse" of radiocarbon that originated in the 1950s and 1960s, allowing identification of changes to distributions of ^{14}C that has entered and mixed within the ocean. We micro-sampled ocean perch (*Helicolenus barathri*) otoliths, collected at ~400–500 m in the Tasman Sea, to obtain measurements of $\Delta^{14}C$ for those depths. We compared our ocean perch $\Delta^{14}C$ series to published otolith-based marine surface water $\Delta^{14}C$ values (Australasian snapper (*Chrysophrys auratus*) and nannygai (*Centroberyx affinis*)) and to published deep-water values (800–1000 m; orange roughy (*Hoplostethus atlanticus*)) from the southwest Pacific to establish a mid-water $\Delta^{14}C$ series. The otolith bomb ^{14}C results from these different depths were consistent with previous water mass results in the upper 1500 m of the southwest Pacific Ocean (e.g. World Ocean Circulation Experiment and Geochemical Ocean Sections Study). A comparison between the initial $\Delta^{14}C$ bomb pulse rise at 400–500 m suggested a ventilation lag of 5 to 10 yr, whereas a comparison of the surface and depths of 800–1000 m detailed a 10 to 20 yr lag in the time history of radiocarbon invasion at this depth. Pre-bomb reservoir ages derived from otolith ^{14}C located in Tasman Sea thermocline waters were ~530 yr, while reservoir ages estimated for Tasman Antarctic intermediate water were ~730 yr.

1. Introduction

Atmospheric testing of thermonuclear weapons in the 1950s and 1960s generated large amounts of radiocarbon. This 'bomb pulse radiocarbon' can be used to trace carbon through the environment, enabling global oceanic circulation patterns to be detected and mapped (e.g. Broecker and Peng, 1982; Nydal, 2000). Atmospheric concentrations of radiocarbon ($\Delta^{14}C$) began increasing worldwide in 1955, while in ocean surface waters the increase was delayed until about 1958 (e.g. Broecker and Peng, 1982; Nydal, 2000). The extended time since atmospheric thermonuclear testing largely ceased in 1963 makes the bomb ^{14}C tracer a powerful device for examining the temporal evolution of ^{14}C and therefore carbon distribution in the ocean (e.g. Druffel, 2002; Jenkins et al., 2010; Key et al., 2004). Radiocarbon, along with physical and geochemical tracers such as salinity, temperature, density, oxygen, stable carbon isotopes, and silicates have vastly improved our understanding of ocean circulation and current dynamics, particularly in the southwest Pacific Ocean (Bostock et al., 2013; Ganachaud et al., 2014; Sokolov and Rintoul, 2000). Our research aims to produce a record of ^{14}C transport from surface waters to depths approaching 1000 m in the oceanic water column of the southwest Pacific.

1.1. Environmental and biological variability of radiocarbon

Levels of ^{14}C in the atmosphere and ocean differ due to the balance between $^{14}CO_2$ inputs to the ocean, the production of ^{14}C in the atmosphere (e.g. anthropogenic inputs, cosmic ray interactions), and ^{14}C exchange with the deep ocean (e.g. circulation inputs, ^{14}C decay) (Broecker and Peng, 1982; Kalish, 2002a). Radiocarbon concentrations (in both the atmosphere and ocean surface waters) exhibit a slight decline due to the increase in fossil fuel burning (Suess Effect; Suess, 1953) from ca. 1880 until about 1955, after which bomb ^{14}C increase disrupts this trend (Broecker and Peng, 1982; Druffel, 2002; Kalish, 2002a). Differences in advection and degrees of vertical mixing contribute to the spatial variability of ^{14}C in marine waters. This is especially evident in surface

* Corresponding author. Tel.: +61 8 8313 1483; fax: +61 8 8313 4364.
E-mail address: gretchen.grammer@adelaide.edu.au (G.L. Grammer).

http://dx.doi.org/10.1016/j.epsl.2015.05.008
0012-821X/

waters where gas exchange is greatest and upward mixing of subsurface waters depleted in ^{14}C occurs (Broecker and Peng, 1982; Druffel, 2002).

Many oceanic biological carbonates reflect ^{14}C in their surrounding environment, providing a valuable record of changes in ^{14}C over both time and space (Druffel, 2002; Kalish et al., 2001; Scourse et al., 2012). Corals are often used for this purpose (e.g. Druffel, 2002), but otoliths (fish earstones; e.g. Campana, 1997; Kalish, 1995) provide a complementary archive. Otoliths are accretionary structures of fish that are acellular and metabolically inert, permanently retaining changes in the chemical composition of the fish's environment (Campana and Neilson, 1985; Campana and Thorrold, 2001). By using the chemical composition of the otolith (e.g. levels of ^{14}C) in tandem with growth increments, temporal changes in the environment can be examined. Therefore, otoliths from long-lived fish can be used to establish pre-bomb levels of ^{14}C and to track the penetration of bomb ^{14}C through the water column on a regional scale. In contrast to coral, otoliths are able to provide records from cooler regions and throughout the water column.

Otoliths were first used as a proxy for $\Delta^{14}C$ levels in the environment in the early 1990s with reference made to the considerable potential of otolith ^{14}C for further investigation into both oceanography and global change (Kalish, 1994). Since that time, there has been a myriad of globally published research relating to $\Delta^{14}C$ in fish otoliths (primarily age validation studies: e.g. Andrews et al., 2011; Armsworthy and Campana, 2010). There has been some use, albeit limited, of otolith ^{14}C to understand ocean circulation or atmosphere/ocean flux of ^{14}C (see Campana et al., 2008; Horn et al., 2010, 2012; Kalish et al., 2001).

When developing proxy records of geochemical or oceanographic characteristics (e.g. $\Delta^{14}C$) of a marine region, it is imperative to understand the species's life history, specifically patterns of movement, diet and habitat. It is also necessary to understand the regional oceanography to give context to the proxy data. Dissolved inorganic carbon (DIC) in seawater contributes about 75% of the carbon found in otoliths; the remaining 25% of carbon is diet-based (Kalish, 1991; Solomon et al., 2006). Discounting upwelling areas, in near surface waters the relationship between ^{14}C in the environment and the otoliths is relatively simple, in part because ^{14}C in DIC equals ^{14}C in the diet as DIC enters the food chain through phytoplankton (e.g. Kalish, 1993, 1995). However, this relationship becomes more complicated when fish reside below the mixed layer (uncertainty of mixing rate at depth and limited ^{14}C data for deeper waters) and/or exhibit ontogenetic depth shifts. For example, values of $\Delta^{14}C$ measured in the otolith cores and edges of both bluenose (*Hyperoglyphe antarctica*; Horn et al., 2010) and rubyfish (*Plagiogeneion rubiginosum*; Horn et al., 2012) had completely different $\Delta^{14}C$ signatures. This was due to the juveniles of both species living in waters <200 m, while the adult fish resided in waters well below that (in depths ~600 m). Adult blue-eye trevalla also undergo extensive vertical and latitudinal migrations, which further confounds ambient water and dietary sources of carbon (Horn et al., 2010).

1.2. Proxy species

Big-eye ocean perch (*Helicolenus barathri*; here after referred to as "ocean perch") were selected as our study species for bomb ^{14}C analysis. This fish occurs in marine waters along the continental shelf of southern Australia and New Zealand in depths >350 m (Park, 1993; Smith et al., 2009). We can examine $\Delta^{14}C$ levels at depth with the otolith records from ocean perch, because these fish are demersal throughout their lives (Park, 1993; Smith et al., 2009), including feeding (Bulman et al., 2001) and reproductive strategies (Pavlov and Emel'yanova, 2013).

To further examine the transport of bomb ^{14}C through the water column in the southwest Pacific Ocean with otolith radiocarbon, we combined our resulting ocean perch $\Delta^{14}C$ time series with previously published otolith $\Delta^{14}C$ series from nannygai (*Centroberyx affinis*; Kalish, 1995), Australasian snapper (*Chrysophrys* (*Pagrus*) *auratus*; Kalish, 1993), and orange roughy (*Hoplostethus atlanticus*; Kalish, 2002b), as well as a hermatypic coral $\Delta^{14}C$ series (Druffel and Griffin, 2004) and a compilation of monthly resolved atmospheric ^{14}C levels in the southern hemisphere (Hua et al., 2013). These otolith series combined with the coral and atmospheric data are representative of the transport of ^{14}C from the atmosphere to oceanic depths approaching 1000 m in the southwest Pacific Ocean.

1.3. Oceanographic setting of the southwest Pacific Ocean

A brief summary of the regional oceanography (≤2000 m of the water column) in the southwest Pacific is necessary to give context to the otolith $\Delta^{14}C$ values; the following is based on Sokolov and Rintoul (2000), Ridgway and Dunn (2003) and Ganachaud et al. (2014) unless otherwise noted (Fig. 1A). The Australia/New Zealand region of the southern Pacific Ocean is primarily influenced by the South Equatorial Current (SEC) of the South Pacific Gyre (SPG) transporting three main water masses: Upper Thermocline Waters (UTW, $\sigma_\theta \sim 24.5$; origin: subducted centre of SPG), Lower Thermocline Waters (LTW, $\sigma_\theta \sim 26.2$; origin: subducted in part northeast of New Zealand) and Southeast Pacific Antarctic Intermediate Water (SP AAIW, $\sigma_\theta \sim 27.1$; origin: subducted ~50°S, 170°W–65°W) (Fig. 1A; see Bostock et al., 2013; Qu et al., 2009). The SEC turns south as it nears Australia and becomes the East Australian Current (EAC), the highly variable, western boundary current of the SPG. The EAC continues south along the Australian coast where it bifurcates into the Tasman Front (flowing eastward around northern New Zealand) and the EAC Extension (flowing southward towards Tasmania) (Fig. 1A). Lower Thermocline Waters and SP AAIW are transported south by the EAC to the Tasman Front and EAC Extension. The EAC Extension is dominated by very intense, warm-core anticyclonic eddies that can reach from the surface to abyssal depths. Around New Zealand, the Tasman Front becomes the southeast flowing East Auckland Current (EAUC) that eventually forms the East Cape Current (ECC), feeding back into the main SPG gyre after flowing east along the Chatham Rise. Anticyclonic eddies, similar to the vigorous EAC Extension warm core eddies, are associated with the flows along the north and eastern coasts of New Zealand and can extend to depths of at least 1500 m.

Three different types of AAIW are found within the Tasman Sea and along the east coast of New Zealand (Figs. 1A, 2): (1) Southeast Pacific AAIW (as above; salinity: 34.2–34.35; origin: main SPG; $\Delta^{14}C$: −120 to +55‰), (2) Tasman AAIW (salinity: 34.45–35.6; origin: Tasman Sea; $\Delta^{14}C$: −75 to −50‰ [limited data]), and (3) Southern Ocean AAIW (SO AAIW; salinity: 34.28–34.4; origin: Southern Ocean 150°E–120°W; $\Delta^{14}C$: −110 to +55‰) (Bostock et al., 2013). The AAIWs of the South Pacific are identified by the distinct salinity minimum typically found near depths of 600 to 1200 m and bounded with potential density isopycnals (σ_θ) of 26.9–27.3 (Fig. 2; Bostock et al., 2010, 2013). The saltier Tasman Sea AAIW is thought to form by mixing of older SP AAIW, that has travelled around the STG, with higher salinity thermocline waters (possibly LWT) within the recirculating central Tasman Sea (Bostock et al., 2013). Some of the Tasman AAIW flows out of the Tasman Sea eastward around the northern coast of New Zealand and east along the Chatham Rise (Fig. 2B; Bostock et al., 2013).

The specific objectives of this research were to (*i*) use carbonate from ocean perch otoliths to produce a mid-water $\Delta^{14}C$ reference record in depths >350 m for the mid-latitudes of the

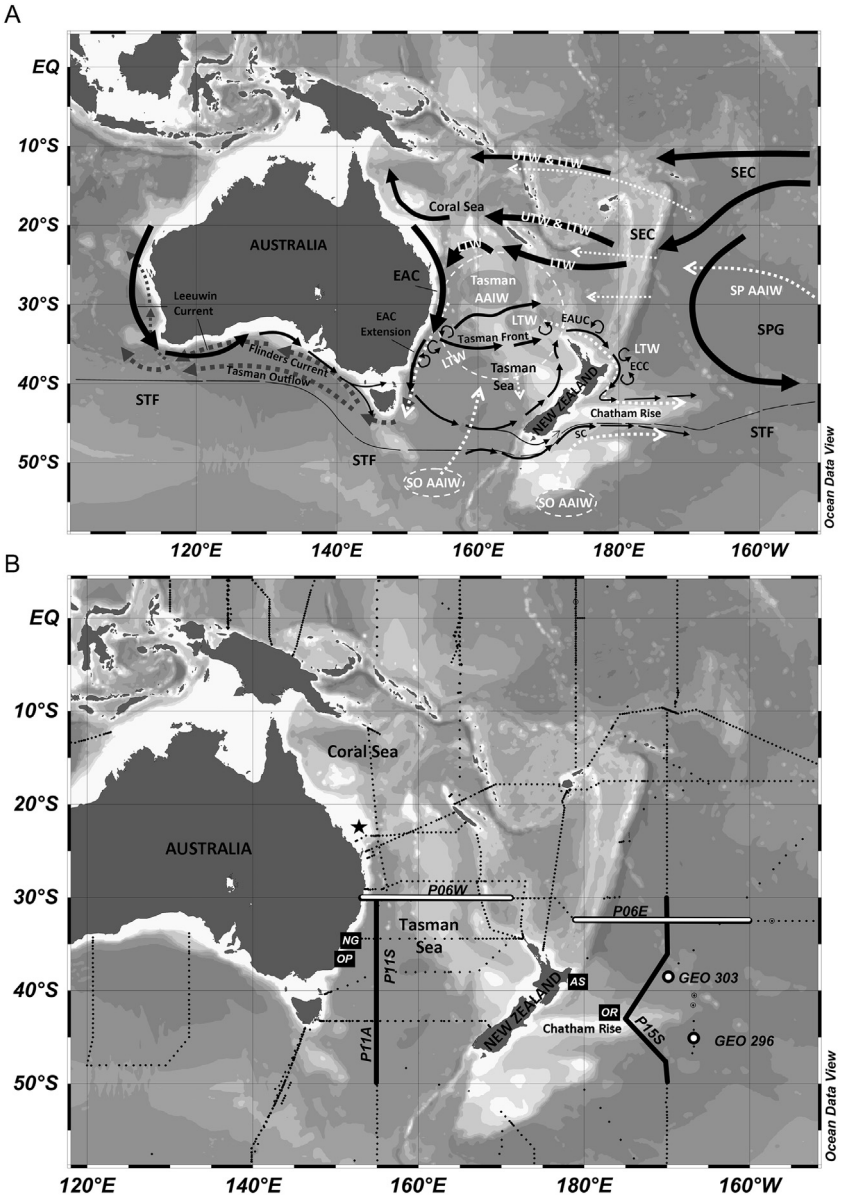

Fig. 1. (A) Schematic of currents and major water masses at depths ≤2000 m in the southwest Pacific region. Currents are represented by solid black (upper flow) and dashed grey (deeper flow) lines: SPG – South Pacific Gyre, SEC – South Equatorial Current, EAC – East Australian Current, EAUC – East Auckland Current, ECC – East Cape Current, SC – Southland Current. Water masses are highlighted in white: UTW – Upper Thermocline Waters, LTW – Lower Thermocline Waters, Tasman AAIW – Tasman Antarctic Intermediate Water, SP AAIW – South Pacific AAIW, SO AAIW – Southern Ocean AAIW. All arrows reflect direction of flow. The Subtropical front (STF) is also denoted. (B) Map of the Word Ocean Circulation Experiment (WOCE) voyages (P11A/P11S; P06 W–E; P15S) and points from the Geochemical Ocean Sections Study (GEOSECS; GEO 296 and 303) that are used for the salinity and/or $\Delta^{14}C$ water values in Figs. 2, 7 and S1 (white: $\Delta^{14}C$ water data). Also shown are locations for the otolith records: Australasian snapper (AS; Kalish, 1993), nannygai (NG; Kalish, 1995), ocean perch (OP), orange roughy (OR; Kalish, 2002b), and hermatypic coral record (star; Druffel and Griffin, 2004). Base maps and transects generated using Ocean Data View software (Schlitzer et al., 2015). (Data sources for A: Bostock et al., 2013; Ganachaud et al., 2014; Qu et al., 2009; Ridgway and Dunn, 2003; Sokolov and Rintoul, 2000.)

southwest Pacific Ocean; (*ii*) compare the linear increase of regional otolith-based $\Delta^{14}C$ curves for the southwest Pacific Ocean to examine temporal ^{14}C transport through the water column; and (*iii*) present a compilation of regional otolith, coral and atmospheric $\Delta^{14}C$ curves for the southwest Pacific Ocean to examine temporal trends in ^{14}C transport.

2. Methods

Archived sagittal otoliths of ocean perch collected off the coast of New South Wales (NSW; Fig. 1B), Australia during the years of 1976 to 2012 were analysed for $\Delta^{14}C$ by accelerator mass spectrometry (AMS; Table S1). Otoliths taken from ocean perch specimens at the Sydney Fish Market were caught during commercial trawling operations between Ulladulla and Eden, NSW (otoliths archived at the Univ. of Adelaide with BMG). We assigned a mean depth estimate of 400–500 m to the archived otoliths based on the recorded depths of scientifically collected specimens and on the range over which the bulk of the commercial NSW ocean perch catch originates (Park, 1993).

2.1. Otolith preparation and age estimation

One otolith from each ocean perch was embedded in epoxy resin, thin-sectioned transversely through the primordium, and mounted on a glass slide (Fig. 3). The presumed annual growth increments (pairs of opaque and hyaline zones) were counted from the core to the proximal margin using a compound microscope

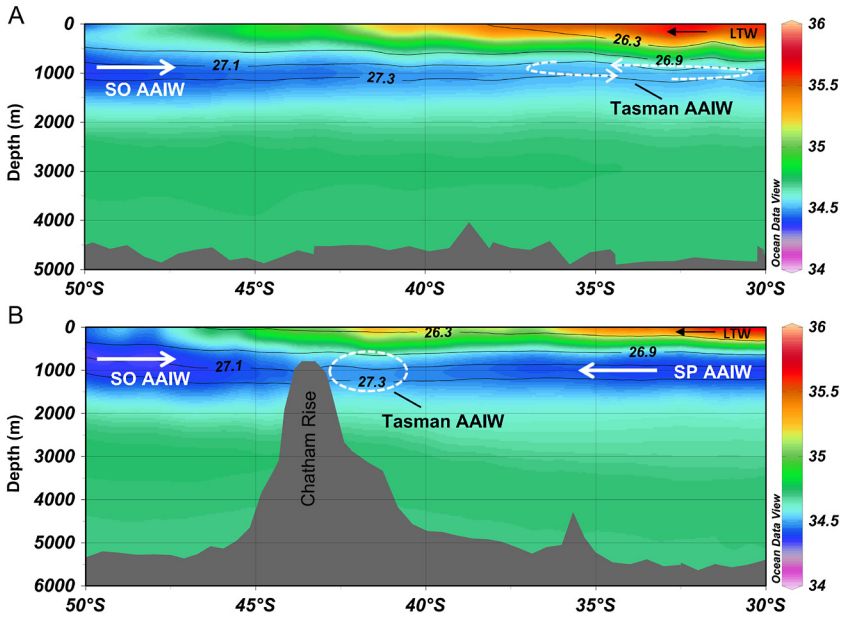

Fig. 2. Salinity data along transects P11S/P11A (A) and P15S (B) (N–S, Fig. 1B) from the electronic atlas of WOCE hydrographic and tracer (eWOCE) dataset (Schlitzer, 2000) plotted with Ocean Data View software (Schlitzer et al., 2015) along the latitudinal gradient of 30°S to 50°S. Isopycnals bounding water masses of AAIW ($\sigma_\theta = 26.9$–27.3) and the lower boundary of LTW ($\sigma_\theta = 26.3$) in the southwest Pacific are overlaid. Tasman AAIW, SO AAIW, and SP AAIW are differentiated and general direction of the water mass movement is reflected by arrows. (B) Flow of Tasman AAIW is perpendicular to the page, flowing towards the east. (For interpretation of the colors in this figure, the reader is referred to the web version of this article.)

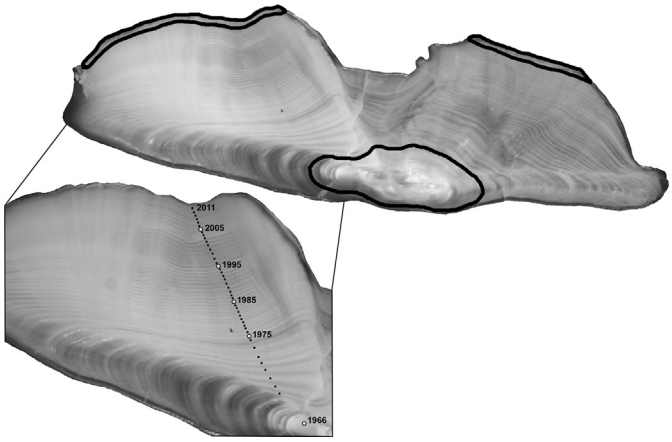

Fig. 3. Thin section of an ocean perch sagittal otolith displaying presumed annual growth increments (pairs of opaque and hyaline zones) under reflected light using a compound microscope (Leica DM LB) at ×87.5 magnification for visual age estimation. The black dotted line represents the aging transect along the dorsal margin of the sulcus. Each black dot marks one annual growth increment; the filled white dots each mark 10 yr of growth starting in the otolith core. This fish was collected in 2012 with the last complete annual growth increment on the edge designated as 2011. This fish was 46 yr old with an estimated birth year of 1966. Carbonate for radiocarbon analysis was milled from the core and along the proximal edges of the otolith (outlined in black).

(Leica DM LB) under reflected light at ×87.5 magnification for visual age interpretation (Fig. 3). The annual increments were also measured using Image-Pro Plus v. 7.0 (MediaCybernetics). Proximal edges of opaque zones (under reflected light) delineated the boundaries of annual growth (Paul and Horn, 2009). The birth year for each fish was adjusted based on an estimated birthdate of October 1 (Park, 1993; Paul and Horn, 2009). Annual growth increments have not been previously validated in ocean perch, but they have been validated in other members of the genus (e.g. *H. percoides*: Paul and Horn, 2009; *H. dactylopterus*: Sequeira et al., 2009). Therefore, growth increments counted in ocean perch otoliths were considered to be annual and representative of 1 yr of growth.

2.2. Carbonate extraction

Otolith carbonate was extracted from the core region (containing the first 1 to 2 yr of growth, Fig. 3), using a computer-controlled micromilling machine (ESI New Wave Research, USA) with a 300 µm carbide cutter (Brasseler, USA). Carbonate from the proximal margin of selected otoliths (Fig. 3) was removed using a 1 mm endmill (Preformance Micro Tool, USA) mounted on a customised, Minitech Machinery Mini-Mill/GX (USA) computer-controlled micromilling machine with 1 µm position repeatability. A transect 120 µm wide was carved into the otolith's edge to a depth of 300 µm. All otolith carbonate samples were stored in clean, glassine envelopes prior to radiocarbon analysis. The milled edge area was overlaid with previously measured annual growth increments to determine the number of increments (yr) that were sampled; the edge samples ranged from 2 to 6 yr of growth depending on the age of the fish. The number of growth increments milled was averaged per otolith to assign a year to the edge material based on the year of capture (Table S1). The amount of carbonate powder milled from each otolith core or edge ranged from 0.14 to 1.00 mg and equalled about 10 to 50 µg of graphitised carbon (Table S1).

2.3. Radiocarbon analysis

Carbonate powder samples were transferred to evacuated ($<10^{-3}$ Torr) Vacutainer® tubes and were acidified with phosphoric acid (0.5 ml, 85%, 80 °C) until the reaction was complete. The CO_2 generated was collected and purified cryogenically before reaction with H_2 over an iron catalyst (Key, 1996) at 500 °C for a maximum of 30 min (dependent upon sample size) for conversion to graphite. Water was removed during the reaction by $Mg(ClO_4)_2$. The graphite was pressed into a target and analysed for ^{14}C using the Australian National University Single Stage Accelerator Mass Spectrometer (SSAMS) (Fallon et al., 2010).

Table 1
Compilation of atmosphere and carbonate series and associated data for the southwest Pacific Ocean used in the $\Delta^{14}C$ multi-curve comparisons. Sampling locations are shown on Fig. 1B.

Species	Depth (m) represented by otolith ^{14}C	Otolith Region (years of growth included)	Collection latitude	Collection longitude	Collection method	Reference
Australasian snapper (*Chrysophrys auratus*)	0–200	core (1 yr)	39°S	179°E	Otolith archive	Kalish (1993)
Nannygai (*Centroberyx affinis*)	0–200	core (<8 months)	35°S	151°E	Commercial fishing	Kalish (1995)
Ocean perch (*Helicolenus barathri*)	400–500	core (first 2 yr of growth) edge (capture year – (2 to 6) yr)	35°S to 37°S	151°E	Commercial fishing	Current study/ Park (1993)
Orange roughy (*Hoplostethus atlanticus*)	800–1000	core (first 4 yr of growth) transition zone (30 to 34 yr of age) inner edge (10 to 20 yr from edge) outer edge (capture year – 10 yr)	42°10′S to 42°54′S	175°W to 178°W	Commercial fishing	Kalish (2002b)
Hermatypic coral	ocean surface waters		22°06′S	153°W		Druffel and Griffin (2004)
Southern Hemisphere Atmospheric monthly record	Atmosphere		Southern Hemisphere			Hua et al. (2013)

Due to the very small size of the otolith carbonate powder samples (Table S1), multiple known value standards of marble, NBS Oxalic Acid-I, NBS Oxalic Acid-II, and in-house oyster carbonate standard (102 pMC) of similar sample weights were graphitised and measured in the SSAMS alongside each set of otolith carbonate samples to ensure the accuracy of the resulting ^{14}C values. Additionally, because the otoliths were embedded in epoxy resin, a sample of pure, hardened resin was acidified to discount it as a possible contamination source; no CO_2 was generated from the resin.

Radiocarbon values resulting from AMS analysis are expressed as $\Delta^{14}C$ (per mil, ‰, deviation of $^{14}C/^{12}C$ of the sample relative to a 95% NBS Oxalic Acid-I standard and corrected for year of formation (Table S1; Stuiver and Polach, 1977). The $\Delta^{14}C$ values from the otolith edges were plotted against the mean year of the milled sample, and values from the cores were plotted against estimated birth year.

2.4. Comparison of regional otolith $\Delta^{14}C$ curves

Otolith-based ^{14}C data from the southwest Pacific region was used to describe the transport of $\Delta^{14}C$ through the water column from marine surface waters to depths approaching 1000 m (Table 1). A general, marine surface reference $\Delta^{14}C$ time series for the southwest Pacific region was derived by combining ^{14}C data from Australasian snapper and nannygai (Fig. 4). There was no significant difference in levels of radiocarbon between the two species (ANOVA, $F_{1,33} = 0.793$, $p = 0.38$), enabling the two species to be pooled into one surface water $\Delta^{14}C$ time series for the region. Currently, there are no reference time series published for biological carbonate $\Delta^{14}C$ in the southwest Pacific Ocean at depths below the mixed layer (>200 m). Therefore, annually resolved ^{14}C values for ocean perch were related to the marine surface water series to establish the ocean perch $\Delta^{14}C$ mid-water series (Fig. 4). Andrews et al. (2009) have validated the ages of orange roughy, allowing us to plot the $\Delta^{14}C$ values obtained by Kalish (2002b; Table S2) against associated age estimates. All radiocarbon data were plotted by year, and each dataset was fitted with locally weighted least-squares regressions with 95% confidence intervals (*loess* function, R 3.0.2, R Development Core Team, 2013). We made additional comparisons of the mean pre-bomb $\Delta^{14}C$ values and post-bomb $\Delta^{14}C$ values/trends between the ocean perch otoliths and marine surface reference to establish the $\Delta^{14}C$ time series for depths of 400–500 m. Reservoir ages for ocean perch and orange roughy otolith ^{14}C data were calculated by subtracting the atmospheric ^{14}C age corresponding to the mean year of the otolith ^{14}C sample from the otolith ^{14}C age. Atmospheric ^{14}C values were determined from INTCAL13 (Reimer et al., 2013). Otolith ^{14}C ages were unavailable for Australasian snapper and nannygai in the published literature.

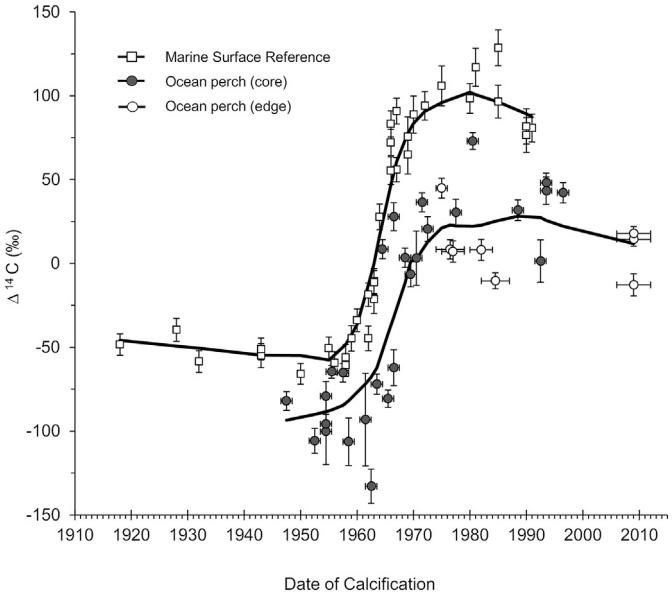

Fig. 4. $\Delta^{14}C$ values from ocean perch otolith aragonite (southeastern Australia) plotted by estimated birth year (cores) or capture year (edges). A marine surface reference curve is pooled from previously published data from the otolith cores of Australasian snapper (Kalish, 1993) and nannygai (Kalish, 1995). Vertical bars are the analytical $\Delta^{14}C$ error of each sample. Horizontal bars represent the range of years included in the ^{14}C sample for ocean perch. Each dataset is fitted with locally weighted least-squares regression curves (bold lines).

To compare otolith-based ^{14}C levels between the different depths, the years corresponding to the time of greatest radiocarbon increase from thermonuclear bomb inputs were selected for each species and the surface reference curve. Years of greatest increase were based on ^{14}C values in seawater in the southwest Pacific Ocean (Broecker and Peng, 1982; Jenkins et al., 2010; Ostlund and Stuiver, 1980) and on previous otolith radiocarbon values (Kalish, 1993, 1995, 2002a). For the surface reference curve, the years from 1960 to 1974 were chosen as these correspond

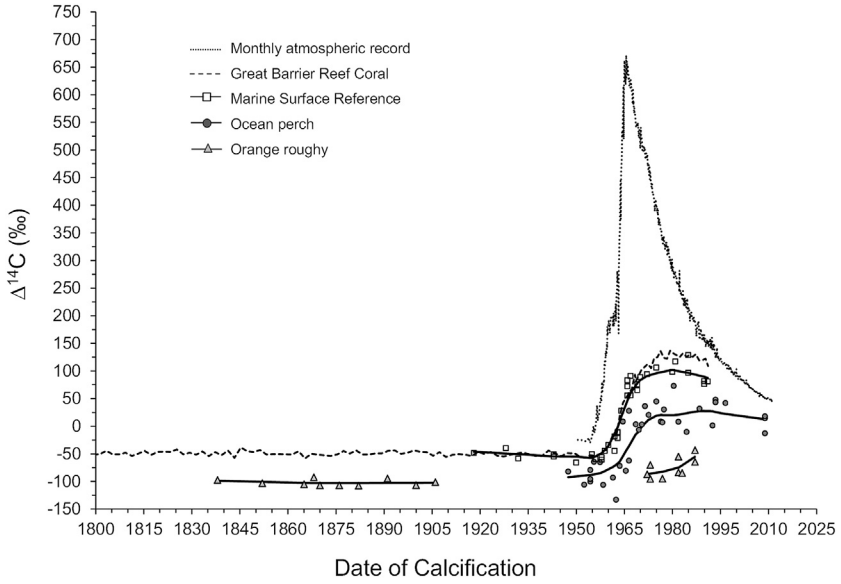

Fig. 5. A compilation of Δ^{14}C time series for the southern Pacific Ocean demonstrating the transport of ^{14}C from the atmosphere to oceanic depths approaching 1000 m. The time series are as follows: monthly atmospheric record for the Southern Hemisphere (Hua et al., 2013), Great Barrier Reef hermatypic coral record (Druffel and Griffin, 2004), fish marine surface reference series (Kalish, 1993, 1995), ocean perch series (present research), orange roughy series (Kalish, 2002b).

to the increase in radiocarbon in marine surface waters (Kalish, 1995). The years from 1963 to 1975 were selected for ocean perch at mid-water depths, 1963 was the first point (−72.00‰) within a 95% CI of the ocean perch time series (data not shown) that was above the mean pre-bomb level of −87.92‰, and 1975 was the last year in the linear trend of the loess curve in that dataset (Fig. 4). Levels of Δ^{14}C in orange roughy otoliths (Table S2) post-bomb were only available for the years 1972 to 1987 with these values representing depths of 800 to 1000 m.

2.5. Statistical analyses

We compared the slope and intercept of the linear trends of Δ^{14}C during the greatest periods of increase for the fish species and the surface reference curve using Comparison of Regression Lines (CRL; Statgraphics Centurion XVI, ver. 16.2.04). To account for negative numbers, a constant of 100 was added to all Δ^{14}C data and the square root taken. The first year in each dataset was designated as 1 regardless of the actual year, and subsequent years were numbered sequentially (e.g. 2, 3, 4, ...). This allocated a common time span for all species and helped to negate serial autocorrelation in the data. The CRL analysis fitted a linear regression model to the data to describe the relationship between Δ^{14}C, year and all species in the model; then the statistical significance of the model terms were tested, allowing the slopes and intercepts of the individual species-based regression lines to be compared at the significance level of $p = 0.05$. The Durbin–Watson statistic was used as a test for autocorrelation.

3. Results

3.1. Radiocarbon analysis of ocean perch

A total of 28 ocean perch otoliths were analysed by AMS to produce a Δ^{14}C time series representing mid-water depths of approximately 400–500 m (Table S1). The fish ranged in age from 6 to 46 yr and were 240 to 443 mm total length with otoliths weighing between 0.0600 and 0.3164 g (Table S1). Age corrected Δ^{14}C in ocean perch otoliths from AMS assays ranged from −132.89 to +72.96‰ with a mean analytical error of ±8.06‰ (Table S1, Fig. 4). Otolith core ($n = 27$) and edge ($n = 8$) Δ^{14}C were combined into one mid-water Δ^{14}C time series. A slight separation between core and edge is evident, but the values still correspond through time (Fig. 4).

A low mean pre-bomb Δ^{14}C value of −87.92‰ (−105.77 to −64.60‰) from ocean perch otolith cores confirms that this record does not represent surface water values between 30°S and 40°S (e.g. Broecker and Peng, 1982). Moreover, post 1975, ocean perch Δ^{14}C values are more depleted than the surface marine reference series (Fig. 4). Reservoir ages calculated from pre-bomb samples (Table S3) of ocean perch ranged from 331 to 701 yr (mean: 532 yr), while orange roughy ^{14}C reflected ages of 652 to 784 yr (mean: 726 yr).

3.2. Southwest Pacific Ocean Δ^{14}C time series compilation

A compilation of Δ^{14}C time series from the atmosphere, hermatypic coral and fish for the southern Pacific Ocean (Table 1) demonstrates the transport of ^{14}C from the atmosphere to oceanic depths approaching 1000 m (Fig. 5). Generally, we observed a shift in the peak of Δ^{14}C values to later years and an overall depression in peak height with increasing depth of the individual series curves (Fig. 5).

Increases of Δ^{14}C in the atmosphere commenced in 1954/1955 and in 1958 for marine surface waters (coral and otoliths). Δ^{14}C values began increasing at mid-water depths around 1963, and increased Δ^{14}C values are observed at deep-water depths about 10 yr later in the early 1970s. Peak values of Δ^{14}C in the marine surface reference curve occurred about 1975, while highest values for the mid-water series followed in the early 1980s (Fig. 5). The pre-bomb (pre-1957) Δ^{14}C orange roughy ("deep-water") series (mean: −102.1‰, range: −107.7 to −92.4‰) is more depleted than the ocean perch mid-water series (mean: −87.9‰, range: −105.8 to 64.6‰; Table S1), which in turn is more depleted than both the otolith marine surface reference (mean: −64.6‰, range: −65.9 to −39.6‰) and the hermatypic coral (Fig. 5). Bomb ^{14}C penetrated to depths of 400–500 m by 1963, when the first post-bomb Δ^{14}C value above the pre-bomb mean for the mid-water series is seen (HBN-009, −72.0‰). The dataset is limited for the

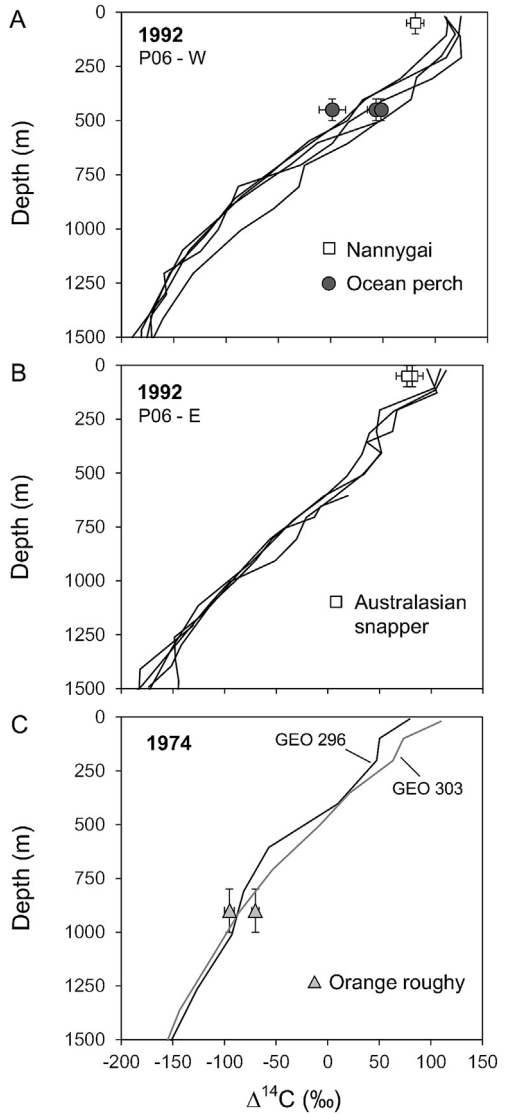

Fig. 6. $\Delta^{14}C$ water values from the eWOCE dataset (Schlitzer, 2000) along (A) P06-W, (B) P06-E in 1992 and (C) GEOSECS stations (Fig. 1A: GEO 296, 303; Ostlund and Stuiver, 1980) in 1974 plotted by depth. Otolith $\Delta^{14}C$ values from corresponding years have been plotted alongside for comparison. (A) Ocean perch (present research) and nannygai (Kalish, 1995) $\Delta^{14}C$ covering the years of 1991–1993 and area of 35°S–37°S, 151°E. (B) Australasian snapper (Kalish, 1993) $\Delta^{14}C$ representing 1990 and the area of 39°S, 179°E. (C) Orange roughy (Kalish, 2002b) $\Delta^{14}C$ representing 1973 and the area of 42°S, 175°W–178°W. Horizontal bars are the analytical $\Delta^{14}C$ error of each sample. Vertical bars denote the estimated depth range of the sample.

deep-water series, only spanning 1972 to 1987, but it is likely that bomb ^{14}C had penetrated to depths of 800–1000 m by 1972 as $\Delta^{14}C$ values from the early 1970s (ORH7/4, −70.0‰) and late 1980s (ORH10/5, −43.2‰) are well above mean pre-bomb values at those depths (Fig. 5, Table S2). Otolith $\Delta^{14}C$ values are also in good agreement with corresponding $\Delta^{14}C$ water values from Geochemical Ocean Sections Study (GEOSECS; Ostlund and Stuiver, 1980) and World Ocean Circulation Experiment (WOCE; Key, 1996; Schlitzer, 2000) surveys (Fig. 6).

Comparisons of the bomb ^{14}C decrease of the 1990s to present can only be made in reference to the atmosphere and mid-water series as data are not available for the surface or deep-water. From 1993 to 2009 the atmosphere exhibited an average rate of change of −5.0‰ yr^{-1} compared to −0.8‰ yr^{-1} estimated for the mid-water series. It is of interest to note that the mid-water and deep-water time series appear to merge as they go back in time. They can only be differentiated in the post-bomb era.

3.3. Regional otolith $\Delta^{14}C$ curves

To more closely examine the otolith $\Delta^{14}C$ data for the three different fish-based ^{14}C time series, we compared the $\Delta^{14}C$ trends during the greatest periods of increase for all three otolith $\Delta^{14}C$ series using a linear regression model (Table 2; Fig. 7). All three time series yielded significantly different intercepts of increase (Overall Model: adjusted $R^2_{Model} = 0.812$, $p_{Model} < 0.001$, $p_{Intercept} < 0.001$, $p_{Slope} = 0.516$, $n = 36$), and no significant difference between the slopes. We estimated lags between each depth series from the plots with fitted loess curves (Fig. 5). These estimates were based on the timing of the bomb pulse increase. A 5 to 10 yr lag was estimated between the surface and depths of 400–500 m, and a 10 to 20 yr lag was estimated between the surface and depths of 800–1000 m.

4. Discussion

Our findings suggest the major, depth segregated water masses in the southwest Pacific Ocean (depths <1500 m) influence $\Delta^{14}C$ values found in fish otoliths. The mean pre-bomb $\Delta^{14}C$ level for each of the three otolith depth series were comparable to reported $\Delta^{14}C$ values for waters of corresponding depths in the southwest Pacific (e.g. Broecker and Peng, 1982; Key et al., 2004). Post-bomb $\Delta^{14}C$ values observed in the otolith depth series were also similar to $\Delta^{14}C$ values reported from GEOSECS (1973 to 1974; Ostlund and Stuiver, 1980) and WOCE (1991 to 1994; Key, 1996; Schlitzer, 2000) surveys of the southwest Pacific and fall within the appropriate modelled $\Delta^{14}C$ ranges as depth increases at 30°S to 45°S (Fig. S1 for comparison; Broecker and Peng, 1982; Jenkins et al., 2010; Key et al., 2004).

While the three otolith radiocarbon records (comprised of four fish species) presented here are spatially separate, the oceanography of the southwestern Pacific allows them to be linked. Both the nannygai $\Delta^{14}C$ record from southeastern Australia (Kalish, 1995) and the Australasian snapper from the north eastern coast of New Zealand (Kalish, 1993) live in surface waters during the time of otolith core formation. The surface water masses in both of these areas are LTW (Fig. 2; $\sigma_\theta = 26.3$: lower boundary; Sokolov and Rintoul, 2000) transported by the EAC to the Tasman Sea (via the EAC Extension) and the northeast coast of New Zealand (via the EAUC). Connectivity between the water masses of these different areas is reflected in the common otolith $\Delta^{14}C$ values of both surface water species (Australasian snapper and nannygai). The Tasman AAIW ($\sigma_\theta = 26.9$–27.3), a distinctive, higher salinity type of AAIW, is found at depths where the orange roughy on the north flank of the Chatham Rise were collected. This water mass originates in the Tasman Sea and is also found along the coast of southeastern Australia (Fig. 1A, Fig. 2a; Bostock et al., 2013), beneath the depths where both the ocean perch and nannygai records originate. Thus, the water column at each location is similarly structured for all otolith radiocarbon records, and allows the records to be considered in the same context and compared through time.

The ocean perch record represents an area dominated by a thermocline layer just above the 26.9 density boundary of the Tasman AAIW and beneath the 26.3 density boundary of the LTW of the surface waters. This area, as well as the region along the northeast coast of New Zealand, is part of a vigorous anticyclonic eddy field. These eddies increase vertical mixing within the upper ocean and can reach to depths beyond 1000 m (Ridgway and Dunn, 2003; Sokolov and Rintoul, 2000). The range of $\Delta^{14}C$ values seen in the mid-water ocean perch series in a given year may be attributed to both vertical mixing and by mixing at the depth boundary of

Table 2
Comparison of the linear trends of $\Delta^{14}C$ during the greatest periods of increase for otolith-based $\Delta^{14}C$ series resulting from ocean perch (this study), orange roughy (Kalish, 2002b), and the marine surface reference curve (Kalish, 1993, 1995). A linear regression model was fitted to transformed data to describe the relationship between $\Delta^{14}C$, year and all series in the model. n = number of samples in each model. The model statistics are presented as: Adjusted R^2_{Model}, df_{Model}, p_{Model}, and Durbin–Watson$_{Model}$ (p value). The statistical significance between the slopes and intercepts of the individual series-based regression lines in each model are given as $p_{Intercept}$, and p_{Slope}.

$\Delta^{14}C$ Series	n	Adjusted R^2_{Model}	df_{Model}	p_{Model}	$p_{Intercept}$	p_{Slope}	Durbin–Watson$_{Model}$ (p value)
Surface + Ocean perch	27	0.715	3, 23	<0.001	<0.001	0.278	2.087 (0.349)
Surface + Orange roughy	25	0.900	3, 21	<0.001	<0.001	0.364	2.161 (0.413)
Ocean perch + Orange roughy	20	0.636	3, 16	0.001	0.006	0.979	2.391 (0.590)
Overall model (all 3 series)	36	0.812	5, 30	<0.001	<0.001	0.516	2.461 (0.716)

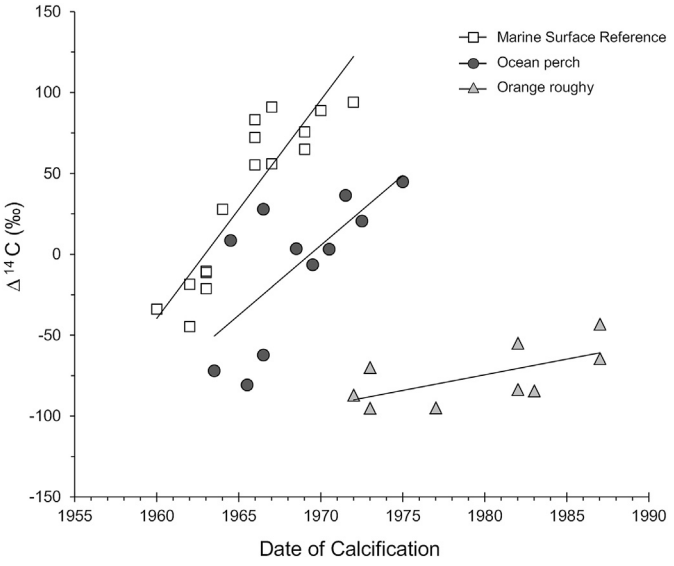

Fig. 7. Linear trends of otolith $\Delta^{14}C$ levels during the periods of greatest ^{14}C increase for the three time series at increasing depths: marine surface reference (Kalish, 1993, 1995), ocean perch (400–500 m), and orange roughy (800–1000 m; Kalish, 2002b). All intercepts were significantly different ($p \leq 0.002$); the slopes did not differ. Untransformed data are presented.

the Tasman AAIW. Other variability in this record is likely due to the necessity of estimating the capture depth of the fish based on commercial fisheries data.

Beginning in 1958, regional diffusion of bomb derived $\Delta^{14}C$ from the atmosphere into the surface waters of the southern Pacific Ocean increased $\Delta^{14}C$ levels found in shallow water coral (e.g. Druffel, 2002) and otoliths (e.g. Kalish, 1993, 1995). A shift of the peak in $\Delta^{14}C$ values to lower values and a general overall decrease with increasing depth of the individual series curves (atmosphere, coral and fish) for the southern Pacific Ocean demonstrates the transport of ^{14}C from the atmosphere to oceanic depths approaching 1000 m. The atmospheric ^{14}C decrease from the mid-1960s to present is a result of absence/reduction of nuclear explosions, rapid atmosphere–biosphere–ocean exchange, and the combustion of fossil fuel free of ^{14}C (Hua et al., 2013). This decrease is replicated to a lesser extent in marine waters and becomes more complex with increasing depth due to latitudinal and vertical mixing (Broecker and Peng, 1982; Jenkins et al., 2010; Rodgers et al., 2011).

$\Delta^{14}C$ found in both coral and otoliths in the surface waters of the southwest Pacific were similar, which again can be attributed to those species living in waters that are LTW (Ganachaud et al., 2014; Sokolov and Rintoul, 2000). However, it is interesting to note that while all carbonate surface records are found in LTW, after the ^{14}C increase in 1958, the coral record $\Delta^{14}C$ peaked much higher than did the otolith values of the marine surface reference series. This could be due to the coral record being located closer to higher $\Delta^{14}C$ values of the main SPG compared to the otoliths sourced from southeastern Australia or northeastern New Zealand (Druffel, 2002; Sokolov and Rintoul, 2000). The slightly lower surface $\Delta^{14}C$ values in these two areas may also reflect increased vertical mixing (Druffel, 2002) by the dynamic eddy fields of these areas (Ridgway and Dunn, 2003).

Pre-bomb reservoir ages estimated for ocean perch (~530 yr) and orange roughy otolith ^{14}C (~730 yr) were lower than current surface water reservoir ages reported for the Tasman Sea (250 to 350 yr: Komugabe et al., 2014). Source waters of AAIW in the southeastern Pacific have an estimated reservoir age of 600 yr (Jenkins et al., 2010). The higher reservoir ages of orange roughy otoliths likely reflect Tasman AAIW along the Chatham Rise. The moderate reservoir ages of ocean perch otoliths suggests mixing of lower ^{14}C Tasman AAIW with higher ^{14}C surface waters in the thermocline of the Tasman Sea.

Lags were revealed in the time history of $\Delta^{14}C$ invasion at different depths. Mid-water and deep-water time series became more discernible by the increased ^{14}C gradient in the post-bomb era. The 10 to 20 yr lag in $\Delta^{14}C$ levels between the surface and depths of 800–1000 m may reflect the ventilation time for Tasman AAIW. Jenkins et al. (2010) estimated the ventilation time for AAIW in the southwest Pacific (possibly in reference to SP AAIW) to be about 30 yr based on ^{14}C patterns. Tasman AAIW forms in the Tasman Sea recirculation gyre from older SP AAIW that has travelled from the main SPG and is then mixed with saltier thermocline water (Bostock et al., 2013). Ventilation time for this water mass could be impacted by its proximity to the energetic eddy field of the EAC Extension (Davis, 2005; Lachkar et al., 2009). The 5 to 10 yr lag between the surface and depths of 400–500 m may represent the ventilation time for those thermocline waters as they are mixed vertically by the eddies as well as mixing with some of the older AAIW water at its depth boundary.

The $\Delta^{14}C$ values from adults of both bluenose (Horn et al., 2010) and rubyfish (Horn et al., 2012) collected off the northeastern coast of New Zealand (near the Australasian ^{14}C snapper record) are comparable to our mid-water ocean perch radiocarbon record off of southeastern Australia. When plotted with the mid-water record (Fig. S2), the peak in the 1980s becomes more defined. The variability within the ^{14}C records of the three species most likely can be attributed to mixing from the anticyclonic eddies found in both areas (Ridgway and Dunn, 2003), ontogenetic feeding and vertical migrations (Horn et al., 2010, 2012), and the inability to precisely pinpoint the exact depth at which each fish was collected.

The ocean perch core and edge $\Delta^{14}C$ values were not offset to the extent displayed by bluenose undergoing ontogenetic depths shifts from surface waters to depths of ≥600 m (Horn et al., 2010). This suggests that juveniles (≤2 yr) and adults may exhibit a slight depth separation and the expected age-related feeding shifts of a non-migratory benthic species (Bulman et al., 2001; Park, 1993; Smith et al., 2009), but generally the fish occupy similar habitats at similar depths. Further separation of this relationship would require more samples at specific depths, especially given the dynamic vertical mixing of the EAC Extension eddies where they were captured.

The otolith material left after thin sections were removed for visual age determination allowed for only very small amounts of otolith carbonate to be milled for AMS. The mean amount of ocean perch otolith carbonate milled for AMS ^{14}C analysis was 0.50 mg (equating to ~50 µg of graphitised carbon), which is 4 to 50 times *less* than the mean amounts (2 to 27 mg) used in previous otolith-based radiocarbon methods (e.g. Andrews et al., 2013; Horn et al., 2010; Kalish, 1993). The use of multiple known-value standards of equally small quantities provided a metric to assess the accuracy of the resultant otolith carbonate ^{14}C values. The mean analytical $\Delta^{14}C$ error associated with previous research ranges from ±3.89 to ±10.36‰ (e.g. Andrews et al., 2013; Horn et al., 2010; Kalish, 1993); the mean error for ocean perch carbonate of ±8.06‰ was well within this range. The ability to analyse small amounts of carbon greatly broadens the scope of samples to which AMS analyses can be applied.

In conclusion, otolith ^{14}C is comparable to other carbonate records and may be used as a tracer of water masses as well as to examine temporal ^{14}C transport. Using otolith bomb ^{14}C, we related three otolith-based depth series to two water masses (LTW, AAIW) and the thermocline waters that are found between the different water masses in the upper 1500 m of the southwest Pacific Ocean. Overall, application of fish otoliths to examine the bomb pulse of ^{14}C provided valuable insights into the timing of ^{14}C transport into depths approaching 1000 m in the southwest Pacific Ocean, particularly the Tasman Sea, an area deficient in instrumental temporal ^{14}C records in waters below the mixed layer. Otolith carbonate records have the capacity to become an accessible mechanism to examine mixing of water masses in areas where instrumental records may not be forthcoming.

Acknowledgements

We acknowledge partial funding from the Dr Paris Goodsell Marine Ecology Research Grant, the Nature Foundation SA, the Sir Mark Mitchell Research Foundation, CSIRO Wealth from Oceans Flagship and the Australian Research Council (FT100100767; DP110100716). We acknowledge Kevin Rowling for assistance in otolith acquisition and general mentoring. This manuscript was markedly improved by constructive comments from Katsumi Matsumoto and two anonymous reviewers.

Appendix A. Supplementary material

Supplementary material related to this article can be found online at http://dx.doi.org/10.1016/j.epsl.2015.05.008.

References

Andrews, A.H., Barnett, B.K., Allman, R.J., Moyer, R.P., Trowbridge, H.D., 2013. Great longevity of speckled hind (*Epinephelus drummondhayi*), a deep-water grouper, with novel use of postbomb radiocarbon dating in the Gulf of Mexico. Can. J. Fish. Aquat. Sci. 70, 1–10. http://dx.doi.org/10.1139/cjfas-2012-0537.

Andrews, A.H., Kalish, J.M., Newman, S.J., Johnston, J.M., 2011. Bomb radiocarbon dating of three important reef-fish species using Indo-Pacific $\Delta^{14}C$ chronologies. Mar. Freshw. Res. 62, 1259–1269. http://dx.doi.org/10.1071/MF11080.

Andrews, A.H., Tracey, D.M., Dunn, M.R., 2009. Lead–radium dating of orange roughy (*Hoplostethus atlanticus*): validation of a centenarian life span. Can. J. Fish. Aquat. Sci. 66, 1130–1140. http://dx.doi.org/10.1139/F09-059.

Armsworthy, S., Campana, S., 2010. Age determination, bomb-radiocarbon validation and growth of Atlantic halibut (*Hippoglossus hippoglossus*) from the Northwest Atlantic. Environ. Biol. Fishes 89, 279–295. http://dx.doi.org/10.1007/s10641-010-9696-8.

Bostock, H.C., Opdyke, B.N., Williams, M.J.M., 2010. Characterising the intermediate depth waters of the Pacific Ocean using $\delta^{13}C$ and other geochemical tracers. Deep-Sea Res., Part I 57, 847–859. http://dx.doi.org/10.1016/j.dsr.2010.04.005.

Bostock, H.C., Sutton, P.J., Williams, M.J.M., Opdyke, B.N., 2013. Reviewing the circulation and mixing of Antarctic Intermediate Water in the South Pacific using evidence from geochemical tracers and Argo float trajectories. Deep-Sea Res., Part I 73, 84–98. http://dx.doi.org/10.1016/j.dsr.2012.11.007.

Broecker, W.S., Peng, T.-H., 1982. Tracers in the Sea. The Lamont-Doherty Geological Observatory. Columbia University, Palisades, New York.

Bulman, C., Althaus, F., He, X., Bax, N., Williams, A., 2001. Diets and trophic guilds of demersal fishes of the south–eastern Australian shelf. Mar. Freshw. Res. 52, 537–548.

Campana, S.E., 1997. Use of radiocarbon from nuclear fallout as a dated marker in the otoliths of haddock *Melanogrammus aeglefinus*. Mar. Ecol. Prog. Ser. 150, 49–56. http://dx.doi.org/10.3354/meps150049.

Campana, S.E., Casselman, J.M., Jones, C.M., 2008. Bomb radiocarbon chronologies in the Arctic, with implications for the age validation of lake trout (*Salvelinus namaycush*) and other Arctic species. Can. J. Fish. Aquat. Sci. 65, 733–743. http://dx.doi.org/10.1139/f08-012.

Campana, S.E., Neilson, J.D., 1985. Microstructure of fish otoliths. Can. J. Fish. Aquat. Sci. 42, 1014–1032.

Campana, S.E., Thorrold, S.R., 2001. Otoliths, increments, and elements: keys to a comprehensive understanding of fish populations? Can. J. Fish. Aquat. Sci. 58, 30–38.

Davis, R.E., 2005. Intermediate-depth circulation of the Indian and South Pacific Oceans measured by autonomous floats. J. Phys. Oceanogr. 35, 683–707. http://dx.doi.org/10.1175/JPO2702.1.

Druffel, E., 2002. Radiocarbon in corals: records of the carbon cycle, surface circulation and climate. Oceanography 15, 122–127.

Druffel, E.R.M., Griffin, S., 2004. Southern Great Barrier Reef coral radiocarbon data. NOAA/NCDC Paleoclimatology Program. IGBP PAGES/World Data Center for Paleoclimatology, Boulder, Colorado, USA. Data Contribution Series #2004-093.

Fallon, S.J., Fifield, L.K., Chappell, J.M., 2010. The next chapter in radiocarbon dating at the Australian National University: status report on the single stage AMS. Nucl. Instrum. Methods B 268, 898–901. http://dx.doi.org/10.1016/j.nimb.2009.10.059.

Ganachaud, A., Cravatte, S., Melet, A., Schiller, A., Holbrook, N.J., Sloyan, B.M., Widlansky, M.J., Bowen, M., Verron, J., Wiles, P., Ridgway, K., Sutton, P., Sprintall, J., Steinberg, C., Brassington, G., Cai, W., Davis, R., Gasparin, F., Gourdeau, L., Hasegawa, T., Kessler, W., Maes, C., Takahashi, K., Richards, K.J., Send, U., 2014. The Southwest Pacific Ocean circulation and climate experiment (SPICE). J. Geophys. Res., Oceans 119, 7660–7686. http://dx.doi.org/10.1002/2013JC009678.

Horn, P.L., Neil, H.L., Paul, L.J., Marriott, P., 2010. Age validation and growth of bluenose Hyperoglyphe antarctica using the bomb chronometer method of radiocarbon ageing. J. Fish Biol. 77, 1552–1563. http://dx.doi.org/10.1111/j.1095-8649.2010.02787.x.

Horn, P.L., Neil, H.L., Paul, L.J., McMillan, P.J., 2012. Age verification, growth and life history of rubyfish *Plagiogeneion rubiginosum*. N. Z. J. Mar. Freshw. Res. 46, 353–368. http://dx.doi.org/10.1080/00288330.2012.676052.

Hua, Q., Barbetti, M., Rakowski, A.Z., 2013. Atmospheric radiocarbon for the period 1950–2010. Radiocarbon 55, 2059–2072.

Jenkins, W.J., Elder, K.L., McNichol, A.P., von Reden, K., 2010. The passage of the bomb radiocarbon pulse into the Pacific Ocean. Radiocarbon 52, 1182–1190.

Kalish, J.M., 1991. Oxygen and carbon stable isotopes in the otoliths of wild and laboratory-reared Australian salmon (*Arripis trutta*). Mar. Biol. 110, 37–47. http://dx.doi.org/10.1007/BF01313090.

Kalish, J.M., 1993. Pre- and post-bomb radiocarbon in fish otoliths. Earth Planet. Sci. Lett. 114, 549–554. http://dx.doi.org/10.1016/0012-821X(93)90082-K.

Kalish, J.M., 1994. Investigating global change and fish biology with fish otolith radiocarbon. Nucl. Instrum. Methods B 92, 421–425. http://dx.doi.org/10.1016/0168-583X(94)96047-X.

Kalish, J.M., 1995. Application of the bomb radiocarbon chronometer to the validation of redfish *Centroberyx affinis* age. Can. J. Fish. Aquat. Sci. 52, 1399–1405. http://dx.doi.org/10.1139/f95-135.

Kalish, J.M., 2002a. Use of the bomb radiocarbon chronometer to validate fish age. Final Report FRDC Project 93/109. Fisheries Research and Development Corporation and Australian National University, Canberra, p. 384.

Kalish, J.M., 2002b. Validation of orange roughy (*Hoplostethus atlanticus*) age by high precision radiocarbon dating. In: Kalish, J.M. (Ed.), Use of the Bomb Radiocarbon Chronometer to Validate Fish Age: Final Report FRDC Project 93/109. Fisheries Research and Development Corporation and Australian National University, Canberra, pp. 238–259.

Kalish, J.M., Nydal, R., Nedreaas, K.H., Burr, G.S., Eine, G.L., 2001. A time history of pre- and post-bomb radiocarbon in the Barrents Sea derived from Arcto-Norwegian cod otoliths. Radiocarbon 43, 843–855.

Key, R.M., 1996. WOCE Pacific Ocean Radiocarbon Program. Radiocarbon 38, 415–423.

Key, R.M., Kozyr, A., Sabine, C.L., Lee, K., Wanninkhof, R., Bullister, J.L., Feely, R.A., Millero, F.J., Mordy, C., Peng, T.H., 2004. A global ocean carbon climatology: results from Global Data Analysis Project (GLODAP). Glob. Biogeochem. Cycles 18, GB4031. http://dx.doi.org/10.1029/2004GB002247.

Komugabe, A.F., Fallon, S.J., Thresher, R.E., Eggins, S.M., 2014. Modern Tasman Sea surface reservoir ages from deep-sea black corals. Deep-Sea Res., Part II 99, 207–212.

Lachkar, Z., Orr, J.C., Dutay, J.-C., Delecluse, P., 2009. On the role of mesoscale eddies in the ventilation of Antarctic intermediate water. Deep-Sea Res., Part I 56, 909–925. http://dx.doi.org/10.1016/j.dsr.2009.01.013.

Nydal, R., 2000. Radiocarbon in the ocean. Radiocarbon 42, 81–98.
Ostlund, H.G., Stuiver, M., 1980. GEOSECS Pacific radiocarbon. Radiocarbon 22, 25–53.
Park, T.J., 1993. A Comparison of the Morphology Growth and Reproductive Biology of Two Colour Forms of Ocean Perch (*Helicolenus percoides*). Faculty of Science, University of Sydney, Sydney, NSW, Australia, p. 201.
Paul, L.J., Horn, P.L., 2009. Age and growth of sea perch (*Helicolenus percoides*) from two adjacent areas off the east coast of South Island, N. Z. Fish. Res. 95, 169–180. http://dx.doi.org/10.1016/j.fishres.2008.08.011.
Pavlov, D.A., Emel'yanova, N.G., 2013. Transition to viviparity in the order Scorpaeniformes: brief review. J. Ichthyol. 53, 52–69. http://dx.doi.org/10.1134/S0032945213010116.
Qu, T., Gao, S., Fukumori, I., Fine, R.A., Lindstrom, E.J., 2009. Origin and pathway of equatorial 13 °C water in the Pacific identified by a simulated passive tracer and its adjoint*. J. Phys. Oceanogr. 39, 1836–1853. http://dx.doi.org/10.1175/2009JPO4045.1.
Reimer, P.J., Bard, E., Bayliss, A., Beck, J.W., Blackwell, P.G., Bronk Ramsey, C., Buck, C.E., Cheng, H., Edwards, R.L., Friedrich, M., Grootes, P.M., Guilderson, T.P., Haflidason, H., Hajdas, I., Hatté, C., Heaton, T.J., Hoffmann, D.L., Hogg, A.G., Hughen, K.A., Kaiser, K.F., Kromer, B., Manning, S.W., Niu, M., Reimer, R.W., Richards, D.A., Scott, E.M., Southon, J.R., Staff, R.A., Turney, C.S.M., van der Plicht, J., 2013. IntCal13 and Marine13 radiocarbon age calibration curves 0–50,000 years cal BP. Radiocarbon 55, 1869–1887. http://dx.doi.org/10.2458/azu_js_rc.55.16947.
Ridgway, K., Dunn, J., 2003. Mesoscale structure of the mean East Australian Current System and its relationship with topography. Prog. Oceanogr. 56, 189–222.
Rodgers, K.B., Mikaloff-Fletcher, S.E., Bianchi, D., Beaulieu, C., Galbraith, E.D., Gnanadesikan, A., Hogg, A.G., Iudicone, D., Lintner, B.R., Naegler, T., 2011. Interhemispheric gradient of atmospheric radiocarbon reveals natural variability of Southern Ocean winds. Clim. Past 7, 1123–1138.
Schlitzer, R., 2015. Ocean data view. odv.awi.de.
Schlitzer, R., 2000. Electronic atlas of WOCE hydrographic and tracer data now available. Eos Trans. AGU 81, 45. http://dx.doi.org/10.1029/00EO00028.
Scourse, J.D., Wanamaker Jr., A.D., Weidman, C., Heinemeier, J., Reimer, P.J., Butler, P.G., Witbaard, R., Richardson, C.A., 2012. The marine radiocarbon bomb pulse across the temperate North Atlantic: a compliation of Δ^{14}C time histories from *Arctica islandica* growth increments. Radiocarbon 54, 165–186.
Sequeira, V., Neves, A., Vieira, A.R., Figueiredo, I., Gordo, L.S., 2009. Age and growth of bluemouth, *Helicolenus dactylopterus*, from the Portuguese continental slope. ICES J. Mar. Sci. 66, 524–531.
Smith, P.J., Struthers, C.D., Paulin, C.D., McVeagh, S.M., Daley, R.K., 2009. Shallow genetic and morphological divergence among seaperches in the South Pacific (family *Scorpaenidae*, genus *Helicolenus*). J. Fish Biol. 74, 1104–1128. http://dx.doi.org/10.1111/j.1095-8649.2008.02172.x.
Sokolov, S., Rintoul, S., 2000. Circulation and water masses of the southwest Pacific: WOCE section P11, Papua New Guinea to Tasmania. J. Mar. Res. 58, 223–268.
Solomon, C.T., Weber, P.K., Cech, J., Joseph, J., Ingram, B.L., Conrad, M.E., Machavaram, M.V., Pogodina, A.R., Franklin, R.L., 2006. Experimental determination of the sources of otolith carbon and associated isotopic fractionation. Can. J. Fish. Aquat. Sci. 63, 79–89.
Stuiver, M., Polach, H.A., 1977. Discussion: reporting of ^{14}C data. Radiocarbon 19, 355–363.
Suess, H.E., 1953. Natural radiocarbon and the rate of exchange of carbon dioxide between the atmosphere and the sea. In: Aldrich, W. (Ed.), Nuclear Processes in Geologic Settings. University of Chicago Press, Chicago, pp. 52–56.

Appendix A: Supplementary Material (for online publication only)

Investigating bomb radiocarbon transport in the southern Pacific Ocean with otolith radiocarbon

Gretchen. L. Grammer[1*], Stewart. J. Fallon[2], Christopher. Izzo[1], Rachel. Wood[2], Bronwyn. M. Gillanders[1]

[1]Southern Seas Ecology Laboratories, School of Biological Sciences, The University of Adelaide, SA 5005, Australia
[2]Radiocarbon Facility, Research School of Earth Sciences, The Australian National University, Canberra, ACT 0200, Australia
*Corresponding Author: Tel.: +61 8 8313 1483; Fax: +61 8 8313 4364;
Email: gretchen.grammer@adelaide.edu.au

Table S1: Data describing ocean perch (*Helicolenus barathri*) samples collected off the coast of New South Wales, Australia used in this study. Ages of ocean perch were estimated from thin sectioned otoliths, and the mean year of the ^{14}C sample was estimated from the birth year as back calculated from the annual growth increment count. All otolith samples were taken from the core region (first 2 years of growth) unless designated as "edge" in the "Estimated age" column. Radiocarbon data are presented as fraction modern (Fm) and $\Delta^{14}C$ (‰). Carbon mass (µg) is the approximate amount of carbon graphitised from the otolith carbonate sample for radiocarbon dating. Carbonate mass (mg) is the amount of otolith carbonate initially extracted for the analysis. A mass of < 0.5 was estimated when the actual mass could not be measured.

Sample no.	SANU no.	Location	Length (mm TL)	Otolith mass (g)	Collection year	C mass (µg)	Carbon-ate mass (mg)	Mean year of ^{14}C sample	Esti-mated age (yrs)	Fm	$\Delta^{14}C$ (‰)	± SD $\Delta^{14}C$
HBN-041	36923	37°S 151°E	380	0.2199	1982	35	0.41	1947.5	35	0.9180	-82.03	5.6
HBN-089	34720	35°S 151°E	400	0.2312	1987	30	< 0.50	1952.5	35	0.8942	-105.77	7.4
HBN-012	34710	37°S 151°E	400	0.2116	1982	10	< 0.50	1954.5	28	0.8998	-100.18	19.8
HBN-035	36921	35°S 151°E	380	0.2008	1979	25	0.29	1954.5	25	0.9043	-95.73	5.8
HBN-058	34714	37°S 151°E	370	0.1475	1984	20	< 0.50	1954.5	30	0.9208	-79.22	8.8
HBN-094	36712	35°S 151°E	370	0.1682	1987	50	0.69	1955.5	32	0.9354	-64.60	3.8
HBN-020	34711	37°S 151°E	400	0.1768	1982	40	< 0.50	1957.5	25	0.9348	-65.22	5.5
HBN-063	34716	37°S 151°E	370	0.1737	1984	15	< 0.50	1958.5	26	0.8937	-106.30	14.2
HBN-005	34709	35°S 151°E	360	0.1633	1979	10	< 0.50	1961.5	18	0.9069	-93.08	27.6
HBN-096	34721	35°S 151°E	390	0.1992	1987	20	< 0.50	1962.5	25	0.8671	-132.89	10.2
HBN-009	36920	35°S 151°E	380	0.1597	1979	25	0.32	1963.5	16	0.9280	-72.00	6.0
HBN-056	36711	37°S 151°E	370	0.1819	1984	35	0.60	1964.5	20	1.0086	8.56	5.7
HBN-080	34718	35°S 151°E	340	0.1630	1987	45	< 0.50	1965.5	22	0.9193	-80.69	5.2
HBN-053	34713	37°S 151°E	350	0.1458	1984	40	< 0.50	1966.5	18	1.0279	27.89	8.3
HBN-115	34726	37°S 151°E	443	0.3164	2012	20	< 0.50	1966.5	46	0.9378	-62.22	10.6
HBN-097	34723	35°S 151°E	350	0.1521	1987	40	< 0.50	1968.5	19	1.0034	3.44	5.8
HBN-082	34719	35°S 151°E	370	0.1876	1987	35	< 0.50	1969.5	18	0.9935	-6.46	7.4
HBN-023	34712	35°S 151°E	240	0.0600	1976	15	< 0.50	1970.5	6	1.0032	3.16	16.2
HBN-074	34717	35°S 151°E	330	0.1720	1987	40	< 0.50	1971.5	16	1.0365	36.46	5.6
HBN-098	34724	35°S 151°E	350	0.1498	1987	40	< 0.50	1972.5	15	1.0206	20.58	7.3
HBN-023E	36832	35°S 151°E	240	0.0600	1976	30	0.70	1975	edge	1.0448	44.85	5.9
HBN-005E	36813	35°S 151°E	360	0.1633	1979	25	0.35	1976.5	edge	1.0084	8.40	5.7
HBN-028E	36831	35°S 151°E	350	0.1507	1979	35	0.76	1977	edge	1.0071	7.06	6.4
HBN-104	34725	35°S 151°E	380	0.1050	1987	35	< 0.50	1977.5	10	1.0304	30.43	7.7
HBN-122	36713	35°S 151°E	433	0.2481	2012	45	0.60	1980.5	32	1.0730	72.96	5.0
HBN-053E	36814	37°S 151°E	350	0.1458	1984	20	0.28	1982	edge	1.0081	8.13	6.2
HBN-094E	36830	35°S 151°E	370	0.1682	1987	25	0.34	1984.5	edge	0.9896	-10.39	4.7
HBN-120	34731	35°S 151°E	388	0.1997	2012	30	< 0.50	1988.5	24	1.0318	31.77	6.2
HBN-118	34729	37°S 151°E	391	0.1752	2012	15	< 0.50	1992.5	20	1.0014	1.41	12.6
HBN-116	34727	37°S 151°E	384	0.1844	2012	35	< 0.50	1993.5	19	1.0433	43.31	8.2
HBN-119	34730	37°S 151°E	398	0.1720	2012	45	< 0.50	1993.5	19	1.0480	48.03	5.8
HBN-117	36818	37°S 151°E	395	0.1660	2012	25	0.14	1996.5	16	1.0422	42.15	6.0
HBN-115E	36812	37°S 151°E	443	0.3164	2012	25	0.30	2009	edge	0.9873	-12.75	6.7
HBN-116E	36833	37°S 151°E	384	0.1844	2012	30	0.67	2009	edge	1.0144	14.40	4.1
HBN-122E	36835	35°S 151°E	433	0.2481	2012	35	1.00	2009	edge	1.0179	17.89	4.1

Table S2: Orange roughy (*Hoplostethus atlanticus*) otolith-based radiocarbon data as estimated from Kalish (2002b).

Sample no.	†Estimated age (yrs)	Estimated birth year	Mean year of ^{14}C sample	Collection year	$\Delta^{14}C$ (‰)	$\pm\Delta^{14}C$ (‰)
Core*						
ORH7/1	120	1868	1870	1988	-106.73	6
ORH8/1	138	1850	1852	1988	-102.83	5.1
ORH10/1	156	1836	1838	1992	-97.3	3
ORH15/1	118	1874	1876	1992	-106.74	3.12
Region 3**						
ORH1/3	154	1833	1865	1987	-105.2	3
ORH4/3	128	1859	1891	1987	-94.488	6.24
ORH7/3	120	1868	1900	1988	-106.53	3.43
ORH8/3	138	1850	1882	1988	-107.73	4.42
ORH10/3	156	1836	1868	1992	-92.4	3
ORH15/3	118	1874	1906	1992	-101.16	3.53
Region 4***						
ORH4/4	128	1859	1972	1987	-87.099	3.07
ORH7/4	120	1868	1973	1988	-70.01	3.72
ORH8/4	138	1850	1973	1988	-95.17	4.57
ORH15/4	118	1874	1977	1992	-95	6.09
Edge****						
ORH1/5	154	1833	1982	1987	-83.6	3
ORH4/5	128	1859	1982	1987	-55.007	3.99
ORH8/5	138	1850	1983	1988	-84.47	4.31
ORH10/5	156	1836	1987	1992	-43.2	3
ORH15/5	118	1874	1987	1992	-64.548	3.13

†Estimated age is derived from annual increment counts on otolith thin sections.

*Core: Contained the first 4 yrs of life. Mean year of ^{14}C sample = (birth year + (birth year + 4 yrs))/2

** Region 3: The transition zone is estimated to be 30 - 34 years from the birthday. The mean year of ^{14}C sample was calculated by estimating a minimum sample year (birth year + 30 yrs) and a maximum sample year (birth year + 34 yrs) then averaging the two.

*** Region 4 was estimated to come from an area that was at maximum of 20 yrs from the otolith edge and at least 10 yrs from the edge. Mean year of ^{14}C sample = ((collection year – 20 yrs) + (collection year – 10 yrs))/2.

****Edge was estimated to be no more than the last 10 yrs of otolith growth. Mean year of ^{14}C sample = (collection year + (collection year – 10 yrs))/2

Table S3: Reservoir ages calculated from ocean perch (*Helicolenus percoides*) and orange roughy (*Hoplostethus atlanticus*) otolith-based ^{14}C data. Orange roughy data are estimated from Kalish (2002b; Table S2). The reservoir age error reflects the error of the atmospheric ^{14}C values determined from INTCAL13 (Reimer et al. 2013) over a given year plus the error associated with the otolith age. Otolith, atmospheric and revervoir ages are presented as radiocarbon years.

	Sample no.	Mean year of ^{14}C sample	Otolith ^{14}C Age (yr)	Atmospheric ^{14}C Age (yr)	Reservoir Age (yr)
Ocean perch	HBN-041	1947.5	690 ± 50	199 ± 8	491 ± 58
	HBN-089	1952.5	900 ± 70	199 ± 8	701 ± 78
	HBN-012	1954.5	840 ± 180	199 ± 8	641 ± 188
	HBN-035	1954.5	800 ± 60	199 ± 8	601 ± 68
	HBN-058	1954.5	660 ± 80	199 ± 8	461 ± 88
	HBN-094	1955.5	530 ± 35	199 ± 8	331 ± 43
	HBN-020	1957.5	535 ± 50	199 ± 8	336 ± 58
	HBN-063	1958.5	890 ± 130	199 ± 8	691 ± 138
Orange roughy	ORH10/1	1838	822 ± 26	122 ± 8	700 ± 34
	ORH8/1	1852	825 ± 45	114 ± 9	711 ± 54
	ORH1/3	1865	893 ± 25	123 ± 6	770 ± 31
	ORH10/3	1868	779 ± 27	114 ± 6	665 ± 33
	ORH7/1	1870	860 ± 55	114 ± 6	746 ± 61
	ORH15/1	1876	860 ± 30	119 ± 7	741 ± 37
	ORH8/3	1882	870 ± 40	104 ± 7	766 ± 47
	ORH4/3	1891	750 ± 55	98 ± 7	652 ± 62
	ORH7/3	1900	855 ± 30	71 ± 7	784 ± 37
	ORH15/3	1906	810 ± 30	83 ± 7	727 ± 37

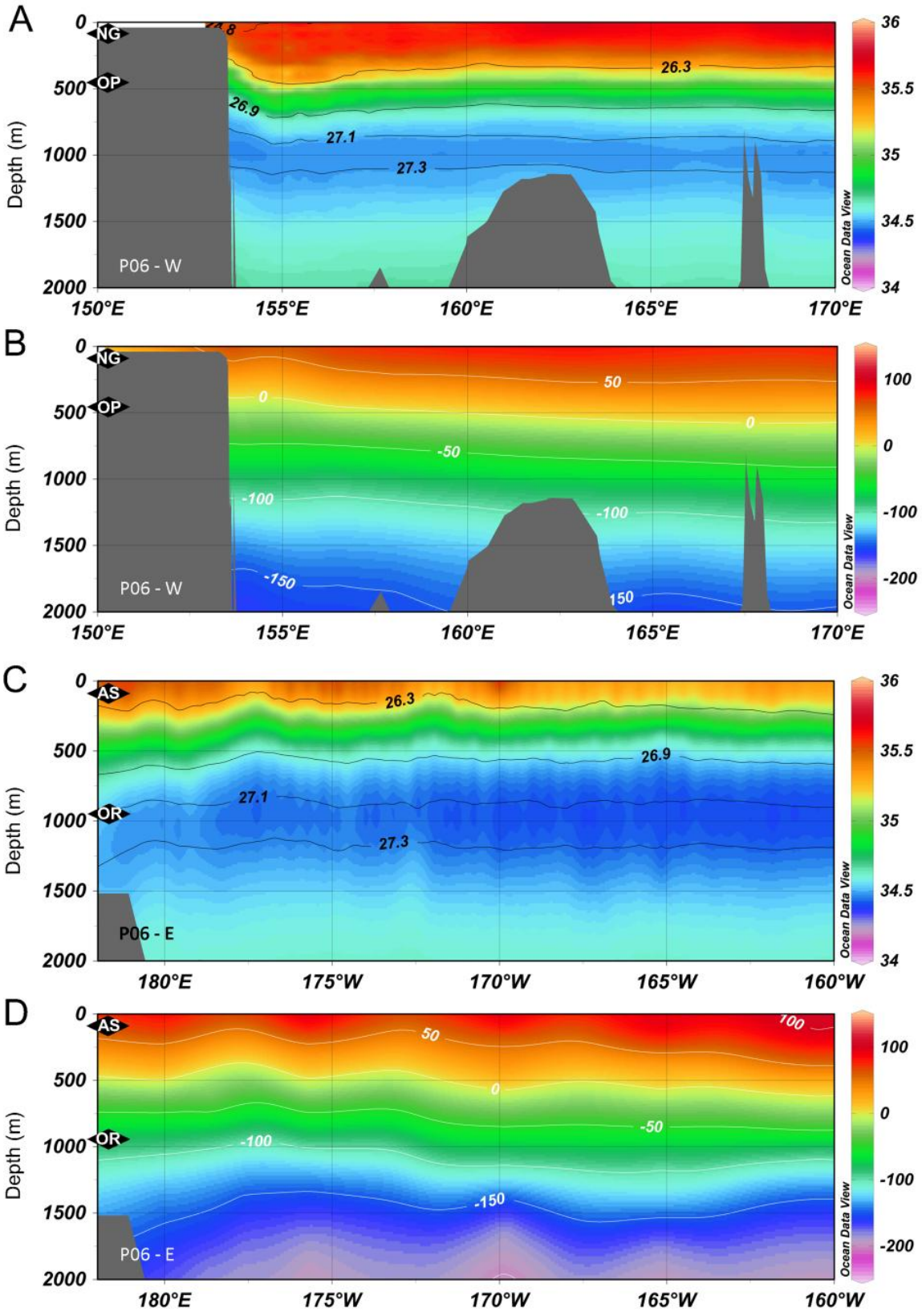

Fig. S1: Salinity (a, b) and $\Delta^{14}C$ (c, d) data from 1992 along P06-W and P06-E (E-W; Fig. 1b) from the eWOCE dataset (Schlitzer, 2000) plotted with Ocean Data View software (Schlitzer, 2015). Isopycnals bounding water masses of AAIW (σ_θ = 26.9 - 27.3) and the lower boundary of LTW (σ_θ = 26.3) in the southwest Pacific are overlaid (a, b). Contours of 50 ‰ are delineated in $\Delta^{14}C$ water values (c, d). Black diamonds signify the different otolith radiocarbon records that correspond to each section and depth for general comparison: NG - Nannygai, OP - Ocean perch, AS - Australasian snapper, OR - Orange roughy.

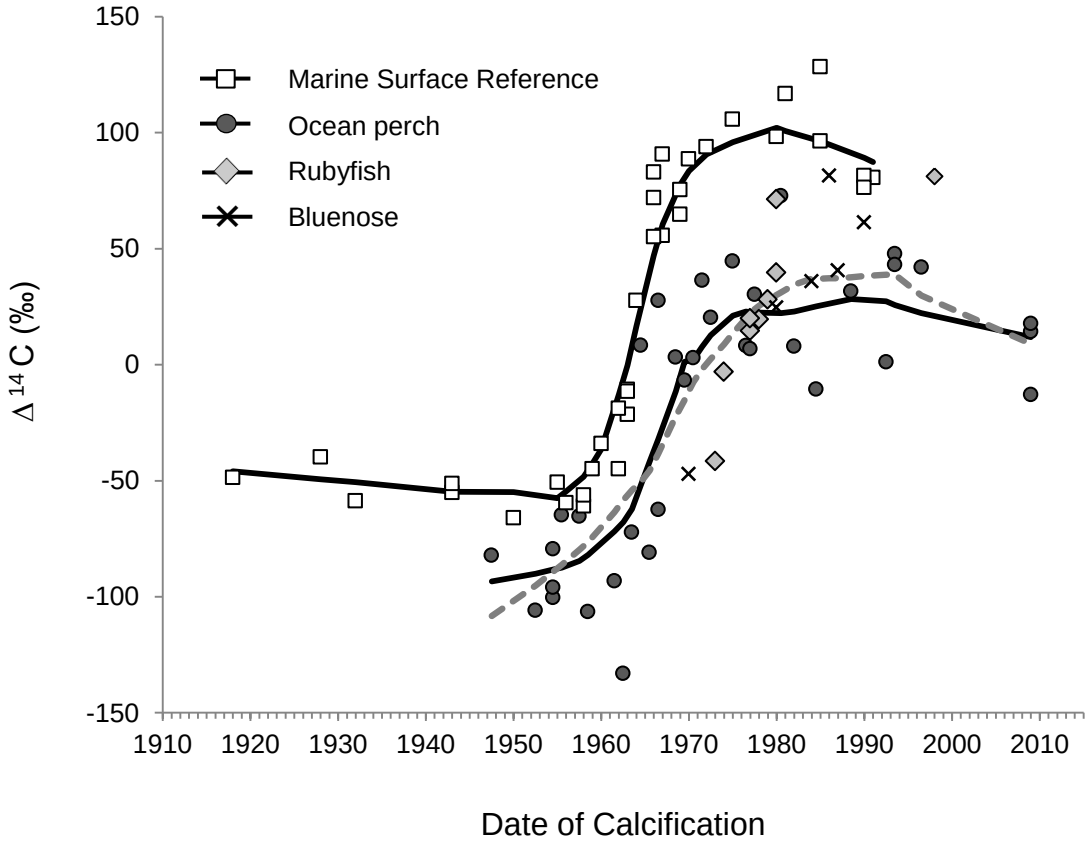

Fig. S2: Previously published Δ^{14}C values from rubyfish (*Plagiogeneion rubiginosum*; northeast New Zealand; Horn et al., 2012) and bluenose (*Hyperoglyphe antarctica*; northeast New Zealand Horn et al., 2010) otolith carbonate plotted with ocean perch otolith Δ^{14}C values (cores and edges) and a marine surface reference curve pooled from the otolith cores of Australasian snapper (Kalish, 1993) and nannygai (Kalish, 1995). Δ^{14}C values from rubyfish were derived from otolith carbonate representing a mid-point age of ≥ 40 years. Values with mid-point ages < 40 years were excluded to ensure only Δ^{14}C values from adults that had migrated to depth were characterised (see Horn et al., 2012 for further details). Bluenose Δ^{14}C values (otolith edges) are also representative of adult fish living at depths below the mixed layer (see Horn et al., 2010). The marine surface reference and ocean perch datasets are fitted with locally weighted least-squares regression curves (*loess* curve; bold solid lines). To further develop the otolith carbonate Δ^{14}C mid-water record, a loess curve was fitted collectively to the rubyfish, bluenose and ocean perch datasets (dashed grey line).

References:

Horn, P.L., Neil, H.L., Paul, L.J., Marriott, P., 2010. Age validation and growth of bluenose *Hyperoglyphe antarctica* using the bomb chronometer method of radiocarbon ageing. J. Fish Biol. 77, 1552-1563. http://dx.doi.org/10.1111/j.1095-8649.2010.02787.x

Horn, P.L., Neil, H.L., Paul, L.J., McMillan, P.J., 2012. Age verification, growth and life history of rubyfish *Plagiogeneion rubiginosum*. N. Z. J. Mar. Freshwat. Res. 46, 353-368. http://dx.doi.org/10.1080/00288330.2012.676052

Kalish, J.M., 1993. Pre- and post-bomb radiocarbon in fish otoliths. Earth Planet. Sci. Lett. 114, 549-554. http://dx.doi.org/10.1016/0012-821X(93)90082-K

Kalish, J.M., 1995. Application of the bomb radiocarbon chronometer to the validation of redfish *Centroberyx affinis* age. Can. J. Fish. Aquat. Sci. 52, 1399-1405. http://dx.doi.org/10.1139/f95-135

Kalish, J.M., 2002b. Validation of orange roughy (*Hoplostethus atlanticus*) age by high precision radiocarbon dating, in: Kalish, J.M. (Ed.), Use of the Bomb Radiocarbon Chronometer to Validate Fish Age. Final Report FRDC Project 93/109. Fisheries Research and Development Corporation and Australian National University, Canberra, pp. 238-259.

Reimer, P. J., E. Bard, A. Bayliss, J. W. Beck, P. G. Blackwell, C. Bronk Ramsey, C. E. Buck, H. Cheng, R. L. Edwards, M. Friedrich, P. M. Grootes, T. P. Guilderson, H. Haflidason, I. Hajdas, C. Hatté, T. J. Heaton, D. L. Hoffmann, A. G. Hogg, K. A. Hughen, K. F. Kaiser, B. Kromer, S. W. Manning, M. Niu, R. W. Reimer, D. A. Richards, E. M. Scott, J. R. Southon, R. A. Staff, C. S. M. Turney, and J. van der Plicht. 2013. IntCal13 and Marine13 Radiocarbon Age Calibration Curves 0–50,000 Years cal BP. Radiocarbon 55, 1869-1887. http://dx.doi.org/10.2458/azu_js_rc.55.16947

Schlitzer, R., 2015. Ocean Data View, odv.awi.de.

Schlitzer, R., 2000. Electronic atlas of WOCE hydrographic and tracer data now available. Eos, Trans. Amer. Geophys. Union. 81, 45-45. http://dx.doi.org/10.1029/00EO00028

CHAPTER 3

A record of contemporary radiocarbon decline derived from otolith carbonate in an upwelling area of the southeastern Indian Ocean

An archive of ocean perch otoliths from the 1970s to 2000s waiting to be sorted and catalogued. Cronulla Fisheries Research Centre, Port Hacking, New South Wales, AUS.

Statement of Authorship

Title of Paper	A record of contemporary radiocarbon decline derived from otolith carbonate in an upwelling area of the southeastern Indian Ocean
Publication Status	☐ Published ☐ Accepted for Publication ☐ Submitted for Publication ☑ Publication Style
Publication Details	This is a co-authored paper and is intended to be published in a scientific journal. Stewart Fallon, Christopher Izzo, Peter Hawthorne, Rachel Wood and Bronwyn Gillanders are co-authors, and therefore, it is written in plural.

Principal Author

Name of Principal Author (Candidate)	Gretchen L. Grammer		
Contribution to the Paper	Collected specimens, extracted otolith carbonate samples, graphitised samples for AMS analyses, performed data analyses, supplied some funding and wrote the manuscript.		
Overall percentage (%)	90		
Signature		Date	17 June 2015

Co-Author Contributions

By signing the Statement of Authorship, each author certifies that:

i. the candidate's stated contribution to the publication is accurate (as detailed above);

ii. permission is granted for the candidate in include the publication in the thesis; and

iii. the sum of all co-author contributions is equal to 100% less the candidate's stated contribution.

Name of Co-Author	Stewart Fallon		
Contribution to the Paper	Assisted with intellectual development, performed AMS analyses, and will provide suggestions, comments and feedback on manuscript drafts prior to submission to a scientific journal		
Signature		Date	17 June 2015

Name of Co-Author	Christopher Izzo		
Contribution to the Paper	Assisted with intellectual development, and provided suggestions, comments and feedback on manuscript drafts		
Signature		Date	17 June 2015

Name of Co-Author	Peter Hawthorne		
Contribution to the Paper	Collected specimens, provided suggestions during manuscript development, and will provide suggestions, comments and feedback on manuscript drafts prior to submission to a scientific journal		
Signature		Date	17 June 2015

Name of Co-Author	Rachel Wood		
Contribution to the Paper	Assisted with AMS analyses, and will provide suggestions, comments and feedback on manuscript drafts prior to submission to a scientific journal		
Signature		Date	17 June 2015

Name of Co-Author	Bronwyn Gillanders		
Contribution to the Paper	Assisted with intellectual development, supplied funding, and provided suggestions, comments and feedback on manuscript drafts		
Signature		Date	17 June 2015

A record of contemporary radiocarbon decline derived from otolith carbonate in an upwelling area of the southeastern Indian Ocean

G. L. Grammer[1], S. J. Fallon[2], P. Hawthorne[3], C. Izzo[1], R. Wood[2], B. M. Gillanders[1]

[1]Southern Seas Ecology Laboratories, School of Biological Sciences, The University of Adelaide, SA 5005, Australia

[2]Radiocarbon Facility, Research School of Earth Sciences, The Australian National University, Canberra, ACT 0200, Australia

[3]South Australian Research and Development Institute (Aquatic Sciences), West Beach, SA 5024, Australia

Correspondence: Gretchen L. Grammer, Southern Seas Ecology Laboratories, School of Biological Sciences, The University of Adelaide, SA 5005, Australia

Tel.: +61 8 8313 1483; Fax: +61 8 8313 4364

Email: gretchen.grammer@adelaide.edu.au

Abstract:

Biogenic carbonates are successfully used to track radiocarbon ($\Delta^{14}C$) evolution through time, and we use otoliths (earstones) of fish to establish a new record of the bomb $\Delta^{14}C$ decline (since ~1980 to the present) in an upwelling area of the southeastern Indian Ocean. Marine surface waters were enriched with ^{14}C during the 1950-60s when thermonuclear weapons testing was at its zenith (bomb $\Delta^{14}C$). Upwelling events ventilate ocean surface waters with subsurface water lower in radiocarbon $\Delta^{14}C$ through a wind-driven, oceanographic process. We assayed otolith carbonate microsampled from ocean perch (*Helicolenus percoides*) for ^{14}C with accelerator mass spectrometry. The ocean perch otolith $\Delta^{14}C$ record extended from 1994 to 2012 and displayed a general decline of $\Delta^{14}C$ levels through time (mean $\Delta^{14}C$ 1994: 75.04‰; mean 2012: 7.57‰). Water depths represented by the otolith records ranged from 42.9 to 118.9 m, and age-based depth segregation between juvenile (< 6 yrs old) and adult fish was not evident. Ocean perch $\Delta^{14}C$ values were lower (62.69 to 82.53‰) than reported seawater values (90.1 to 95.5‰) in depths < 200 m in adjacent non-upwelling areas. Comparisons of ocean perch $\Delta^{14}C$ with published Indo-Pacific coral records showed the ocean perch $\Delta^{14}C$ record was lower than $\Delta^{14}C$ values in coral of tropical surface water, but had higher levels than coral in areas of equatorial upwelling. The ocean perch $\Delta^{14}C$ record characterises temperate marine waters well mixed throughout the year by both upwelling and downwelling and with sources of upwelled waters being formed at higher latitudes. Documenting levels of $\Delta^{14}C$ in the marine environment along the coast of southern Australia has improved existing ^{14}C data relating to ocean circulation in the southeastern Indian Ocean.

Introduction

Radiocarbon ($\Delta^{14}C$) levels within the ocean are powerful tracers of water mass circulation through time. Radiocarbon produced in the atmosphere enters the ocean as ^{14}C-enriched CO_2 by mixing across the ocean-atmosphere interface (e.g. Broecker and Peng 1982). Atmospheric ^{14}C production rates and deep water inputs (waters depleted in ^{14}C due to radioactive decay) both influence $\Delta^{14}C$ levels in surface waters and shallow water masses through air-sea exchange and physical mixing (Broecker and Peng 1982). Until 1950, natural sources of ^{14}C in the ocean originated from cosmic-ray interactions in the upper atmosphere (Bard et al. 1997). This was augmented by anthropogenic inputs of ^{14}C generated from atmospheric testing of thermonuclear weapons in the 1950s and 1960s. The resultant radiocarbon 'bomb-pulse' (peaking in 1964/65) caused an increase of atmospheric $\Delta^{14}C$ levels to nearly twenty-five times the natural levels of 1950 (e.g. Hua et al. 2013). As such, these higher $\Delta^{14}C$ levels were also incorporated into the surface ocean, causing a distinctive spike in the radiocarbon surface water signal.

Surface waters are ventilated with subsurface water deficient in $\Delta^{14}C$ during upwelling events, which is a wind-driven, oceanographic process that brings cold, nutrient-rich, bottom water to the ocean's surface (Bigg 2003). In the early 1970s, this phenomenon was first recognised in equatorial waters where upwelled waters caused the $\Delta^{14}C$ levels to be lower by a factor of five compared to adjacent mid-latitude waters (Broecker et al. 1978). Time series of $\Delta^{14}C$ values measured from coral carbonate across the tropics and subtropics further verified upwelling of deeper waters in these areas (Toggweiler et al. 1991, Guilderson and Schrag 1998, Druffel 2002) and also the distribution of radiocarbon by convection through the oceans (Mahadevan 2001).

Coastal upwelling occurs along continental margins where winds blowing parallel to the coastline and associated Ekman transport causes water to be moved offshore (Bigg 2003). Along the southern Australian shelf-slope, a unique northern boundary current system, influenced by the Flinders Current, flows westward and helps to induce upwelling (Middleton and Cirano 2002, Kämpf et al. 2004, Middleton and Bye 2007). Multiple upwelling events develop along the southern Australian shelf in the austral summer, with each event lasting three to ten days in duration, interspersed by episodes of weak

downwelling and surface water mixing (Kämpf et al. 2004, Middleton and Bye 2007). The largest and most predictable upwelling area of this northern boundary current system is the Bonney upwelling (Fig 1a-b) (Middleton et al. 2007, Middleton and Bye 2007).

Biogenic carbonates from coral, molluscs, echinoderms, foraminifera and fish have been successfully used to track $\Delta^{14}C$ evolution through time (Berkman and Forman 1996, Druffel 2002, Chapter 2: Grammer et al. 2015). Here, we focus on otoliths (earstones) of fish to establish a new record of the bomb ^{14}C decline, for a period after the $\Delta^{14}C$ peak to the present, in an upwelling area of the southeastern Indian Ocean. Fish accrete calcium carbonate onto otoliths, which are typically aragonite-based and used to maintain balance and facilitate hearing (Secor et al. 1995, Campana 1999). Similar to other biogenic carbonates, the chemical composition of the fish's environment is permanently retained within the otolith, as these structures are acellular and metabolically inert (Campana and Neilson 1985, Campana and Thorrold 2001). To generate a $\Delta^{14}C$ record for a region, an annually resolved archive yielding known-age increments is required (Scourse et al. 2012). Propitiously, the microstructural formation of growth-increments in otoliths allows the individual fish's age to be resolved (Campana and Thorrold 2001). Therefore, $\Delta^{14}C$ levels measured in otoliths can be assigned specific calcification years similar to techniques used with coral time series. Only one other study has specifically used otolith $\Delta^{14}C$ levels to examine the signature of an upwelled water mass, and this was in the California Current along the western coast of North America (Haltuch et al. 2013). In the Southern Hemisphere, $\Delta^{14}C$ levels in upwelled water have never before been quantified using otolith carbonate.

Migratory behaviour (vertical or latitudinal) of the candidate species or ingesting prey from a different depth/water mass can have confounding effects on the amount of $\Delta^{14}C$ measured in biogenic carbonates. Dietary sources contribute ~25% of carbon to fish otoliths, while the remaining 75% originates from dissolved inorganic carbon in seawater (Kalish 1991, Solomon et al. 2006). Consequently, it is key to know life history characteristics of a candidate species. We chose reef ocean perch (*Helicolenus percoides*, Sebastidae) as our candidate species for ^{14}C analyses in an upwelling region. This species is found along the continental shelf of southern Australia and New Zealand and is both non-

migratory and benthic. They may attain ages of ~40 years and grow to lengths of > 400 mm (Withell and Wankowski 1988, Paul and Horn 2009). Ocean perch are live bearing (lecithotrophic; Pavlov and Emel'yanova 2013) and reach maturity at 5 to 6 years (Park 1993). All life stages are demersal (Park 1993, Furlani 1997) with both juveniles and adults preying on benthic crustaceans and fish (Bulman et al. 2001, Horn et al. 2012). The carcasses of salps (food-falls) are also important dietary items for all ages of ocean perch (Henschke et al. 2013).

The broad aim of this project is to investigate the use of $\Delta^{14}C$ values as an indicator of upwelling in the southeastern Indian Ocean. The specific objectives are to: 1) produce a $\Delta^{14}C$ decline record for an upwelling area in the southeastern Indian Ocean from otolith carbonate; 2) examine the range of $\Delta^{14}C$ values found in the otolith carbonate record by depth and through time; 3) compare otolith ^{14}C values to seawater $\Delta^{14}C$ values measured in non-upwelling areas of the region; and 4) compare this record with coral $\Delta^{14}C$ records from the eastern Indian Ocean and Pacific Ocean.

Methods

Oceanographic setting

The southeastern corner of the Indian Ocean is influenced by two major current systems: the Flinders Current system flowing westward and the Leeuwin Current system flowing eastward (e.g. Middleton and Bye 2007, James and Bone 2011) (Fig. 1a). It is bounded by the continental landmass of Australia to the north and the Antarctic Circumpolar Current to the south. The Flinders Current results from wind curl stress and the equatorward Sverdrup transport of water in the Southern Ocean (Bye 1972, Middleton and Cirano 2002, Middleton and Bye 2007). It flows along the Australian continental shelf-slope and is similar to larger western boundary currents. This current flows west at depths of 400 to 800 m and transports Tasmanian Subantarctic Mode Water (TSAMW) and Tasmanian Intermediate Water (TIW) to the northwest (Barker 2004, Middleton and Bye 2007). TSAMW is formed in surface waters off the southwest coast of Tasmania (47°S) and is subducted to 500 m, and TIW is formed at depths of ~1000 m in the same region (Barker 2004). The Flinders Current also transports remnants of the East Australian Current from the Pacific Ocean via the

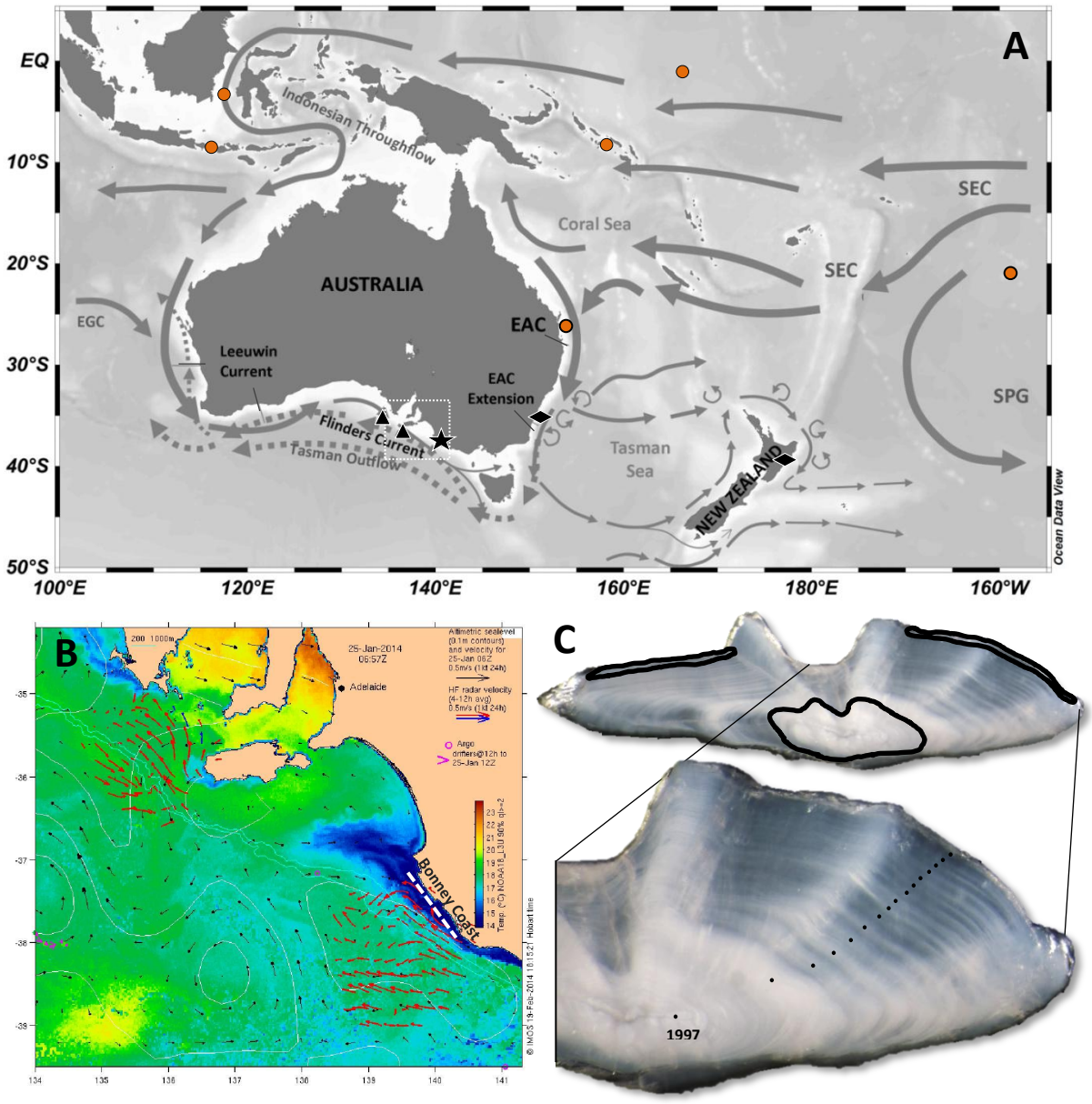

Fig. 1. A) Schematic of ocean currents in the southwest Pacific and southeast Indian Ocean, and ^{14}C records used in this study (orange circles: coral; black star: ocean perch otoliths; black triangles: water records; black diamonds: Australasian snapper and nannygai otoliths). SPG - South Pacific Gyre, SEC - South Equatorial Current, EAC - East Australian Current, EGC - East Gyral Current. Location and reference details of the ^{14}C records are given in Table 2. B) The Bonney upwelling off the coast of South Australia during an upwelling event in January 2014 where ocean perch were collected (dashed white line). Sea surface temperatures range from 14°C (dark blue) to 23°C (red). C) Thin section of an otolith from a 16 year old ocean perch collected in 2012 (birth year: 1997). Annual growth increments were counted from the core to the proximal edge (black dots). The carbonate extraction regions (core and edge) for ^{14}C analysis are also shown (outlined in black). [SST image credit: Data was sourced from the Integrated Marine Observing System (IMOS) - IMOS is a national collaborative research infrastructure, supported by Australian Government; Data sources for currents in A: Bostock et al., 2013; Ganachaud et al., 2014; Qu et al., 2009; Ridgway and Dunn, 2003; Sokolov and Rintoul, 2000]

Tasman Outflow (Middleton and Bye 2007). The Leeuwin Current system (depths < 200 m) has its origins in the tropical east Indian Ocean and advects water from both the Indonesian Flowthrough and East Gyral Current into the Great Australian Bight (GAB; Feng et al. 2003, James and Bone 2011). The main Leeuwin Current becomes weaker as it flows westward, joining with the South Australian current in the central GAB and the Zeehan Current off western Tasmania (James and Bone 2011).

Both the Flinders and Leeuwin Current systems are wind-dominated and this results in seasonal strengthening or weakening of either current system. The main Flinders Current has its strongest westward flow in the austral summer, which helps to produce the seasonal coastal upwelling along the Bonney Coast (Fig. 1b). A reversal in current strength is seen in the winter months where the main Leeuwin Current becomes dominant and flows strongly eastward producing downwelling (Middleton and Bye 2007, James and Bone 2011).

Sample collection and visual age determination

Sagittal otoliths from ocean perch assayed for ^{14}C with accelerator mass spectrometry (AMS) were collected during fishery-dependent surveys off the coast of South Australia in the Bonney upwelling region from 2011 to 2013 (Fig. 1b, Table 1). Otoliths were stored dry in paper envelopes prior to analyses and archived at the University of Adelaide (under care of BMG). Water depths where the fish were collected ranged from ~40 to 120 m.

Otoliths were embedded in epoxy resin and thin-sectioned transversely through the primordium to visually determine the fish's age. Sections were mounted on a glass slide and annual growth increments (pairs of opaque and hyaline zones) were counted with a compound microscope (Leica DM LB) under reflected light at × 87.5 magnification (Fig. 1c). Annual growth increments have been previously validated in ocean perch (Paul and Horn 2009), which allows a specific year to be assigned to each growth increment (based on date of capture and estimated birthdate). Annual growth increment boundaries were defined by the proximal edges of the opaque zones, and the age of each fish was adjusted with the estimated birthdate of October 1 (Park 1993, Furlani 1997, Paul and Horn 2009). Growth

Table 1. Data describing ocean perch (*Helicolenus percoides*) samples collected off the coast of South Australia. Fish ages are based on visual age determination using annual otolith growth increments. All samples extracted from the otolith edge are designated with an 'E' on the end of the sample number. Year of ^{14}C sample is back calculated from the capture date based on the annually resolved otolith growth increment count: core = birth year; edge = amalgamation of last full year of growth plus marginal increment. Other samples were taken from the core region (first year of growth). Radiocarbon data are presented as fraction modern (Fm) and $\Delta^{14}C$ (‰). Carbon mass (µg): amount of carbon graphitised from the otolith carbonate sample for radiocarbon dating. Carbonate mass (mg): amount of otolith carbonate milled for analysis.

Sample no.	SANU no.	Location	Water depth (m)	Length (TL mm)	Otolith mass (g)	Collection year	C mass (µg)	Carbon-ate mass (mg)	Year of ^{14}C sample	Fish age (yrs)	Fm	$\Delta^{14}C$ (‰)	± SD $\Delta^{14}C$
HPS-070	36720	37°39'S 140°02'E	58.5	283	0.10807	2011	46	0.95	1994	18	1.0825	82.53	4.3
HPS-027	36716	37°39'S 140°01'E	54.9	291	0.11202	2011	42	0.70	1994	18	1.0799	79.91	4.6
HPS-053	36916	37°44'S 139°54'E	91.4	313	0.12057	2011	55	1.05	1994	18	1.0627	62.69	3.7
HPS-110	36827	37°46'S 139°55'E	117.0	291	0.10208	2012	40	0.66	1995	18	1.0753	75.35	6.6
HPS-097	36918	37°38'S 139°57'E	65.0	344	0.12461	2012	40	0.99	1995	18	1.0663	66.31	5.3
HPS-163	36917	37°45'S 139°54'E	96.9	322	0.12789	2012	58	1.15	1995	18	1.0648	64.84	5.1
HPS-184	36733	37°50'S 140°06'E	69.5	285	0.09644	2012	19	0.40	1997	16	1.0846	84.58	6.8
HPS-055	36829	37°44'S 139°54'E	91.4	264	0.09964	2011	68	0.69	1997	15	1.0739	73.93	4.8
HPS-141	36729	37°48'S 140°04'E	86.0	288	0.09802	2012	33	0.45	1997	16	1.0701	70.11	7.0
HPS-063	36717	37°39'S 140°02'E	58.5	272	0.09345	2011	23	0.62	1997	15	1.0695	69.48	6.7
HPS-004	36714	37°38'S 139°58'E	44.0	298	0.09571	2011	39	0.67	1997	15	1.0669	66.92	5.2
HPS-022	36819	37°39'S 140°00'E	60.4	296	0.11677	2011	26	0.20	1997	15	1.0473	47.26	5.3
HPS-140	36924	37°48'S 140°04'E	86.0	277	0.10097	2012	19	0.20	1997	16	1.0372	37.19	6.0
HPS-088	36723	37°42'S 139°53'E	82.3	283	0.08198	2012	25	0.52	2002	10	1.0501	50.11	7.0
HPS-172	36732	38°10'S 140°31'E	50.5	203	0.05702	2013	22	0.56	2003	10	1.0679	67.92	8.0
HPS-166	36731	37°41'S 139°55'E	42.9	265	0.08562	2012	49	0.82	2003	10	1.0605	60.50	4.8
HPS-101	36724	37°43'S 139°53'E	89.6	207	0.04899	2012	32	0.60	2005	8	1.0501	50.15	5.8
HPS-085	36721	37°44'S 139°50'E	118.9	196	0.04389	2011	19	0.40	2006	6	1.0544	54.37	8.5
HPS-161	36730	37°41'S 139°46'E	89.6	190	0.04361	2012	30	0.66	2006	7	1.0471	47.10	5.6
HPS-120	36725	37°39'S 139°45'E	86.0	210	0.04912	2012	43	0.52	2006	7	1.0469	46.87	5.2
HPS-066	36718	37°39'S 140°02'E	58.5	193*	0.04308	2011	42	0.64	2006	6	1.0459	45.87	5.8
HPS-125	36727	38 45'S 140°01'E	87.8	218	0.05814	2013	29	0.45	2006	7	1.0338	33.81	6.8
HPS-062	36820	37°39'S 140°02'E	58.5	160	0.02747	2011	20	0.24	2006	6	1.0267	26.74	5.8

* The total length of this fish was estimated from its standard length measurement of 154 mm.

Table 1. *Continued:* Data describing ocean perch (*Helicolenus percoides*) samples collected off the coast of South Australia.

Sample no.	SANU no.	Location	Water depth (m)	Length (TL mm)	Otolith mass (g)	Collection year	C mass (µg)	Carbon-ate mass (mg)	Year of ^{14}C sample	Fish age (yrs)	Fm	$\Delta^{14}C$ (‰)	± SD $\Delta^{14}C$
HPS-123	36726	37°43'S 139°53'E	87.8	201	0.04002	2013	26	0.37	2008	5	1.0490	48.96	5.8
HPS-197	36735	37°39'S 139°44'E	86.0	178	0.03623	2012	22	0.30	2008	5	1.0457	45.68	7.8
HPS-067	36719	37°39'S 140°02'E	58.5	162	0.03267	2011	22	0.32	2009	3	1.0527	52.71	6.4
HPS-121	36816	37°35'S 139°44'E	75.0	179	0.03744	2012	30	0.50	2009	4	1.0293	29.29	6.5
HPS-062E	36926	37°39'S 140°02'E	58.5	160	0.02747	2011	16	0.25	2010	6	1.0049	4.86	8.6
HPS-088E	36823	37°42'S 139°53'E	82.3	283	0.08198	2012	9	0.22	2011	10	1.0141	14.09	12.1
HPS-055E	36824	37°44'S 139°54'E	91.4	264	0.09964	2011	13	0.20	2011	15	1.0075	7.51	7.1
HPS-053E	36927	37°44'S 139°54'E	91.4	313	0.12057	2011	16	0.27	2011	18	1.0051	5.08	6.1
HPS-067E	36821	37°39'S 140°02'E	58.5	162	0.03267	2011	13	0.21	2011	3	1.0044	4.44	9.7
HPS-027E	36925	37°39'S 140°01'E	54.9	291	0.11202	2011	14	0.24	2011	18	1.0007	0.75	9.8
HPS-161E	36825	37°41'S 139°46'E	89.6	190	0.04361	2012	17	0.26	2012	7	1.0301	30.13	7.9
HPS-120E	36826	37°39'S 139°45'E	86.0	210	0.04912	2012	16	0.26	2012	7	1.0082	8.16	8.8
HPS-125E	36811	39 45'S 140°01'E	87.8	218	0.05814	2013	16	0.21	2012	7	1.0045	4.49	7.8
HPS-101E	36817	37°43'S 139°53'E	89.6	207	0.04899	2012	12	0.47	2012	8	0.9875	-12.51	8.2

increments were counted and measured from the core to the proximal margin using Image-Pro Plus v. 7.0 (MediaCybernetics).

Radiocarbon (^{14}C) analysis

Otolith carbonate for ^{14}C analysis was milled from the otolith material left after thin sections were removed for visual age determination. A computer-controlled micromilling machine (ESI New Wave Research, USA) fitted with a 300 µm carbide cutter (Brasseler, USA) was used to extract the otolith carbonate from core and edge regions. The extracted core carbonate contained the first year of growth while the edge carbonate included the last year of growth plus the marginal increment (Fig. 1c). After milling, the carbonate powder was stored in clean, glassine envelopes prior to radiocarbon analysis. Years were assigned to the milled carbonate based on annually resolved growth increments resulting from visual age determination (Table 1). A mean year was calculated when the milled carbonate included multiple growth years (as with the edges). Extracted carbonate masses ranged from 0.20 to 1.15 mg, and equated to ~30 µg of graphitised carbon (Table 1).

For ^{14}C analysis, carbonate powder samples were completely acidified with phosphoric acid (0.5 ml, 85%, 80°C) in evacuated Vacutainer® tubes. The evolved CO_2 was cryogenically purified before reaction with H_2 over an iron catalyst (Key, 1996) at 500° C for a maximum of 30 mins for conversion to graphite. Graphite samples were pressed into targets and analysed for ^{14}C using a Single Stage Accelerator Mass Spectrometer at the Australian National University (Fallon et al. 2010). Multiple known value standards of marble, NBS Oxalic Acid-I, NBS Oxalic Acid-II, and in-house oyster carbonate standard (102 pMC) of similar sample weights to the small otolith carbonate samples (Table 1) were graphitized and measured at the same time as the otolith carbonate to confirm the resultant ^{14}C values (Chapter 2; Grammer et al. 2015). Radiocarbon values are reported as $\Delta^{14}C$ following the conventions of Stuiver and Polach (1977) where $\Delta^{14}C$ is the per mil (‰) deviation of $^{14}C/^{12}C$ of the sample relative to a 95% NBS Oxalic Acid-I standard and corrected for year of formation (Table 1).

Contemporary Indo-Pacific ^{14}C carbonate and seawater records

We compared the ocean perch otolith $\Delta^{14}C$ record from South Australia with previously published otolith and hermatypic coral $\Delta^{14}C$ records from the Indo-Pacific to place the new record in a regional context. Since $\Delta^{14}C$ carbonate time series are not available for the southeastern Indian Ocean, coral records from both the northeastern Indian Ocean and western Pacific Ocean were used for comparison as well as two southwestern Pacific otolith records (Table 2, Fig. 1). We also included a $\Delta^{14}C$ coral record from the Galápagos Islands as a representation of an upwelling dominated area. The two southwest Pacific otolith records (*Chrysophrys auratus* and *Centroberyx affinis*) were combined and treated as one ^{14}C reference series for the region (for more details see Grammer et al. 2015; Chapter 2). Two seawater $\Delta^{14}C$ depth profiles from the GAB measured in 1994 (Table 2; Ribbe et al. 1996) were used as local references for our otolith record in corresponding years. The seawater samples were taken in proximity to, but outside of, the Bonney upwelling area (Fig. 1b). These are the only $\Delta^{14}C$ water values available for the region. All carbonate records were fitted with locally weighted least-squares regression (loess) curves to assist general comparisons (Chapter 2; Grammer et al. 2015).

Results:

The ocean perch otolith $\Delta^{14}C$ record extended from 1994 to 2012 and displayed a general decline of $\Delta^{14}C$ levels through time (mean $\Delta^{14}C$ 1994: 75.04‰; mean 2012: 7.57‰) (Table 1; Fig. 2). Otoliths from 27 fish, aged 3 to 18 years, were analysed by AMS to produce this record. Water depths represented by the otolith records ranged from 42.9 to 118.9 m. An age-based depth segregation between juvenile (< 6 yrs old) and adult fish was not evident (Fig. 3).

The ocean perch $\Delta^{14}C$ record, representing upwelled seawater in the southeastern Indian Ocean, was compared with eight previously published $\Delta^{14}C$ time series measured from Indo-Pacific corals (7 individual time series) and fish otoliths (1 combined time series) (Table 2; Fig. 2). There was only overlap between the coral/otolith and ocean perch records in the mid-1990s. The loess curve fitted to the ocean perch record was lower than all records it overlapped, and generally appeared to decline more steeply through its trajectory than the carbonate records representing marine surface waters in the Indo-

Table 2. Contemporary Indo-Pacific hermatypic coral, otolith, and sea water data showing collection location, depth of record and species information.

Source of ^{14}C record	Depth (m) of ^{14}C record	Collection Latitude	Collection Longitude	Location	Reference
Ocean perch (*Helicolenus percoides*)	40 - 120	37°35'S to 39°45'S	139°44'E to 140°31'S	southern Australia	Current study
Australasian snapper (*Chrysophrys auratus*)	< 200	39°S	179°E	eastern New Zealand	Kalish (1993)
Nannygai (*Centroberyx affinis*)	< 200	35°S	151°E	southeastern Australia	Kalish (1995)
Hermatypic coral (*Porites lutea*)	4	5°02'S	119°04'E	Makassar Strait, Indonesia	Fallon and Guilderson (2008)
Hermatypic coral (*Porites sp.*)	14	0.5°S	166°30'E	Nauru Island	Guilderson et al. (1998)
Hermatypic coral (*Porites sp.*)	5	8°15'S	115°30'E	Lombok Strait, Indonesia	Guilderson et al. (2009)
Hermatypic coral (*Porites lutea*)	18	21°S	160°W	Rarotonga, Cook Islands	Guilderson et al. (2000)
Hermatypic coral (*Porites australiensis*)	14	9°S	160°E	Guadalcanal, Solomon Islands	Guilderson et al. (2004)
Hermatypic coral (*Porites lobata*)	1	0.5°S	90°W	Galápagos Islands	Guilderson and Schrag (1998)
Hermatypic coral (*Porites australiensis*)	10	22°06'S	153°W	Abraham Reef, GBR, Australia	Druffel and Griffin (2004)
Sea Water (GAB A22)	200 - 1750	35.5°S	134°E	Great Australian Bight	Ribbe et al. (1996)
Sea Water (GAB A8)	Surface - 2750	38°S	136°E	Great Australian Bight	Ribbe et al. (1996)

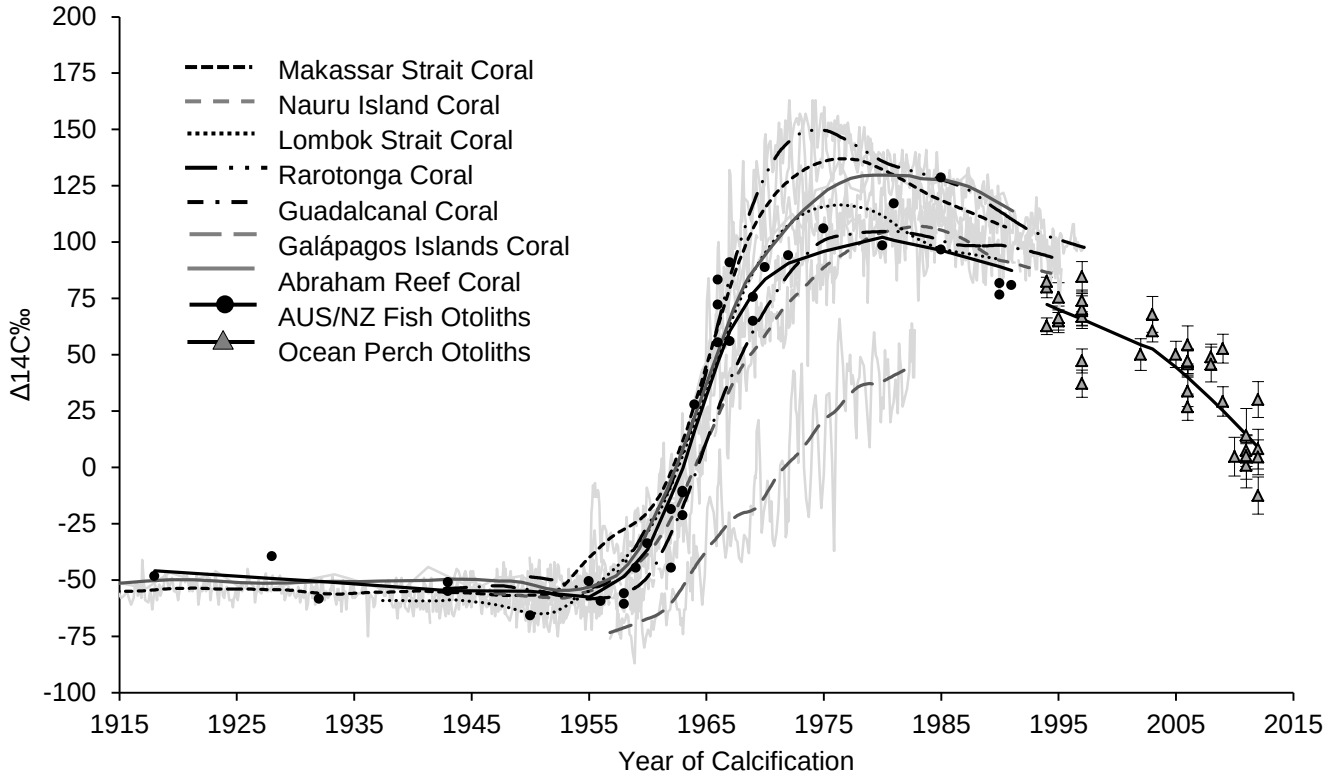

Fig. 2. Ocean perch otolith Δ ^{14}C record from an upwelling region of southern Australia plotted with previously published otolith and hermatypic coral Δ ^{14}C records from the Indo-Pacific. Coral records originate in the northeastern Indian Ocean and western Pacific Ocean, while the otolith records are from the southwest Pacific Ocean (see Table 2 for details). Also included is a Δ^{14}C coral record from the Galapagos Islands to represent strong upwelling. [References used in plot - Makassar Strait Coral: Fallon and Guilderson (2008); Nauru Island Coral: Guilderson et al. (1998); Lombok Strait Coral: Guilderson et al. (2009); Rarotonga Coral: Guilderson et al. (2000); Guadalcanal Coral: Guilderson et al. (2004); Galápagos Islands Coral: Guilderson and Schrag (1998); Abraham Reef Coral: Druffel and Griffin (2004); AUS/NZ Fish Otoliths: Kalish (1993), Kalish (1995)]

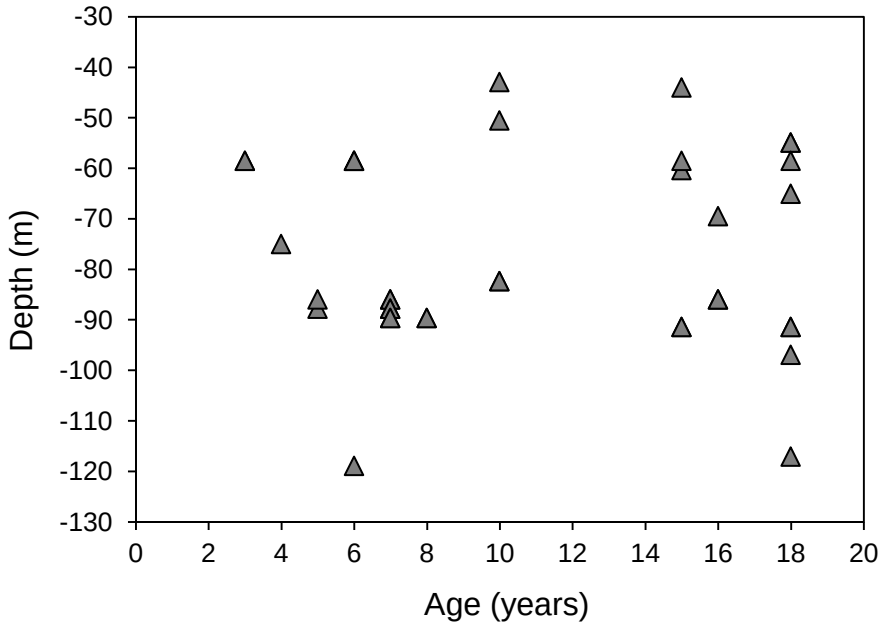

Fig. 3. Age (years) of ocean perch plotted by capture depth. Fish ages are the result of visual age determination using annual otolith growth increments.

Pacific (Fig. 2). The exception to this was the coral record from the Galápagos Islands. While this record did not overlap with the ocean perch record, its trajectory during the bomb ^{14}C increase (late 1950s to 1970s) was much lower and lagged in time than other Indo-Pacific coral and otolith records due to ^{14}C deficient upwelled water. The ocean perch record appears to fall between the Galápagos coral record and the rest of the coral and otolith records (Fig. 2). This suggests that the ocean perch record does indeed come from a source of seawater depleted in ^{14}C.

To further investigate the lower $\Delta^{14}C$ levels measured in the ocean perch otoliths, we compared ^{14}C values measured directly in seawater of a non-upwelling area of the eastern GAB in December 1994 with otolith ^{14}C values from 1994 to 1995 (Fig. 4). The ocean perch $\Delta^{14}C$ values were lower (62.69 to 82.53‰) than the reported seawater values (90.1 to 95.5‰) in depths < 200 m (Fig. 4).

Within the ocean perch record, $\Delta^{14}C$ levels were similar over the water depth range of samples in a given year (Fig. 5a) and decreased through time (Fig. 5a,b). The rate of decline through time did not differ between depths (Fig. 5b), and the mean rate of decline based on the loess curve for all samples was 3.5‰ year^{-1}.

Discussion:

The ocean perch otolith $\Delta^{14}C$ record is the first contemporary time series of $\Delta^{14}C$ documented in the southeastern Indian Ocean. Furthermore, there are very few marine carbonate records of the $\Delta^{14}C$ decline for years after 1997 and especially for the Southern Hemisphere. Two published $\Delta^{14}C$ coral records by Glynn et al. (2013) and Druffel-Rodriguez et al. (2012) are available for the Pacific Ocean just north of the equator. Glynn et al. (2013) presents a record for the Palau Archipelago (7°N, 134°E) spanning the years 1945 to 2008, and Druffel-Rodriguez et al. (2012) documents the $\Delta^{14}C$ signal at Palmyra Atoll (5°51'N, 162°06'W) from 1896 to 2005. Most contemporary $\Delta^{14}C$ carbonate records representing marine surface waters for the Southern Hemisphere end in 1997 and are from tropical areas (e.g. Druffel 2002). Carbonate records that continue to document $\Delta^{14}C$ in a range of environments are valuable for observing changes in El Niño-Southern Oscillation (ENSO),

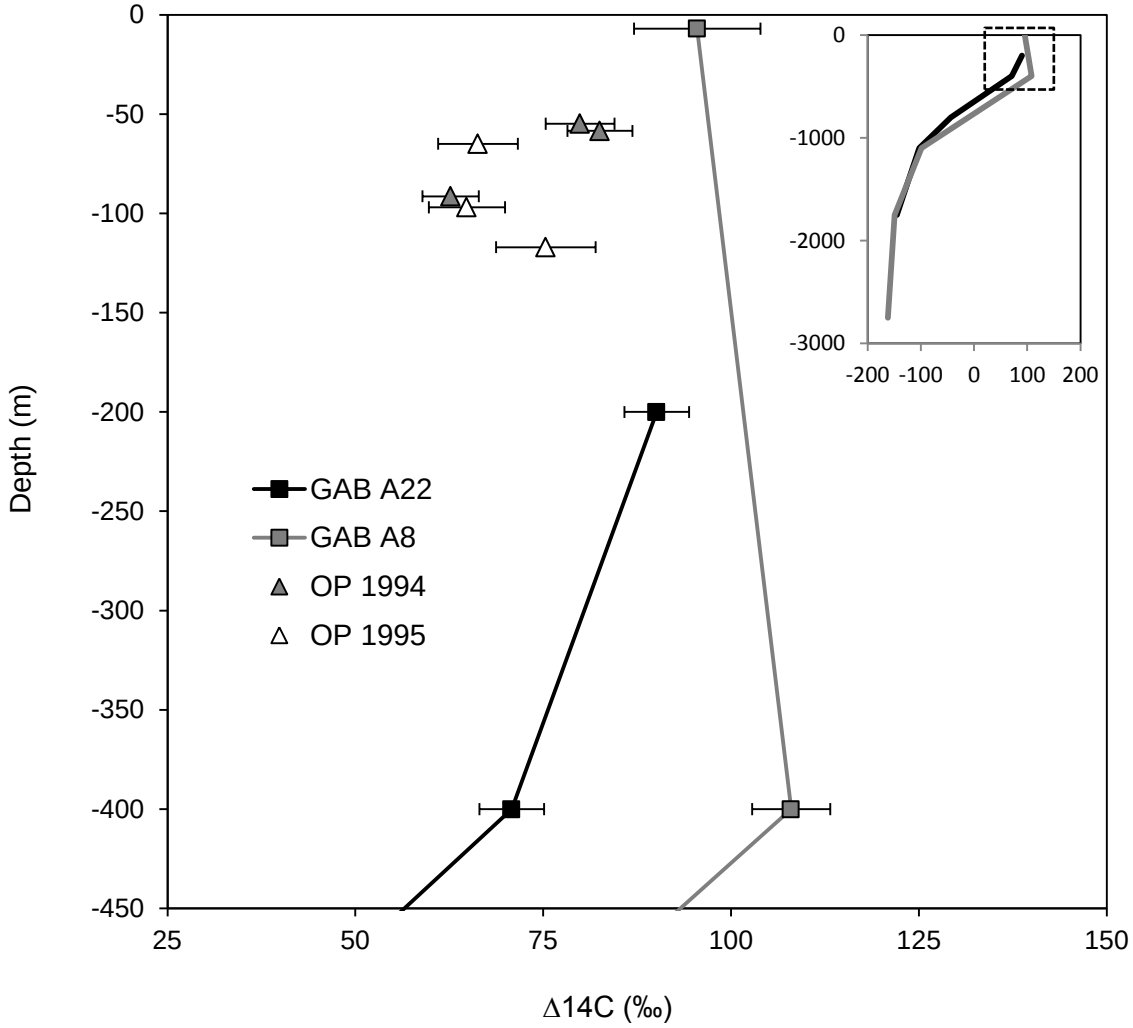

Fig. 4. $\Delta^{14}C$ values recorded in the water column of the Great Australian Bight (GAB) in 1994 plotted by depth to -450 m (GAB A22, GAB A8; Ribbe et al. 1996). Ocean perch otolith $\Delta^{14}C$ values from 1994 and 1995 are plotted by collection depth for comparison (OP 1994, OP 1995). Sample positions were: GAB A22: 35.5°S, 134°E; GAB A8: 38°S, 136°E; OP 1994 and 1995: 37.7°S, 140°E. Inset: Entire $\Delta^{14}C$ depth profile for GAB A22 (black) and GAB A8 (grey) from the ocean surface to -2750 m (dashed box indicates area of main plot).

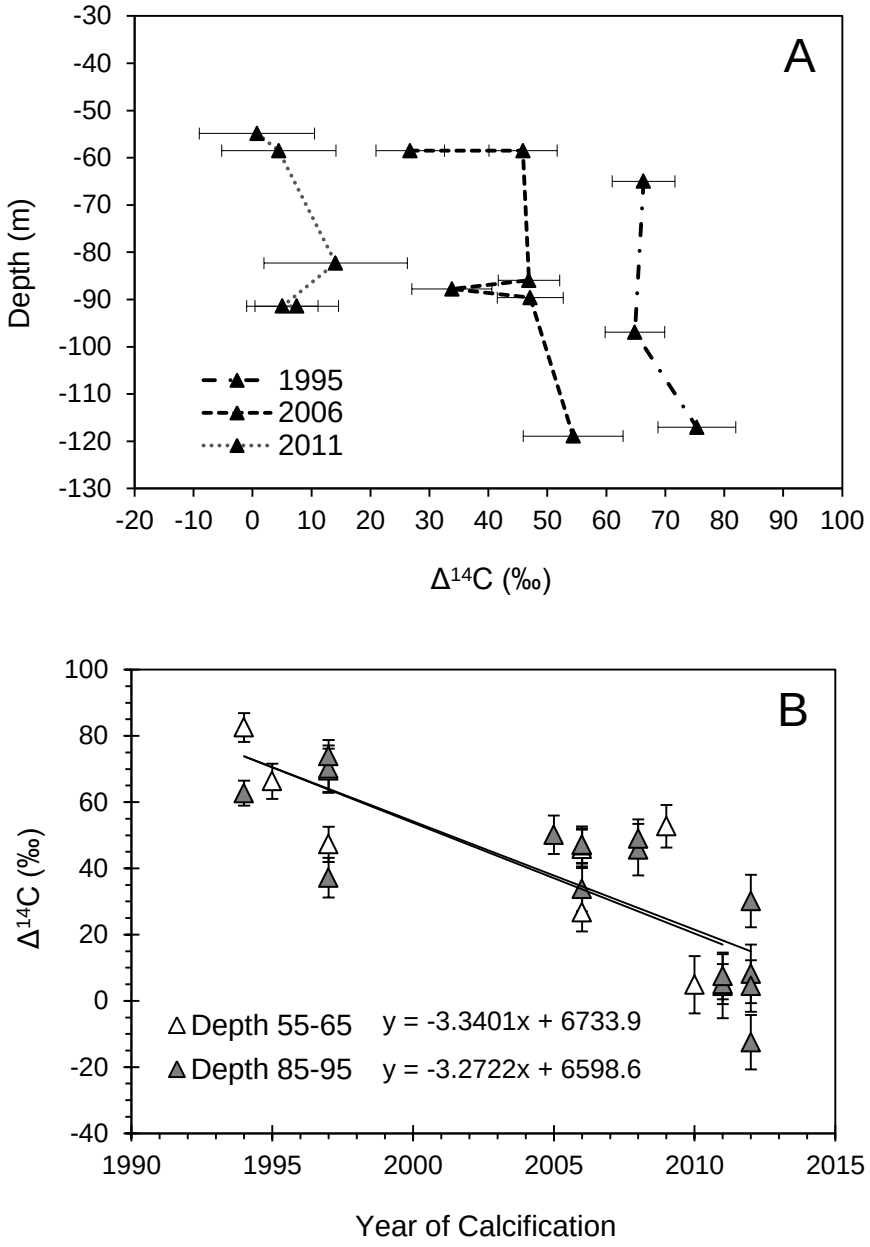

Fig. 5. A) $\Delta^{14}C$ depth profiles resulting from ocean perch otoliths for only the years of 1995, 2006 and 2011 to illustrate changes in ^{14}C through time. Otolith $\Delta^{14}C$ levels are similar over the sample depth and decline through time. B) Ocean perch otolith $\Delta^{14}C$ values representing the specific depths of 55 to 65 m (n = 9) and 85 to 95 m (n = 16) over the time period of 1994 to 2012.

upwelling intensity, ocean circulation and CO_2 inputs (e.g. Guilderson and Schrag 1998, Druffel 2002, Druffel et al. 2014).

Within the Bonney upwelling region, the ocean perch otolith $\Delta^{14}C$ levels declined at the same rate through time and were similar over the range of depths that samples were collected (< 120 m). This is indicative of the dynamic mixing that occurs within the upper water column of this region. Alongshore current speeds in the austral summer can be as great as 40 $cm \cdot s^{-1}$ and vertical scales of upwelling are on the order of 250 m (Middleton and Bye 2007). During winter months, surface water is downwelled up to depths of 200 to 400 m below the surface (Schwing et al. 1996). Upwelled waters tend to have lower $\Delta^{14}C$ signatures than those of the surrounding surface waters. This may be due to upwelled source waters i) being formed in higher latitude surface waters that are low in $\Delta^{14}C$, then subducted and transported at depth; ii) originating from a deep, sub-surface source depleted in $\Delta^{14}C$; or iii) a combination of both (e.g. Broecker and Peng 1982, Guilderson and Schrag 1998, Druffel et al. 2014). Low $\Delta^{14}C$ surface water values due to upwelling are especially evident in the $\Delta^{14}C$ time series measured in coral carbonate from the Galápagos Islands (Guilderson and Schrag 1998). The source water ultimately is the eastward flowing, subsurface Equatorial Undercurrent, which transports a mix of water from both the northern and southern subpolar Pacific, subtropical surface water, and deep water of the tropical thermocline (Guilderson and Schrag 1998, Thorrold and Shuttleworth 2000, Druffel et al. 2014). The low $\Delta^{14}C$ levels of the ocean perch record appear to be higher than those of the Galápagos Islands but lower than $\Delta^{14}C$ values in carbonate records of tropical surface water. This is consistent with the ocean perch record representing waters that are mixed throughout the year by both upwelling and downwelling and with sources of upwelled waters being formed at higher latitudes (near ~47°S southwest of Tasmania; TSAMW and TIW).

Comparison of the ocean perch and GAB water $\Delta^{14}C$ levels support previous studies regarding the source of upwelled water off the coast of southern Australia and general circulation patterns of the GAB. The otolith $\Delta^{14}C$ values from 1994/95 are lower than those reported in the upper water column (depths < 200 m) of the GAB outside of the upwelling region. These lower values most likely represent a mix of $\Delta^{14}C$ levels from the Flinders

Current (summer upwelled waters) and Leeuwin Current/South Australian Current (winter downwelled waters). The upper water column $\Delta^{14}C$ values of the GAB are characteristic of the Leeuwin Current/South Australian Current dominating that area and depth (Ribbe et al. 1996). The lower ocean perch $\Delta^{14}C$ values are more comparable to GAB water $\Delta^{14}C$ values at depths ≥ 400 m. At the GAB water sites, ~400 m is the upper depth boundary of the Flinders Current flowing westward across the GAB (e.g. Middleton and Bye 2007).

Different influences on contemporary ^{14}C records can be further examined by comparing the rates of decline within each record. Ocean perch $\Delta^{14}C$ values within the Bonney upwelling decline at a mean rate of 3.5‰ year^{-1} (1994 to 2012). Mean rates of ^{14}C decline from 1993 to 2009 for the Southern Hemisphere atmosphere and in shelf waters at depths of ~450 m on the east coast of Australia (otolith carbonate record) have been estimated to be 5.0‰ year^{-1} and 0.8 year^{-1}, respectively (Chapter 2; Grammer et al. 2015). The mean rate of decline estimated for tropical surface waters from 1993 to 2008 was 2.6‰ year^{-1} (coral record; estimated from Glynn et al. 2013). Interestingly, the ocean perch record is declining more rapidly than both the tropical surface water coral record and the mid-water otolith record. The ocean perch $\Delta^{14}C$ time series falls between these carbonate records in term of values but has a different rate of decline. The lower decline rate estimated for the surface waters of the tropical Pacific Ocean may be influenced by a complex interaction between seasonal variation in local winds forced by El Nino-Southern Oscillation (ENSO) and converging surface currents (Guilderson and Schrag 1998, Glynn et al. 2013).

Otoliths and bivalve shells are valuable alternative ^{14}C sources to hermatypic corals. Both fish and bivalves produce accretionary structures that, like coral, contain distinct growth bands. It is important for the alternative biogenic structure to have growth bands that can be resolved to seasonal or annual time scales, allowing the extracted carbonate to be time constrained. Ideally, the target species would also be site-attached (non-migratory in any form), and life history parameters known and accounted for when interpreting ^{14}C values (i.e. reproductive strategies, larval/juvenile/adult habitats, and dietary composition). Alternative sources of biogenic carbonate are especially useful at higher latitudes or deeper waters where coral samples are not available (e.g. Scourse et al. 2012, Grammer et al. 2015). Moreover, since many species of fish and bivalves are commercially harvested,

samples of the target species can be easily accessible. One drawback to using commercially fished specimens is the need for specific information relating to a specimen, such as depth and location of capture, to negate variability within the resultant $\Delta^{14}C$ record when trying to associate it with an explicit depth or water mass (Chapter 2; Grammer et al. 2015).

The 'bomb ^{14}C chronometer' is also extensively used as a precision tool for dating hard-to-age fish species to improve fish resource management and stock assessments (e.g. Campana 2001, Haltuch et al. 2013, Morin et al. 2013). Extension of $\Delta^{14}C$ carbonate records to present years allow younger fish to be age validated based on the bomb $\Delta^{14}C$ decline (after ~1980) as opposed to the $\Delta^{14}C$ increase of the 1960s (Andrews et al. 2013). $\Delta^{14}C$ reference records constructed from the bomb $\Delta^{14}C$ decline will become more important through time. Additionally, it is key for earlier otolith reference records (e.g. *Chrysophrys auratus*: Kalish 1993, *Centroberyx affinis*: Kalish 1995) to be extended to include the present $\Delta^{14}C$ decline.

In summary, we have presented the first contemporary time series of $\Delta^{14}C$ documented for the southeastern Indian Ocean. This otolith-based record documents the bomb $\Delta^{14}C$ decline (after ~1980) and represents an area of seasonal upwelling. We compared the ocean perch otolith $\Delta^{14}C$ with Indo-Pacific coral records and found that the ocean perch $\Delta^{14}C$ record was higher than the Galápagos Islands $\Delta^{14}C$ record but lower than $\Delta^{14}C$ values in coral of tropical surface water. The ocean perch record characterises waters well mixed throughout the year by both upwelling and downwelling and with sources of upwelled waters being formed at higher latitudes. Documenting levels of $\Delta^{14}C$ in the marine environment along the coast of southern Australia has augmented current ^{14}C data relating to ocean circulation in the southeastern Indian Ocean.

Acknowledgements:

We acknowledge partial funding from the Dr Paris Goodsell Marine Ecology Research Grant, the Nature Foundation SA, the Ecological Society of Australia, the Sir Mark Mitchell Research Foundation, CSIRO Wealth from Oceans Flagship and the Australian Research

Council (FT100100767; DP110100716). Thanks to J. Redman and S. Redman of Southend, SA for help with specimen collection.

References:

Bard, E., G. M. Raisbeck, F. Yiou, and J. Jouzel. 1997. Solar modulation of cosmogenic nuclide production over the last millennium: comparison between ^{14}C and ^{10}Be records. Earth and Planetary Science Letters **150**:453-462.

Barker, P. M. 2004. The circulation and formation of water masses south of Australia and the inter-annual wind variability along the southern Australian coast. PhD Thesis. The University of Melbourne, Victoria, Australia.

Berkman, P. A. and S. L. Forman. 1996. Pre-bomb radiocarbon and the reservoir correction for calcareous marine species in the Southern Ocean. Geophysical Research Letters **23**:363-366.

Bigg, G. R. 2003. The Oceans and Climate. Cambridge University Press.

Broecker, W. S. and T.-H. Peng. 1982. Tracers in the Sea. The Lamont-Doherty Geological Observatory, Columbia University, Palisades, New York.

Broecker, W. S., T.-H. Peng, and M. Stuiver. 1978. An estimate of the upwelling rate in the equatorial Atlantic based on the distribution of bomb radiocarbon. Journal of Geophysical Research **83**:6179-6186.

Bulman, C., F. Althaus, X. He, N. Bax, and A. Williams. 2001. Diets and trophic guilds of demersal fishes of the south-eastern Australian shelf. Marine and Freshwater Research **52**:537-548.

Campana, S. E. 1999. Chemistry and composition of fish otoliths: pathways, mechanisms and applications. Marine Ecology Progress Series **188**:263-297.

Campana, S. E. and J. D. Neilson. 1985. Microstructure of fish otoliths. Canadian Journal of Fisheries and Aquatic Sciences **42**:1014-1032.

Campana, S. E. and S. R. Thorrold. 2001. Otoliths, increments, and elements: keys to a comprehensive understanding of fish populations? Canadian Journal of Fisheries and Aquatic Sciences **58**:30-38.

Druffel-Rodriguez, K. C., D. Vetter, S. Griffin, E. R. M. Druffel, R. B. Dunbar, D. A. Mucciarone, L. A. Ziolkowski, and J.-A. Sanchez-Cabeza. 2012. Radiocarbon and stable isotopes in Palmyra corals during the past century. Geochimica et Cosmochimica Acta **82**:154-162.

Druffel, E. 2002. Radiocarbon in corals: records of the carbon cycle, surface circulation and climate. Oceanography **15**:122-127.

Druffel, E. R. M. and S. Griffin. 2004. Southern Great Barrier Reef coral radiocarbon data. NOAA/NCDC Paleoclimatology Program. IGBP PAGES/World Data Center for Paleoclimatology. Boulder, Colorado, USA. Data Contribution Series #2004-093.

Druffel, E. R. M., S. Griffin, D. S. Glynn, R. B. Dunbar, D. A. Mucciarone, and J. R. Toggweiler. 2014. Seasonal radiocarbon and oxygen isotopes in a Galapagos coral: Calibration with climate indices. Geophysical Research Letters **41**:5099-5105.

Fallon, S. J., L. K. Fifield, and J. M. Chappell. 2010. The next chapter in radiocarbon dating at the Australian National University: Status report on the single stage AMS. Nuclear Instruments and Methods in Physics Research Section B: Beam Interactions with Materials and Atoms **268**:898-901.

Fallon, S. J. and T. P. Guilderson. 2008. Surface water processes in the Indonesian throughflow as documented by a high-resolution coral $\Delta^{14}C$ record. Journal of Geophysical Research: Oceans **113**:C09001.

Feng, M., G. Meyers, A. Pearce, and S. Wijffels. 2003. Annual and interannual variations of the Leeuwin Current at 32°S. Journal of Geophysical Research **108**:1-20.

Furlani, D. M. 1997. Development and ecology of ocean perch larvae, *Helicolenus percoides* (Richardson, 1842) (Pisces:Scorpaenidae), from southern Australian waters, with notes on the larvae of other sympatric scorpaenid genera. Marine and Freshwater Research **48**:311-320.

Glynn, D., E. Druffel, S. Griffin, R. Dunbar, M. Osborne, and J. A. Sanchez-Cabeza. 2013. Early bomb radiocarbon detected in Palau Archipelago Corals. Radiocarbon **55**:1659–1664.

Grammer, G. L., S. J. Fallon, C. Izzo, R. Wood, and B. M. Gillanders. 2015. Investigating bomb radiocarbon transport in the southern Pacific Ocean with otolith radiocarbon. Earth and Planetary Science Letters **424**:59-68.

Guilderson, T. P., S. Fallon, M. D. Moore, D. P. Schrag, and C. D. Charles. 2009. Seasonally resolved surface water $\Delta^{14}C$ variability in the Lombok Strait: a coralline perspective. Journal of Geophysical Research: Oceans **114**:C07029.

Guilderson, T. P. and D. P. Schrag. 1998. Abrupt shift in subsurface temperatures in the tropical Pacific associated with changes in El Niño. Science **281**:240-243.

Guilderson, T. P., D. P. Schrag, and M. A. Cane. 2004. Surface water mixing in the solomon sea as documented by a high-resolution coral ^{14}C record. Journal of Climate **17**:1147-1156.

Guilderson, T. P., D. P. Schrag, E. Goddard, M. Kashgarian, G. M. Wellington, and B. K. Linsley. 2000. Southwest subtropical Pacific surface water radiocarbon in a high-resolution coral record. Radiocarbon **42**:249-256.

Guilderson, T. P., D. P. Schrag, M. Kashgarian, and J. Southon. 1998. Radiocarbon variability in the western equatorial Pacific inferred from a high-resolution coral record from Nauru Island. Journal of Geophysical Research: Oceans **103**:24641-24650.

Haltuch, M. A., O. S. Hamel, K. R. Piner, P. McDonald, C. R. Kastelle, and J. C. Field. 2013. A California Current bomb radiocarbon reference chronology and petrale sole (*Eopsetta jordani*) age validation. Canadian Journal of Fisheries and Aquatic Sciences **70**:22-31.

Henschke, N., D. A. Bowden, J. D. Everett, S. P. Holmes, R. J. Kloser, R. W. Lee, and I. M. Suthers. 2013. Salp-falls in the Tasman Sea: a major food input to deep-sea benthos. Marine Ecology Progress Series **491**:165-175.

Horn, P. L., J. S. Forman, and M. R. Dunn. 2012. Dietary partitioning by two sympatric fish species, red cod (*Pseudophycis bachus*) and sea perch (*Helicolenus percoides*), on Chatham Rise, New Zealand. Marine Biology Research **8**:624-634.

Hua, Q., M. Barbetti, and A. Z. Rakowski. 2013. Atmospheric radiocarbon for the period 1950 - 2010. Radiocarbon **55**:2059-2072.

James, N. P. and Y. Bone. 2011. Neritic Carbonate Sediments in a Temperate Realm: Southern Australia. Springer, London.

Kalish, J. M. 1991. Oxygen and carbon stable isotopes in the otoliths of wild and laboratory-reared Australian salmon (*Arripis trutta*). Marine Biology **110**:37-47.

Kalish, J. M. 1993. Pre- and post-bomb radiocarbon in fish otoliths. Earth and Planetary Science Letters **114**:549-554.

Kalish, J. M. 1995. Application of the bomb radiocarbon chronometer to the validation of redfish *Centroberyx affinis* age. Canadian Journal of Fisheries and Aquatic Sciences **52**:1399-1405.

Kämpf, J., M. Doubell, D. Griffin, R. L. Matthews, and T. M. Ward. 2004. Evidence of a large seasonal coastal upwelling system along the southern shelf of Australia. Geophysical Research Letters **31**:1-4.

Mahadevan, A. 2001. An analysis of bomb radiocarbon trends in the Pacific. Marine Chemistry **73**:273-290.

Middleton, J. F., C. Arthur, P. Van Ruth, T. M. Ward, J. L. McClean, M. E. Maltrud, P. Gill, A. Levings, and S. Middleton. 2007. El Nino effects and upwelling off South Australia. Journal of Physical Oceanography **37**:2458-2477.

Middleton, J. F. and J. A. T. Bye. 2007. A review of the shelf-slope circulation along Australia's southern shelves: Cape Leeuwin to Portland. Progress in Oceanography **75**:1-41.

Middleton, J. F. and M. Cirano. 2002. A northern boundary current along Australia's southern shelves: The Flinders Current. Journal of Geophysical Research. C. Oceans **107**:1-11.

Park, T. J. 1993. A comparison of the morphology, growth and reproductive biology of two colour forms of ocean perch (*Helicoleus percoides*), NSW, Australia. Masters. University of Sydney, Sydney, Australia.

Paul, L. J. and P. L. Horn. 2009. Age and growth of sea perch (*Helicolenus percoides*) from two adjacent areas off the east coast of South Island, New Zealand. Fisheries Research **95**:169-180.

Pavlov, D. A. and N. G. Emel'yanova. 2013. Transition to viviparity in the order Scorpaeniformes: Brief review. Journal of Ichthyology **53**:52-69.

Ribbe, J., J. T. Bye, M. Tomczak, G. E. Jacobsen, E. M. Lawson, A. M. Smith, D. Fink, M. C. Hotchkis, and C. Tuniz. 1996. First ^{14}C observations in waters of the Great Australian Bight. Radiocarbon **38**:1-10.

Schwing, F. B., M. O'Farrell, J. Steger, and K. Baltz. 1996. Coastal Upwelling Indices, West coast of North America, 1946-1995. U.S. Dept. of Commerce, NOAA Tech. Memo. NOAA-TM-NMFS-SWFC-231.

Scourse, J. D., A. D. Wanamaker Jr, C. Weidman, J. Heinemeier, P. J. Reimer, P. G. Butler, R. Witbaard, and C. A. Richardson. 2012. The marine radiocarbon bomb pulse across the temperate North Atlantic: a compliation of $\Delta^{14}C$ time histories from *Arctica islandica* growth increments. Radiocarbon **54**:165-186.

Secor, D. H., J. M. Dean, and S. E. Campana. 1995. Recent Developments in Fish Otolith Research. University of South Carolina Press, Columbia, SC, USA.

Solomon, C. T., P. K. Weber, J. Cech, Joseph J, B. L. Ingram, M. E. Conrad, M. V. Machavaram, A. R. Pogodina, and R. L. Franklin. 2006. Experimental determination of the sources of otolith carbon and associated isotopic fractionation. Canadian Journal of Fisheries and Aquatic Sciences **63**:79-89.

Stuiver, M. and H. A. Polach. 1977. Discussion: reporting of ^{14}C data. Radiocarbon **19**:355-363.

Thorrold, S. R. and S. Shuttleworth. 2000. In situ analysis of trace elements and isotope ratios in fish otoliths using laser ablation sector field inductively coupled plasma mass spectrometry. Canadian Journal of Fisheries and Aquatic Sciences **57**:1232-1242.

Toggweiler, J. R., K. Dixon, and W. S. Broecker. 1991. The Peru upwelling and the ventilation of the south Pacific thermocline. Journal of Geophysical Research: Oceans **96**:20467-20497.

Withell, A. and J. Wankowski. 1988. Estimates of age and growth of ocean perch, *Helicolenus percoides* Richardson, in south-eastern Australian waters. Marine and Freshwater Research **39**:441-457.

CHAPTER 4
Local and regional effects of climate forcing detected in long-term fish growth chronologies

Big-eye ocean perch (*Helicolenus barathri*) being sold by a fishmonger at the Sydney Fish Market, Sydney, New South Wales, AUS

Statement of Authorship

Title of Paper	Local and regional effects of climate forcing detected in long-term fish growth chronologies
Publication Status	☐ Published ☐ Accepted for Publication ☐ Submitted for Publication ☑ Publication Style
Publication Details	This is a co-authored paper and is intended to be published in a scientific journal. Christopher Izzo, Peter Hawthorne, John Middleton, and Bronwyn Gillanders are co-authors, and therefore, it is written in plural.

Principal Author

Name of Principal Author (Candidate)	Gretchen L. Grammer		
Contribution to the Paper	Collected specimens, extracted otoliths, performed all laboratory analyses, performed statistical analyses, supplied some funding, and wrote the manuscript.		
Overall percentage (%)	90		
Signature		Date	17 June 2015

Co-Author Contributions

By signing the Statement of Authorship, each author certifies that:

iv. the candidate's stated contribution to the publication is accurate (as detailed above);

v. permission is granted for the candidate in include the publication in the thesis; and

vi. the sum of all co-author contributions is equal to 100% less the candidate's stated contribution.

Name of Co-Author	Christopher Izzo		
Contribution to the Paper	Assisted with intellectual development and statistical analyses, and provided suggestions, comments and feedback on manuscript drafts		
Signature		Date	17 June 2015

Name of Co-Author	Peter Hawthorne		
Contribution to the Paper	Collected specimens, assisted with intellectual development, and will provide suggestions, comments, and feedback on manuscript drafts prior to submission to a scientific journal		
Signature		Date	17 June 2015

Name of Co-Author	John Middleton		
Contribution to the Paper	Provided Bluelink temperature data, provided suggestions during manuscript development, and will provide feedback on manuscript drafts prior to submission to a scientific journal		
Signature		Date	17 June 2015

Name of Co-Author	Bronwyn M. Gillanders		
Contribution to the Paper	Assisted with intellectual development, supplied funding, and provided suggestions, comments and feedback on manuscript drafts		
Signature		Date	17 June 2015

Local and regional effects of climate forcing detected in long-term fish growth chronologies

Gretchen L. Grammer[1], Christopher Izzo[1], Peter J. Hawthorne[2], John F. Middleton[2], and Bronwyn M. Gillanders[1]

[1]Southern Seas Ecology Laboratories, School of Biological Sciences, The University of Adelaide, SA 5005, Australia

[2]South Australian Research and Development Institute (Aquatic Sciences), West Beach, SA 5024, Australia

Correspondence: Gretchen L. Grammer, Southern Seas Ecology Laboratories, School of Biological Sciences, The University of Adelaide, SA 5005, Australia

Tel.: +61 8 8313 1483; Fax: +61 8 8313 4364

Email: gretchen.grammer@adelaide.edu.au

Abstract:

Variability in fish populations is closely related to weather and climate dynamics. Broad scale climate patterns originate in atmospheric processes modulated through complex interactions with oceans and surrounding landmasses, and cause ecosystem forcing at various time scales. Synchrony of geographically separate populations of fish is believed to relate to low frequency climate variability. Annually resolved growth chronologies can be produced from the otoliths (earstones) of fishes and offer a metric to further examine synchrony in growth and possible climatic drivers across regions. We compare chronologies of fish growth derived from the otoliths of ocean perches (*Helicolenus* spp.) from southern Australia and New Zealand across multiple regions spanning 3000 km and species with broad- and local-scale climatic/oceanographic variables. We used univariate mixed-effects models to partition age-dependent drivers of growth through time, allowing other sources of variability to be extracted from the growth record. Specific broad- and local-scale environmental parameters were then added to the models to determine their potential influence on growth. Long-term growth responses of the ocean perches revealed the synergistic effects of climate forcing at different environmental scales on fish growth. Age was a key intrinsic driver of growth, as anticipated. Temporal growth responses at the broadest level were influenced by solar activity and the Madden-Julien Oscillation (MJO). Other regional drivers included the El Niño-Southern Oscillation (ENSO) and the Southern Annular Mode (SAM). Over the local variation in sea level and sea level pressure, fish growth showed different directionality within each population. Broad-scale climate variables typically produced more percent change to growth than did the local parameters. We detected climate forcing in multiple fish species over a distance of 3000 km and found growth responses were associated with variation in ocean-atmosphere coupling. We demonstrated climate forcing is reflected in fish growth, and otoliths can be used as a tool to examine these effects. Broad scale climate patterns and weather have synergistic effects on the environment, which are related to fish growth.

Introduction:

Broad scale climate signals originate in atmospheric processes modulated through complex interactions with oceans and surrounding landmasses (e.g. Peterson and White 1998, Mo 2000, Zhang 2005). These broad scale patterns influence ecosystems at different time scales from diurnal to centennial or longer (Stabeno et al. 2006, Overland et al. 2010, Jin et al. 2012). Indices of teleconnections (i.e. simultaneous physical variations in climate over large distances) have been developed to describe broad climate patterns, e.g. sea level pressure differences between Tahiti and Darwin (Southern Oscillation Index; SOI) describe the El Niño-Southern Oscillation (ENSO). Large-scale climate patterns can affect the ocean mixed layer (Hayward 1997, Sallee et al. 2010, Chi et al. 2014). The mixed layer mediates interactions between the atmosphere and ocean; its depth is regulated by wind forcing and atmospheric heating (Sallee et al. 2010). Changes in the mixed layer depth specifically affects the amount of light and nutrients available for phytoplankton growth, and thus, overall biological productivity (Polovina et al. 1995, Sallee et al. 2010).

Local weather patterns on hourly or daily time scales are quite different from broad-scale climate phenomena, and the relationships between local weather and broad-scale climate patterns are not always clear. The Madden-Julian Oscillation (MJO) is a key mechanism that links weather and climate (Zhang 2005, Jin et al. 2012). The MJO is an eastward propagating, equatorial deep convection system with baroclinic wind patterns that influence environments of the tropics and extratropics (mid-latitudes) (Zhang 2005, Woolnough et al. 2007, Risbey et al. 2009). This atmospheric phenomenon is a direct driver of rainfall in the tropics and indirectly forces weather patterns of the extratropics through interactions with the Southern Annular Mode (SAM; Matthews and Meredith 2004) and changes in tropical convection (e.g. Matthews et al. 2004, Wheeler et al. 2009). The SAM is also known as the Antarctic Oscillation (AAO).

Variability in fish populations maybe correlated with weather and climate dynamics. Climate variability influences distribution, migratory patterns, abundances, and growth in fishes (Attrill and Power 2002, Möllmann et al. 2005, Lehodey et al. 2006). Explaining this interannual variability has become an active area of research (e.g. Thresher et al. 2007, Black et al. 2008, Morrongiello et al. 2012). Synchrony in geographically separate

populations of fish has drawn attention to low frequency climate variability such as the Pacific Decadal Oscillation (PDO) and ENSO (Lehodey et al. 2006). Annually resolved growth chronologies can be produced from the otoliths (earstones) of fishes and offer a metric to further examine synchrony in growth and possible drivers across regions (Black et al. 2008, Gillanders et al. 2012, Morrongiello et al. 2012). Otolith growth increment chronologies are akin to bivalve, coral or tree-ring chronologies in their ability to provide indirect records of the environment. Fish growth records gleaned from otoliths, particularly in the Northern Hemisphere, have shown some of the interconnections existing with both large-scale climate phenomenon and localised oceanographic variables (e.g. Matta et al. 2010, Black et al. 2015).

Otolith-based growth increment chronologies have not been developed for the Southern Hemisphere to the extent that they have in the Northern Hemisphere. Many species used for chronological studies in the Southern Hemisphere have been shallow water species (e.g. Gillanders et al. 2012, Coulson et al. 2014, Rountrey et al. 2014), whilst few have focused on deep water fish (living at the boundary of or below the mixed layer; $\geq$ ~200 m) (Thresher et al. 2007, Thresher et al. 2014, Nguyen et al. 2015). Previous research has generally examined the growth responses of fish to an aspect(s) of climate or oceanography, with limited consideration of multiples species (e.g. Thresher et al. 2007) or comparisons across locations (e.g. Thresher et al. 2014, Morrongiello and Thresher 2015).

Here, we relate otolith-based growth increment chronologies from *Helicolenus*, a deepwater fish genus, to broad-scale climate processes as well as localised oceanographic variables across the southwest Pacific region. Specifically, we examine growth responses to large-scale climate variables for fish from the same genus across an area spanning ~3000 km. Then, we investigate the influence of broad and localised climate/oceanographic variables on interspecific growth between *H. barathri* and *H. percoides* from one region in southeastern Australia. Next, we compare intraspecific growth responses of *H. percoides* to broad climate/oceanographic variables across southeastern Australia. Finally, we correlate the individual growth of each species (two species and two species complexes) at each location in southeastern Australia and New Zealand with both broad- and local-scale climate/oceanographic variables.

Methods:

Study Species

Ocean perches (*Helicolenus* spp., family: Sebastidae) are demersal fishes that occur in continental waters, offshore ridges and seamounts of the Atlantic, Pacific and Indian Oceans. In the southwest Pacific, *H. percoides* and *H. barathri* are distributed in southeast Australian and New Zealand waters, with a third undescribed *Helicolenus* species found on the Chatham Rise, east of New Zealand (Smith et al. 2009). We focused primarily on reef ocean perch (*H. percoides*) in depths of < 350 m and big-eye ocean perch (*H. barathri*) in depths > 350 m (Park 1993, Smith et al. 2009), but also included *Helicolenus* spp. collected off the Chatham Rise for comparison. The *Helicolenus* species complex is fished commercially in New South Wales (NSW), Australia as well as New Zealand (Park 1993, Paul and Horn 2009); they are also frequently captured as bycatch in the southern rock lobster fishery in southeast Australia (Brock et al. 2007). *Helicolenus* can reach lengths of > 40 cm and attain ages > 50 yrs (Bentley et al. 2014).

Ocean perches are highly evolved in their reproductive strategies and display a transition from oviparity to viviparity within the genus (Pavlov and Emel'yanova 2013). *Helicolenus percoides* is lecithotrophic viviparous (Pavlov and Emel'yanova 2013), whilst the specific reproductive strategy (embryoparous or lecithotrophic) of *H. barathri* has yet to be confirmed (Park 1993). Both of these species of ocean perch mature around five years of age and spawn in the austral winter/spring and summer, depending on latitude (July to January; Park 1993, Paul and Horn 2009); a birthdate of 1 October was assigned for ageing purposes. Ocean perches are benthopelagic omnivores (Bulman et al. 2001) and demersal as both juveniles and adults (Park 1993).

Study area and sample collection

Fish from six areas in the southwest Pacific were used to examine climate drivers of growth in *Helicolenus* (Table 1, Fig. 1). Otoliths from *H. percoides* were sourced from Kangaroo Island, South Australia (SA), the Bonney Coast, SA (Robe to Port MacDonnell), and southeastern NSW (Ulladulla to Eden). *Helicolenus barathri* otoliths were obtained from southeastern NSW (Ulladulla to Eden). Otoliths from New Zealand were not identified to species at the time of collection, but they came from two geographically separate locations:

Table 1. Collection information for *Helicolenus* samples. SA: South Australia, NSW: New South Wales, NZ: New Zealand

Location	Species	Species - Location identifier	Fish (n)	Increments measured (n)	Age range (yrs)	Chronology range (yrs)
Kangaroo Island, SA	*Helicolenus percoides*	HP - KI	45	434	2-22	1994-2012
Bonney Coast, SA	*Helicolenus percoides*	HP- BC	155	1762	2-25	1993-2012
Southeastern NSW	*Helicolenus percoides*	HP - NSW	80	817	2-30	1975-2011
Southeastern NSW	*Helicolenus barathri*	HB - NSW	104	1767	2-46	1955-2011
West NZ	*Helicolenus* spp.	Hspp. - WNZ	88	916	2-26	1980-2010
Chatham Rise NZ	*Helicolenus* spp.	Hspp. - ENZ	117	1953	2-31	1969-2012

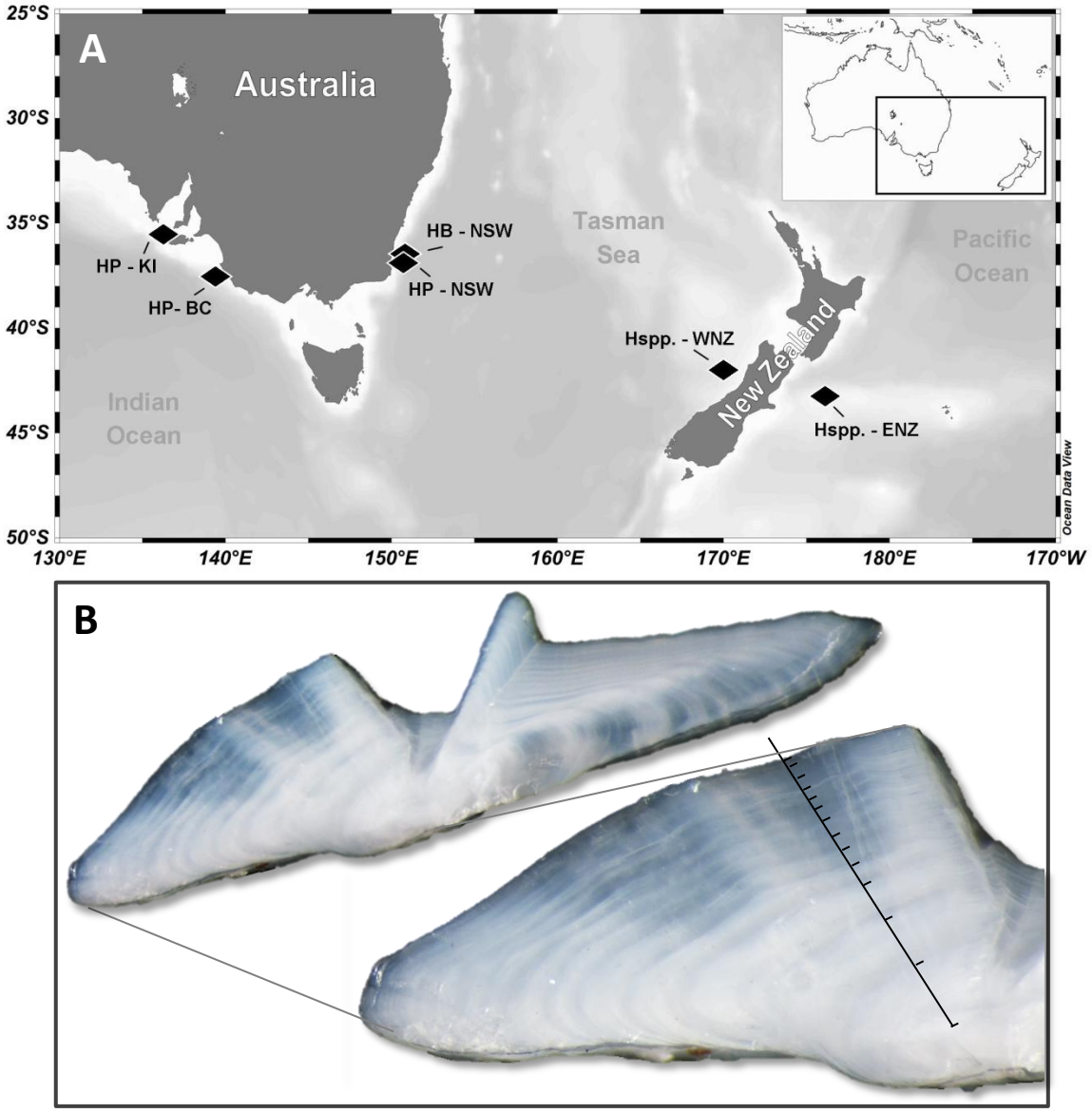

Fig. 1. A) Map of study area in the southwestern Pacific and southeastern Indian Ocean regions. Locations of growth chronologies (black diamonds) are Kangaroo Island, South Australia (SA, HP - KI), Bonney Coast, SA (HP - BC), southeastern New South Wales (NSW, HP - NSW, HB - NSW), western New Zealand (NZ, Hspp. - WNZ), and eastern NZ (Hspp. - ENZ). B) Thin section of a *Helicolenus percoides* otolith. Growth increments were measured from the core to the proximal edge (black line; tics designate annual increments along the axis of measurement). This fish was 12+ years old.

the west coast of the South Island near the Challenger Plateau and the east of New Zealand on the Chatham Rise. Based on phylogenetic analyses, we can infer that the west coast specimens were *H. percoides* and/or *H. barathri*, whilst the Chatham Rise otoliths most likely came from the undescribed *Helicolenus* species or a mix of that species and *H. percoides* (Smith et al. 2009). The majority of the *Helicolenus* otoliths originated from archived collections taken during stock assessment surveys in both Australia (NSW Department of Primary Industries) and New Zealand (New Zealand National Institute of Water and Atmospheric Research). These collections were expanded with more recent otoliths from commercial catches, research sampling, and sampling from fish markets. All otoliths were stored dry in paper envelopes prior to analysis.

Otolith preparation & growth increment analysis

One sagittal otolith from each fish was used for growth increment analysis. Each otolith was weighed (g), measured (length, width; mm), embedded in epoxy resin, and then sectioned transversely through the primordium. Sections (~350 µm thick) were mounted on glass slides and examined using a compound microscope (× 87.5 magnification; Leica DM LB) for age interpretation. Each otolith section was photographed (Leica DFC320; digital camera on microscope), first under reflected light and then using transmitted light without moving the section or refocusing the microscope. Overlaying the two images allowed the growth increments to be checked as they were being marked, thereby ensuring that growth increments were not missed and were measured accurately. Each annual growth increment was comprised of one opaque growth zone and one hyaline growth zone. Annual growth increments have been validated in *H. percoides* (Paul and Horn 2009) and verified in *H. barathri* (Chapter 2; Grammer et al. 2015). The growth increments in each otolith were marked and measured (mm; Image-Pro Plus v. 7.0, MediaCybernetics) just dorsal to the sulcus groove from the core to the proximal margin (Fig. 1b). Each growth increment was assigned a year back-calculated from the date of capture taking into account the marginal increment. Growth years were designated as November 1 to October 1 based on estimates of the timing of increment formation in *H. percoides* (Park 1993, Paul and Horn 2009) and *H. barathri* (Park 1993). The core (age 0) and marginal increment were excluded from all analyses, as neither of these growth increments represented one complete year of growth.

For all species, otoliths were shown to grow in proportion to somatic growth (Supplementary Table 1).

Otolith chronology development and climate comparisons

We developed a suite of linear mixed-effect models following Morrongiello and Thresher (2015) and Weisberg et al. (2010) to examine variations in *Helicolenus* growth relative to broad-scale and local climatic variation. A hierarchical, two-stage procedure was followed, wherein a series of intrinsic (biological) and extrinsic (environmental) covariates were added in ever-increasing complexity to obtain an optimal model to predict fish growth: (i) across species and regions (identifying broad-scale drivers of growth across all species and regions); (ii) among species within a region (identifying broad and local-scale drivers of growth among species in a specific region); (iii) within species among regions (population level growth drivers across regions), and (iv) species and region specific (individual species responses within their habitat). Intrinsic covariates used in all comparisons of growth were the age of the fish at each annual growth increment (*Age*) and age at capture (*AgeCap*) (Table 2). Extrinsic covariates represented broad-scale and local climatic variables potentially acting on fish growth in each region (see Table 3 for complete list and descriptions). Sea surface temperature (SST) was not used as an environmental parameter, because the *Helicolenus* populations used in this study live at depths where SST is not a suitable proxy for bottom temperature.

To develop an optimal model for each comparison of fish growth (i-iv above), a series of random effect structures (Tables 2, 4 and 5) were fit to the full array of fixed intrinsic effects (*Age*, *AgeCap*) using restricted maximum likelihood estimates of error (REML). Selection of the best structure was based on ΔAICc values. Next, the best random effects structure was fit with the specific fixed effects structure of *Age* or *Age* + *AgeCap* using maximum likelihood estimates of error (ML), and again, ΔAICc values were used for model comparisons. Then, best models were refit with REML to produce unbiased parameter estimates (Zuur et al. 2009) (Table 6). Finally, broad-scale environmental variables were added as fixed effects to each optimal model to relate growth variability to climate (Supplementary Table 2 and 3). We also fitted interaction terms for environmental variables to test for synergistic environmental effects on growth for growth comparisons ii

Table2. Descriptions of variables used in mixed-effects modelling showing whether they were treated as random or fixed effects (R = random effect; F = Fixed effect)

Variable	**Description**	**Type**
FishID	Unique fish identifier	R
Age	Fish age (in years) when annual growth increment formed	F, R
AgeCap	Fish age (in years) when captured	F, R
Year	Year annual growth increment formed	F, R
YearClass	Birth year of fish; used to indicate cohorts of fish from the same spawning season	R
Location	Location fish collected for otolith growth record	R
Species	Fish species from which growth record is derived	R
Climate Variable	See Table 3 for details	F

Table 3. Climate variables, their descriptions and to what region they are associated. MJO: Madden-Julian Oscillation.

Climate Variable	Description	Source	Region Associated				
			Kangaroo Island	Bonney Coast	NSW	West NZ	Chatham Rise
Broad							
Sunspots	Mean number of sunspots recorded per year	SILSO data, Royal Observatory of Belgium, Brussels	X	X	X	X	X
AAO	Antarctic Oscillation: leading mode of empirical orthogonal function analysis of monthly mean 700 hPa; Index of the Southern Annular Mode	National Oceanic and Atmospheric Association	X	X	X	X	X
SOI	Southern Oscillation Index: standardised anomaly of the mean sea level pressure difference between Tahiti and Darwin	Australian Bureau of Meteorology	X	X	X	X	X
PDO	Pacific Decadal Oscillation: leading principle component of North Pacific monthly sea surface temperature variability	National Oceanic and Atmospheric Association	X	X	X	X	X
MJOindex20E	MJO Index centred at 20°E	Indices of enhanced atmospheric convection centred at 20°E, 70°E, 80°E, 100°E, 120°E, 140°E, 160°E, 120°W, 40°W or 10°W determined from extended empirical orthogonal function analysis applied to pentad 200-hPa velocity potential anomalies	X	X	X	X	X
MJOindex70E	MJO Index centred at 70°E		X	X	X	X	X
MJOindex80E	MJO Index centred at 80°E		X	X	X	X	X
MJOindex100E	MJO Index centred at 100°E		X	X	X	X	X
MJOindex120E	MJO Index centred at 120°E		X	X	X	X	X
MJOindex140E	MJO Index centred at 140°E		X	X	X	X	X
MJOindex160E	MJO Index centred at 160°E		X	X	X	X	X
MJOindex120W	MJO Index centred at 120°W		X	X	X	X	X
MJOindex40W	MJO Index centred at 140°W		X	X	X	X	X
MJOindex10W	MJO Index centred at 10°W		X	X	X	X	X
OMImjoAmplitude	OMI MJO index: outgoing longwave radiation MJO index; negative: enhanced convection, positive: supressed convection	National Oceanic and Atmospheric Association	X	X	X	X	X
Local							
SeaLevel	Mean annual local sea level (mm)	Permanent Service for Mean Sea Level (PSMSL), 2014	X	X	X	X	X
YearSLP	Mean annual local sea level pressure (hPa)	KNMI Climate Explorer based on HadSLP2	X	X	X	X	X
YearlyUI	Mean annual upwelling index	National Oceanic and Atmospheric Association	X	X			
YearBotTemp	Mean annual bottom temperature (°C)	South Australian Research and Development Institute	X	X			

Table 4. Best random effect structure (highlighed in **bold**) fitted with the full fixed effect structure of *Age* + *AgeCap* (i: identifying broad-scale drivers of growth), among *Helicolenus percoides* and *H. barathri* in NSW (ii: identifying local-scale drivers of growth), and within *H. percoides* from different locations in SA and NSW (iii). For growth comparison ii, the term *Location* was replaced within each model structure with the term *Species*. Random slope term designated with A|B. Nested terms are signified by A: B. LL: log likelihood.

Random effect structure	**(i) Across species and regions**				**(ii) Among species within a region**				**(iii) within species among regions**			
Model	df	AICc	ΔAICc	LL	df	AICc	ΔAICc	LL	df	AICc	ΔAICc	LL
(1|FishID)	5	-118.72	224.01	64.37	5	-51.09	75.96	30.56	5	-547.98	134.45	279.00
(Age|FishID)	7	-235.27	107.46	124.65	7	-109.83	17.23	61.95	7	-667.83	14.60	340.94
(Age|FishID) + (1|Year)	8	-300.62	42.11	158.33	8	-122.29	4.77	69.19	8	-672.58	9.84	344.32
(Age|FishID) + (1|YearClass)	8	-244.49	98.24	130.27	8	-107.81	19.25	61.95	8	-665.83	16.60	340.95
(Age|FishID) + (Age|Year)	10	-314.92	27.81	167.49	10	-118.60	8.45	69.37	10	-672.65	9.78	346.37
(Age|FishID) + (Age|YearClass)	10	-265.73	77.00	142.89	10	-103.76	23.29	61.95	10	-673.21	9.21	346.66
(Age|FishID) + (1|Location:Year) + (1|Location) + (1|Location:YearClass)	10	-293.87	48.86	156.96	10	-118.86	8.20	69.50	10	-672.58	9.84	346.34
(Age|FishID) + (Age|Location:Year) + (Age|Location) + (Age|Location:YearClass)	**16**	**-342.73**	**0**	**187.44**	16	-118.91	8.14	75.62	16	-682.11	0.31	357.18
(Age|FishID) + (Age|Location:Year) + (1|Location) + (1|Location:YearClass)	12	-323.82	18.91	173.95	**12**	**-127.05**	**0**	**75.62**	12	-678.30	4.12	351.22
(Age|FishID) + (1|Location:Year) + (Age|Location) + (1|Location:YearClass)	12	-307.37	35.36	165.73	12	-114.90	12.15	69.55	12	-673.12	9.30	348.63
(Age|FishID) + (1|Location:Year) + (1|Location) + (Age|Location:YearClass)	12	-312.18	30.56	168.13	12	-114.80	12.26	69.50	12	-682.27	0.15	353.21
(Age|FishID) + (Age|Location:Year) + (Age|Location) + (1|Location:YearClass)	14	-333.01	9.72	180.56	14	-122.99	4.07	75.62	14	-678.00	4.43	353.09
(Age|FishID) + (Age|Location:Year) + (1|Location) + (Age|Location:YearClass)	14	-334.29	8.44	181.20	14	-122.99	4.07	75.62	**14**	**-682.43**	**0**	**355.31**
(Age|FishID) + (1|Location:Year) + (Age|Location) + (Age|Location:YearClass)	14	-320.88	21.85	174.50	14	-110.83	16.22	69.55	14	-682.24	0.19	355.21
(Age|FishID) + (Age|Location:Year) + (AgeCap|Location) + (Age|Location:YearClass)	16	-333.11	9.62	182.63	16	-119.29	7.76	75.82	16	-678.37	4.06	355.31
(Age|FishID) + (1|Location:Year) + (AgeCap|Location) + (Age|Location:YearClass)	14	-309.39	33.35	168.75	14	-111.06	15.99	69.66	14	-678.22	4.20	353.21
(Age|FishID) + (Age|Location:Year) + (AgeCap|Location) + (1|Location:YearClass)	14	-325.70	17.03	176.91	14	-123.37	3.68	75.82	14	-674.25	8.17	351.22
(Age|FishID) + (1|Location:Year) + (AgeCap|Location) + (1|Location:YearClass)	12	-295.23	47.50	159.66	12	-115.13	11.93	69.66	12	-668.54	13.88	346.34

Table 5. Best random effect structure (highlighed in **bold**) fitted with the full fixed effect structure of *Age* + *AgeCap* for growth comparison iv: species and region specific. Random slope term designated with A|B. LL: log likelihood. Species and region codes are provided in Table 1.

Growth Comparison (iv)	**HP - BC**				**HP - KI**				**HP - NSW**			
Model	df	AICc	ΔAICc	LL	df	AICc	ΔAICc	LL	df	AICc	ΔAICc	LL
(1|FishID)	5	-399.01	129.04	204.52	5	-94.78	15.33	52.46	5	-103.93	94.21	57.00
(Age|FishID)	7	-497.39	30.66	255.73	**7**	**-110.11**	**0**	**62.19**	7	-169.81	28.33	91.98
(Age|FishID) + (1|Year)	8	-508.67	19.38	262.38	8	-108.25	1.86	62.29	8	-190.71	7.43	103.44
(Age|FishID) + (1|YearClass)	8	-495.37	32.68	255.73	8	-108.09	2.02	62.22	8	-167.77	30.37	91.98
(Age|FishID) + (Age|Year)	10	-516.53	11.52	268.33	10	-107.91	2.20	64.21	**10**	**-198.14**	**0**	**109.21**
(Age|FishID) + (Age|YearClass)	10	-510.23	17.82	265.18	10	-104.64	5.48	62.58	10	-163.68	34.46	91.98
(Age|FishID) + (1|Year) + (1|YearClass)	9	-506.65	21.40	262.38	9	-106.21	3.90	62.32	9	-188.66	9.48	103.44
(Age|FishID) + (Age|Year) + (1|YearClass)	11	-514.51	13.55	268.33	11	-105.82	4.29	64.22	11	-196.08	2.05	109.21
(Age|FishID) + (1|Year) + (Age|YearClass)	11	-527.04	1.01	274.60	11	-102.87	7.24	62.75	11	-184.62	13.52	103.47
(Age|FishID) + (Age|Year) + (Age|YearClass)	**13**	**-528.05**	**0**	**277.13**	13	-102.01	8.11	64.44	13	-191.96	6.18	109.21

Growth Comparison (iv)	**HB - NSW**				**Hspp - WNZ**				**Hspp - ENZ**			
Model	df	AICc	ΔAICc	LL	df	AICc	ΔAICc	LL	df	AICc	ΔAICc	LL
(1|FishID)	5	168.64	68.05	-79.30	5	-41.42	60.78	25.74	5	505.64	162.83	-247.81
(Age|FishID)	7	100.61	0.01	-43.27	7	-85.84	16.36	49.98	7	439.01	96.20	-212.48
(Age|FishID) + (1|Year)	8	102.54	1.95	-43.23	8	-83.80	18.39	49.98	8	389.64	46.83	-186.78
(Age|FishID) + (1|YearClass)	**8**	**100.59**	**0**	**-42.26**	8	-84.70	17.50	50.43	8	437.44	94.63	-210.68
(Age|FishID) + (Age|Year)	10	104.45	3.86	-42.16	10	-101.05	1.14	60.65	10	357.52	14.71	-168.70
(Age|FishID) + (Age|YearClass)	10	104.63	4.03	-42.25	10	-87.83	14.37	54.03	10	437.81	95.00	-208.85
(Age|FishID) + (1|Year) + (1|YearClass)	9	102.54	1.94	-42.22	9	-82.66	19.54	50.43	9	387.26	44.45	-184.59
(Age|FishID) + (Age|Year) + (1|YearClass)	11	104.15	3.55	-41.00	11	-98.18	4.02	60.23	11	356.05	13.24	-166.95
(Age|FishID) + (1|Year) + (Age|YearClass)	11	106.58	5.98	-42.21	11	-85.78	16.42	54.03	11	379.52	36.71	-178.69
(Age|FishID) + (Age|Year) + (Age|YearClass)	13	108.20	7.61	-41.00	**13**	**-102.20**	**0**	**64.30**	**13**	**342.81**	**0**	**-158.31**

Table 6. Selection for base model fixed effect structures (highlighted in **bold**) for each growth comparison (i to iv) first fit with estimates of maximum likelihood (ML) and refitted with restricted estimates of maximum likelihood (REML). Conditional (c) R^2 values were calculated after models were refit with REML. LL: log likelihood

Growth Comparison		Fixed Effect Structure	df	AICc	ΔAICc	LL	R^2c
i	Across species and regions	**Age**	**15**	**-360.91**	**0**	**195.52**	**0.876**
		Age + AgeCap	16	-359.34	1.58	195.74	0.877
ii	Among species within a region	**Age**	**11**	**-144.71**	**0**	**83.44**	**0.899**
		Age + AgeCap	12	-143.27	1.44	83.73	0.901
iii	Within species among regions	**Age**	**13**	**-702.63**	**0**	**364.40**	**0.885**
		Age + AgeCap	14	-700.70	1.94	364.44	0.886
iv	Species and region specific						
	HP - KI	**Age**	**6**	**-127.77**	**0**	**69.99**	**0.873**
		Age + AgeCap	7	-126.19	1.59	70.22	0.874
	HP - BC	**Age**	**12**	**-546.23**	**0**	**285.20**	**0.894**
		Age + AgeCap	13	-544.20	2.03	285.20	0.894
	HP - NSW	**Age**	**9**	**-216.08**	**0**	**117.15**	**0.900**
		Age + AgeCap	10	-214.23	1.85	117.25	0.901
	HB - NSW	**Age**	**7**	**80.88**	**0**	**-33.41**	**0.864**
		Age + AgeCap	8	82.42	1.54	-33.17	0.865
	Hspp - WNZ	**Age**	**12**	**-118.88**	**0**	**71.61**	**0.877**
		Age + AgeCap	13	-118.61	0.27	72.51	0.880
	Hspp - ENZ	**Age**	**12**	**325.58**	**0**	**-150.71**	**0.847**
		Age + AgeCap	13	326.53	0.95	-150.17	0.848

(among species within a region) and iv (species and region specific). A series of interactions were applied between the best supported broad scale climatic parameter and uncorrelated local scale parameters (Supplementary Table 4). We used the statistical programming environment of R 3.0.3 with the packages of 'lme4' ('lmer' function; Bates et al. 2014), 'effects', and 'AICcmodagv' (Mazerolle 2015) to perform analyses (R Development Core Team 2014). Additionally, the 'Hmisc' package ('rcorr' function; Harrell 2014) was used to produce pairwise Pearson's correlation coefficients (Harrell 2014) to compare among the climatic/oceanographic variables. Annual growth increment width (*Growth*) and age related data (*Age*, *AgeCap*) were natural-log transformed to meet model assumptions and all fixed predictor variables were mean centred to assist model convergence and interpretation of interaction terms (Morrongiello et al. 2014, Morrongiello and Thresher 2015). The relative support for each model was tested using Akaike's Information Criterion (*AIC*) corrected for small sample sizes (*AICc*) (Burnham and Anderson 2004). The proportion of variance for fixed effects alone and combined fixed and random effects in the models were estimated using marginal and conditional R^2 metrics for mixed-effects models (Nakagawa and Schielzeth 2013, Johnson 2014). For growth comparisons i to iii, truncated datasets were used that spanned common time periods (Table 1).

Growth data contained repeated yearly measures from individual fish across multiple years. Random effects structures were comprised of both random intercepts combined with random slopes, which differed for each of the growth comparisons. All comparisons contained random intercepts for *FishID*, *Year*, *YearClass* (Table 2 for descriptions) in combination with random slopes for *Age*. *FishID*, *Year*, and *YearClass* added as random intercepts generate correlations among growth increments within each fish, within a year, or among fish born in the same year, respectively. *FishID* as a random intercept enabled individual fish growth to vary in comparison to the model average, while *Year* gives temporally resolved (annual) estimates of whether good or poor growth conditions were provided by the environmental drivers relative to the long term mean. Likewise, *YearClass* provides a similar temporal estimate to *Year* but is an estimate of growth conditions for groups of fish over their lifetimes (Morrongiello et al. 2014, Morrongiello and Thresher 2015). Random *Age* slopes permit the fixed effect *Age* ~ *Growth* relationship to vary based on the random intercept with which it is associated and allows age dependant trends to be

inferred. To compare among regions (i and iii) or species (ii), additional random intercept terms of *Location* or *Species* were added, respectively (Table 2 and 4). For these additional terms, *Year* or *YearClass* was nested within *Location* or *Species* and had random slopes of *Age* or *AgeCap*. Nested terms generated temporal correlations among growth increments within a given species or location. The *AgeCap* term helps to identify growth-based selectivity that may occur in a species and corrects for sampling biases (Morrongiello et al. 2012, Morrongiello and Thresher 2015).

Chronologies for all growth combinations were produced by extracting the *Year* random effect conditional modes (best linear unbiased predictors 'BLUPs') from the best *Year* only model created during the hierarchal modelling procedure (e.g. Table 4) (Morrongiello and Thresher 2015). We extracted estimates of temporal growth synchrony across individuals for each comparison (i-iv) by calculating the interclass correlation coefficient (ICC) based on a model containing random intercepts for both *FishID* and *Year* (random *Age* slope for *FishID* only) with the full set of fixed effects (Morrongiello and Thresher 2015). Temporal growth synchrony is the amount of correlation of growth increments among individuals through time (Morrongiello and Thresher 2015). Additionally, a temporal fixed *Year* effect was added to each optimal model of growth comparison iv (without environmental variables) to examine general growth trends of species with their specific habitats through time.

Results:

For all growth comparison analyses (i-iv), the most important factor determining variation in *Helicolenus* growth rate was *Age*, with all growth rates declining with increasing age (Fig. 2a). There was a positive temporal growth trend for all species within their local region, but each had different slopes and intercepts through time (Fig. 2b). After accounting for age effects, growth varied substantially among years for all species and regions, although the magnitude of the variation differed (Fig. 3, 4). Localised climatic/oceanographic parameters of sea level and sea level pressure (two parameters common to all species locales) generated unique growth responses of ocean perches in our study region (Fig. 2c, 2d).

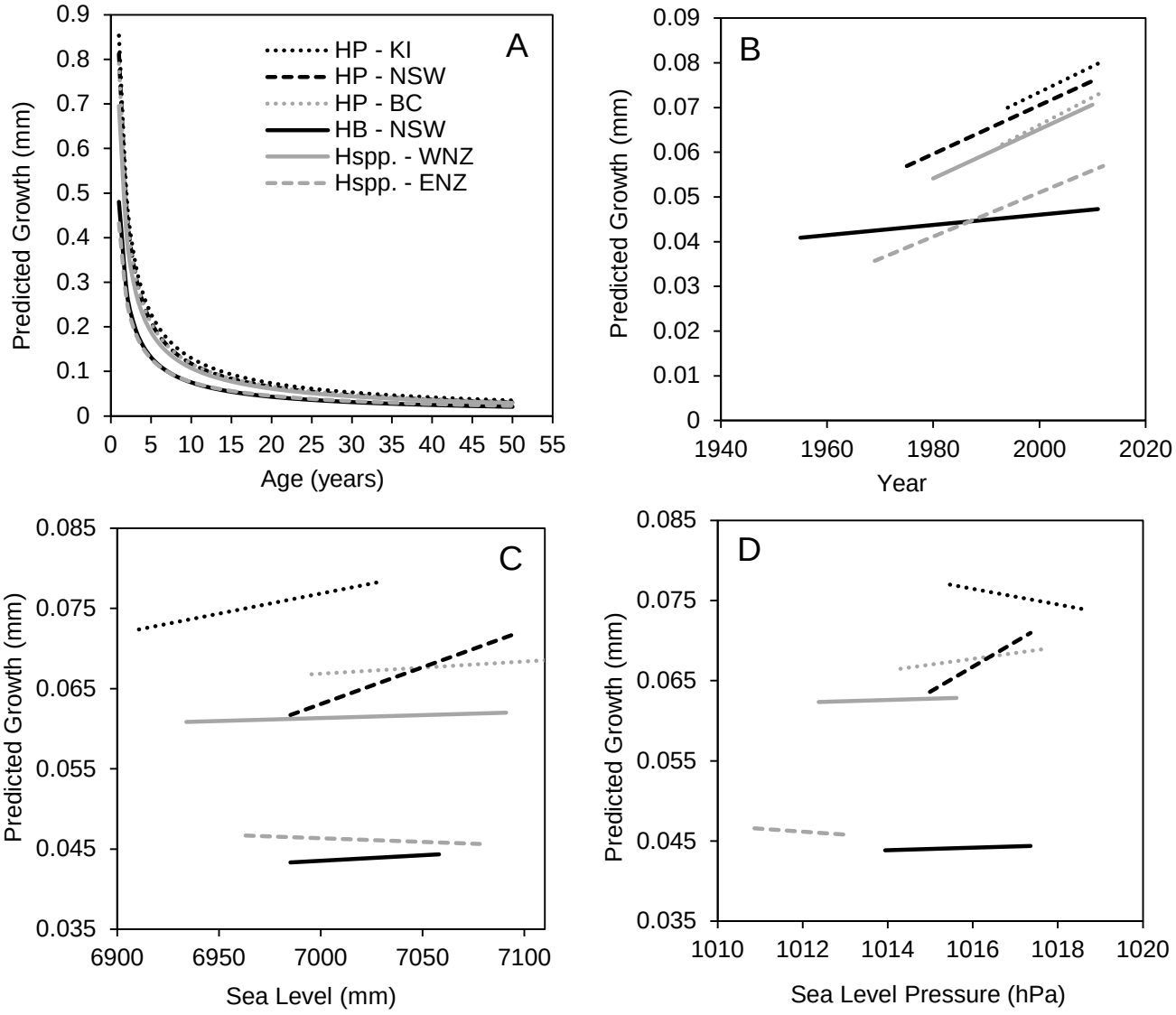

Fig. 2. Predicted growth effects of individual *Helicolenus* species from different regions (growth comparison iv) with age (A), time (temporal year trend, B), local sea level (C), local sea level pressure (D). Species and region codes correspond to those used in Fig. 1.

Fig. 3. (on following page) Predicted annual growth for *Helicolenus* in the southwest Pacific region with key, broad-scale, climatic/oceanographic variables. Growth increment chronologies (solid lines) are produced from the *Year* random effect term (best linear unbiased predictors 'BLUPs') (± 1 SE). Dashed lines represent the broad-scale variable that accounted for the most variance within each optimal model. Predicted growth scales differ on the y axis.

Fig. 3

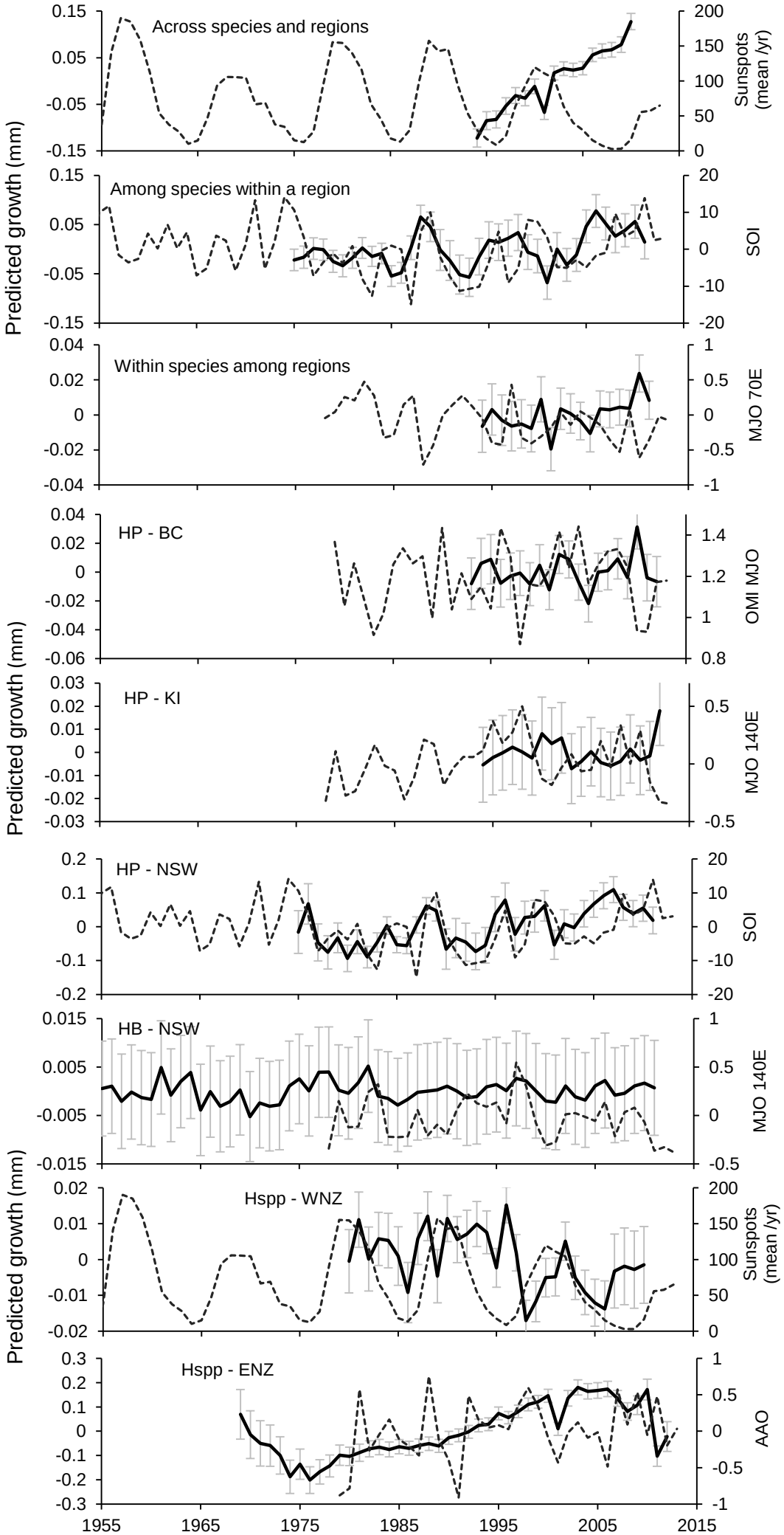
Across species and regions
Sunspots (mean /yr)
Among species within a region
SOI
Within species among regions
MJO 70E
HP - BC
OMI MJO
HP - KI
MJO 140E
HP - NSW
SOI
HB - NSW
MJO 140E
Hspp - WNZ
Sunspots (mean /yr)
Hspp - ENZ
AAO
Predicted growth (mm)
Predicted growth (mm)
Predicted growth (mm)
1955
1965
1975
1985
1995
2005
2015

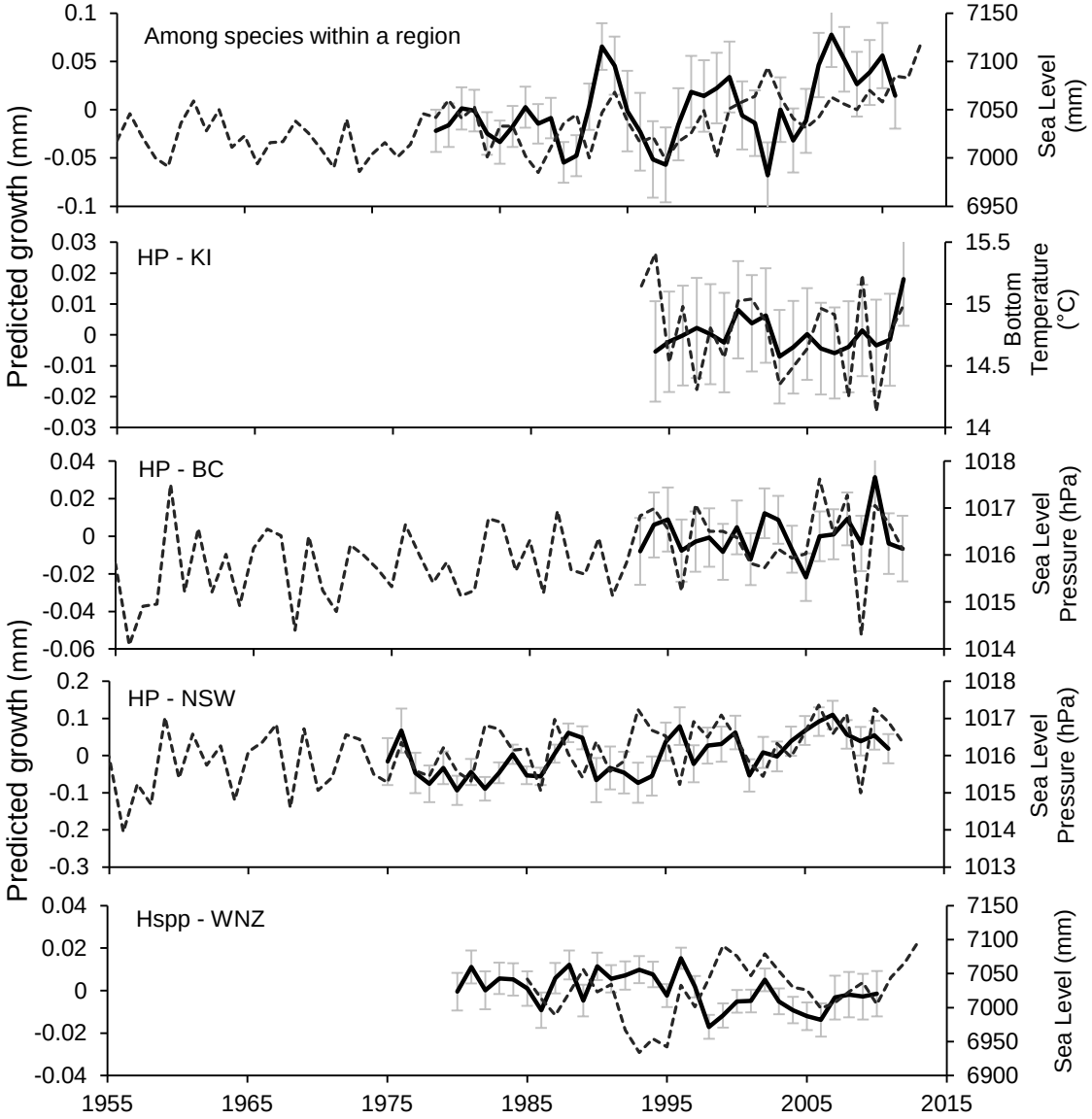

Fig. 4. Predicted annual growth for *Helicolenus* in the southwest Pacific region with key, local-scale, climatic/oceanographic variables. Growth increment chronologies (solid lines) were produced form the *Year* random effect term (best linear unbiased predictors 'BLUPs') (± 1 SE). Dashed lines represent the local-scale variable that accounted for the most variance within each optimal model. Predicted growth scales differ on the y axis.

Different slopes and intercepts of growth and directional responses were evident for every species and region.

In all optimal models, the best fixed effect structure included *Age* only (Table 6). The best random structures had the common term of *FishID* as a random intercept with a random *Age* slope, which means the *Growth ~ Age* relationship varied among individuals (Tables 4 and 5). Subsequently, all optimal models became more complex and comprised various combinations of *Year* and/or *YearClass* as random intercepts (nested within *Location* or *Species* where appropriate), usually with random *Age* slopes. Random *Age* slopes on *Year*, *YearClass*, *Location* or *Species* suggests that *Growth ~ Age* varies among years, birth years, locations and/or species, respectively (Tables 4 and 5).

Across species and regions (i)

Broad-scale drivers of growth across all *Helicolenus* species and regions were examined at the genus level from the *Locations* of Kangaroo Island, SA to the Chatham Rise, New Zealand, spanning ~3000 km (Fig. 1a). This growth record covered 1994 to 2010, the time period common to all *Helicolenus* chronologies (17 yrs, Fig. 3). The optimal model included the fixed effect of *Age* and a random effect structure with random *Age* slopes for random intercepts of *FishID*, *Location*, *Year*, and *YearClass* (Table 4 and 6). Thus, within the entire geographical region, growth rates of *Helicolenus* varied across individuals, across locations, across cohorts and through time. Growth synchrony for the overall region was 7.4% (Table 7).

Solar activity (number of *Sunspots* per year) had the most influence on fish growth across all six different *Helicolenus* populations in what is a multi-basin oceanic region (Supplementary Table 2; Fig. 3). Growth declined 3% as solar activity increased (Table 8 and 9). Not all broad-scale climatic/oceanographic variables added to the optimal model improved model performance (Supplementary Table 2).

Among species within a region (ii)

We explored the influence of broad and localised climate/oceanographic variables on interspecific growth between *H. barathri* and *H. percoides* from southeastern NSW (Fig. 1a).

Table 7. Intraclass correlation coefficients (ICC) of the growth comparisons (i to iv) for *Year*

Growth Comparison		ICC Year (%)
i	Across species and regions	7.4
ii	Among species within a region	2.8
iii	Within species among regions	0.7
iv	Species and region specific	
	HP-KI	0.4
	HP-BC	1.4
	HP-NSW	5.3
	HB-NSW	0.1
	Hspp -WNZ	1.2×10^{-14}
	Hspp -ENZ	15.0

Table 8. Parameter estimates and test statistics for optimal models, and broad- and local-scale environmental models with best climatic/oceanographic variables. Where an interaction term is the best environmental parameter (*), the two parameters making up that term are also included.

Growth Comparison		Model	Parameter	Fixed effects		
				Estimate	±SE	t-statistic
i	Across species and regions	Optimal	Intercept	-2.8026	0.0242	-115.96
			Age	-0.7807	0.0333	-23.47
		Broad	*Sunspots*	-0.0003	0.0001	-1.99
ii	Among species within a region	Optimal	Intercept	-3.0631	0.0407	-75.23
			Age	-0.8276	0.0189	-43.71
		Broad	SOI	0.0031	0.0014	2.23
		Local	SeaLevel	0.0014	0.0004	3.21
			YearSLP	0.0372	0.0153	2.43
iii	Within species among regions	Optimal	Intercept	-2.6612	0.0136	-196.12
			Age	-0.8025	0.0231	-34.72
		Broad	MJOindex70E	-0.0466	0.0276	-1.69
iv	Species and region specific					
	HP - BC	Optimal	Intercept	-2.6925	0.0242	-111.23
			Age	-0.8275	0.0405	-20.41
		Broad	*OMImjoAmplitude*	-0.1162	0.0457	-2.55
		Local	*YearSLP*OMImjoAmplitude*	-0.2036	0.0803	-2.54
			YearSLP	0.0136	0.0077	1.76
			OMImjoAmplitude	-0.0521	0.0441	-1.18
	HP - KI	Optimal	Intercept	-2.5845	0.0175	-148.15
			Age	-0.8170	0.0261	-31.35
		Broad	*MJOindex140E*	-0.1237	0.0473	-2.62
		Local	*YearBotTemp*MJOindex140E*	-0.4775	0.1887	-2.53
			MJOindex140E	-0.1290	0.0574	-2.25
			YearBotTemp	0.0417	0.0374	1.12
	HP - NSW	Optimal	Intercept	-2.7012	0.0217	-124.67
			Age	-0.8395	0.0275	-30.49
		Broad	*SOI*	0.0056	0.0022	2.59
		Local	*YearSLP*	0.0664	0.0228	2.91
			SeaLevel	0.0017	0.0006	2.87
	HB - NSW	Optimal	Intercept	-3.1210	0.0142	-219.61
			Age	-0.8041	0.0147	-54.83
		Broad	*MJOindex120E*	0.0789	0.0447	1.76
		Local	*MJOindex120E*	0.0789	0.0447	1.76
	Hspp. - WNZ	Optimal	Intercept	-2.7714	0.0164	-169.11
			Age	-0.8109	0.0311	-26.08
		Broad	*Sunspots*	-0.0003	0.0002	-1.53
		Local	*SeaLevel*	0.0001	0.0002	0.63
	Hspp. - ENZ	Optimal	Intercept	-3.0757	0.0244	-126.31
			Age	-0.7534	0.0344	-21.92
		Broad	*AAO*	0.0423	0.0212	1.99
		Local	*AAO*	0.0423	0.0212	1.99

Table 9. Predicted climate effects on fish growth (% change) over the environmental range to which the fish were exposed. Where an interaction term is the best environmental parameter (*), the two parameters making up that term are also included.

Growth Comparison		Model	Parameter	Range (units)	Predicted Effects (% change)	
					across range	per unit
i	Across species and regions	Broad	*Sunspots*	2.9 - 119.6 (num·yr^{-1})	-3.19	-0.03
ii	Among species within a region	Broad	*SOI*	-14.9 - 13.9	9.25	0.31
		Local	*SeaLevel*	6985 - 7094 (mm)	10.97	0.10
			YearSLP	1015.0 - 1017.4 (hPa)	4.35	17.77
iii	Within species among regions	Broad	*MJOindex70E*	-0.6 - 0.4	4.99	4.46
iv	Species and region specific					
	HP - BC	Broad	*OMImjoAmplitude*	0.8 - 1.4	-11.65	-6.86
		Local	*YearSLP*OMImjoAmplitude*			
			YearSLP	1014.3 - 1017.6 (hPa)	3.66	1.09
			OMImjoAmplitude	0.9 - 1.4	-11.65	-6.86
	HP - KI	Broad	*MJOindex140E*	-0.3 - 0.5	-10.79	-13.85
		Local	*YearBotTemp*MJOindex140E*			
			YearBotTemp	14.1 - 15.4 (°C)	4.86	36.56
			MJOindex140E	-0.3 - 0.5	-10.79	-13.85
	HP - NSW	Broad	*SOI*	-14.9 - 13.9	17.54	5.59
		Local	*SeaLevel*	6985 - 7094 (mm)	16.16	0.14
			YearSLP	1015.0 - 1017.4 (hPa)	11.52	45.53
	HB - NSW	Broad	*MJOindex120E*	-0.4 - 0.5	7.43	7.99
		Local	*MJOindex120E*	-0.4 - 0.5	7.43	7.99
	Hspp - WNZ	Broad	*Sunspots*	2.9 - 157.6 (num·yr^{-1})	-4.05	-0.02
		Local	*SeaLevel*	6934 - 7091 (mm)	1.89	0.01
	Hspp - ENZ	Broad	*AAO*	-0.9 - 0.8	7.28	4.42
		Local	*AAO*	-0.9 - 0.8	7.28	4.42

This growth chronology spanned 37 years from 1975 to 2011 (Fig. 3). The random effect structure included in the optimal model contained *FishID*, *Species*, *Year*, and *YearClass* random intercepts, but with a random *Age* slope only for *FishID* and *Year* nested within *Species*; *Age* was the sole fixed effect (Table 4 and 6). Fish growth in NSW varied by year within a species and across individuals. Growth synchrony among *H. percoides* and *H. barathri* was 2.8% (Table 7).

For this analysis, both broad- and local-scale models were used to examine drivers of among species fish growth. The *SOI* was the best explanatory broad- scale driver, while, at the local level, there was an additive effect between sea level pressure (*YearSLP*) and sea level (*SeaLevel*) on growth (Supplementary Table 2 and 4, Fig. 3). Between the two *Helicolenus* species, fish growth in the NSW region increased as the SOI increased (Table 9) and also showed positive growth with an increase in both sea level and sea level pressure (Table 8 and 9).

Within species among regions (iii)

Intraspecific growth responses of *H. percoides* were compared to broad climatic/oceanographic variables across southeastern Australia and included the *Locations* of Kangaroo Island (SA), Bonney Coast (SA) and southeastern NSW (Fig. 1a). The growth chronology extended over the years of 1994 to 2012 (19 yrs, Fig. 3). In this optimal model, *Age* was, again, the only fixed effect. The random effects structure contained random intercepts of *FishID*, *Location*, *Year*, and *Yearclass* with random *Age* slopes on *FishID*, and *Year* and *YearClass* nested within *Location* (Table 4 and 6). This indicates that fish growth of *H. percoides* in southeastern Australia varies across individuals and by year and cohort within each location. Less than 1% growth synchrony was observed among the *H. percoides* populations (Table 7).

The MJO Index centred at 70°E (*MJOindex70E*) was the broad-scale driver that best correlated with regional growth of *H. percoides* in southeastern Australia (Supplementary Table 2, Fig. 3). Fish growth declined 5% (over the range of the MJO experienced) as the convectively active phase of MJO centred at 70°E became less negative (Table 8 and 9). Weatherwise, this generally equates to a lack of anomalous low-level zonal (850 hPa) winds

or rainfall over southeastern Australia in November to April (Bureau of Meteorology Australian Government 2015a, NOAA/National Weather Service 2015), which is the growing season of *H. percoides* (Chapter 5; Paul and Horn 2009).

Species and region specific (iv)

Finally, we correlated the individual growth response of each *Helicolenus* species (2 species and 2 species complexes) within their local regions in southeastern Australia and New Zealand with both broad- and local-scale climatic/oceanographic variables (Fig. 3 and 4). Based on optimal models for each species/region (described below), two different growth rates were evident (Fig. 2a). We observed a lower growth rate in *H. barathri* and the species complex from eastern New Zealand (Hspp.-ENZ) and a faster growth rate in all *H. percoides* and the species complex from western New Zealand (Hspp.-WNZ). The slower growing populations (*H. barathri* and Hspp.-ENZ) also exhibited lower overall growth through time (Fig. 2b) and lower overall growth responses in changes to sea level or sea level pressure (Fig. 2c-d). Temporal growth rates were similar for all populations of *H. percoides* (Fig. 2b), but varied markedly in relation to local sea level or sea level pressure (Fig. 2c-d). The NSW *H. percoides* (HP-NSW) population had a much steeper growth rate than all other populations relative to sea level and sea level pressure, while the slower growing fish (HB-NSW and Hspp.-ENZ) displayed only slight changes in growth related to sea level pressure or sea level (Fig. 2c-d). *Helicolenus percoides* from Kangaroo Island (HP-KI) had the fastest growth rate as well as different directional growth responses to sea level (+) and sea level pressure (-). All optimal models included an *Age* only fixed effect (Table 6).

H. percoides, Bonney Coast (HP-BC)

The chronology for *H. percoides* along the Bonney Coast, SA covered 20 years from 1993 to 2012 (Fig. 3). The optimal model contained a random effect structure of *FishID*, *Year* and *YearClass* as random intercepts and random slopes of *Age* (Table 6). Therefore, fish growth within the Bonney Coast varied among individuals, years and year classes. Growth synchrony within the population was 1.4% (Table 7).

The outgoing longwave radiation MJO index (*OMImjoAmplitude*) was the broad-scale climatic driver that was most correlated with growth of HP-BC (Supplementary Table 3,

Table 8, Fig 3). Growth decreased (increased) as the MJO index increased (decreased). In the local-scale model, the best explanatory variable associated with growth was an interactive effect between sea level pressure (*YearSLP*) and the outgoing longwave radiation MJO index (*OMImjoAmplitude*), where growth decreased with the increasing effects of the MJO and sea level pressure (Supplementary Table 4, Table 8, Fig. 4). Growth decreased ~12% over the range of the MJO index experienced by the fish, but increased ~4% in relation to sea level pressure (Table 9).

H. percoides, Kangaroo Island (HP-KI)

Growth of *H. percoides* from Kangaroo Island fluctuated through time but with a general increasing trend (Fig. 3). This chronology extended from 1994 to 2012 (19 yrs). The optimal model included only *FishID* as a random intercept with a random *Age* slope (Table 5). However, the next highest ranked model included a random *Year* intercept, which was used to extract the random year effects (BLUPs) to compare with the climatic/oceanographic variables. The optimal model indicated fish growth varied across individuals. Growth synchrony was very low at < 1% (Table 7).

Growth variation through time was most correlated with the broad-scale predictor of the MJO Index centred at 140° (*MJOindex140E*) (Supplementary Table 3, Fig. 3). As the convectively active phase of MJO centred at 140°E became less negative, fish growth declined (Table 8). At the local-scale, the best explanatory parameter was an interaction between *MJOindex140E* and bottom temperature (*YearBotTemp*) that resulted in a negative effect on growth (Supplementary Table 4, Table 8). Growth was reduced by ~11% over the range of the MJO 140°E index and increased ~5% over the range of the bottom temperatures (Table 9).

H. percoides, southeastern NSW (HP-NSW)

The growth record spanned 1975 to 2011 (37 yrs) with an increasing trend through time (Fig. 3). Fish growth varied among individuals and by year with a growth synchrony of 5.3% (Table 7). A random effects structure of *FishID* and *Year* with random *Age* slopes formed the optimal model (Table 5).

Annual growth was broadly driven by the *SOI* (Supplementary Table 3, Fig. 3), and locally by an additive effect of sea level pressure (*YearSLP*) and sea level (*SeaLevel*) (Supplementary Table 4, Fig. 4). Growth increased with increases in the environmental parameters by 17.5% over the range of the SOI, 16.2% with sea level and 11.5% with sea level pressure (Table 9).

H. barathri, southeastern NSW (HB-NSW)

The growth record for *H. barathri* in NSW was the longest chronology, stretching over 57 years from 1955 to 2011. There was very little growth synchrony (Table 7) or fluctuations through time (Fig. 3). Similar to HP-KI, the optimal model (Table 5) did not contain a random intercept for Year, and a comparable procedure was used to extract the BLUPs for climatic/oceanographic comparison. There was a large degree of growth variation among individuals (random *Age* slope on *FishID* random intercept).

In both the broad and local-scale models, fish growth was most correlated with the broad-scale MJO Index centred at 120° (*MJOindex120E*) (Supplementary Table 3 and 4, Fig 3.). Growth increased as the convectively active phase of MJO centred at 120°E became less negative (Table 8). Over the range of the MJO 120°E Index experienced by *H. barathri*, growth increased 7.4% (Table 9).

Helicolenus species complex, western New Zealand (Hspp.-WNZ)

The *Helicolenus* species complex from western New Zealand produced a chronology that covered 31 years from 1980 to 2010. Growth synchrony within the population was again < 1%. Fish growth varied among individuals, by year and year class, as the optimal model included random *Age* slopes on all random intercepts (Table 5).

Broad-scale growth variation was most attributed to solar acidity (*Sunspots*, Supplementary Table 3), while the most influential local-scale parameter was sea level (*SeaLevel*, Supplementary Table 4). Increasing solar activity caused fish growth to decrease ~4% over the parameter range; conversely, growth increased with increasing sea level by ~2% (Table 9, Fig. 3 and 4).

Helicolenus species complex, Chatham Rise, New Zealand (Hspp.-ENZ)

Growth was the most synchronous (15%) in the *Helicolenus* species complex from eastern New Zealand on the Chatham Rise. This growth record extended over 44 years from 1969 to 2012 (Fig. 3). The optimal model suggested growth varied among individuals, by year and by year class (random *Age* slopes on all random intercepts; Table 5).

At both the broad and local scales, growth was most influenced by the *AAO* (Antarctic Oscillation; Supplementary Table 3 and 4). Fish growth increased as the AAO increased (Fig. 3, Table 8) by 7.3% over the range of the AAO experienced (Table 9).

Discussion:

Long-term growth responses derived from the otoliths of *Helicolenus* species from southern Australia and New Zealand revealed the synergistic effects of climate forcing within local environments on fish growth. We compared chronologies of fish growth across multiple regions and species with broad- and local-scale climatic/oceanographic variables using univariate mixed-effects models to account for biological influences on growth. Age was a key intrinsic driver of growth, and partitioning this allowed other sources of variability to be extracted from the growth record. Across the entire study region (~3000 km distance), age-dependent growth of ocean perches varied among years, cohorts, locations and *Helicolenus* species. In each local region, different combinations of climatic/oceanographic variables affected species specific growth.

Growth synchrony

We detected a collective, temporal growth signal, across 3000 km and parts of three ocean basins, despite the low synchrony in the individual *Helicolenus* populations. At this geographic scale only very large-scale climatic drivers should be detectable (Morrongiello and Thresher 2015). In our case, solar activity was the leading harmonizer, and growth declined with increased solar activity. The MJO index centred at 140°E (*MJOindex140E*) was ranked second to solar activity during model selection, and growth increased as the MJO became more positive (i.e. growth was better when the MJO situated at 140°E was weak). Very simply, the MJO index describes enhanced or supressed convection in the tropics that

begins over the Maritime Continent and propagates eastward over 30 to 60 days. The MJO is a key driver of variation in intraseasonal rainfall and atmospheric circulation in Australia and New Zealand (Risbey et al. 2009, Wheeler et al. 2009). Solar activity enhances the MJO during periods of solar maxima (solar activity increases cloudiness and, at times of solar maxima, causes the MJO to become more negative) (Takahashi et al. 2010). During the solar maxima in the early 2000s, fish growth decreased dramatically across the entire study region. Three other MJO indices were also ranked above the optimal growth model, but below solar activity. This suggests there are multiplicative effects of climate acting on fish growth.

This study is the first investigation of climate forcing in multiple fish species over a broad region. Currently, there are a few single species studies (e.g. Black et al. 2014, Thresher et al. 2014) that have attempted to gauge climate forcing by using fish growth as a proxy. Growth records from juvenile orange roughy (*Hoplostethus atlanticus*) revealed a bihemispheric oceanic response of climate forcing from the subpolar annular modes of both hemispheres (NH: North Atlantic Oscillation, SH: SAM) on intermediate water mass temperatures (Thresher et al. 2014). Black et al. (2014) described broad physical-ecological connections in the Pacific northeast region forced by ENSO from chronologies sourced from fish, trees, birds and zooplankton.

Within NSW, the SOI was the principal broad-scale driver for growth of *H. percoides* and *H. barathri*, with an additive local effect of sea level and sea level pressure. Fish growth was positively related to SOI (a measurement of the intensity of an ENSO event). During a sustained positive SOI (La Niña), the climate in southeastern Australia/New Zealand is cooler with more rainfall and physical disturbances (Holbrook et al. 2009). A major oceanographic feature within this region is the East Australian Current (EAC), the large western boundary current of the South Pacific Gyre (Ridgway and Dunn 2003). However, limited ENSO variability has been detected within the EAC.

Sea level variations in the Pacific basin are also regulated by ENSO, as well as a range of other factors, including thermal expansion through warming and melting sea ice (Walsh et al. 2012). ENSO modifies sea level in the Pacific through a ‘bath tub’-like sloshing effect of

Kelvin and Rossby waves. Eastward moving Kelvin waves, caused by westerlies blowing over the Pacific, deepen the thermocline in the east Pacific and increase sea level. Then, Kelvin waves 'bounce' off South America, producing internal, westward propagating Rossby waves that cause the thermocline to deepen in the west and increases sea level (Glantz 2001). Incoming Rossby waves also increase EAC transport, thereby connecting sea level, ENSO and the EAC along the NSW coast (Holbrook et al. 2011). Variations in the EAC (e.g. temperatures, transport) and thermocline depth (i.e. impacts on food resources) would lead to changes in fish growth (Holbrook et al. 2009).

The growth synchrony between *H. percoides* in SA and NSW was quite small. The populations inhabit two different ocean basins with potentially no overarching growth synchronizer between the two regions. In other words, the NSW coast is dominated by the EAC (regulated by physical processes of the main Pacific basin) while the Bonney Coast and Kangaroo Island are under the influence of the Flinders current (with regular seasonal upwelling; Middleton and Bye 2007) and are geographically part of the Indian Ocean.

Annual growth synchrony varied between all individual regions and species, with the least seen in the *Helicolenus* species complex from western New Zealand (< 1%), whilst the *Helicolenus* species complex on the Chatham Rise east of New Zealand was most synchronous (15%). Growth synchrony reported in other marine fish populations is generally higher at around 50 to 80% (e.g. Black et al. 2008, Black et al. 2011, Gillanders et al. 2012). However, many species of fish have much lower levels of within-population growth synchrony (2 to 20%; Rountrey et al. 2014, Morrongiello and Thresher 2015, Nguyen et al. 2015). Lack of synchrony may reflect growth complacency in a species (i.e. low annual growth variation), an environment where climate signals are dampened (e.g. deep ocean depths), and/or variations in local microhabitat quality (e.g. food resources, habitat structure). Thus, variability in individual growth can increase, and subsequent integration into a population-level growth response adds unexplained variation and diminishes synchrony (Morrongiello and Thresher 2015). In such cases, mixed-effects modelling approaches tend to be more effective for extracting environmentally driven growth variability (Morrongiello et al. 2012) rather than dendrochronological techniques as

pioneered in the northeast Pacific region where strong climate signals prevail (Black et al. 2014).

Growth variation

The magnitude of the year to year variation within the individual growth chronologies varied substantially across the entire study region. Interannual growth variability in two chronologies was at least an order of magnitude larger than the others: Hspp.-ENZ and HP-NSW. Interannual growth variability of the *Helicolenus* species complex found on the Chatham Rise of New Zealand (Hspp.-ENZ) was much larger, especially compared with the neighbouring *Helicolenus* spp. growth record on the Challenger Plateau west of New Zealand (Hspp.-WNZ). This is potentially due to the energetics of the two regions. The Chatham Rise is one of the most productive areas around the New Zealand landmass due to active upwelling. Benthic-pelagic coupling is strong in this region; high levels of particulate organic carbon (POC) reaching the benthos mirror surface primary productivity (Ministry for Primary Industries 2013). Conversely, the oceanography around the Challenger Plateau is much less dynamic, as it is fed by weak eastward flow crossing the southern Tasman Sea (Ridgway and Dunn 2003). This region is not as productive, being nutrient limited (Ministry for Primary Industries 2013). A similar situation is found along the coast of NSW where the *H. percoides* chronology from NSW (HP-NSW) originates. The coast of NSW would be comparable in terms of ocean dynamics to the Chatham Rise area, since it is dominated by the EAC. The stronger oceanographic dynamics of the Chatham Rise and NSW regions may reduce individual variation in fish growth by acting as environmentally-based synchronizers.

Annual growth variation of *H. barathri* in NSW was much lower than in all other chronologies. *Helicolenus barathri* lives at deeper depths (peak abundances ~600 m) than its counterpart, *H. percoides* (peak abundances ~150 m) (Park 1993, Smith et al. 2009, Bentley et al. 2014). In southern NSW, the EAC is weaker at the deeper depths of *H. barathri* than at the shallower depths of *H. percoides* (Sokolov and Rintoul 2000, Ridgway and Dunn 2003). Therefore, the EAC signal may not be a strong growth synchronizer for fish populations in deeper depths. Additionally, since the otolith specimens came from commercial fishing activities, we lacked the ability to pinpoint the exact location of each individual included in the growth chronology. Therefore, the fish incorporated into this

growth record were likely to have experienced many different microhabitats resulting in greater individual variation in growth.

Age-dependent growth

Age accounted for the majority of growth variance in the fish (~70 to 80%), which was expected. It was, however, unexpected to see two distinct, age-related growth rates within our *Helicolenus* species, particularly with respect to the species complexes from New Zealand. Genetic analyses have detected a third, undescribed species of ocean perch inhabiting New Zealand waters on the Norfolk Ridge, Kermadac Ridge, and Chatham Rise (Smith et al. 2009). The undescribed species is thought to have a similar life history to *H. barathri*, as it resides in deeper waters and reaches comparable older ages (Smith et al. 2009, Bentley et al. 2014). Our results show *H. barathri* has lower growth rates than *H. percoides*. Comparing the two New Zealand species complexes to our known species reveals similar growth rates of Hspp.-ENZ to *H. barathri* and Hspp.-WNZ to *H. percoides*. These growth rate patterns are also evident in the linear temporal growth trend as well as in predicted effects of local oceanographic parameters on growth; growth of *H. barathri* and Hspp.-ENZ are always lower compared to all *H. percoides* populations and Hspp.-WNZ. Furthermore, the range of *H. barathri* does not extend to the eastern side of New Zealand (Smith et al. 2009, Bentley et al. 2014). For these reasons, we suggest the fish of Hspp.-WNZ are likely *H. percoides*, and Hspp.-ENZ represents a population of the undescribed ocean perch (referred to as the 'CR–KR–NR' clade; Smith et al. 2009).

Growth responses and the environment

Within our analyses, broad-scale climate variability typically correlated with greater changes in growth than local parameters, again demonstrating climate forcing affects fish growth. Broad scale climate patterns and weather can have effects on the environment that are amplified or dampened depending on the type of interaction (Stenseth et al. 2004, Brierley and Kingsford 2009, Travers-Trolet et al. 2014). The MJO represents direct ocean-atmospheric coupling and indirectly affects deep water fish growth in the southwest Pacific with changes to both the surface and deep water layers. A temperature change of ± 1°C in the equatorial ocean mixed layer can occur in a strong MJO event due to fluxes of solar radiation (changes in cloudiness) and cooling/heating from changes in wind speeds

(Shinoda et al. 1998). MJO events also generate eastward propagating oceanic equatorial Kelvin waves that reach depths of 1500 m and may enhance or trigger ENSO events (Matthews et al. 2007). Additionally, the MJO intraseasonally forces the SAM in both the austral summer and winter (Matthews and Meredith 2004, Carvalho et al. 2005).

Temporal magnitude and environmental directionality of growth responses differed substantially between the separate *Helicolenus* populations. In all populations, growth increased through time. Interestingly, Hspp.-ENZ had a similar annual growth rate to the shallower living *H. percoides* populations, although the age-dependant growth rate was the same as *H. barathri*. This, again, may be due to the dynamic and productive nature of the Chatham Rise area (Ministry for Primary Industries 2013). The annual growth rate of *H. barathri* was much lower compared to all other species; this may reflect the deeper depth at which the fish is living (Koslow et al. 2000) or lower quality habitat (i.e. decreased food availability, sub-optimal temperature for growth; Arendt 1997), or a combination of the two.

Predicted growth over the range of local sea level and sea level pressure experienced by the fish showed different environmental directionality for each population. Generally, growth increased with increasing sea level for all *Helicolenus* populations, except Hspp.-ENZ. The greatest rate of increased growth with sea level was seen in HP-NSW. Similar patterns were evident in growth responses to sea level pressure, with the two deeper water populations (HB-NSW and Hspp.-ENZ) having overall lower growth responses and HP-NSW with the fastest rate of increasing growth. Growth decreased with sea level pressure in the Kangaroo Island population of *H. percoides.*

Differences in growth responses to sea level and sea level pressure reflect effects of climate forcing. For example, the Kangaroo Island fish responded with negative growth to sea level pressure but positive growth to increased sea level. Kangaroo Island fish growth was negatively correlated with the highest ranked broad-scale climatic parameter of MJO index centred at 140°E. These results suggest the fish grow better under weather patterns of disturbance, i.e. stronger winds, cloudiness, weather systems moving through the region. Since *H. percoides* grow most rapidly in the warmer months (Park 1993, Paul and Horn

2009), we suggest these weather patterns likely occur in the late spring, summer and early autumn. Our growth models also indicated a positive synergistic effect between the MJO and bottom temperature for the Kangaroo Island ocean perch. Bottom temperature decreases when sustained southeasterlies produce coastal upwelling in the region. Upwelling favourable winds occur when high pressure systems move through the area just south of the continent in the summer (Schahinger 1987).

Growth of Hspp.-ENZ had a distinct increasing trend through time and was most highly correlated with the SAM at both the broad and local level. The SAM describes the movement to the north or south of the westerly wind belt that dominates the mid to high latitudes of the Southern Hemisphere (Bureau of Meteorology Australian Government 2015b). During a positive SAM, the westerly wind belt contracts towards Antarctica (higher pressures over Australia), while the opposite occurs during a negative event (more storms and low pressure over Australia) (Bureau of Meteorology Australian Government 2015b). Effects of the SAM are diverse, ranging from increased/decreased rainfall over the Australian continent to changes in the ocean mixed layer. A positive SAM event in the western Pacific (140°E-140°W north of 40°S) causes the mixed layer to become shallower, and chlorophyll-a (plankton biomass) increases with decreasing depth of the mixed layer, thereby increasing the productivity of a region (Sallee et al. 2010). During a negative SAM event, the opposite is true; as surface waters cool, the water becomes denser and the surface water sinks, deepening the mixed layer. The mixed layer can get too deep, and the phytoplankton get 'mixed out' of the light penetrating zone leading to lower biological productivity (Sallee et al. 2010).

Most interestingly, the annual positive trend in SAM has been linked to increasing CO_2 in the atmosphere (Cai et al. 2005, Metzl 2009). Physical mixing and cooling of ocean waters below 40°S during a positive SAM event causes increased CO_2 incorporation into the ocean water, whilst north of 40°S, less CO_2 is incorporated. This happens because westerlies are stronger south of 40°S during positive SAM and weaker north of 40°S (Metzl 2009). Fish growth on the Chatham Rise may reflect this mechanism, since that area is quite productive and located below 40°S. We hypothesise this region is benefiting from CO_2 incorporation

(to a point) into the deep ocean via elevated primary production, and this is reflected by the general increase in annual growth of ocean perch over more than three decades.

Conclusion

We have demonstrated that climate forcing is reflected in fish growth, and otoliths can be used as a tool to examine these effects. Broad scale climate patterns and weather have additive or synergistic effects on the environment, and these interactions were seen in fish growth. We have detected climate forcing in multiple fish species over a broad region and related different levels of growth responses to ocean-atmosphere coupling. Fish growth has not been extensively used to examine broad-scale climate in this manner. Directions for future research may include deducing if the effects of broad climate forcing are more pronounced in systems exposed to large ocean basins and dynamic oceanographic processes, and examining long-term records of fish growth in climate 'hot spots' to discern if growth indirectly reflects increases in greenhouse gasses in the atmosphere.

Acknowledgements:

We acknowledge partial funding from the Dr Paris Goodsell Marine Ecology Research Grant, the Nature Foundation SA, the Ecological Society of Australia, the Sir Mark Mitchell Research Foundation, CSIRO Wealth from Oceans Flagship and the Australian Research Council (FT100100767; DP110100716). We thank Kevin Rowling for assistance in otolith acquisition and general mentoring. We acknowledge the National Institute of Water and Atmospheric Research (NIWA) for providing access to their otolith archives. Thanks to J. Redman and S. Redman of Southend, SA, and R. Smith of Kangaroo Island, SA for help with specimen collection.

References:

Arendt, J. D. 1997. Adaptive intrinsic growth rates: an integration across taxa. The Quarterly Review of Biology **72**:149-177.

Attrill, M. J. and M. Power. 2002. Climatic influence on a marine fish assemblage. Nature **417**:275-278.

Bates, D., M. Maechler, B. Bolker, and S. Walker. 2014. lme4: Linear mixed-effects models using Eigen and S4. R package version 1.1-7. http://cran.r-project.org/web/packages/lme4/.

Bentley, N., T. H. Kendrick, and D. J. MacGibbon. 2014. Fishery characterisation and catch-per-unit-effort analyses for sea perch (*Helicolenus* spp.) in New Zealand, 1989–90 to 2009–10. New Zealand Fisheries Assessment Report 2014/27. 181 p.

Black, B. A., R. J. Allman, I. D. Schroeder, and M. J. Schirripa. 2011. Multidecadal otolith growth histories for red and gray snapper (*Lutjanus* spp.) in the northern Gulf of Mexico, USA. Fisheries Oceanography **20**:347-356.

Black, B. A., G. W. Boehlert, and M. M. Yoklavich. 2008. Establishing climate-growth relationships for yelloweye rockfish (*Sebastes ruberrimus*) in the northeast Pacific using a dendrochronological approach. Fisheries Oceanography **17**:368-379.

Black, B. A., J. B. Dunham, B. W. Blundon, J. Brim-Box, and A. J. Tepley. 2015. Long-term growth-increment chronologies reveal diverse influences of climate forcing on freshwater and forest biota in the Pacific Northwest. Global Change Biology **21**:594-604.

Black, B. A., W. J. Sydeman, D. C. Frank, D. Griffin, D. W. Stahle, M. García-Reyes, R. R. Rykaczewski, S. J. Bograd, and W. T. Peterson. 2014. Six centuries of variability and extremes in a coupled marine-terrestrial ecosystem. Science **345**:1498-1502.

Brierley, A. S. and M. J. Kingsford. 2009. Impacts of climate change on marine organisms and ecosystems. Current Biology **19**:R602-R614.

Brock, D. J., P. J. Hawthorne, T. M. Ward, and A. J. Linnane. 2007. Two monitoring methods that assess species composition and spatio-temporal trends in bycatch from an important temperate rock lobster (*Jasus edwardsii*) fishery. Marine and Freshwater Research **58**:273-285.

Bulman, C., F. Althaus, X. He, N. Bax, and A. Williams. 2001. Diets and trophic guilds of demersal fishes of the south-eastern Australian shelf. Marine and Freshwater Research **52**:537-548.

Bureau of Meteorology Australian Government. 2015a. Madden-Julian Oscillation (MJO). http://www.bom.gov.au/climate/mjo/. Accessed 16 June 2015.

Bureau of Meteorology Australian Government. 2015b. The Southern Annular Mode (SAM). http://www.bom.gov.au/climate/enso/history/ln-2010-12/SAM-what.shtml. Accessed 17 June 2015.

Burnham, K. P. and D. R. Anderson. 2004. Multimodel inference: understanding AIC and BIC in model selection. Sociological Methods & Research **33**:261-304.

Cai, W., G. Shi, T. Cowan, D. Bi, and J. Ribbe. 2005. The response of the Southern Annular Mode, the East Australian Current, and the southern mid-latitude ocean circulation to global warming. Geophysical Research Letters **32**:1-4.

Carvalho, L. M. V., C. Jones, and T. Ambrizzi. 2005. Opposite phases of the Antarctic Oscillation and relationships with intraseasonal to interannual activity in the tropics during the austral summer. Journal of Climate **18**:702-718.

Chi, N.-H., R.-C. Lien, E. A. D'Asaro, and B. B. Ma. 2014. The surface mixed layer heat budget from mooring observations in the central Indian Ocean during Madden–Julian Oscillation events. Journal of Geophysical Research: Oceans **119**:4638-4652.

Coulson, P. G., B. A. Black, I. C. Potter, and N. G. Hall. 2014. Sclerochronological studies reveal that patterns of otolith growth of adults of two co-occurring species of *Platycephalidae* are synchronised by water temperature variations. Marine Biology **161**:383-393.

Gillanders, B. M., B. A. Black, M. G. Meekan, and M. A. Morrison. 2012. Climatic effects on the growth of a temperate reef fish from the Southern Hemisphere: a biochronological approach. Marine Biology **159**:1327-1333.

Glantz, M. H. 2001. Currents of Change: Impacts of El Niño and La Niña on Climate and Society. Cambridge University Press, London.

Grammer, G. L., S. J. Fallon, C. Izzo, R. Wood, and B. M. Gillanders. 2015. Investigating bomb radiocarbon transport in the southern Pacific Ocean with otolith radiocarbon. Earth and Planetary Science Letters **424**:59-68.

Harrell, F. E. J. 2014. Hmisc: Harrell Miscellaneous. R package version 3.14-5. http://cran.r-project.org/web/packages/Hmisc/.

Hayward, T. L. 1997. Pacific Ocean climate change: atmospheric forcing, ocean circulation and ecosystem response. Trends in Ecology & Evolution **12**:150-154.

Holbrook, N. J., J. Davidson, M. Feng, A. J. Hobday, J. M. Lough, S. McGregor, and J. S. Risbey. 2009. El Niño-Southern Oscillation. *in* E.S. Poloczanska, A. J. Hobday, and A. J. Richardson, editors. A Marine Climate Change Impacts and Adaptation Report Card for Australia 2009. NCCARF Publication 05/09.

Holbrook, N. J., I. D. Goodwin, S. McGregor, E. Molina, and S. B. Power. 2011. ENSO to multi-decadal time scale changes in East Australian Current transports and Fort Denison sea level: Oceanic Rossby waves as the connecting mechanism. Deep Sea Research Part II: Topical Studies in Oceanography **58**:547-558.

Jin, D., R. Murtugudde, and D. E. Waliser. 2012. Tropical Indo-Pacific Ocean chlorophyll response to MJO forcing. Journal of Geophysical Research: Oceans **117**:1-20.

Johnson, P. C. D. 2014. Extension of Nakagawa & Schielzeth's R^2GLMM to random slopes models. Methods in Ecology and Evolution **5**:944-946.

Koslow, J. A., G. W. Boehlert, J. D. M. Gordon, R. L. Haedrich, P. Lorance, and N. Parin. 2000. Continental slope and deep-sea fisheries: implications for a fragile ecosystem. ICES Journal of Marine Science: Journal du Conseil **57**:548-557.

Lehodey, P., J. Alheit, M. Barange, T. Baumgartner, G. Beaugrand, K. Drinkwater, J. M. Fromentin, S. R. Hare, G. Ottersen, R. I. Perry, C. Roy, C. D. van der Lingen, and F. Werner. 2006. Climate variability, fish, and fisheries. Journal of Climate **19**:5009-5030.

Matta, M. E., B. A. Black, and T. K. Wilderbuer. 2010. Climate-driven synchrony in otolith growth-increment chronologies for three Bering Sea flatfish species. Marine Ecology Progress Series **413**:137-145.

Matthews, A. J., B. J. Hoskins, and M. Masutani. 2004. The global response to tropical heating in the Madden–Julian oscillation during the northern winter. Quarterly Journal of the Royal Meteorological Society **130**:1991-2011.

Matthews, A. J. and M. P. Meredith. 2004. Variability of Antarctic circumpolar transport and the Southern Annular Mode associated with the Madden-Julian Oscillation. Geophysical Research Letters **31**:1-5.

Matthews, A. J., P. Singhruck, and K. J. Heywood. 2007. Deep ocean impact of a Madden-Julian Oscillation observed by Argo floats. Science **318**:1765-1769.

Mazerolle, M. J. 2015. Model selection and multimodel inference based on (Q)AIC(c). R package version 2.0-3. http://cran.r-project.org/web/packages/AICcmodavg/index.html.

Metzl, N. 2009. Decadal increase of oceanic carbon dioxide in Southern Indian Ocean surface waters (1991–2007). Deep Sea Research Part II: Topical Studies in Oceanography **56**:607-619.

Middleton, J. F. and J. A. T. Bye. 2007. A review of the shelf-slope circulation along Australia's southern shelves: Cape Leeuwin to Portland. Progress in Oceanography **75**:1-41.

Ministry for Primary Industries. 2013. Aquatic environment and biodiversity annual review 2013. Compiled by the Fisheries Management Science Team, Ministry for Primary Industries. Wellington, New Zealand. 538 p.

Mo, K. C. 2000. Relationships between low-frequency variability in the Southern Hemisphere and sea surface temperature anomalies. Journal of Climate **13**:3599-3610.

Möllmann, C., G. Kornilovs, M. Fetter, and F. W. Köster. 2005. Climate, zooplankton, and pelagic fish growth in the central Baltic Sea. ICES Journal of Marine Science: Journal du Conseil **62**:1270-1280.

Morrongiello, J. R. and R. E. Thresher. 2015. A statistical framework to explore ontogenetic growth variation among individuals and populations: a marine fish example. Ecological Monographs **85**:93-115.

Morrongiello, J. R., R. E. Thresher, and D. C. Smith. 2012. Aquatic biochronologies and climate change. Nature Climate Change **2**:849-857.

Morrongiello, J. R., C. T. Walsh, C. A. Gray, J. R. Stocks, and D. A. Crook. 2014. Environmental change drives long-term recruitment and growth variation in an estuarine fish. Global Change Biology **20**:1844-1860.

Nakagawa, S. and H. Schielzeth. 2013. A general and simple method for obtaining R^2 from generalized linear mixed-effects models. Methods in Ecology and Evolution **4**:133-142.

Nguyen, H. M., A. N. Rountrey, J. J. Meeuwig, P. G. Coulson, M. Feng, S. J. Newman, A. M. Waite, C. B. Wakefield, and M. G. Meekan. 2015. Growth of a deep-water, predatory fish is influenced by the productivity of a boundary current system. Scientific Reports **5**:1-6.

NOAA/ National Weather Service. 2015. Monitoring Weather & Climate. http://www.cpc.noaa.gov/products/precip/CWlink/daily_mjo_index/details.html. Accessed 16 June 2015. NOAA Climate Prediction Center.

Overland, J. E., J. Alheit, A. Bakun, J. W. Hurrell, D. L. Mackas, and A. J. Miller. 2010. Climate controls on marine ecosystems and fish populations. Journal of Marine Systems **79**:305-315.

Park, T. J. 1993. A comparison of the morphology, growth and reproductive biology of two colour forms of ocean perch (*Helicoleus percoides*), NSW, Australia. Masters. University of Sydney, Sydney, Australia.

Paul, L. J. and P. L. Horn. 2009. Age and growth of sea perch (*Helicolenus percoides*) from two adjacent areas off the east coast of South Island, New Zealand. Fisheries Research **95**:169-180.

Pavlov, D. A. and N. G. Emel'yanova. 2013. Transition to viviparity in the order Scorpaeniformes: Brief review. Journal of Ichthyology **53**:52-69.

Peterson, R. G. and W. B. White. 1998. Slow oceanic teleconnections linking the Antarctic Circumpolar Wave with the tropical El Niño-Southern Oscillation. Journal of Geophysical Research: Oceans **103**:24573-24583.

Polovina, J. J., G. T. Mitchum, and G. T. Evans. 1995. Decadal and basin-scale variation in mixed layer depth and the impact on biological production in the Central and North Pacific, 1960-88. Deep Sea Research Part I: Oceanographic Research Papers **42**:1701-1716.

Ridgway, K. R. and J. R. Dunn. 2003. Mesoscale structure of the mean East Australian Current System and its relationship with topography. Progress in Oceanography **56**:189-222.

Risbey, J. S., M. J. Pook, P. C. McIntosh, M. C. Wheeler, and H. H. Hendon. 2009. On the remote drivers of rainfall variability in Australia. Monthly Weather Review **137**:3233-3253.

Rountrey, A. N., P. G. Coulson, J. J. Meeuwig, and M. Meekan. 2014. Water temperature and fish growth: otoliths predict growth patterns of a marine fish in a changing climate. Global Change Biology **20**:2450-2458.

Sallee, J. B., K. G. Speer, and S. R. Rintoul. 2010. Zonally asymmetric response of the Southern Ocean mixed-layer depth to the Southern Annular Mode. Nature Geosci **3**:273-279.

Schahinger, R. 1987. Structure of coastal upwelling events observed off the south-east coast of South Australia during February 1983 - April 1984. Marine and Freshwater Research **38**:439-459.

Shinoda, T., H. H. Hendon, and J. Glick. 1998. Intraseasonal variability of surface fluxes and sea surface temperature in the tropical western Pacific and Indian Oceans. Journal of Climate **11**:1685-1702.

Smith, P. J., C. D. Struthers, C. D. Paulin, S. M. McVeagh, and R. K. Daley. 2009. Shallow genetic and morphological divergence among seaperches in the South Pacific (family Scorpaenidae; genus *Helicolenus*). Journal of Fish Biology **74**:1104-1128.

Sokolov, S. and S. Rintoul. 2000. Circulation and water masses of the southwest Pacific: WOCE section P11, Papua New Guinea to Tasmania. Journal of Marine Research **58**:223-268.

Stabeno, P. J., J. G. L. Hunt, J. M. Napp, and J. D. Schumacher. 2006. Physical forcing of ecosystem dynamics on the Bering Sea Shelf. Harvard University Press, Cambridge, MA.

Stenseth, N. C., G. Ottersen, J. W. Hurrell, and A. Belgrano. 2004. Marine ecosystems and climate variation. Oxford University Press, Oxford.

Takahashi, Y., Y. Okazaki, M. Sato, H. Miyahara, K. Sakanoi, P. K. Hong, and N. Hoshino. 2010. 27-day variation in cloud amount in the Western Pacific warm pool region and relationship to the solar cycle. Atmospheric Chemistry and Physics **10**:1577-1584.

Thresher, R., J. Morrongiello, B. M. Sloyan, K. Krusic-Golub, S. Shephard, C. Minto, C. P. Nolan, F. Cerna, and L. Cid. 2014. Parallel decadal variability of inferred water temperatures for Northern and Southern Hemisphere intermediate water masses. Geophysical Research Letters **41**:2013GL058638.

Thresher, R. E., J. A. Koslow, A. K. Morison, and D. C. Smith. 2007. Depth-mediated reversal of the effects of climate change on long-term growth rates of exploited marine fish. Proceedings of the National Academy of Sciences, USA **104**:7461-7465.

Travers-Trolet, M., Y.-J. Shin, L. J. Shannon, C. L. Moloney, and J. G. Field. 2014. Combined fishing and climate forcing in the southern Benguela upwelling ecosystem: an end-to-end modelling approach reveals dampened effects. PLoS ONE **9**:e94286.

Walsh, K. J. E., K. L. McInnes, and J. L. McBride. 2012. Climate change impacts on tropical cyclones and extreme sea levels in the South Pacific - A regional assessment. Global and Planetary Change **80–81**:149-164.

Weisberg, S., G. Spangler, and L. S. Richmond. 2010. Mixed effects models for fish growth. Canadian Journal of Fisheries and Aquatic Sciences **67**:269-277.

Wheeler, M. C., H. H. Hendon, S. Cleland, H. Meinke, and A. Donald. 2009. Impacts of the Madden-Julian Oscillation on Australian rainfall and circulation. Journal of Climate **22**:1482-1498.

Woolnough, S. J., F. Vitart, and M. A. Balmaseda. 2007. The role of the ocean in the Madden-Julian Oscillation: implications for MJO prediction. Quarterly Journal of the Royal Meteorological Society **133**:117-128.

Zhang, C. 2005. Madden-Julian Oscillation. Reviews of Geophysics **43**:1-36.

Zuur, A., E. N. Ieno, N. Walker, A. A. Saveliev, and G. M. Smith. 2009. Mixed effects models and extensions in ecology with R. Springer, New York.

Supplementary Material:

Supplementary Table 1. Otolith growth increments are assumed to grow in proportion to the somatic growth of the fish, thus allowing growth histories to be reconstructed. To assess this assumption, we regressed the total length (TL; mm) and whole body weight (g; when available) of each species (or species complex) within a region against their otolith length (anterior to posterior edge, mm), otolith width (dorsal to ventral edge; mm), and otolith weight (mg). The intercept, slope and R^2 of the linear regression are presented along with the significance (*p*) value. n: total number of fish.

Species - Location code	Fish parameter	Otolith dimension	n	Intercept	Slope	R^2	*p* value
HP - BC	TL (160 - 365 mm)	length	177	2.93	0.03	0.75	<0.001
		width	178	2.24	0.01	0.56	<0.001
		weight	178	-58.68	0.55	0.70	<0.001
	whole weight	length	179	8.43	0.01	0.67	<0.001
		width	180	4.43	0.00	0.44	<0.001
		weight	180	-46.87	4.52	0.64	<0.001
HP - KI	TL (160 - 313 mm)	length	54	3.44	0.03	0.60	<0.001
		width	54	2.23	0.01	0.58	<0.001
		weight	54	-68.70	0.60	0.71	<0.001
	whole weight	length	53	8.20	0.01	0.61	<0.001
		width	53	4.30	0.00	0.53	<0.001
		weight	53	34.81	0.15	0.70	<0.001
HP - NSW	TL (244 - 341 mm)	length	59	1.14	0.02	0.60	<0.001
		width	59	1.14	0.02	0.60	<0.001
		weight	60	-114.94	0.76	0.45	<0.001
	whole weight	length	57	8.77	0.01	0.40	<0.001
		width	57	4.11	8.77	0.55	<0.001
		weight	58	28.35	0.17	0.42	<0.001
HB - NSW	TL (210 - 443 mm)	length	126	1.60	0.03	0.60	<0.001
		width	126	2.36	0.01	0.49	<0.001
		weight	126	-153.58	0.88	0.71	<0.001
	whole weight	length	85	11.73	0.00	0.23	<0.001
		width	85	6.34	0.00	0.08	0.008
		weight	85	98.05	0.08	0.33	<0.001
Hspp. - WNZ	TL (150 - 490 mm)	length	93	3.62	0.25	0.93	<0.001
		width	93	2.73	0.10	0.86	<0.001
		weight	93	-83.00	6.07	0.91	<0.001
Hspp. - ENZ	TL (270 - 510 mm)	length	118	5.31	0.21	0.71	<0.001
		width	118	3.52	0.08	0.44	<0.001
		weight	118	-145.34	7.69	0.78	<0.001

Supplementary Table 2. Optimal model with broad-scale climate variables added as fixed effects for growth comparisons i to iii: (i) Across all species and regions, (ii) among *Helicolenus percoides* and *H. barathri* in NSW, and (iii) within *H. percoides* from different locations in SA and NSW. Models were first fit with estimates of maximum likelihood (ML) and refit with restricted estimates of maximum likelihood (REML). Marginal (m) and conditional (c) R^2 values were calculated after models were refit with REML. Best ranked variable highlighted in **bold**. LL: log likelihood.

Growth Comparison:	**(i) Across species and regions**						**(ii) Among species within a region**						**(iii) Within species among regions**					
Model	df	AICc	ΔAICc	LL	R^2m	R^2c	df	AICc	ΔAICc	LL	R^2m	R^2c	df	AICc	ΔAICc	LL	R^2m	R^2c
Growth - optimal base model	15	-360.91	1.92	195.52	0.790	0.876	11	-144.71	2.90	83.44	0.829	0.899	13	-702.63	0.75	364.40	0.814	0.885
+ *Sunspots*	**16**	**-362.83**	**0**	**197.49**	**0.792**	**0.876**	12	-146.08	1.53	85.14	0.831	0.900	14	-701.56	1.82	364.87	0.812	0.886
+ *AAO*	16	-360.66	2.17	196.40	0.790	0.876	12	-98.07	49.54	61.16	0.833	0.903	14	-700.61	2.77	364.40	0.813	0.886
+ *SOI*	16	-358.90	3.93	195.52	0.790	0.876	**12**	**-147.61**	**0**	**85.90**	**0.830**	**0.900**	14	-701.47	1.91	364.83	0.812	0.886
+ *PDO*	16	-354.14	8.69	193.14	0.790	0.876	12	-146.17	1.44	85.18	0.827	0.899	14	-701.94	1.44	365.06	0.813	0.886
+ *MJOindex20E*	16	-361.49	1.34	196.82	0.790	0.875	12	-117.44	30.17	70.84	0.837	0.901	14	-702.89	0.50	365.54	0.813	0.885
+ *MJOindex70E*	16	-359.35	3.48	195.75	0.790	0.876	12	-111.71	35.90	67.97	0.835	0.902	**14**	**-703.38**	**0**	**365.78**	**0.813**	**0.886**
+ *MJOindex80E*	16	-358.94	3.89	195.55	0.790	0.876	12	-108.23	39.38	66.23	0.834	0.902	14	-702.62	0.77	365.40	0.813	0.886
+ *MJOindex100E*	16	-359.04	3.79	195.59	0.790	0.876	12	-104.34	43.27	64.28	0.832	0.902	14	-701.75	1.63	364.97	0.813	0.886
+ *MJOindex120E*	16	-360.09	2.74	196.12	0.790	0.876	12	-102.23	45.38	63.23	0.831	0.902	14	-700.74	2.64	364.46	0.813	0.886
+ *MJOindex140E*	16	-361.90	0.93	197.02	0.789	0.875	12	-112.47	35.14	68.35	0.834	0.901	14	-701.41	1.97	364.80	0.813	0.885
+ *MJOindex160E*	16	-360.01	2.82	196.08	0.790	0.876	12	-114.19	33.42	69.21	0.836	0.902	14	-703.32	0.07	365.75	0.813	0.885
+ *MJOindex120W*	16	-358.95	3.88	195.55	0.790	0.876	12	-108.24	39.37	66.23	0.834	0.902	14	-702.79	0.59	365.49	0.813	0.886
+ *MJOindex40W*	16	-359.14	3.69	195.65	0.790	0.876	12	-103.48	44.13	63.86	0.831	0.902	14	-701.54	1.84	364.86	0.813	0.886
+ *MJOindex10W*	16	-360.92	1.91	196.54	0.789	0.875	12	-104.52	43.09	64.38	0.831	0.901	14	-700.62	2.77	364.40	0.813	0.886
+ *OMImjoAmplitude*	16	-359.19	3.64	195.67	0.790	0.876	12	-94.48	53.13	59.36	0.830	0.902	14	-701.53	1.85	364.86	0.812	0.886

Supplementary Table 3. Optimal model with broad-scale climate variables added as fixed effects for growth comparison iv: species and region specific. Models were first fit with estimates of maximum likelihood (ML) and refit with restricted estimates of maximum likelihood (REML). Marginal (m) and conditional (c) R^2 values were calculated after models were refit with REML. Best ranked variable highlighted in **bold**. LL: log likelihood.

Growth comparison (iv)	**HP - BC**						**HP - KI**						**HP - NSW**					
Model	df	AICc	ΔAICc	LL	R^2m	R^2c	df	AICc	ΔAICc	LL	R^2m	R^2c	df	AICc	ΔAICc	LL	R^2m	R^2c
Growth - optimal base model	12	-546.23	2.75	285.20	0.798	0.892	6	-127.77	4.71	69.99	0.822	0.873	9	-216.08	2.40	117.15	0.824	0.900
+ *Sunspots*	13	-544.20	4.78	285.20	0.798	0.892	7	-130.85	1.63	72.56	0.822	0.876	10	-217.34	1.15	118.81	0.827	0.900
+ *AAO*	13	-544.38	4.59	285.30	0.798	0.892	7	-126.72	5.77	70.49	0.822	0.873	10	-191.36	27.12	105.83	0.810	0.889
+ *SOI*	13	-545.58	3.40	285.89	0.796	0.893	7	-126.28	6.20	70.27	0.823	0.873	**10**	**-218.48**	**0**	**119.38**	**0.825**	**0.899**
+ *PDO*	13	-545.45	3.52	285.83	0.796	0.892	7	-131.65	0.83	72.96	0.825	0.876	10	-215.37	3.12	117.82	0.825	0.899
+ *MJOindex20E*	13	-545.62	3.35	285.92	0.799	0.891	7	-131.66	0.83	72.96	0.823	0.875	10	-212.84	5.65	116.56	0.815	0.890
+ *MJOindex70E*	13	-546.55	2.42	286.38	0.798	0.891	7	-127.67	4.82	70.96	0.822	0.873	10	-211.95	6.53	116.12	0.814	0.892
+ *MJOindex80E*	13	-546.26	2.72	286.23	0.798	0.892	7	-126.53	5.96	70.39	0.822	0.873	10	-209.07	9.42	114.67	0.814	0.892
+ *MJOindex100E*	13	-545.79	3.19	286.00	0.796	0.892	7	-125.82	6.67	70.04	0.822	0.873	10	-204.31	14.17	112.30	0.814	0.893
+ *MJOindex120E*	13	-544.65	4.32	285.43	0.796	0.893	7	-128.90	3.59	71.58	0.824	0.875	10	-200.08	18.40	110.18	0.813	0.894
+ *MJOindex140E*	13	-544.58	4.40	285.39	0.799	0.892	**7**	**-132.49**	**0**	**73.38**	**0.824**	**0.876**	10	-206.42	12.06	113.35	0.815	0.891
+ *MJOindex160E*	13	-546.35	2.63	286.28	0.799	0.891	7	-129.65	2.84	71.95	0.823	0.874	10	-212.70	5.78	116.49	0.815	0.891
+ *MJOindex120W*	13	-546.44	2.53	286.33	0.797	0.892	7	-126.28	6.21	70.27	0.822	0.873	10	-208.86	9.62	114.57	0.814	0.892
+ *MJOindex40W*	13	-545.61	3.37	285.91	0.796	0.893	7	-126.21	6.28	70.24	0.822	0.873	10	-202.83	15.65	111.56	0.814	0.893
+ *MJOindex10W*	13	-544.25	4.72	285.23	0.797	0.893	7	-130.78	1.71	72.52	0.824	0.875	10	-200.79	17.70	110.54	0.814	0.894
+ *OMImjoAmplitude*	**13**	**-548.98**	**0**	**287.59**	**0.794**	**0.892**	7	-125.71	6.78	69.99	0.822	0.873	10	-190.96	27.53	105.62	0.808	0.890

Supplementary Table 3. *Continued*: Optimal model with broad-scale climate variables added as fixed effects for growth comparison iv: species and region specific.

Growth comparison (iv)	**HB - NSW**						**Hspp - WNZ**						**Hspp - ENZ**					
Model	df	AICc	ΔAICc	LL	R^2m	R^2c	df	AICc	ΔAICc	LL	R^2m	R^2c	df	AICc	ΔAICc	LL	R^2m	R^2c
Growth - optimal base model	7	80.88	15.78	-33.41	0.821	0.864	12	-118.88	0.17	71.61	0.798	0.877	12	325.58	24.82	-150.71	0.708	0.847
+ *Sunspots*	8	81.23	16.13	-32.58	0.821	0.864	**13**	**-119.05**	**0.00**	**72.73**	**0.799**	**0.878**	13	325.94	25.19	-149.88	0.709	0.848
+ *AAO*	8	68.39	3.29	-26.05	0.768	0.829	13	-117.45	1.60	71.93	0.798	0.877	**13**	**300.76**	**0.00**	**-137.27**	**0.663**	**0.820**
+ *SOI*	8	82.80	17.69	-33.36	0.821	0.864	13	-117.12	1.93	71.76	0.798	0.877	13	325.86	25.10	-149.83	0.708	0.847
+ *PDO*	8	82.79	17.69	-33.35	0.821	0.864	13	-116.97	2.09	71.69	0.798	0.877	13	327.18	26.42	-150.49	0.708	0.847
+ *MJOindex20E*	8	68.00	2.90	-25.88	0.753	0.820	13	-118.56	0.49	72.48	0.799	0.877	13	305.69	4.94	-139.74	0.667	0.824
+ *MJOindex70E*	8	67.30	2.20	-25.52	0.752	0.820	13	-117.28	1.77	71.84	0.799	0.877	13	307.04	6.28	-140.41	0.675	0.817
+ *MJOindex80E*	8	66.56	1.46	-25.16	0.752	0.820	13	-116.98	2.07	71.69	0.798	0.877	13	307.44	6.69	-140.62	0.666	0.825
+ *MJOindex100E*	8	65.50	0.40	-24.62	0.753	0.821	13	-116.83	2.23	71.61	0.798	0.877	13	307.74	6.99	-140.77	0.667	0.824
+ *MJOindex120E*	**8**	**65.10**	**0.00**	**-24.42**	**0.754**	**0.821**	13	-116.38	2.67	71.39	0.798	0.877	13	307.46	6.71	-140.63	0.667	0.823
+ *MJOindex140E*	8	66.52	1.41	-25.13	0.755	0.821	13	-118.46	0.59	72.43	0.799	0.877	13	305.73	4.98	-139.76	0.667	0.823
+ *MJOindex160E*	8	68.09	2.99	-25.92	0.752	0.820	13	-117.71	1.34	72.06	0.799	0.877	13	306.61	5.85	-140.20	0.667	0.825
+ *MJOindex120W*	8	66.53	1.42	-25.14	0.752	0.820	13	-116.97	2.08	71.69	0.798	0.877	13	307.49	6.73	-140.64	0.667	0.825
+ *MJOindex40W*	8	65.44	0.34	-24.60	0.753	0.821	13	-116.84	2.22	71.62	0.798	0.877	13	307.76	7.00	-140.77	0.674	0.816
+ *MJOindex10W*	8	65.36	0.26	-24.55	0.755	0.822	13	-117.64	1.42	72.02	0.798	0.877	13	306.78	6.02	-140.29	0.667	0.823
+ *OMImjoAmplitude*	8	68.08	2.98	-25.90	0.767	0.829	13	-118.67	0.38	72.54	0.800	0.878	13	304.09	3.33	-138.94	0.663	0.819

Supplementary Table 4. Optimal model with all local-scale environmental variables and best broad-scale variable added as fixed effects for growth comparisons ii and iv: (ii) among *Helicolenus percoides* and *H. barathri* in NSW and (iv) species and region specific. Models were first fit with estimates of maximum likelihood (ML) and refit with restricted estimates of maximum likelihood (REML). Marginal (m) and conditional (c) R^2 values were calculated after models were refit with REML. Best ranked variable highlighted in **bold**. LL: log likelihood. *Signifies an interaction.

Growth comparison		Fixed effects structure	df	AICc	ΔAICc	LL	R^2m	R^2c
ii	Among Species within a region							
		Growth - optimal base model	11	-144.71	7.83	83.44	0.829	0.899
		+ *SOI*	12	-147.61	4.93	85.90	0.834	0.900
		+ *SeaLevel*	12	-148.49	4.06	86.34	0.830	0.899
		+ *YearSLP*	12	-144.34	8.20	84.27	0.831	0.900
		+ ***YearSLP*** + ***SeaLevel***	**13**	**-152.54**	**0.00**	**89.39**	**0.833**	**0.900**
		+ *YearSLP * SeaLevel*	14	-151.05	1.49	89.66	0.833	0.900
		+ *SeaLevel + SOI*	13	-147.01	5.54	86.62	0.830	0.900
		+ *SeaLevel * SOI*	14	-145.64	6.91	86.95	0.828	0.900
iv	Species and region specific							
	HP - KI	*Growth* - optimal base model	6	-127.77	6.92	69.99	0.822	0.873
		+ *MJOindex140E*	7	-132.49	2.21	73.38	0.824	0.876
		+ *YearlyUI*	7	-126.05	8.65	70.16	0.822	0.873
		+ *SeaLevel*	7	-130.45	4.24	72.36	0.825	0.875
		+ *YearSLP*	7	-126.77	7.93	70.52	0.823	0.873
		+ *YearBotTemp*	7	-127.59	7.11	70.93	0.822	0.874
		+ *YEarSLP+YearBotTemp*	8	-125.62	9.08	70.98	0.822	0.873
		+ *YearlyUI+SeaLevel*	8	-128.63	6.07	72.48	0.825	0.875
		+ *YearlyUI+BotTemp*	8	-126.06	8.64	71.20	0.823	0.874
		+ *YearlyUI+YearSLP*	8	-125.84	8.85	71.09	0.824	0.874
		+ *SeaLevel+YearBotTemp*	8	-128.60	6.10	72.47	0.824	0.875
		+ *YearSLP*YearBotTemp*	9	-123.62	11.08	71.02	0.822	0.873
		+ *YearlyUI*SeaLevel*	9	-126.79	7.91	72.61	0.825	0.875
		+ *YearlyUI*YearBotTemp*	9	-123.97	10.73	71.20	0.822	0.873
		+ *SeaLevel*YearBotTemp*	9	-128.75	5.95	73.59	0.825	0.876
		+ *YearlyUI*YearSLP*	9	-123.97	10.72	71.20	0.823	0.873
		+ *YearBotTemp+MJOindex140E*	8	-130.44	4.26	73.39	0.824	0.876
		+ *SeaLevel+MJOindex140E*	8	-131.87	2.83	74.10	0.825	0.877
		+ *YearlyUI+MJOindex140E*	8	-131.04	3.65	73.69	0.825	0.876
		+ ***YearBotTemp*MJOindex140E***	**9**	**-134.70**	**0.00**	**76.56**	**0.826**	**0.879**
		+ *SeaLevel*MJOindex140E*	9	-132.71	1.99	75.57	0.826	0.879
		+ *YearlyUI*MJOindex140E*	9	-130.44	4.26	74.43	0.825	0.876

Supplementary Table 4. *Continued:* Optimal model with all local-scale environmental variables and best broad-scale variable added as fixed effects.

Growth comparison	Fixed effects structure	df	AICc	ΔAICc	LL	R^2m	R^2c
HP - BC	*Growth* - optimal base model	12	-546.23	4.71	285.20	0.798	0.892
	+ *YearlyUI*	13	-544.20	6.74	285.20	0.798	0.892
	+ *Sealevel*	13	-544.41	6.52	285.31	0.797	0.893
	+ *YearSLP*	13	-545.35	5.58	285.78	0.798	0.892
	+ *YearBotTemp*	13	-546.27	4.66	286.24	0.798	0.891
	+ *OMImjoAmplitude*	13	-548.98	1.96	287.59	0.794	0.892
	+ *YearSLP+YearBotTemp*	14	-544.51	6.42	286.37	0.798	0.891
	+ *YearlyUI+Sealevel*	14	-542.40	8.54	285.32	0.796	0.893
	+ *YearlyUI+YearBotTemp*	14	-544.36	6.58	286.30	0.799	0.891
	+ *YearlyUI+YearSLP*	14	-544.87	6.06	286.56	0.802	0.890
	+ *SeaLevel+YearBotTemp*	14	-546.46	4.47	287.35	0.796	0.892
	+ *YearSLP*YearBotTemp*	15	-543.67	7.26	286.97	0.798	0.890
	+ *YearlyUI*Sealevel*	15	-542.61	8.32	286.44	0.793	0.894
	+ *YearlyUI*YearBotTemp*	15	-543.68	7.25	286.98	0.799	0.891
	+ *SeaLevel*YearBotTemp*	15	-544.59	6.34	287.43	0.796	0.892
	+ *YearlyUI*YearSLP*	15	-544.00	6.93	287.14	0.803	0.891
	+ *YearSLP+OMImjoAmplitude*	14	-547.14	3.79	287.69	0.794	0.892
	+ *YearBotTemp+OMImjoAmplitude*	14	-548.36	2.57	288.30	0.794	0.892
	+ *SeaLevel+OMImjoAmplitude*	14	-547.35	3.58	287.79	0.793	0.893
	+ *YearlyUI+OMImjoAmplitude*	14	-547.68	3.25	287.96	0.795	0.893
	+ *YearSLP*OMImjoAmplitude*	**15**	**-550.93**	**0.00**	**290.60**	**0.794**	**0.891**
	+ *YearBotTemp*OMImjoAmplitude*	15	-548.83	2.10	289.55	0.796	0.891
	+ *SeaLevel*OMImjoAmplitude*	15	-546.53	4.40	288.40	0.792	0.894
	+ *YearlyUI*OMImjoAmplitude*	15	-548.98	1.95	289.63	0.793	0.893
HP - NSW	*Growth* - optimal base model	9	-216.08	6.45	117.15	0.823	0.900
	+ *SOI*	10	-218.48	4.05	119.38	0.824	0.900
	+ *SeaLevel*	10	-216.83	5.70	118.55	0.822	0.899
	+ *YearSLP*	10	-219.07	3.46	119.67	0.822	0.900
	+ *YearSLP+SeaLevel*	**11**	**-222.53**	**0.00**	**122.43**	**0.821**	**0.897**
	+ *YearSLP*SeaLevel*	12	-221.12	1.42	122.75	0.821	0.897
	+ *SeaLevel+SOI*	11	-216.79	5.74	119.56	0.823	0.900
	+ *SeaLevel*SOI*	12	-215.38	7.15	119.89	0.822	0.899
HB - NSW	*Growth* - optimal base model	7	80.88	15.78	-33.41	0.821	0.864
	+ *MJOindex120E*	**8**	**65.10**	**0.00**	**-24.42**	**0.754**	**0.821**
	+ *SeaLevel*	8	81.44	16.34	-32.68	0.821	0.864
	+ *YearSLP*	8	82.72	17.62	-33.32	0.821	0.864
	+ *YearSLP+c.SeaLevel*	9	81.55	16.45	-31.72	0.822	0.864
	+ *YearSLP*c.SeaLevel*	10	82.00	16.90	-30.94	0.822	0.864
	+ *YearSLP+c.MJOindex120E*	9	67.09	1.99	-24.39	0.754	0.821
	+ *YearSLP*c.MJOindex120E*	10	66.67	1.57	-23.14	0.753	0.822
Hspp - WNZ	*Growth* - optimal base model	12	-118.88	19.19	71.61	0.800	0.876
	+ *Sunspots*	13	-119.05	19.02	72.73	0.801	0.877
	+ *SeaLevel*	**13**	**-138.08**	**0.00**	**82.25**	**0.794**	**0.877**
	+ *YearSLP*	13	-116.89	21.19	71.65	0.800	0.876
	+ *YearSLP+c.SeaLevel*	14	-136.11	1.97	82.30	0.794	0.877
	+ *YearSLP*c.SeaLevel*	15	-134.57	3.50	82.57	0.794	0.878
	+ *YearSLP+c.Sunspots*	14	-117.04	21.04	72.75	0.801	0.877
	+ *YearSLP*c.Sunspots*	15	-115.57	22.50	73.05	0.801	0.877
Hspp - ENZ	*Growth* - optimal base model	12	325.58	24.82	-150.71	0.708	0.847
	+ *AAO*	**13**	**300.76**	**0.00**	**-137.27**	**0.663**	**0.820**
	+ *SeaLevel*	13	327.25	26.50	-150.53	0.708	0.848
	+ *YearSLP*	13	327.45	26.69	-150.63	0.708	0.847
	+ *YearSLP+AAO*	14	302.75	2.00	-137.25	0.672	0.811
	+ *SeaLevel+AAO*	14	301.66	0.91	-136.71	0.672	0.811
	+ *YearSLP*AAO*	15	304.66	3.90	-137.19	0.663	0.820
	+ *SeaLevel*AAO*	15	303.44	2.69	-136.58	0.663	0.820

CHAPTER 5
Highly resolved chemical-growth chronologies reveal physiological and environmental influences on trace element assimilation in otoliths

Helicolenus larger than life: the striking, red fish are on a billboard advertising a fish market to international buyers.

Statement of Authorship

Title of Paper	Highly resolved chemical-growth chronologies reveal physiological and environmental influences on trace element assimilation in otoliths
Publication Status	☐ Published ☐ Accepted for Publication ☐ Submitted for Publication ☑ Publication Style
Publication Details	This is a co-authored paper and is intended to be published in a scientific journal. John Morrongiello, Christopher Izzo, Peter Hawthorne, John Middleton, and Bronwyn Gillanders are co-authors, and therefore, it is written in plural.

Principal Author

Name of Principal Author (Candidate)	Gretchen L. Grammer		
Contribution to the Paper	Collected specimens, extracted otoliths, performed all laboratory analyses, performed univariate analyses, supplied some funding, and wrote the manuscript.		
Overall percentage (%)	85		
Signature		Date	17 June 2015

Co-Author Contributions

By signing the Statement of Authorship, each author certifies that:

vii. the candidate's stated contribution to the publication is accurate (as detailed above);

viii. permission is granted for the candidate in include the publication in the thesis; and

ix. the sum of all co-author contributions is equal to 100% less the candidate's stated contribution.

Name of Co-Author	John Morrongiello		
Contribution to the Paper	Assisted with intellectual development, performed multivariate analyses, and provided suggestions, comments and feedback on manuscript drafts		
Signature		Date	17 June 2015

Name of Co-Author	Christopher Izzo		
Contribution to the Paper	Assisted with intellectual development, and provided suggestions, comments and feedback on manuscript drafts		
Signature		Date	17 June 2015

Name of Co-Author	Peter Hawthorne		
Contribution to the Paper	Collected specimens, assisted with intellectual development, and will provide suggestions, comments, and feedback on manuscript drafts prior to submission to a scientific journal		
Signature		Date	17 June 2015

Name of Co-Author	John Middleton		
Contribution to the Paper	Provided Bluelink temperature data, provided suggestions during manuscript development, and will provide feedback on manuscript drafts prior to submission to a scientific journal		
Signature		Date	17 June 2015

Name of Co-Author	Bronwyn M. Gillanders		
Contribution to the Paper	Assisted with intellectual development, supplied funding, and provided suggestions, comments and feedback on manuscript drafts		
Signature		Date	17 June 2015

Highly resolved chemical-growth chronologies reveal physiological and environmental influences on trace element assimilation in otoliths

Gretchen L. Grammer[1], John R. Morrongiello[2], Christopher Izzo[1], Peter J. Hawthorne[3], John F. Middleton[3], and Bronwyn M. Gillanders[1]

[1]Southern Seas Ecology Laboratories, School of Biological Sciences, The University of Adelaide, SA 5005, Australia

[2]School of BioSciences, The University of Melbourne, VIC 3010, Australia

[3]South Australian Research and Development Institute (Aquatic Sciences), West Beach, SA 5024, Australia

Correspondence: Gretchen L. Grammer, Southern Seas Ecology Laboratories, School of Biological Sciences, The University of Adelaide, SA 5005, Australia

Tel.: +61 8 8313 1483; Fax: +61 8 8313 4364

Email: gretchen.grammer@adelaide.edu.au

Abstract:

Biogeochemical tracers found in the hard parts of organisms are frequently used to answer key ecological questions by linking the organism with the environment. However, biogenic structures are not always in direct contact with the environment and their formation may be under some level of physiological control. As physiological processes become more complex in higher organisms, the biogeochemical relationship between the environment and the biogenic structure becomes less predictable. Here, we used the simultaneous combination of biogeochemical tracers (trace elements: Na, Sr, Mg, Ba, Li) and fish growth with univariate and multivariate mixed modelling, in a novel approach, to describe physiological and environmental controls on otolith chemistry. First, univariate mixed models were used to examine fish growth and elemental relationships within the otolith through time to enable intrinsic influences (e.g. age effects) to be partitioned. Then, specific extrinsic sources (i.e. environmental parameters) were added to the models to look at other factors potentially influencing otolith chemistry or growth. Finally, we used multivariate models to examine the directionality and strength between element-to-element and growth relationships to test hypotheses around physiological and environmental controls on elemental assimilation in otoliths. Otolith chemistry and fish growth displayed cyclic seasonal signals over a 17 year time period in a marine upwelling system. Age-dependent relationships existed in the trace element and growth profiles, and responses to the environment differed as the fish aged. Temporal signals were correlated with seasonal upwelling events. Some elements (Sr:Ca and Na:Ca) were predominantly controlled by physiological processes, while other elements (Ba:Ca and Li:Ca) were more influenced by the environment. Ba:Ca negatively tracked upwelling events, suggesting an upwelled water mass not enriched in Ba. Li:Ca correlated positively with chlorophyll-a, indicating a possible proxy for marine productivity. Resolving element:Ca and growth profiles from otoliths to monthly increments over 17 years has allowed an unprecedented level of information to be obtained. Signals from marine systems are heterogeneous with respect to otolith chemistry or growth, and population level responses to the environment are evident in element:Ca concentrations and growth rates. Chronologies of otolith chemistry coupled with fish growth have the scope to be used as ecological proxies, whereby temporal fluctuations in the physical environment can be directly correlated with changes in reproduction, diet or other biological factors to reconstruct responses of past populations.

Introduction:

How does environmental variation influence species biology? Can we use this insight to hindcast past conditions and forecast future states? These are key ecological questions asked by many researchers. Biogeochemical tracers (e.g. trace elements, stable isotopes, chemical pollutants, lipids) are commonly used to make the link between an organism and the environment. There remain, however, a number of outstanding issues that need to be addressed for successful data interpretation, as each tracer has a unique set of properties, controls and assumptions that need to be recognized before it is applied to an ecological question. For example, careful consideration should be given to the assimilation mechanism of the tracer into the biogenic structure, time scales for integration, and how the tracer is distributed/integrated in the environment (Ramos and González-Solís 2012). Furthermore, different tracers reflect different biological/ecological processes, and thus, it is desirable to simultaneously measure multiple biogeochemical tracers and effects of growth or other physiological factors to allow for synergistic interactions to be explored (Ramos and González-Solís 2012).

Trace elements are frequently used as biogeochemical tracers in biogenic structures to make inferences about past environments (e.g. Montaggioni et al. 2006, Batenburg et al. 2011) or organismal movement across environmental gradients (e.g. Lamson et al. 2006, Steer et al. 2009). Key assumptions underpinning these corollaries rely on the predictability of element assimilation in relation to the surrounding environment and minimal or constant influence of biological effects ('vital effects'). However, the biogeochemical relationship between the environment and the biogenic structure becomes less predictable in higher organisms as physiological processes become more complex (Weiner and Dove 2003, Stanley 2006, Cusack and Freer 2008). Understanding and accounting for these processes allow biological and environmental influences on element assimilation to be disentangled.

Fish earstones or otoliths are biogenic structures that are easily accessible in almost every aquatic environment. These structures contain growth increments that can be time resolved, making them one of the most extensively studied calcified structures of a higher organism. Not only are otoliths favoured as chronometers of growth, otolith

biogeochemical (here after referred to as chemistry or chemical) profiles are extensively used as natural tags to examine stock structure, population connectivity, and movement patterns through different aquatic environments (e.g. Gillanders 2002, Elsdon and Gillanders 2003a, Reis-Santos et al. 2013). They are also used as palaeoproxies to infer past environments (Disspain et al. 2011, Disspain et al. 2015). Distinct chemical profiles found in otoliths are assumed to reflect the fish's ambient environment, and much experimental work has centred on directly relating water chemistry and environmental conditions to otolith elemental composition (e.g. Elsdon and Gillanders 2002, 2003b, de Vries et al. 2005). Studies have also examined the contribution of water versus dietary sources to otolith element composition (Walther and Thorrold 2006, Webb et al. 2012, Doubleday et al. 2013). Early otolith research from the late 1980s/1990s focused on differentiating the effects of biological and environmental controls upon element composition (Kalish 1989, 1991, Campana 1999). Recently, there has been renewed interest in this area (e.g. Sturrock et al. 2014, Sturrock et al. 2015), as complex and conflicting results have been revealed between otolith chemistry and ambient water (Thresher 1999, Elsdon et al. 2008, Berumen et al. 2010). These issues need to be resolved if we are to have confidence in the use of otoliths as an environmental proxy.

Otoliths are encapsulated in the fish's head, surrounded by endolymph, and are not in direct contact with the environment (Campana 1999). This places a first order limit on the responsiveness of otolith chemistry to variations in ambient water chemistry (Sturrock et al. 2014). Fluctuations in the physical environment (e.g. temperature, salinity, current strength) directly affect fish physiology by altering metabolism, respiratory function, osmotic processes, feeding behaviour, and/or diet (Brett and Groves 1979, Wootton 2011). Therefore, the chemical composition of the otolith will also be affected. Physiological processes such as growth or reproduction can cause otolith chemistry to respond both directly or indirectly to changes in the ambient environment, because these processes themselves are often cued by extrinsic factors (Walther et al. 2010, Sturrock et al. 2014, Sturrock et al. 2015). Some elements tend to be less physiologically regulated than others; Ba, Mg, and Li in blood plasma of fish were found to display the least biological fractionation compared to Sr (Sturrock et al. 2014). Otolith Sr:Ca has been shown to be highly influenced by reproductive processes in marine fish (Kalish 1991, Sturrock et al.

2015). Most research examining physiological controls on otoliths is laboratory based and primarily targeted at early life history stages for limited experimental durations (i.e. days to weeks). Moreover, laboratory based results may not accurately represent the same responses in wild caught fish (Elsdon and Gillanders 2005).

Based on current research, we developed a conceptual model explaining element concentrations and growth correlations within an otolith and among individual fish inhabiting the same marine environment (Fig. 1a). We propose that certain elements assimilated into otoliths are primarily under physiological control, environmental control or both. We hypothesise Na:Ca and Sr:Ca will be predominantly influenced by an individual's physiology, while Ba:Ca and Li:Ca would be primarily affected by environmental parameters (Fig. 1a). We also predict growth and Mg:Ca would be moderately influenced by both physiology and the environment. It is likely that there will be stronger correlations within physiological or environmental variables (elements or growth), but less so between the two groups due to the different controls on element assimilation or growth. Furthermore, the level at which correlation occurs (within or among individuals) will vary among physiologically and environmentally controlled variables. Those elements most influenced by physiological processes, such as reproduction or metabolic processes, are expected to be correlated within an otolith as they reflect processes intrinsic to the individual ('vital effects'). Conversely, variables driven by environmental conditions will correlate both within an otolith, reflecting the time dependency of growth and elemental assimilation, and among individual fish that experience a similar set of external conditions (Fig. 1a).

To test these hypotheses, we develop a series of increasingly complex, univariate mixed-effects models to partition variation in otolith elemental concentration or growth between intrinsic (e.g. individual, age) and extrinsic (e.g. local upwelling, temperature) drivers (Weisberg et al. 2010, Morrongiello and Thresher 2015). We apply these models to continuous, multi-year, otolith chemistry and growth increment profiles derived from our test species, a wild-caught, site-attached, fully marine fish. Finally, we develop a multivariate mixed-effect model, based on the univariate models, to generate estimates of between element/growth correlations within and among individuals and investigate the strength and directionality of those relationships.

Fig.1. A) Hypothesised correlations between age-corrected element:Ca ratios and estimated growth within otoliths and among individuals. Some otolith traits are correlated via physiological or environmental pathways. Solid black arrows: within individual correlations; Dashed grey arrows: among individual correlations. B) Supported correlations (point estimate credible intervals not spanning zero) from (A) based on the multivariate model. Correlation direction denoted by + or - and strength by line width. Within individual correlations are in black, among-individual correlations in grey. Full correlation matrices are found in Tables 7 and 8.

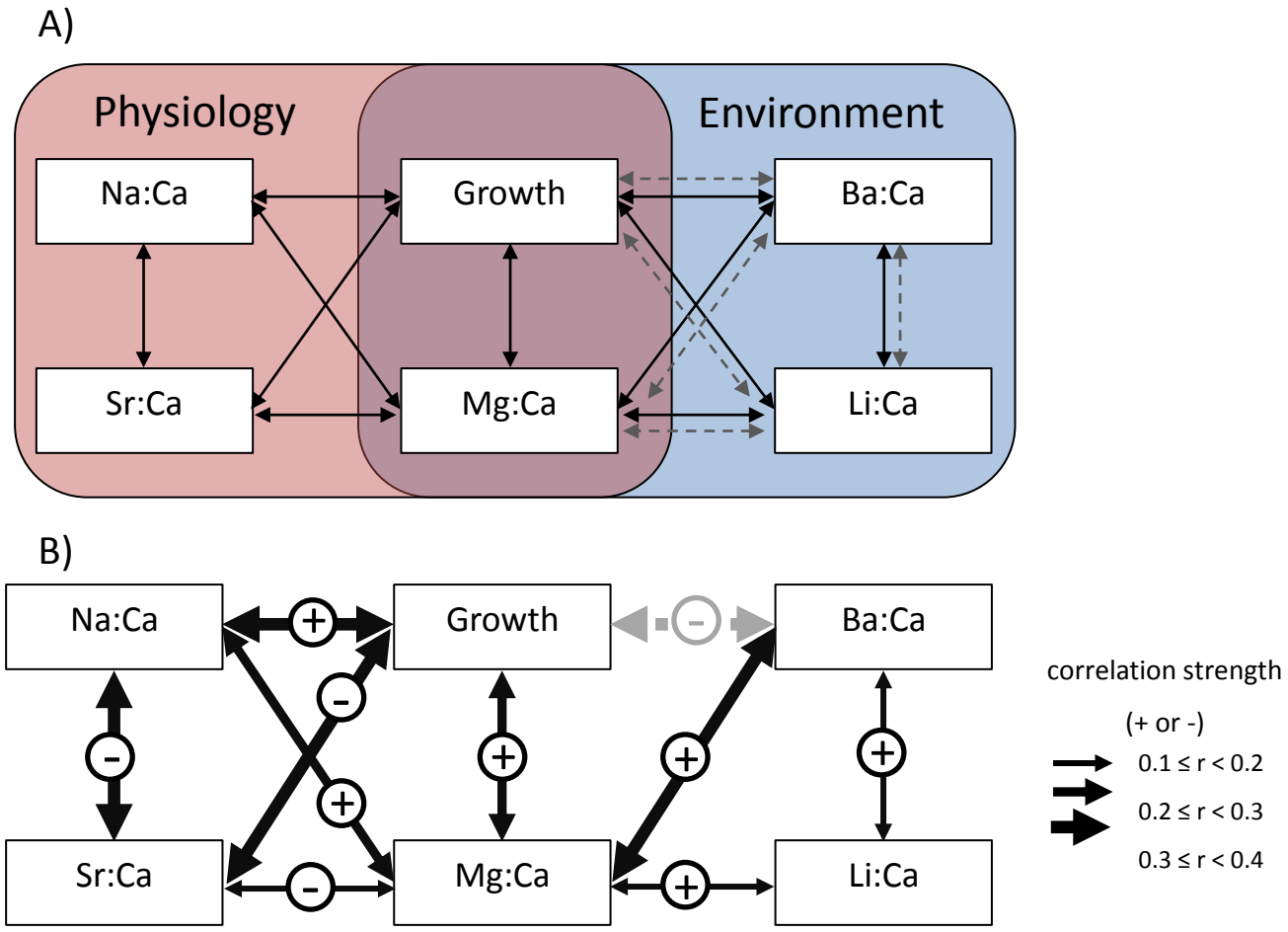

Our test species is the reef ocean perch (*Helicolenus percoides*; here after referred to as 'ocean perch'), a long-lived, benthic fish found in continental marine waters of southern Australia and New Zealand. We focused on this species for both biological (i.e. longevity, non-migratory, benthic, fully marine) and environmental reasons. Ocean perch for this study were collected from a region dominated by seasonal upwelling (Fig. 2a). Upwelling is a wind-driven, oceanographic process that brings cold, nutrient-rich, deep-water masses to the ocean's surface (Botsford et al. 2003). Upwelled waters typically leave distinctive trace element signatures in biological carbonates due to differences in water mass chemistry and associated links to primary productivity (e.g. coral: Lea et al. 1989, otoliths: Kingsford et al. 2009, molluscs: Hatch et al. 2013). Coastal upwelling events along Australia's southern coast are distinct, seasonal occurrences (austral summer: December to April; Middleton and Bye 2007) that provide much needed nutrients to the oligotrophic waters of this region (Nieblas et al. 2009, van Ruth et al. 2010).

Here, we use the simultaneous combination of biogeochemical tracers and fish growth with univariate and multivariate mixed-effects modelling to describe physiological and environmental controls on otolith chemistry. We examine intrinsic age-dependent relationships on trace element assimilation and growth over multiple years at a monthly timescale. We apply the strong, local upwelling signal as an extrinsic cue to explore synergistic effects of age and environment on chemical assimilation into the otolith and on fish growth.

Methods:

Oceanographic setting & study species

In the southeastern Indian Ocean, upwelling occurs along the Bonney Coast of southern Australia in the austral summer as two to four upwelling events, each lasting three to ten days in duration, interspersed by episodes of weak downwelling and surface water mixing (Kämpf et al. 2004, Middleton and Bye 2007). These upwelling areas are wind-forced and influenced by the Flinders Current flowing westward along the shelf-slope of southern Australia (Middleton and Bye 2007). The Flinders Current results from wind curl stress and the equatorward Sverdrup transport of water in the Southern Ocean; it is similar to larger

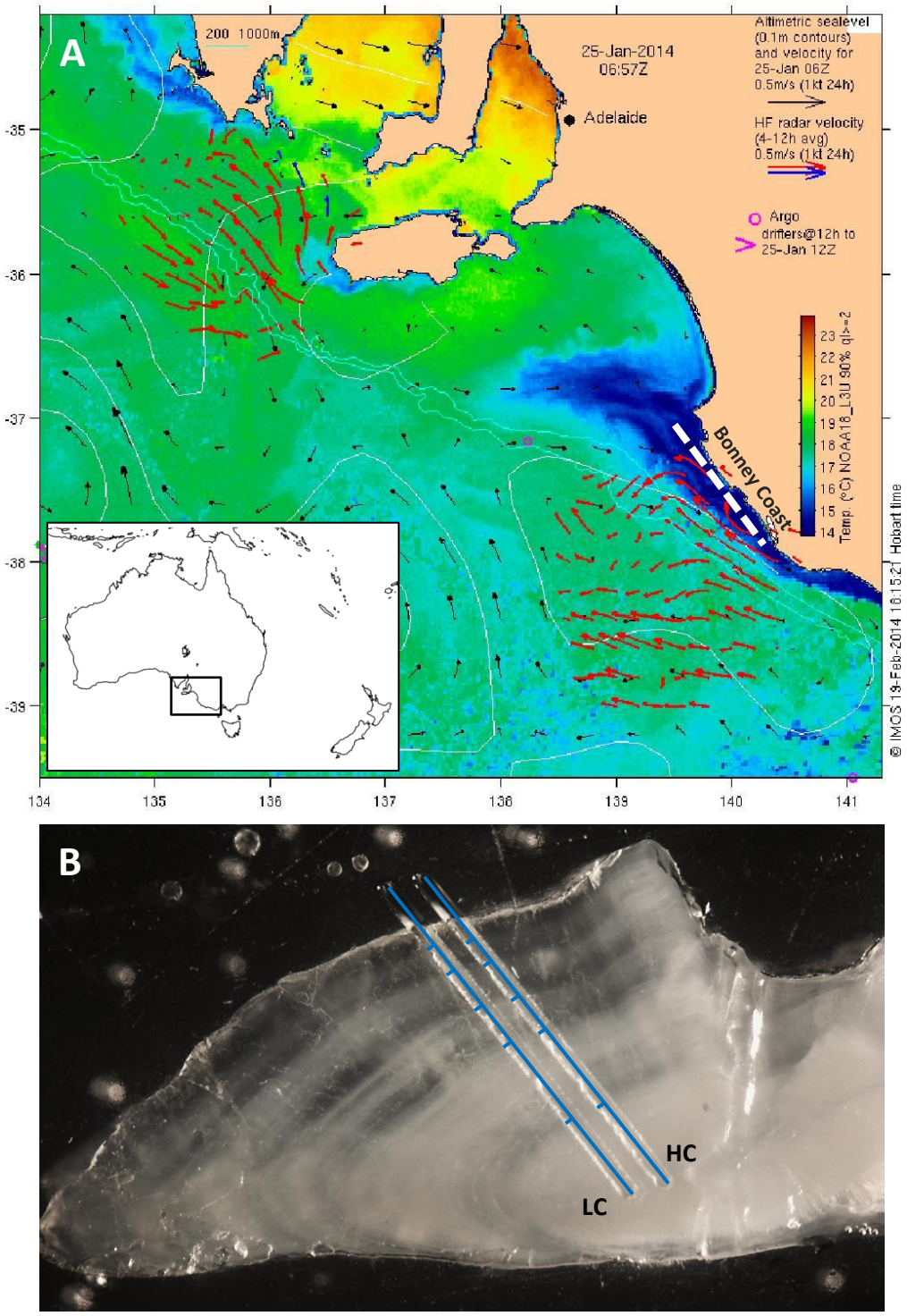

Fig. 2: A) Map of the southeastern coast of South Australia during an upwelling event in January 2014. The strongest area of upwelling occurs off the Bonney Coast region where ocean perch otoliths were collected (dashed white line). Sea surface temperatures range from 14°C (dark blue) to 23°C (red). B) Ventral lobe of a thin-sectioned ocean perch otolith with dual laser transects (highlighted in blue) from low element concentration (LC) and high element concentration (HC) scans. Transects run from the otolith's core to the proximal edge. This fish was 5+ years old when collected in 2011 (tics on blue lines mark each annual growth increment). [SST image credit: Data was sourced from the Integrated Marine Observing System (IMOS) - IMOS is a national collaborative research infrastructure, supported by the Australian Government]

western boundary currents but is actually part of a northern boundary current system that produces upwelling areas (Middleton and Cirano 2002, Middleton and Bye 2007). A reversal in current strength occurs in the winter months of southern Australia where an eastward flowing current, the Leeuwin Current, becomes dominant and produces downwelling. Both the Flinders and Leeuwin Current systems are wind-dominated, which causes the seasonal strengthening or weakening of either current system (Middleton and Bye 2007, James and Bone 2011).

Ocean perch were collected from the upwelling area along the Bonney Coast of southern Australia (near 37°40'S, 139°50'E; Fig. 2a) at depths between 43 and 119 m (mean: 80 m). Ocean perch are lecithotrophic (live bearing; Pavlov and Emel'yanova 2013) and demersal as both juveniles and adults (Park 1993, Smith et al. 2009). Juveniles and adults are benthopelagic omnivores (Bulman et al. 2001) with ontogenetic diet shifts from smaller crustaceans (mysids and galatheids) to larger crustaceans (scampi and two-spine crab; Horn et al. 2012). Benthic fish and salps (carcasses as food-fall; Henschke et al. 2013) are also important dietary components for all ages (Bulman et al. 2001, Horn et al. 2012).

Otolith preparation

Ocean perch were caught from October 2011 to January 2013 and ranged in size from 160 to 344 mm total length (TL). Sagittal otoliths were removed from the fish, cleaned and stored dry. One otolith from each fish (n = 38) was embedded in epoxy resin, transversely thin sectioned to include the primordium, polished with lapping film, and mounted on a microscope slide using thermoplastic cement. Both the epoxy resin and thermoplastic cement were spiked with indium chloride as an indicator of those substances. Slides were cleaned in ultrapure water and air dried.

Analysis of elemental otolith chemistry

Concentrations of elements were measured in the otolith from the core to the proximal, dorsal edge using a Resonetics M-50-LR 193nm Excimer laser ablation system coupled to an Agilent 7700cx quadrupole ICP-MS (housed at Adelaide Microscopy, The University of Adelaide). The laser was operated at a scan speed of 4 $\mu m \cdot s^{-1}$ with a frequency of 10 Hz using a 33 µm diameter to produce continuous laser transects across the otoliths. Prior to

each ablation, background levels of elements in the ablation chamber were measured for 30 s and a pre-ablation path 45 µm diameter was made. Instrument drift and precision was measured by analysing a reference standard (NIST612) after about every 10 samples and a carbonate standard (MACS3; US Geological Survey) at the beginning and end of each laser session (~5 hrs). Dual transects were ablated on each otolith to allow the laser to be optimized for higher and lower concentration elements. High concentration elements measured were ^{23}Na (dwell time: 50 ms), ^{88}Sr (100 ms), ^{24}Mg (100 ms) and ^{138}Ba (100 ms). ^{7}Li (150 ms) was the only low concentration element measured. For both transects, ^{43}Ca (5 ms), ^{44}Ca (5 ms) and ^{115}In (high concentration: 10 ms; low concentration: 5 ms) were also measured to produce element:Ca ratios and confirm otolith material was constantly ablated. Raw data were processed using GLITTER software (Griffin et al. 2008) and all elements were normalised to Ca and presented as element:Ca (mmol·mol^{-1}).

Monthly resolution of growth increments and element:Ca profiles

Ablated otolith sections were viewed with a compound microscope and digital camera system (×87.5 magnification; Leica DFC320 digital camera) for age interpretation and growth increment measurement. Along each ablation path, the annual growth increments were marked and measured (mm; Image-Pro Plus v. 7.0, MediaCybernetics); then, the hyaline and opaque zones were measured (mm) within each annual increment. The proportion of hyaline to opaque material within an annual growth increment was approximately 50%. We designated the hyaline growth zone as forming from November to March (5 months), and the opaque zones as being deposited from April to October (7 months). These timeframes are based on combined ocean perch age data from age validations (Paul and Horn 2009), marginal increment analysis (Park 1993), and the status of the otolith's marginal edge at the time of capture in the current study. Ages of ocean perch have been validated and each annual growth increment is comprised of one opaque growth zone and one hyaline growth zone (Paul and Horn 2009). Ocean perch from the Bonney Upwelling region were assigned a birthdate of October 1 based on the peak spawning season (September to November) of ocean perch in southeastern Australia (Park 1993).

We assigned each annual growth increment a year relative to the date of capture taking into account the marginal increment. Then, starting at the outer edge of the opaque core

region (represents transition of growth at end of fish's first winter; Paul and Horn 2009) and progressing towards the otolith's edge, the hyaline and opaque zones were resolved to monthly increments by dividing the total measurement of each zone by its corresponding number of months, e.g. hyaline measurement divided by five months or opaque measurement divided by seven months. The element:Ca transect data were resolved in a similar fashion. Since the laser was operated in a time resolved mode, we used the scan speed ($\mu m \cdot s^{-1}$) to convert each time dated element:Ca data point (s) to a distance measurement (μm). Next, we aligned these data to the growth increment measurements using the otolith edge as the reference point to assign appropriate years. Finally, we resolved the element:Ca data to monthly increments as above, starting at the outer edge of the opaque core region and progressing outwards. The element:Ca transect data and growth measurements were trimmed to only include years 2 to 7 (maximum). This allowed certainty of the starting point of the data when resolving to monthly increments (year 2 begins at the edge of opaque core region) and provided at least two element:Ca data points for each month. Generally after year 7, the width of the monthly growth increment decreased to the point where the laser scan speed, coupled with the ablation diameter, was equal to or greater than that increment width. Because growth was resolved to monthly increments on both the low concentration and high concentration elemental transects, these measurements were averaged and combined into one growth transect (*Growth*) for subsequent analyses.

Univariate mixed modelling to estimate intrinsic and extrinsic variation

We applied six univariate mixed models to the monthly resolved element:Ca (*Na:Ca, Sr:Ca, Mg:Ca, Ba:Ca, Li:Ca*) and growth (*Growth*) data extracted from the otoliths to examine relationships with upwelling events. These models enabled us to partition monthly variation of the response variables (*Na:Ca, Sr:Ca, Mg:Ca, Ba:Ca, Li:Ca* or *Growth*) between intrinsic (e.g. age) and extrinsic (e.g. upwelling index) drivers (Weisberg et al. 2010, Morrongiello et al. 2014). The intrinsic covariates were fish age in months (*Age*) and age in months at capture (*age.month.cap*), whilst extrinsic variables demarcated monthly characteristics of upwelling: an upwelling index (*Bonney UI*), bottom temperature (*Bottom Temp*) and levels of chlorophyll a (*Chl-a*) (full descriptions in Table 1).

Table 1. Description of fixed (intrinsic and extrinsic) and random effects used in the analyses of trace elements and growth derived from the otoliths of ocean perch.

Variable	Description	Data Range
Intrinsic Fixed effects		
Age	Age when each monthly increment was formed.	14 - 85 mo (1.2 - 7.1 yrs)
age.month.cap	Age of the fish in months at date of capture	37 - 223 mo (3.1 - 18.6 yrs)
Random Effects		
FishID	Unique identifier for each fish	n = 38
Month	A code designating the specific month and year of each monthly resolved increment (i.e. 75 = Dec 1996, 76 = Jan 1997)	204 mo (17 yrs) (Nov 1995 - Oct 2012)
Extrinsic Fixed effects		
Bonney UI	Monthly NOAA PFEL Global 1-degree Upwelling Index calculated for the Bonney Coast region of South Australia (37.6°S, 139.8°E; coast angle: 144°) *Source: http://www.pfeg.noaa.gov/products/las/docs/global_upwell.html*	1981 - 2014
Bottom Temp	Corrected monthly Bluelink bottom temperature (°C) derived in Middleton et al. (2012) and extended with bottom temperature logger data from Southend, SA	1993 - 2013
Chl-a	MODIS Aqua Level 3 Global Monthly Mapped 4 km Chlorophyll a ($mg \cdot m^3$) for the Bonney Coast, SA (37°S, 139°E) *Source: http://thredds.jpl.nasa.gov/las/getUI.do*	2002 - 2013

Following the two-stage procedure of Morrongiello and Thresher (2015), we developed a series of linear mixed-effect models that combined fixed intrinsic variables (*Age*, *age.month.cap*) with different random effect structures in a hierarchical manner to isolate sources of variation in otolith trace element concentrations or fish growth (Table 2). Then, we introduced extrinsic environmental variables into the resulting best models to relate the observed variability to the environment. We used R 3.0.3 with the packages of 'lme4' ('lmer' function; Bates et al. 2014), 'effects' (Fox et al. 2014), and 'AICcmodavg' (Mazerolle 2015) to perform model analyses (R Development Core Team 2014), and the 'Hmisc' package ('rcorr' function; Harrell 2014) to compare among upwelling variables with pairwise Pearson's correlation coefficients. All response variables and *Age* were natural-log transformed to meet model assumptions and fixed predictor variables were mean centred to assist model convergence (Morrongiello et al. 2014, Morrongiello and Thresher 2015). Akaike's Information Criterion (*AIC*) corrected for small sample sizes (*AICc*) was used to test relative support for each model (Burnham and Anderson 2004). We also used marginal and conditional R^2 metrics for mixed effects models (Nakagawa and Schielzeth 2013, Johnson 2014) to estimate the proportion of variance for fixed effects alone and combined fixed and random effects, respectively.

The element:Ca and growth data were comprised of repeated monthly measures (trace element concentrations or growth increment width) from each individual across multiple years. Random effects structures (n = 4; Table 2) contained random intercepts for *FishID* and *Month* (see Table 1 for descriptions) in combination with random slopes for *Age*. Random intercepts for *FishID* and *Month* generate correlation among measurements within an individual and correlation among trace element concentrations or growth increments assimilated in the same month per year, respectively. Individual trace element concentration or growth was allowed to vary in comparison to the model average by using a *FishID* random intercept. Likewise, a random *Month* intercept gives temporally resolved (month per year) estimates of whether extrinsic drivers provided good or poor conditions for trace element assimilation or growth relative to the long term mean (Morrongiello et al. 2014, Morrongiello and Thresher 2015). Random slopes for *Age* enabled the fixed effect *Age ~ element:Ca* or *Growth* relationship to vary among individuals and among months per year. Random *Age* slopes for each fish permit a distinct age-dependent trace element

Table 2. Best random effect structure (highlighted in **bold**) fitted with the full fixed effect structure of *Age + age.month.cap* for each element:Ca ratio and average growth. Best model rankings were assessed using AICc. Random slope term designated with A|B.

	Ba:Ca				Na:Ca				Sr:Ca			
Model	df	AICc	ΔAICc	Log Likelihood	df	AICc	ΔAICc	Log Likelihood	df	AICc	ΔAICc	Log Likelihood
FishID	5	-1034.60	561.11	522.31	5	-6180.57	483.68	3095.30	5	-5681.03	462.22	2845.53
Age|FishID	7	-1470.50	125.21	742.27	7	-6419.22	245.03	3216.64	7	-5997.87	145.38	3005.96
Age|FishID + Month	8	-1513.44	82.27	764.75	8	-6660.21	4.05	3338.13	8	-6116.31	26.94	3066.18
Age|FishID + Age|Month	**10**	**-1595.71**	**0.00**	**807.90**	**10**	**-6664.25**	**0.00**	**3342.17**	**10**	**-6143.25**	**0.00**	**3081.67**

	Mg:Ca				Li:Ca				AvGrowth			
Model	df	AICc	ΔAICc	Log Likelihood	df	AICc	ΔAICc	Log Likelihood	df	AICc	ΔAICc	Log Likelihood
FishID	5	-2025.91	323.48	1017.97	5	1889.82	813.49	-939.90	5	-696.97	1099.24	353.50
Age|FishID	7	-2291.68	57.71	1152.87	7	1225.35	149.01	-605.65	7	-1182.57	613.64	598.31
Age|FishID + Month	8	-2321.44	27.96	1168.75	8	1135.86	59.52	-559.90	8	-1568.77	227.45	792.41
Age|FishID + Age|Month	**10**	**-2349.39**	**0.00**	**1184.75**	**10**	**1076.34**	**0.00**	**-528.12**	**10**	**-1796.22**	**0.00**	**908.15**

assimilation or growth trajectory while still inferring an age response for the population. Similarly, a random *Age* slope for *Month* allows for age-dependent responses to environmental effects through time (Morrongiello et al. 2014, Morrongiello and Thresher 2015).

The best random effect structures for the six response variables were selected by adding all fixed intrinsic effects (*Age*, *age.month.cap*) to each possible random effects structure and fitting the models using restricted maximum likelihood estimates of error (REML). The most complex model took the form:

$$y_{ijkl} = \alpha_0 + \alpha_i^F + \alpha_k^M + \beta_1 x_{ij} + b_{1i}^F x_{ij} + b_{1k}^M x_{jk} + \beta_2 x_l + \varepsilon_{ijk}$$

$$\begin{bmatrix} \alpha_i^F \\ b_{1i}^F \end{bmatrix} \sim N(0, \Sigma_i), \qquad \begin{bmatrix} \alpha_k^M \\ b_{1k}^M \end{bmatrix} \sim N(0, \Sigma_k), \qquad \varepsilon_{ijk} \sim N(0, \sigma^2)$$

Where y_{ijkl} is a response variable measurement for fish *i* at age *j* from month *k,* caught at age (*age.month.cap*) *l*. α_0 is the overall mean monthly response intercept, α_i^F is the random intrinsic effect for fish *I*, and α_k^Y is the random extrinsic environmental effect for month *k*. β_1 is the fixed effect *Age* coefficient, β_2 is the fixed effect *age.month.cap* coefficient, and b_{1i}^F and b_{1k}^M are random *Age* slopes for fish *I* and month *k* respectively.

Next, the fixed effect structures of either *Age* or *Age* + *age.month.cap* were fit to the best random effects structure (from above) for each response variable with maximum likelihood estimates of error (ML). Each candidate set of models were compared with ΔAICc values. Then, unbiased parameter estimates were produced for each response variable by refitting the best ranked models with REML (Zuur et al. 2009). We estimated the temporal synchrony of trace element assimilation or growth across individuals by calculating the interclass correlation coefficient (ICC). The ICC model contained random intercepts for both *FishID* and *Month*, but a random *Age* slope was only included for *FishID* to ensure interpretability of the *Month* variance component (Morrongiello and Thresher 2015). Finally, we added the upwelling specific, environmental covariates (*Bonney UI*, *Bottom Temp*, *Chl-a*; Table 1) to each optimal model to assess extrinsic effects within and among the response variables. We also tested for *Age* specific responses of elements or growth for each environmental covariate by fitting interaction terms.

Multivariate mixed model to estimate within and among individual correlations

Because the six response variables represent repeated measures of multiple elements and growth within the otolith of each fish, it is of interest to estimate correlations among these otolith 'traits' both within and among individuals (response variables here after are referred to as traits). This will allow us to estimate the strength and direction of relationships between the trace elements themselves, as well as growth, and begin linking these to either physiology (intrinsic effects), the environment (extrinsic effects) or both. It is important to note that the six traits (elements: n = 5; growth: n = 1) are dependent on the same intrinsic and extrinsic drivers at a given time and are not independent of one another. Whilst among individual correlations can be based on average trait values for each individual derived from the series of univariate models outlined above, these values will be biased due to unaccounted-for within-individual variation and do not properly account for uncertainty around element:Ca or growth estimates (Hadfield et al. 2010, Dingemanse and Dochtermann 2013). Furthermore, such an approach precludes the estimation of trait correlation within otoliths (e.g. is a period of high growth related to an increase or decrease in a particular element). Multivariate mixed-effects models avoid these limitations and allow for the concordant estimation of both within and among individual trait variation across multiple traits (Dingemanse and Dochtermann 2013).

We used a multivariate mixed effects linear model fitted in the 'MCMCglmm' package of R (Hadfield 2010) which applies a Bayesian approach to estimate variance-covariance matrices within individuals (**I**) and among individuals (**R**) for all six traits (bold font denotes matrices). These matrices were then used to generate point estimates and 95% credible intervals for each pair-wise within and among individual otolith trait correlation; credible intervals that do not overlap zero indicate statistical significance. Multivariate mixed models fit with MCMCglmm can cope with missing response values, which was beneficial as not all otolith traits were measured at each point along an otolith transect (e.g. Li could not be monthly resolved past a certain age due to decreasing otolith growth increment widths and limitations of the laser ablation ICP-MS system).

Similar to univariate analyses, all traits were natural log-transformed to meet assumptions of normality. They were then standardised (observation-mean/SD) to ensure similar scales, which aids model convergence and parameter interpretation. Our multivariate mixed model included fixed effects for trait-specific *Age* (natural log-transformed) and trait-specific *age.month.cap* terms to account for intrinsic effects on growth and elemental assimilation into the otolith (Table 1). In the majority of the univariate models, a random effect structure allowing for individual- and month-specific differences in the *Age* coefficient performed best. We therefore used this random effect structure here as well, adding the additional complexity that these individual and month random slopes could vary across elements (e.g. an individual might have a steeper than average Na:Ca-age relationship but a shallower than average growth-age relationship).

We used parameter expanded priors (Hadfield 2010), ran our model for 110,000 iterations with a burn-in phase of 10,000 and a thinning interval of 25. This resulted in a well-mixed chain, no autocorrelation and a sample size of 4,000 values for each estimate.

Results:

Sources of element:Ca and growth variation

The best random effects structure for all otolith traits included a random *Age* slope on both *FishID* and *Month* (Table 2), which means the *element:Ca ~ age* and *Growth ~ age* relationships vary among individual fish and months. For Sr:Ca, Ba:Ca and Li:Ca, the best fixed effects structure included both *Age* and *age.month.cap* terms, while Na:Ca, Mg:Ca and growth included *Age* only (Table 3). Growth, Ba:Ca, Na:Ca, Mg:Ca and Li:Ca all decreased with age, while Sr:Ca increased with age (Table 3, Fig. 3). Older fish at capture had higher overall levels of Ba:Ca and Sr:Ca than younger fish (positive *age.month.cap* slope), while the negative *age.month.cap* slope seen in Li:Ca indicated that younger fish had overall higher Li:Ca levels than older fish (Table 3). These differences suggest older fish most likely have experienced slightly different environmental/dietary conditions during the earlier years of their lives than the younger fish have experienced during that same portion of their own lives. Power functions fit to *element:Ca ~ age* and *Growth ~ age* relationships

Table 3. Variance components, parameter estimates and test statistics for the optimal model of each element:Ca and average growth fitted with restricted maximum likelihood (REML). Random slope term designated with A|B.

	Ba:Ca			Na:Ca			Sr:Ca		
Random Effect	Var.	±SD	Corr.	Var.	±SD	Corr.	Var.	±SD	Corr.
FishID	0.020	0.142		0.005	0.074		0.002	0.047	
Age|FishID	0.033	0.180	0.220	0.003	0.053	0.470	0.005	0.068	0.330
Month	0.002	0.048		0.001	0.026		0.001	0.024	
Age|Month	0.010	0.100	-0.800	0.000	0.008	-1.000	0.001	0.022	-0.840
Residual	0.024	0.155		0.003	0.053		0.004	0.060	
Fixed Effect	Estimate	±SE	t-statistic	Estimate	±SE	t-statistic	Estimate	±SE	t-statistic
Intercept	0.492	0.024	20.491	9.338	0.012	754.100	8.082	0.008	991.400
Age	-0.187	0.032	-5.830	-0.189	0.009	-20.400	0.143	0.012	12.100
age.month.cap	0.001	0.000	1.684	-	-	-	0.000	0.000	2.300

	Mg:Ca			Li:Ca			AvGrowth		
Random Effect	Var.	±SD	Corr.	Var.	±SD	Corr.	Var.	±SD	Corr.
FishID	0.026	0.160		0.077	0.277		0.032	0.178	
Age|FishID	0.015	0.122	0.300	0.197	0.443	0.200	0.060	0.245	0.310
Month	0.001	0.032		0.008	0.088		0.008	0.091	
Age|Month	0.004	0.060	-0.890	0.026	0.160	-0.810	0.019	0.138	0.710
Residual	0.017	0.131		0.076	0.275		0.020	0.140	
Fixed Effect	Estimate	±SE	t-statistic	Estimate	±SE	t-statistic	Estimate	±SE	t-statistic
Intercept	3.903	0.027	142.700	2.212	0.046	47.830	2.137	0.030	71.570
Age	-0.188	0.022	-8.390	-0.344	0.075	-4.550	-0.883	0.042	-20.930
age.month.cap	-	-	-	-0.002	0.001	-2.650	-	-	-

Fig. 3. Predicted monthly variation in otolith trace elements (element:Ca; µmol/mol) and average growth (Growth; µm) of ocean perch from the Bonney upwelling region. Power functions shown describe element:Ca assimilation rate (AR; µmol·mol^{-1}·month^{-1}) or growth rate (GR; µm·month^{-1}).

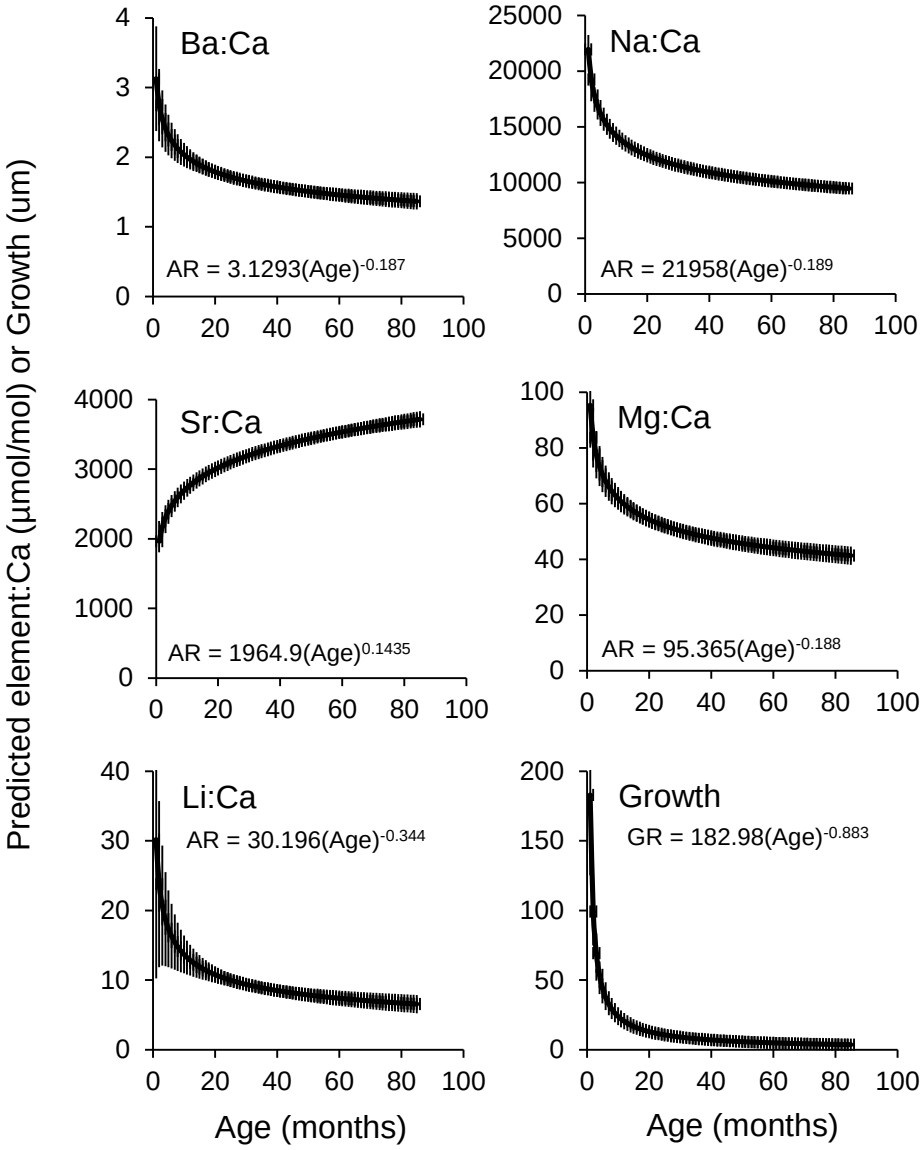

estimated assimilation/growth rates (AR: µmol·mol^{-1}·month^{-1}; GR: µm·month^{-1}) for ocean perch (Fig. 3).

Random variability around mean *element:Ca* or *Growth* was greatest among fish (*FishID*) followed by among months (*Month*) (Table 3). *Element:Ca* or *Growth ~ Age* slopes had the highest variation among individuals followed by variation among months. All *element:Ca* data displayed negative correlations between the *Month* random intercept and *Age* slope, signifying that younger fish assimilate higher concentrations of trace elements compared to older fish when conditions are favourable for element assimilation (older fish assimilate relatively higher concentrations than younger fish when conditions are less favourable for element assimilation; Table 3). A positive correlation between the *Month* random intercept and *Growth ~ Age* slope (slopes are shallower at higher intercepts) indicates older fish are growing proportionally better than younger fish during months of good growth (younger fish grow better in poor times). Random *Age* slopes of the otolith traits were positively correlated with *FishID*, meaning there is variation in growth or trace element assimilation across individuals (larger *FishID* effects lead to greater growth variation across individuals). Trace element assimilation of Na:Ca and Sr:Ca varied the least across individuals as they aged (corr: 0.470 and 0.330, respectively), whereas Ba:Ca and Li:Ca varied the most (corr: 0.220 and 0.200, respectively). When compared to trace element assimilation, growth varied moderately across individuals (corr: 0.310).

Patterns in temporal variation of the otolith traits (extracted from the *Month* random effect term) all showed a cyclic signal (Fig. 4). Na:Ca and Sr:Ca varied the least through time, but displayed periodicity. The amount of synchrony seen in each trace element among individuals in each month ranged from a low ICC of 1.74% (Mg:Ca) to a high of 5.08% (Na:Ca) (Table 4). Growth had the highest ICC of 8.50%.

Relating temporal variation of element:Ca and growth data to environmental parameters

Upwelling-specific environmental covariates improved all intrinsic effect models (Tables 5 and 6). The upwelling index with an age interaction (*Age * Bonney UI*) best explained variation for Na:Ca, Sr:Ca and growth (Table 3). The upwelling index alone (*Bonney UI*) best explained variation for Ba:Ca and Mg:Ca, and chlorophyll-a (*Chl-a*) concentrations

Fig. 4. Monthly resolved otolith trace elements (ratioed to calcium) and average growth predicted for ocean perch in the Bonney upwelling region in South Australia. Chronologies (black lines) are produced from the *Month* random effect term (best linear unbiased predictors 'BLUPs') and are plotted along with the regional upwelling index (grey line).

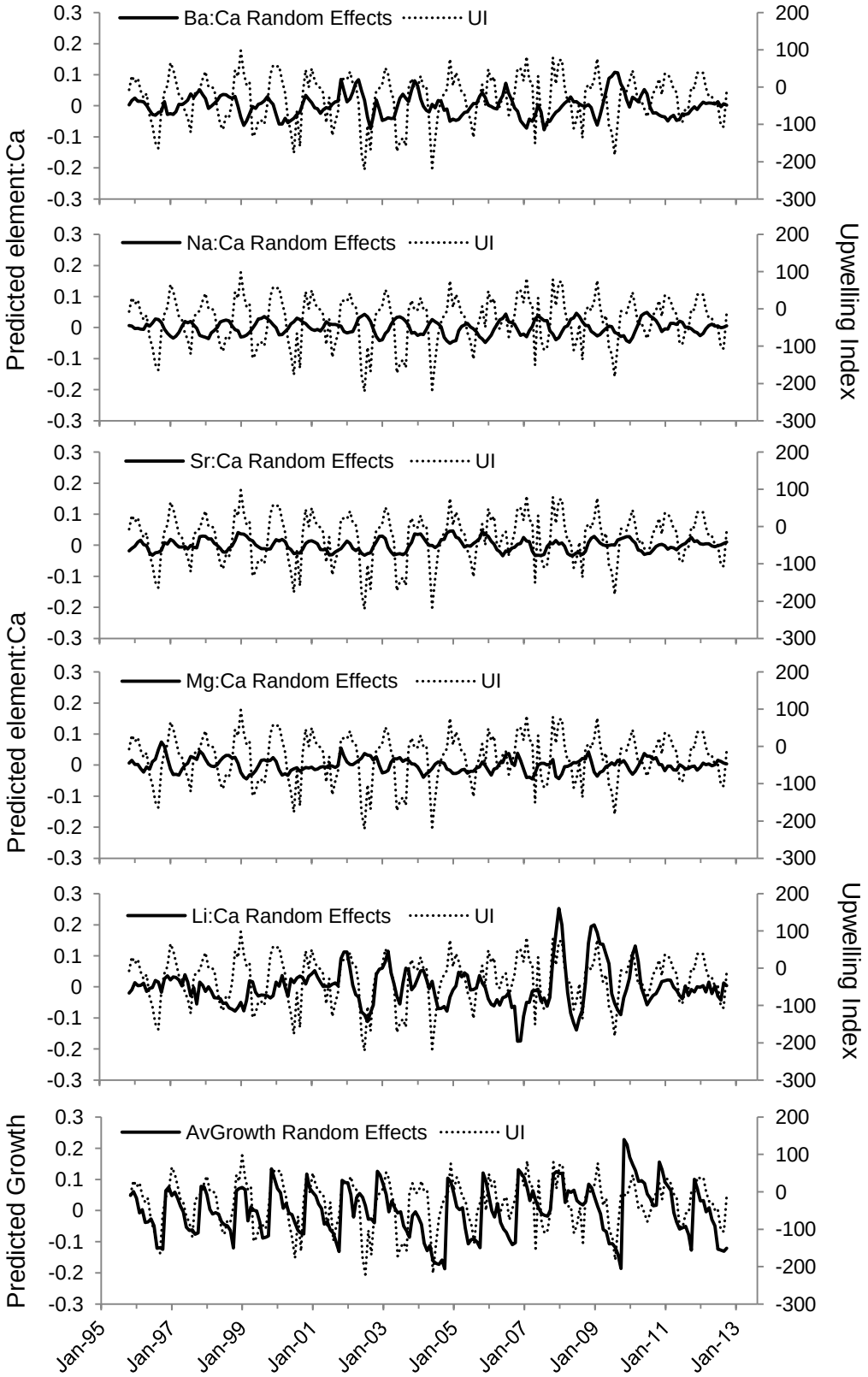

Table 4. Intraclass correlation coefficients (ICC) of the six otolith traits for *Month*

	ICC *Month* (%)
Ba:Ca	2.05
Na:Ca	5.08
Sr:Ca	5.02
Mg:Ca	1.74
Li:Ca	3.30
AvGrowth	8.50

Table 5. Pearson's correlation coefficients (*r,* unshaded areas) for pairwise comparisons of environmental effects. Shaded areas indicate *P* values for correlations.

	Bonney UI	Bottom Temp	Chl-a
Bonney UI		-0.410	0.340
Bottom Temp	<0.001		-0.320
Chl-a	<0.001	<0.001	

Table 6. Model selection for environmental variables fitted to each optimal model with maximum likelihood (ML). Best explanatory variable or combination of variables is highlighted in **bold.** The second ranked variable(s) is *italicized*. Marginal (m) and conditional (c) R^2 values were calculated after models were refit with restricted maximum likelihood (REML). Also displayed are the parameter estimates and test statistics for the top and second ranked models.

Response Variable	Environmental Variables	df	AICc	ΔAICc	Log Likelihood	R^2m	R^2c	Estimate	±SE	t-statistic
Ba:Ca	+ Growth	10	-1620.3	4.7	820.2	0.127	0.626			
	+ Bonney UI	**11**	**-1625.0**	**0.0**	**823.5**	**0.128**	**0.626**	**-0.0002**	**0.0001**	**-2.616**
	+ Bottom Temp	11	-1618.7	6.3	820.4	0.127	0.627			
	+ Chl-a	11	-1047.0	577.9	534.6	0.123	0.603			
	*+ Age * Bonney UI*	*12*	*-1623.4*	*1.5*	*823.8*	*0.128*	*0.626*	*0.0001*	*0.0002*	*0.710*
	+ Age * Bottom Temp	12	-1619.4	5.5	821.8	0.128	0.627			
	+ Age * Chl-a	12	-1045.2	579.7	534.7	0.123	0.603			
Na:Ca	+ Growth	9	-6696.2	95.0	3357.1	0.461	0.842			
	+ Bonney UI	*10*	*-6778.9*	*12.3*	*3399.5*	*0.469*	*0.839*	*-0.0003*	*0.0000*	*-10.600*
	+ Bottom Temp	10	-6720.4	70.8	3370.2	0.464	0.840			
	+ Chl-a	10	-4111.2	2680.0	2065.7	0.443	0.839			
	+ Age * Bonney UI	**11**	**-6791.2**	**0.0**	**3406.7**	**0.470**	**0.839**	**0.0001**	**0.0000**	**3.800**
	+ Age * Bottom Temp	11	-6724.7	66.5	3373.4	0.465	0.840			
	+ Age * Chl-a	11	-4113.4	2677.8	2067.8	0.444	0.840			
Sr:Ca	+ Growth	10	-6174.2	75.5	3097.1	0.416	0.724			
	+ Bonney UI	*11*	*-6225.4*	*24.3*	*3123.7*	*0.438*	*0.719*	*0.0002*	*0.0000*	*8.600*
	+ Bottom Temp	11	-6197.8	51.9	3110.0	0.425	0.721			
	+ Chl-a	11	-3851.3	2398.4	1936.7	0.383	0.740			
	+ Age * Bonney UI	**12**	**-6249.7**	**0.0**	**3136.9**	**0.440**	**0.717**	**-0.0003**	**0.0000**	**-5.400**
	+ Age * Bottom Temp	12	-6199.0	50.6	3111.6	0.426	0.721			
	+ Age * Chl-a	12	-3854.6	2395.1	1939.4	0.385	0.739			

Table 6. *continued.* Model selection for environmental variables fitted to each optimal model with maximum likelihood (ML). Best explanatory variable or combination of variables is highlighted in **bold.** The second ranked variable(s) is *italicized*. Marginal (m) and conditional (c) R^2 values were calculated after models were refit with restricted maximum likelihood (REML). Also displayed are the parameter estimates and test statistics for the top and second ranked models.

Response Variable	Environmental Variables	df	AICc	ΔAICc	Log Likelihood	R^2m	R^2c	Estimate	±SE	t-statistic
Mg:Ca	+ Growth	9	-2376.1	16.9	1197.1	0.145	0.695			
	+ Bonney UI	**10**	**-2393.0**	**0.0**	**1206.6**	**0.147**	**0.695**	**-0.0002**	**0.0000**	**-4.430**
	+ Bottom Temp	10	-2375.6	17.4	1197.9	0.146	0.695			
	+ Chl-a	10	-1531.2	861.9	775.7	0.152	0.672			
	*+ Age * Bonney UI*	*11*	*-2392.2*	*0.8*	*1207.2*	*0.147*	*0.696*	*0.0001*	*0.0001*	*1.080*
	+ Age * Bottom Temp	11	-2377.7	15.3	1199.9	0.147	0.696			
	+ Age * Chl-a	11	-1541.1	851.9	781.7	0.154	0.673			
Li:Ca	+ Growth	10	1056.1	198.5	-518.0	0.184	0.706			
	+ Bonney UI	11	1047.3	189.6	-512.6	0.191	0.709			
	+ Bottom Temp	11	1055.5	197.9	-516.7	0.186	0.706			
	+ Chl-a	**11**	**857.7**	**0.0**	**-417.7**	**0.204**	**0.693**	**0.1416**	**0.0324**	**4.373**
	+ Age * Bonney UI	12	1043.0	185.4	-509.4	0.197	0.709			
	+ Age * Bottom Temp	12	1053.2	195.5	-514.5	0.188	0.706			
	*+ Age * Chl-a*	*12*	*859.4*	*1.7*	*-417.6*	*0.207*	*0.693*	*-0.0424*	*0.0795*	*-0.534*
AvGrowth	+ Growth	9	-1821.4	63.2	919.7	0.699	0.924			
	+ Bonney UI	*10*	*-1849.2*	*35.3*	*934.7*	*0.710*	*0.924*	*0.0006*	*0.0001*	*6.350*
	+ Bottom Temp	10	-1839.4	45.2	929.7	0.703	0.925			
	+ Chl-a	10	-1018.5	866.1	519.3	0.698	0.928			
	+ Age * Bonney UI	**11**	**-1884.6**	**0.0**	**953.3**	**0.713**	**0.925**	**0.0011**	**0.0002**	**6.480**
	+ Age * Bottom Temp	11	-1837.5	47.1	929.8	0.703	0.925			
	+ Age * Chl-a	11	-1020.2	864.3	521.2	0.698	0.928			

significantly improved model fit for Li:Ca (Table 3). Na:Ca, Mg:Ca, and Ba:Ca concentrations were all significantly and negatively related to the upwelling index; in contrast, Sr:Ca and growth were significantly and positively related to the upwelling index (Table 3, Figs. 5a - d, f). Li:Ca was positively related to monthly chlorophyll-a concentrations (Fig. 5e).

The elemental concentrations of younger fish showed a steeper rate of change over the range of environmental variables experienced by fish, suggesting younger fish increase or decrease their elemental assimilation more rapidly than older fish (Fig. 5g - k). This pattern was reversed when comparing growth at a given age with the upwelling index. Very young fish responded with negative, less rapid growth to increased upwelling, while older fish increased their growth rate when upwelling increased (Fig. 5l).

Estimating within and among individual correlations with multivariate mixed models

Within individual correlations of otolith traits revealed the strength and direction of relationships between the otolith traits (Table 7; Fig. 1b). Growth was moderately to weakly correlated with Na:Ca (0.304), Sr:Ca (-0.307), and Mg:Ca (0.270) (Table 7; Fig. 1b), whereas no significant correlation existed between growth and Ba:Ca or Li:Ca within an individual. A moderate, negative correlation was found between Na:Ca and Sr:Ca (-0.398). Mg:Ca was moderately correlated with Ba:Ca (0.301) and weakly correlated with Na:Ca (0.256). Very weak correlations existed between other pairs of traits (Table 7).

When comparing otolith traits among individuals, only Ba:Ca and growth were significantly correlated (-0.316; Table 8; Fig 5b). This suggests that individuals with overall higher growth generally have lower Ba:Ca, but this relationship was not found between monthly increments measured within an individual otolith. All other otolith traits were not correlated among individuals (Table 8; Fig. 1b).

Fig. 5. (on following page) Predicted effects for each element:Ca and average growth resulting from the best additive environmental effect model (a-f: left panels; dotted lines: ± SE) and the best environmental interaction with *Age* model (g-l: right panels). An asterisk in the upper right corner indicates the top ranked model as selected by AICc values (ΔAICc = 0; shown in Table 5).

Fig. 5

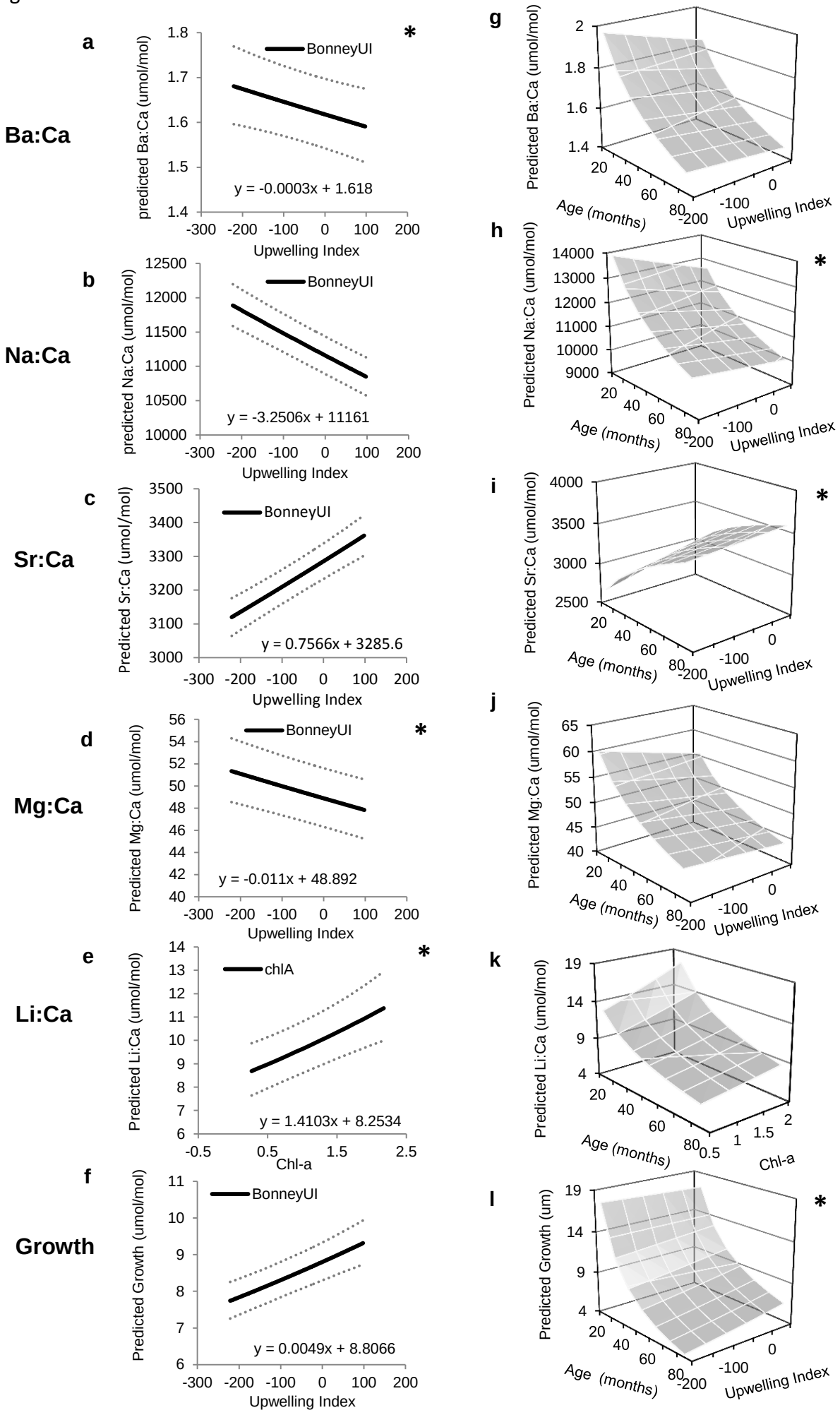
a
Ba:Ca
predicted Ba:Ca (umol/mol)
BonneyUI
y = -0.0003x + 1.618
Upwelling Index
b
Na:Ca
predicted Na:Ca (umol/mol)
BonneyUI
y = -3.2506x + 11161
Upwelling Index
c
Sr:Ca
Predicted Sr:Ca (umol/mol)
BonneyUI
y = 0.7566x + 3285.6
Upwelling Index
d
Mg:Ca
Predicted Mg:Ca (umol/mol)
BonneyUI
y = -0.011x + 48.892
Upwelling Index
e
Li:Ca
Predicted Li:Ca (umol/mol)
chlA
y = 1.4103x + 8.2534
Chl-a
f
Growth
Predicted Growth (umol/mol)
BonneyUI
y = 0.0049x + 8.8066
Upwelling Index
g
Predicted Ba:Ca (umol/mol)
Age (months)
Upwelling Index
h
Predicted Na:Ca (umol/mol)
Age (months)
Upwelling Index
i
Predicted Sr:Ca (umol/mol)
Age (months)
Upwelling Index
j
Predicted Mg:Ca (umol/mol)
Age (months)
Upwelling Index
k
Predicted Li:Ca (umol/mol)
Age (months)
Chl-a
l
Predicted Growth (um)
Age (months)
Upwelling Index

Table 7: Within-individual covariances (light grey), variances (dark grey) and correlation (un-shaded) point estimates and 95% credible intervals (in parentheses) among six otolith traits (element:Ca ratios and growth) derived from a multivariate mixed model. This model accounted for individual, monthly and trait-specific variation in *Age* and *age.month.cap*. Bold indicates a significant relationship.

	Growth	Sr	Ba	Li	Na	Mg
Growth	**0.046** **(0.219,0.246)**	**-0.307** **(-0.186,-0.086)**	-0.056 (-0.071,0.016**)**	0.088 (-0.006,0.083)	**0.304** **(0.1,0.167)**	**0.27** **(0.083,0.158)**
Sr	**-0.047** **(-0.06,-0.031**)	**0.514** **(0.483,0.545)**	**0.109** **(0.066,0.138)**	**0.05** **(0.011,0.091)**	**-0.398** **(-0.465,-0.327)**	**-0.102** **(-0.153,-0.053)**
Ba	-0.01 (-0.027,0.007)	**0.065** **(0.037,0.089)**	**0.706** **(0.67,0.755)**	**0.152** **(0.118,0.187**)	**0.136** **(0.1,0.169)**	**0.301** **(0.27,0.327**)
Li	0.015 (-0.002,0.033)	**0.028** **(0.006,0.054)**	**0.1** **(0.073,0.131)**	**0.61** **(0.58,0.655)**	**0.068** **(0.019,0.098)**	**0.152** **(0.113,0.187)**
Na	**0.046** **(0.032,0.06)**	**-0.2** **(-0.219,-0.174)**	**0.08** **(0.056,0.106)**	**0.037** **(0.01,0.057)**	**0.493** **(0.459,0.518)**	**0.256** **(0.227,0.29)**
Mg	**0.048** **(0.031,0.067)**	**-0.06** **(-0.085,-0.033)**	**0.208** **(0.177,0.241)**	**0.098** **(0.069,0.129)**	**0.148** **(0.123,0.177)**	**0.677** **(0.639,0.723)**

Table 8: Among-individual covariances (light grey), variances (dark grey) and correlation (un-shaded) point estimates and 95% credible intervals (in parentheses) among six otolith traits (element:Ca ratios and growth) derived from a multivariate mixed model. This model accounted for individual, monthly and trait-specific variation in *Age* and *age.month.cap*. Bold indicates a statistical significant relationship.

	Growth	Sr	Ba	Li	Na	Mg
	0.238	-0.105	**-0.316**	0.272	0.247	-0.304
Growth	**(0.127,0.381)**	(-0.855,0.173)	**(-1.433,-0.004)**	(-0.111,0.421)	(-0.307,0.392)	(-1.535,0.057)
	-0.029	**0.322**	0.28	0.216	-0.13	0.214
Sr	(-0.129,0.079)	**(0.18,0.544)**	(-0.146,0.424)	(-0.189,0.408)	(-1.242,0.099)	(-1.195,0.152)
	-0.115	0.118	**0.554**	0.004	-0.143	0.102
Ba	**(-0.288,-0.002)**	(-0.035,0.303)	**(0.318,0.94)**	(-0.55,0.259)	(-1.047,0.141)	(-0.525,0.327)
	0.129	0.119	0.003	**0.941**	0.006	-0.322
Li	(-0.029,0.322)	(-0.059,0.373)	(-0.23,0.311)	**(0.549,1.535)**	(-0.626,0.272)	(-1.594,0.031)
	0.05	-0.031	-0.044	0.002	**0.172**	0.293
Na	(-0.034,0.14)	(-0.161,0.043)	(-0.181,0.079)	(-0.142,0.196)	**(0.094,0.336)**	(-0.153,0.474)
	-0.089	0.073	0.046	-0.189	0.073	**0.364**
Mg	(-0.229,0.029)	(-0.212,0.091)	(-0.124,0.258)	(-0.494,0.031)	(-0.02,0.223)	**(0.175,0.659)**

Discussion:

Otolith chemistry and fish growth displayed cyclic seasonal signals over a 17 year period in a marine system. Age-dependent relationships existed in the element:Ca and growth profiles, and responses to the environment differed as the fish aged. Temporal signals were correlated with seasonal upwelling events. Since elemental concentrations and growth were measured simultaneously within the otolith, direct comparisons among otolith traits, both within and among individual fish, were made through time. Multivariate mixed modelling revealed the strength and direction of relationships between element:Ca and growth and supported our conceptual model hypothesising physiological-environmental controls on otolith chemistry. We found that within individual correlations among physiologically regulated elements were generally stronger than those primarily controlled by environmental drivers.

Sources of intrinsic variation in element:Ca and growth

Age-related responses differed with each element:Ca and growth in ocean perch otoliths. The rate of element assimilation decreased as the fish aged in four of the five elements (except Sr:Ca), and growth rate also decreased with age, as is typical in most fish species. Similar age-related relationships for Na:Ca and Sr:Ca have been reported for other marine species, e.g. blue grenadier (*Macruronus novaezelandiae*; Kalish 1989), Australian salmon (*Arripis trutta*; Hughes et al. 2015) and southern bluefin tuna (*Thunnus maccoyii*; Proctor et al. 1995). Comparable directional relationships were also evident in otolith Li:Ca, Ba:Ca, and Mg:Ca from Australian salmon (Hughes et al. 2015). It is interesting to note that, while comparable *element:Ca ~ age* responses are evident, these fish species inhabit different marine environments and have varied reproductive strategies: blue grenadier (benthic/continental slope waters, vertical migrations, isochronal spawner), Australian salmon (coastal, migratory, heterochronal spawner), southern bluefin tuna (pelagic, migratory, heterochronal spawner) and ocean perch (benthic/continental shelf waters, non-migratory, live-bearing) (e.g. Bruce et al. 2002). This suggests that these chemical patterns are a conserved and a robust proxy for fish responses to changing environmental conditions. Assimilation rates of Sr:Ca and Na:Ca ($\mu mol \cdot mol^{-1} \cdot yr^{-1}$) differed between ocean perch and blue grenadier (Kalish 1989) although directional relationships were the same as the fish aged. Most likely this is due to their disparate life history strategies. Lifetime assimilation rates of Ba:Ca, Li:Ca, and Mg:Ca in otoliths have not been previously estimated

for a marine fish. Age-related assimilation rates of elements should be considered when reconstructing migratory histories. As we have demonstrated, this is easily done through the use of univariate models that include age components as intrinsic effects.

Mg:Ca exhibited the least amount of synchrony between individuals through time. In marine fish, Mg in otoliths is not correlated with either temperature or salinity (as reviewed by Sturrock et al. 2012), but it is correlated with growth rate (Sturrock et al. 2015). Mg is required in many major metabolic pathways (Kaim et al. 2013), and the lack of synchrony could reflect individual metabolic processes and growth. Concentrations of Li:Ca and Ba:Ca showed moderate temporal synchrony compared to the other elements, and also displayed seasonal, cyclic signals. Both Li:Ca and Ba:Ca tend to primarily correlate with environmental parameters as opposed to physiological processes, such as reproduction (e.g. Sturrock et al. 2012, Sturrock et al. 2015). However, Ba:Ca has been linked to diet (positive: Sanchez-Jerez et al. 2002, Buckel et al. 2004) and growth rate (negative: Miller 2011, Sturrock et al. 2015). Indeed, dietary sources have been shown to contribute up to 25% of otolith Ba in marine settings (Webb et al. 2012, Izzo et al. 2015).

Temporal patterns among element:Ca and growth displayed distinct seasonal trends. Na:Ca and Sr:Ca were the most consistent through time and had the highest individual synchrony among the element:Ca traits, but displayed an inverse relationship (i.e. Sr:Ca peaked in spring/summer; Na:Ca peaks in autumn/winter). Seasonal sinusoidal patterns in otolith Sr:Ca over shorter time periods have been previously documented and are attributed to seasonal temperature changes aliased by reproductive physiology or other biological processes (Radtke and Targett 1984, Thorrold and Shuttleworth 2000, Hughes et al. 2015). Otolith Sr:Ca levels in plaice (*Pleuronectes platessa*) were highly correlated with physiological processes, particularly reproduction (Sturrock et al. 2015). Ocean perch are live-bearing (Pavlov and Emel'yanova 2013) and have a winter reproductive period with fertilisation occurring in May/June, followed by gestation through the winter and parturition in October/November (Park 1993). The timing of increases in otolith Sr:Ca corresponds with gestation and parturition, and it is possible the seasonal environmental signal (i.e. upwelling) aliases the underlying cause of Sr:Ca fluctuation in ocean perch otoliths. Further research is required to conclusively define this relationship.

Environmental influences on element:Ca and growth

While age and individual variation accounted for most of the variability seen within the otolith trait profiles, some variation was attributed to environmental parameters. Seasonal upwelling is a key environmental driver of the local ecosystem, and we used this strong environmental signal to examine the otolith elemental composition and growth relationships experienced by a fully marine fish *in situ*. The upwelling process has a 'cascading' effect where multiple changes occur in the environment due to increased wind stress. As deeper water is brought to the surface, salinity and temperature change, and there is an influx of nutrients. The amount of change within the local environment is dependent on the characteristics of the water mass being upwelled in addition to the strength/duration of the wind driving the upwelling event (Bigg 2003). During an upwelling event within the Bonney upwelling system, both temperature and salinity decrease (e.g. temp: $\Delta \geq 4°C$; sal: 35.6 to 35.2‰) (Lewis 1981, Middleton et al. 2007) and chlorophyll-a increases due to nutrient influx (Nieblas et al. 2009, van Ruth et al. 2010). All elements and growth, except Li:Ca, were correlated with the upwelling index as opposed to bottom temperature or chlorophyll-a. There were different directional relationships among the otolith traits with the upwelling index, and these persisted through time.

Otolith Ba:Ca was negatively related to the Bonney upwelling index and generally displayed maximas during autumn/winter and minimas during spring/summer. This is the opposite relationship to that documented in carbonate records from other upwelling systems. In strong upwelling areas, usually dominated by large continental boundary currents or equatorial currents, waters tend to be enriched in Ba due to dissolution of barite in deep ocean water and marine sediments (e.g. Lea and Boyle 1991, Shimmield 2015). Increased concentrations of Ba:Ca in coral skeletons and otoliths from those areas have been positively correlated with seasonal upwelling signals (Lea et al. 1989, Montaggioni et al. 2006, Kingsford et al. 2009). Positive relationships between Ba:Ca concentrations of ambient water and those measured in fish otoliths have been well documented (as reviewed in Sturrock et al. 2012). Therefore, the otolith Ba:Ca profile found in the Bonney upwelling region likely reflect reduced concentrations of Ba of the actual water mass being upwelled.

We hypothesise, given the negative correlation with Ba:Ca to the upwelling index, that the water upwelled from the Flinders Current is not Ba enriched as occurs in other systems. Source waters of the Flinders Current are primarily Tasmanian Subantarctic Mode Water (TSAMW) formed in surface waters southwest of Tasmania at ~ 47°S and subducted to depths of 400 to 800 m as it flows northwest (Barker 2004, Middleton and Bye 2007). We suggest that the water mass transported by the Flinders Current and upwelled along the Bonney Coast has had very minimal contact with Ba enriched bottom waters/sediments and therefore, does not produce a 'typical' increased Ba:Ca upwelling signal in the otoliths. Furthermore, while nutrient inputs and the productivity of the Bonney upwelling are well documented (e.g. Nieblas et al. 2009, van Ruth et al. 2010), mass accumulation rates of biogenic compounds (including Ba) in the marine sediments of southern Australia are 1 to 2 orders of magnitude lower than the upwelling areas of Africa (Benguela Current) and South America (Peru Current) (Veeh et al. 1999). Ba accumulation in marine sediments is related to regional primary productivity, and thus, highly productive areas tend to accumulate large amounts of Ba (as barite) in associated sediments (Dymond et al. 1992, Shimmield 2015). Lower regional Ba sediment concentrations reflect the general oligotrophic nature of southern Australian waters.

The otolith Ba:Ca maximas in the autumn/winter months indicate alternative (non-upwelled) sources of Ba to southern Australian marine waters. These sources may include seasonal riverine inputs (Moore 1997, Sinclair and McCulloch 2004) from the River Murray (drainage encompasses the southeastern region of continental Australia), wintertime strengthening of the Leeuwin/South Australian Current flows to the east (Middleton and Bye 2007), and/or wintertime transport of dense, saline, coastal waters from the shelf to the deeper ocean (caused by regional evaporation exceeding precipitation; Kämpf et al. 2010).

Li:Ca was more strongly correlated with chlorophyll-a than either the upwelling index or bottom temperature. Given this, otolith Li:Ca could be a potential indicator of productivity within the marine environment. For example, increased concentrations of Li:Ca in scallop shells were linked to Li-rich phytoplankton in their diet (Thébault and Chauvaud 2013),

while a direct physiological response to changes in dissolved inorganic carbon (DIC) of seawater caused an increase of Li:Ca in foraminifera tests (phytoplankton photosynthesis decreases seawater DIC, low DIC causes Li:Ca to increase in foraminifera tests) (Vigier et al. 2015). Furthermore, we recorded increased Li:Ca concentrations from the hyaline component of the otolith as opposed to the opaque portion. In ocean perch, hyaline zones equate to the faster, summer growth (Paul and Horn 2009). Li:Ca concentrations were positively correlated with opaque zones in plaice otoliths (Sturrock et al. 2015). This suggests that Li:Ca is tied to environmental influences (i.e. increases in primary productivity) rather than to specific features of the otolith.

The addition of an age-environmental interaction term allowed the response of fish at a given age to be examined from both the perspective of chemical assimilation in the otolith and growth. Younger fish adjusted their elemental assimilation more rapidly to changing environmental conditions than older fish. For example, younger fish assimilated Li:Ca more rapidly than older fish as chlorophyll-a concentrations increased, and younger fish also decreased their assimilation rate of Ba:Ca more quickly as upwelling increased. Similar increases or decreases in relation to age were seen with the other elements and environmental parameters. Whilst overall there was a positive relationship between growth and upwelling, when explored across ages, it became apparent that older fish grew better with increased upwelling, while growth rate marginally decreased in very young fish. Because physical changes are happening at a rapid rate in an upwelling system (e.g. drops in temperature/salinity, increased nutrients), young fish may expend greater energy on metabolic processes, thereby repartitioning energy that could be used for growth (e.g. Brett and Groves 1979, Wootton 2011). Rapid changes to metabolic processes could potentially cause rapid adjustment of element assimilation rates. Fish within an upwelling environment will experience drops in metabolic rates as temperature decreases, regulation of ionic homeostasis with changing salinity, and increased water movement. Growth rates are influenced by changes to metabolic processes caused by interactions of multiple environmental parameters, including changes to food resources, relative to fish size and age (Brett and Groves 1979, Wootton 2011). Therefore, growth rates in very young fish may decrease slightly in response to upwelling events while older fish have positive growth rates. Comparing overall levels of an element or growth across a fish's lifetime also enables

differences to be examined between younger and older fish. This type of information can be used to infer differences in 'lifestyle' that fish might have had during certain portions of their lives (e.g. influences of diets, microhabitat).

Physiological versus environmental influences

The multivariate modelling results corroborated our hypotheses regarding physiological controls on elements in otoliths and present the first instance where correlations between elements within individual otoliths and among fish have been determined (Fig. 1 b). Within an individual fish, Na:Ca and Sr:Ca were most highly correlated with each other and growth, and were only very weakly correlated with Ba:Ca and Li:Ca. Neither Ba:Ca or Li:Ca were significantly correlated with growth and exhibited a weak negative correlation between themselves. These results suggest Ba:Ca and Li:Ca are indeed less controlled by physiological processes and more reflective of extrinsic influences. Mg:Ca was weakly correlated with growth (+) and Na:Ca (+), moderately with Ba:Ca (+) and very weakly with both Sr:Ca (-) and Li:Ca (+). This demonstrates Mg:Ca, along with growth, is regulated simultaneously by physiological and environmental factors. Similar directional relationships have been reported for marine fish when examining growth versus a single element: Na:Ca - positive (with age as a proxy for growth: Kalish 1989, Proctor et al. 1995, Hughes et al. 2015); Sr:Ca - negative (Sadovy and Severin 1994, Sturrock et al. 2015; with age as a proxy for growth: Kalish 1989, Proctor et al. 1995, Hughes et al. 2015). Otolith Mg:Ca has been positively correlated with growth rate (Sturrock et al. 2015). Lastly, element:Ca and growth were also compared among individuals, and only Ba:Ca and growth were significantly correlated (-). This means fish with overall higher growth rates equated to overall lower Ba:Ca. Given that upwelled water had lower Ba concentrations, but upwelling were times of higher average growth, a potential explanation is that fish whose lives spanned periods with stronger upwelling events would have elevated growth and reduced Ba; those inhabiting weaker upwelling periods would have the opposite.

Conclusions

The application of univariate and multivariate mixed-effects modelling to highly resolved element:Ca and growth profiles has provided a novel method to disentangle the effects of physiology and the environment on otolith chemistry and fish growth. If changes to

element concentrations in otoliths driven by physiology are unaccounted for (e.g. age, reproductive parameters, diet), then elemental data used to reconstruct lifetime movements or as palaeoproxies can be misinterpreted (Thresher 1999, Elsdon et al. 2008, Sturrock et al. 2012). Our models accounted for age-related effects but did not include reproductive parameters or diet as these data were unavailable. However, since both male and female fish were included in the models, the element:Ca profiles and growth are integrated to reflect the response of all fish, regardless of sex. The Sr:Ca temporal signal and its association with reproduction should be thoroughly explored, as this relationship has potential for use as a proxy to reconstruct reproductive histories. This would be especially useful when examining exploited populations for changes in reproductive characteristics through time (e.g. changes in age-at-maturity, shifts in spawning season with climate variability). Since both Ba:Ca and Li:Ca were under limited physiological control, these elements are the most likely candidates for use as environmental proxies. Otolith Li:Ca is particularly promising as an indicator of productivity in the marine environment. Describing the assimilation mechanism of Li from the environment into the otolith will be an important first step. In a similar vein, Ba:Ca seems to track Ba concentrations within the ambient water mass, if the Bonney upwelled water does indeed reflect a unenriched Ba source. Of all the elements examined, Ba was the only one to be correlated among individuals, which suggests that population-level fluctuations in ambient Ba are simultaneously recorded by all individuals. Therefore, fluctuations in Ba:Ca are likely to represent broad-scale environmental change as opposed to individual-based differences in assimilation. Further research directions should include quantifying physiological (e.g. metabolism, reproductive condition) and environmental influences on element assimilation by focusing on all life history stages, since element assimilation is inherently linked with age-based growth.

Acknowledgements:

We acknowledge partial funding from the Dr Paris Goodsell Marine Ecology Research Grant, the Nature Foundation SA, the Ecological Society of Australia, CSIRO Wealth from Oceans Flagship and the Australian Research Council (FT100100767; DP110100716). We acknowledge Aoife McFadden and Benjamin Wade of Adelaide Microscopy for assistance

with LA ICP-MS. Thanks to J. Redman and S. Redman of Southend, SA for help with specimen collection.

References:

Barker, P. M. 2004. The circulation and formation of water masses south of Australia and the inter-annual wind variability along the southern Australian coast. PhD Thesis. The University of Melbourne, Victoria, Australia.

Batenburg, S. J., G.-J. Reichart, T. Jilbert, M. Janse, F. P. Wesselingh, and W. Renema. 2011. Interannual climate variability in the Miocene: High resolution trace element and stable isotope ratios in giant clams. Palaeogeography, Palaeoclimatology, Palaeoecology **306**:75-81.

Bates, D., M. Maechler, B. Bolker, and S. Walker. 2014. lme4: Linear mixed-effects models using Eigen and S4. R package version 1.1-7. http://cran.r-project.org/web/packages/lme4/.

Berumen, M. L., H. J. Walsh, N. Raventos, S. Planes, G. P. Jones, V. Starczak, and S. R. Thorrold. 2010. Otolith geochemistry does not reflect dispersal history of clownfish larvae. Coral Reefs **29**:883-891.

Bigg, G. R. 2003. The Oceans and Climate. Cambridge University Press.

Botsford, L. W., C. A. Lawrence, E. P. Dever, A. Hastings, and J. Largier. 2003. Wind strength and biological productivity in upwelling systems: an idealized study. Fisheries Oceanography **12**:245-259.

Brett, J. R. and T. D. D. Groves. 1979. Physiological energetics. Pages 279-352 *in* W. S. Hoar, D. J. Randall, and J. R. Brett, editors. Fish Physiology: Bioenergetics and Growth. Academic Press, London.

Bruce, B. D., R. Bradford, R. Daley, M. Green, and K. Phillips. 2002. Targeted review of biological and ecological information from fisheries research in the South East Marine Region National Oceans Office, CSIRO Marine Research, Hobart.

Buckel, J. A., B. L. Sharack, and V. S. Zdanowicz. 2004. Effect of diet on otolith composition in *Pomatomus saltatrix*, an estuarine piscivore. Journal of Fish Biology **64**:1469-1484.

Bulman, C., F. Althaus, X. He, N. Bax, and A. Williams. 2001. Diets and trophic guilds of demersal fishes of the south-eastern Australian shelf. Marine and Freshwater Research **52**:537-548.

Burnham, K. P. and D. R. Anderson. 2004. Multimodel inference: understanding AIC and BIC in model selection. Sociological Methods and Research **33**:261-304.

Campana, S. E. 1999. Chemistry and composition of fish otoliths: pathways, mechanisms and applications. Marine Ecology Progress Series **188**:263-297.

Cusack, M. and A. Freer. 2008. Biomineralization: elemental and organic influence in carbonate systems. Chemical Reviews **108**:4433-4454.

de Vries, M. C., B. M. Gillanders, and T. S. Elsdon. 2005. Facilitation of barium uptake into fish otoliths: Influence of strontium concentration and salinity. Geochimica et Cosmochimica Acta **69**:4061-4072.

Dingemanse, N. J. and N. A. Dochtermann. 2013. Quantifying individual variation in behaviour: mixed-effect modelling approaches. Journal of Animal Ecology **82**:39-54.

Disspain, M., L. A. Wallis, and B. M. Gillanders. 2011. Developing baseline data to understand environmental change: a geochemical study of archaeological otoliths from the Coorong, South Australia. Journal of Archaeological Science **38**:1842-1857.

Disspain, M. C. F., S. Ulm, and B. M. Gillanders. 2015. Otoliths in archaeology: methods, applications and future prospects. Journal of Archaeological Science: Reports: http://dx.doi.org/10.1016/j.jasrep.2015.1005.1012.

Doubleday, Z. A., C. Izzo, S. H. Woodcock, and B. M. Gillanders. 2013. Relative contribution of water and diet to otolith chemistry in freshwater fish. Aquatic Biology **18**:271-280.

Dymond, J., E. Suess, and M. Lyle. 1992. Barium in deep-sea sediment: a geochemical proxy for paleoproductivity. Paleoceanography **7**:163-181.

Elsdon, T. S. and B. M. Gillanders. 2002. Interactive effects of temperature and salinity on otolith chemistry: challenges for determining environmental histories of fish. Canadian Journal of Fisheries and Aquatic Sciences **59**:1796-1808.

Elsdon, T. S. and B. M. Gillanders. 2003a. Reconstructing migratory patterns of fish based on environmental influences on otolith chemistry. Reviews in Fish Biology and Fisheries **13**:217-235.

Elsdon, T. S. and B. M. Gillanders. 2003b. Relationship between water and otolith elemental concentrations in juvenile black bream *Acanthopagrus butcheri*. Marine Ecology Progress Series **260**:263-272.

Elsdon, T. S. and B. M. Gillanders. 2005. Consistency of patterns between laboratory experiments and field collected fish in otolith chemistry: an example and applications for salinity reconstructions. Marine and Freshwater Research **56**:609-617.

Elsdon, T. S., B. K. Wells, S. E. Campana, B. M. Gillanders, C. M. Jones, K. E. Limburg, D. H. Secor, S. R. Thorrold, and B. D. Walther. 2008. Otolith chemistry to describe movements and life-history parameters of fishes: Hypotheses, assumptions, limitations and inferences. Pages 297-330 *in* R. N. Gibson, R. J. A. Atkinson, and J. D. M. Gordon, editors. Oceanography and Marine Biology: An Annual Review, Vol 46. Crc Press-Taylor & Francis Group, Boca Raton.

Fox, J., S. Weisberg, and J. Hong. 2014. effects: Effect displays for linear, generalized linear, and other models. R package version 3.0-3. http://cran.r-project.org/web/packages/effects/index.html.

Gillanders, B. M. 2002. Temporal and spatial variability in elemental composition of otoliths: Implications for determining stock identity and connectivity of populations. Canadian Journal of Fisheries and Aquatic Sciences **59**:669-679.

Griffin, W. L., W. J. Powell, N. J. Pearson, and S. Y. O'Reilly. 2008. GLITTER: data reduction software for laser ablation ICP-MS. Pages 204-207 *in* P. Sylvester, editor. Laser Ablation: ICP-MS in the Earth Sciences Mineralogical Association of Canada Short Course Series.

Hadfield, J. D. 2010. MCMC methods for multi-response generalised linear mixed models: the MCMCglmm R package. Journal of Statistical Software **33**:1-22.

Hadfield, J. D., A. J. Wilson, D. Garant, B. C. Sheldon, and L. E. B. Kruuk. 2010. The misuse of BLUP in ecology and evolution. American Naturalist **175**:116-125.

Harrell, F. E. J. 2014. Hmisc: Harrell Miscellaneous. R package version 3.14-5. http://cran.r-project.org/web/packages/Hmisc/.

Hatch, M. B. A., S. A. Schellenberg, and M. L. Carter. 2013. Ba/Ca variations in the modern intertidal bean clam *Donax gouldii*: An upwelling proxy? Palaeogeography, Palaeoclimatology, Palaeoecology **373**:98-107.

Henschke, N., D. A. Bowden, J. D. Everett, S. P. Holmes, R. J. Kloser, R. W. Lee, and I. M. Suthers. 2013. Salp-falls in the Tasman Sea: a major food input to deep-sea benthos. Marine Ecology Progress Series **491**:165-175.

Horn, P. L., J. S. Forman, and M. R. Dunn. 2012. Dietary partitioning by two sympatric fish species, red cod (*Pseudophycis bachus*) and sea perch (*Helicolenus percoides*), on Chatham Rise, New Zealand. Marine Biology Research **8**:624-634.

Hughes, J. M., J. Stewart, B. M. Gillanders, D. Collins, and I. M. Suthers. 2015. Relationship between otolith chemistry and age in a widespread pelagic teleost *Arripis trutta*: influence of adult movements on stock structure and implications for management. Marine and Freshwater Research: http://dx.doi.org/10.1071/MF14247.

Izzo, C., Z. A. Doubleday, A. G. Schultz, S. H. Woodcock, and B. M. Gillanders. 2015. Contribution of water chemistry and fish condition to otolith chemistry: comparisons across salinity environments. Journal of Fish Biology **86**:1680-1698.

James, N. P. and Y. Bone. 2011. Neritic Carbonate Sediments in a Temperate Realm: Southern Australia. Springer, London.

Johnson, P. C. D. 2014. Extension of Nakagawa & Schielzeth's R^2GLMM to random slopes models. Methods in Ecology and Evolution **5**:944-946.

Kaim, W., B. Schwederski, and A. Klein. 2013. Bioinorganic Chemistry--Inorganic Elements in the Chemistry of Life: An Introduction and Guide. 2nd edition. John Wiley & Sons, United Kingdom.

Kalish, J. M. 1989. Otolith microchemistry: validation of the effects of physiology, age and environment on otolith composition. Journal of Experimental Marine Biology and Ecology **132**:151-178.

Kalish, J. M. 1991. Determinants of otolith chemistry: seasonal variation in the composition of blood plasma, endolymph and otoliths of bearded rock cod *Pseudophycis barbatus*. Marine Ecology Progress Series **74**:137-159.

Kämpf, J., M. Doubell, D. Griffin, R. L. Matthews, and T. M. Ward. 2004. Evidence of a large seasonal coastal upwelling system along the southern shelf of Australia. Geophysical Research Letters **31**:1-4.

Kämpf, J., N. Payne, and P. Malthouse. 2010. Marine connectivity in a large inverse estuary. Journal of Coastal Research **26**:1047-1056.

Kingsford, M. J., J. M. Hughes, and H. M. Patterson. 2009. Otolith chemistry of the non-dispersing reef fish *Acanthochromis polyacanthus*: cross-shelf patterns from the central Great Barrier Reef. Marine Ecology Progress Series **377**:279-288.

Lamson, H., J.-C. Shiao, Y. Iizuka, W.-N. Tzeng, and D. Cairns. 2006. Movement patterns of American eels (*Anguilla rostrata*) between salt- and freshwater in a coastal watershed, based on otolith microchemistry. Marine Biology **149**:1567-1576.

Lea, D. W. and E. A. Boyle. 1991. Barium in planktonic foraminifera. Geochimica et Cosmochimica Acta **55**:3321-3331.

Lea, D. W., G. T. Shen, and E. A. Boyle. 1989. Coralline barium records temporal variability in equatorial pacific upwelling. Nature **340**:373-373.

Lewis, R. 1981. Seasonal upwelling along the south-eastern coastline of South Australia. Marine and Freshwater Research **32**:843-854.

Mazerolle, M. J. 2015. Model selection and multimodel inference based on (Q)AIC(c). R package version 2.0-3. http://cran.r-project.org/web/packages/AICcmodavg/index.html.

Middleton, J. F., C. Arthur, P. Van Ruth, T. M. Ward, J. L. McClean, M. E. Maltrud, P. Gill, A. Levings, and S. Middleton. 2007. El Nino effects and upwelling off South Australia. Journal of Physical Oceanography **37**:2458-2477.

Middleton, J. F. and J. A. T. Bye. 2007. A review of the shelf-slope circulation along Australia's southern shelves: Cape Leeuwin to Portland. Progress in Oceanography **75**:1-41.

Middleton, J. F. and M. Cirano. 2002. A northern boundary current along Australia's southern shelves: The Flinders Current. Journal of Geophysical Research. C. Oceans **107**:1-11.

Miller, J. A. 2011. Effects of water temperature and barium concentration on otolith composition along a salinity gradient: Implications for migratory reconstructions. Journal of Experimental Marine Biology and Ecology **405**:42-52.

Montaggioni, L. F., F. Le Cornec, T. Correge, and G. Cabioch. 2006. Coral barium/calcium record of mid-Holocene upwelling activity in New Caledonia, South-West Pacific. Palaeogeography, Palaeoclimatology, Palaeoecology **237**:436-455.

Moore, W. S. 1997. High fluxes of radium and barium from the mouth of the Ganges-Brahmaputra River during low river discharge suggest a large groundwater source. Earth and Planetary Science Letters **150**:141-150.

Morrongiello, J. R. and R. E. Thresher. 2015. A statistical framework to explore ontogenetic growth variation among individuals and populations: a marine fish example. Ecological Monographs **85**:93-115.

Morrongiello, J. R., C. T. Walsh, C. A. Gray, J. R. Stocks, and D. A. Crook. 2014. Environmental change drives long-term recruitment and growth variation in an estuarine fish. Global Change Biology **20**:1844-1860.

Nakagawa, S. and H. Schielzeth. 2013. A general and simple method for obtaining R^2 from generalized linear mixed-effects models. Methods in Ecology and Evolution **4**:133-142.

Nieblas, A. E., B. M. Sloyan, A. J. Hobday, R. Coleman, and A. J. Richardson. 2009. Variability of biological production in low wind-forced regional upwelling systems: A case study off southeastern Australia. Limnology and Oceanography **54**:1548-1558.

Park, T. J. 1993. A comparison of the morphology, growth and reproductive biology of two colour forms of ocean perch (*Helicoleus percoides*), NSW, Australia. Masters. University of Sydney, Sydney, Australia.

Paul, L. J. and P. L. Horn. 2009. Age and growth of sea perch (*Helicolenus percoides*) from two adjacent areas off the east coast of South Island, New Zealand. Fisheries Research **95**:169-180.

Pavlov, D. A. and N. G. Emel'yanova. 2013. Transition to viviparity in the order Scorpaeniformes: Brief review. Journal of Ichthyology **53**:52-69.

Proctor, C. H., R. E. Thresher, J. S. Gunn, D. J. Mills, I. R. Harrowfield, and S. H. Sie. 1995. Stock structure of the southern bluefin tuna *Thunnus maccoyii:* an investigation based on probe microanalysis of otolith composition. Marine Biology **122**:511-526.

Radtke, R. L. and T. E. Targett. 1984. Rhythmic structural and chemical patterns in otoliths of the Antarctic fish *Notothenia larseni*: Their application to age determination. Polar Biology **3**:203-210.

Ramos, R. and J. González-Solís. 2012. Trace me if you can: the use of intrinsic biogeochemical markers in marine top predators. Frontiers in Ecology and the Environment **10**:258-266.

Reis-Santos, P., S. E. Tanner, R. P. Vasconcelos, T. S. Elsdon, H. N. Cabral, and B. M. Gillanders. 2013. Connectivity between estuarine and coastal fish populations: contributions of estuaries are not consistent over time. Marine Ecology Progress Series **491**:177-186.

Sadovy, Y. and K. P. Severin. 1994. Elemental patterns in red hind (*Epinephelus guttatus*) otoliths from bermuda and Puerto Rico reflect growth rate, not temperature. Canadian Journal of Fisheries and Aquatic Sciences **51**:133-141.

Sanchez-Jerez, P., B. M. Gillanders, and M. J. Kingsford. 2002. Spatial variability of trace elements in fish otoliths: comparison with dietary items and habitat constituents in seagrass meadows. Journal of Fish Biology **61**:801-821.

Shimmield, G. 2015. Biogenic barium. Pages 1-2 *in* J. Harff, M. Meschede, S. Petersen, and J. Thiede, editors. Encyclopedia of Marine Geosciences. Springer Netherlands.

Sinclair, D. J. and M. T. McCulloch. 2004. Corals record low mobile barium concentrations in the Burdekin River during the 1974 flood: evidence for limited Ba supply to rivers? Palaeogeography, Palaeoclimatology, Palaeoecology **214**:155-174.

Smith, P. J., C. D. Struthers, C. D. Paulin, S. M. McVeagh, and R. K. Daley. 2009. Shallow genetic and morphological divergence among seaperches in the South Pacific (family Scorpaenidae; genus *Helicolenus*). Journal of Fish Biology **74**:1104-1128.

Stanley, S. M. 2006. Influence of seawater chemistry on biomineralization throughout phanerozoic time: Paleontological and experimental evidence. Palaeogeography, Palaeoclimatology, Palaeoecology **232**:214-236.

Steer, M., A. J. Fowler, and B. M. Gillanders. 2009. Age-related movement patterns and population structuring in southern garfish, *Hyporhamphus melanochir*, inferred from otolith chemistry. Fisheries Management and Ecology **16**:265-278.

Sturrock, A. M., E. Hunter, J. A. Milton, E. Eimf, R. C. Johnson, C. P. Waring, and C. N. Trueman. 2015. Quantifying physiological influences on otolith microchemistry. Methods in Ecology and Evolution: doi: 10.1111/2041-1210X.12381.

Sturrock, A. M., C. N. Trueman, A. M. Darnaude, and E. Hunter. 2012. Can otolith elemental chemistry retrospectively track migrations in fully marine fishes? Journal of Fish Biology **81**:766-795.

Sturrock, A. M., C. N. Trueman, J. A. Milton, C. P. Waring, M. J. Cooper, and E. Hunter. 2014. Physiological influences can outweigh environmental signals in otolith microchemistry research. Marine Ecology Progress Series **500**:245-264.

Thébault, J. and L. Chauvaud. 2013. Li/Ca enrichments in great scallop shells (*Pecten maximus*) and their relationship with phytoplankton blooms. Palaeogeography, Palaeoclimatology, Palaeoecology **373**:108-122.

Thorrold, S. R. and S. Shuttleworth. 2000. *In situ* analysis of trace elements and isotope ratios in fish otoliths using laser ablation sector field inductively coupled plasma mass spectrometry. Canadian Journal of Fisheries and Aquatic Sciences **57**:1232-1242.

Thresher, R. E. 1999. Elemental composition of otoliths as a stock delineator in fishes. Fisheries Research **43**:165-204.

van Ruth, P. D., G. G. Ganf, and T. M. Ward. 2010. Hot-spots of primary productivity: an alternative interpretation to conventional upwelling models. Estuarine, Coastal and Shelf Science **90**:142-158.

Veeh, H. H., D. T. Heggie, and A. J. Crispe. 1999. Biogeochemistry of southern Australian continental slope sediments. Australian Journal of Earth Sciences **46**:563-575.

Vigier, N., C. Rollion-Bard, Y. Levenson, and J. Erez. 2015. Lithium isotopes in foraminifera shells as a novel proxy for the ocean dissolved inorganic carbon (DIC). Comptes Rendus Geoscience **347**:43-51.

Walther, B., M. Kingsford, M. O'Callaghan, and M. McCulloch. 2010. Interactive effects of ontogeny, food ration and temperature on elemental incorporation in otoliths of a coral reef fish. Environmental Biology of Fishes **89**:441-451.

Walther, B. D. and S. R. Thorrold. 2006. Water, not food, contributes the majority of strontium and barium deposited in the otoliths of a marine fish. Marine Ecology Progress Series **311**:125-130.

Webb, S. D., S. H. Woodcock, and B. M. Gillanders. 2012. Sources of otolith barium and strontium in estuarine fish and the influence of salinity and temperature. Marine Ecology Progress Series **453**:189-199.

Weiner, S. and P. M. Dove. 2003. An overview of biomineralization processes and the problem of the vital effect. Reviews in Mineralogy and Geochemistry **54**:1-29.

Weisberg, S., G. Spangler, and L. S. Richmond. 2010. Mixed effects models for fish growth. Canadian Journal of Fisheries and Aquatic Sciences **67**:269-277.

Wootton, R. J. 2011. Energy utilization in growth | Growth: environmental effects. Pages 1629-1635 *in* A. P. Farrell, editor. Encyclopedia of Fish Physiology. Academic Press, San Diego.

Zuur, A., E. N. Ieno, N. Walker, A. A. Saveliev, and G. M. Smith. 2009. Mixed effects models and extensions in ecology with R. Springer, New York.

CHAPTER 6

General Discussion

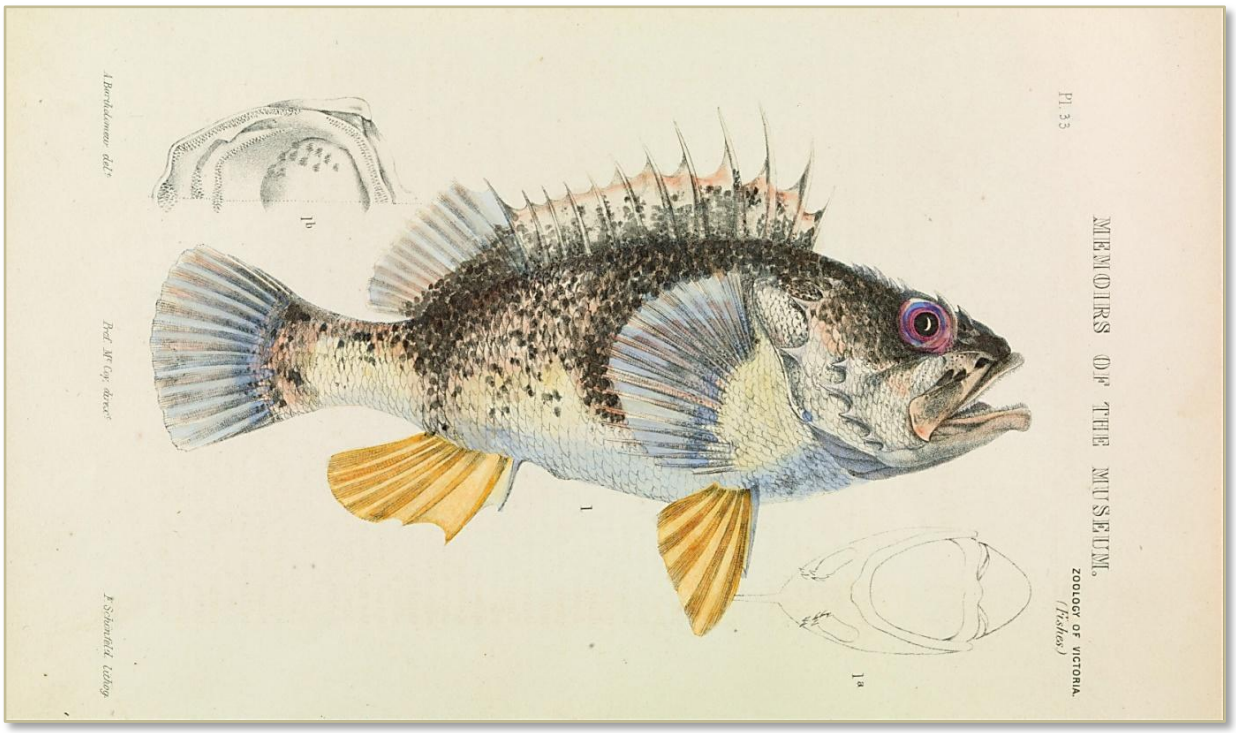

Ocean Perch, *Helicolenus percoides* by Arthur Bartholomew (1834 - 1909), an Australian explorer, natural history illustrator and lithographer. Lithographic ink, varnish and water colour on paper (1887). No known copyright restrictions

General Discussion

The southwest Pacific and southeast Indian Oceans are dynamic areas of the Southern Hemisphere where there is still a paucity of instrumental records relating to ocean and climate. Alternatives to *in situ* instrumental measurements are necessary in areas where it is too expensive or logistically difficult for rigorous data collection of physical or chemical parameters. Otolith carbonate records are accessible archives that provide a mechanism to examine environmental change in specific regions in both space and time. Throughout this thesis, I used the otoliths from the benthic deep-water fish, *Helicolenus,* as bioarchives of biogeochemistry and growth to provide new data describing environmental change in marine systems of southern Australia and New Zealand. Specifically, I (i) identified changes to distributions of $\Delta^{14}C$ in different ocean circulation systems, (ii) related growth responses from *Helicolenus* to broad-scale climate processes and localised oceanographic parameters, and (iii) concurrently used biogeochemical tracers and fish growth to explore synergistic effects of physiology and the environment on chemical assimilation into otoliths in an area of seasonal upwelling. I exploited advancing technologies for processing both data and geochemical samples to produce higher resolution datasets from otolith carbonate. For example, refinements to carbonate graphitising/AMS procedures enabled minuscule quantities of carbonate to be analysed, which limited temporal error in the resultant ^{14}C data (Chapters 2 and 3). Further, I created high resolution element:Ca profiles at monthly time scales, because the current LA ICP-MS technologies have greatly increased the scope to extract chemical profiles from otoliths (Chapter 5). Additionally, evolving software and statistical packages provided the capacity for high precision measuring of otolith growth increments and subsequent statistical analyses (Chapters 2 to 5). Combining advanced techniques with the time-resolved structure of otoliths culminated in robust proxies on which to reconstruct both ecological and environmental histories. In this chapter, I discuss the main findings of my research and provide suggestions for future research.

Otolith radiocarbon as an environmental tracer

Otoliths were first used as a proxy for $\Delta^{14}C$ levels in the environment in the early 1990s with reference made to the considerable potential of otolith ^{14}C for further investigation into both oceanography and global change (Kalish 1994). My results showed that by using levels of otolith ^{14}C in tandem with growth increments, temporal changes of $\Delta^{14}C$ in

different marine environments could be examined. Otolith $\Delta^{14}C$ levels were equivalent to regional seawater records of $\Delta^{14}C$ in the respective locations. Both ocean perch species (*H. barathri* and *H. percoides*) were equally effective as archives for ^{14}C, and both displayed $\Delta^{14}C$ levels representative of their differing marine environments, e.g. mid-water depths (*H. barathri*, Chapter 2) or an upwelling area (*H. percoides*, Chapter 3). This provides further evidence that otoliths from long-lived fish can be used to establish pre-bomb levels of ^{14}C and to track the invasion of bomb ^{14}C through the water column on a regional scale. In contrast to coral, otoliths are able to provide records from cooler regions and throughout the water column (Chapters 2 and 3).

Ocean perches are an 'ideal species' for use with ^{14}C, as they are non-migratory, live at a specific depth (benthic in this case), and have feeding and reproductive strategies in similar depths. Dissolved inorganic carbon (DIC) in seawater contributes about 75% of the carbon found in otoliths; the remaining 25% of carbon is diet-based (Kalish 1991b, Solomon et al. 2006). If a deep water fish with ontogenetic migration patterns were used as the proxy species, associations with regional water ^{14}C values could not have been made. For example, values of $\Delta^{14}C$ measured in the otolith cores and edges of both bluenose (*Hyperoglyphe antarctica*; Horn et al. 2010) and rubyfish (*Plagiogeneion rubiginosum*; Horn et al. 2012) had completely different $\Delta^{14}C$ signatures. The juveniles of both species live in waters < 200 m, while the adult fish resided at depths well below that (~ 600 m). Adult bluenose also undergo extensive vertical and latitudinal migrations, which further confound ambient water and dietary sources of carbon (Horn et al. 2010).

Since the 1990s, numerous studies have measured $\Delta^{14}C$ in fish otoliths (e.g. Kerr et al. 2005, Andrews et al. 2011). Until now, measurements of otolith $\Delta^{14}C$ values were primarily used for age validation (e.g. Kalish 1995, Campana 1997, Andrews et al. 2011) with limited exploration of the physical aspects of ^{14}C levels in otoliths, such as water mass tracers or atmosphere/ocean flux of ^{14}C (but see Kalish et al. 2001, Campana et al. 2008). My research demonstrates the power of compiling $\Delta^{14}C$ records from multiple sources within a location to examine regional ocean circulation patterns.

Growth responses recorded in otoliths as climate proxies

Climate variability influences distribution, migratory patterns, abundances, and growth in fishes (Attrill and Power 2002, Möllmann et al. 2005, Lehodey et al. 2006), and explaining this interannual variability is an active area of research (e.g. Thresher et al. 2007, Black et al. 2008, Morrongiello et al. 2012). Synchrony in geographically separate populations of fish has drawn attention to low frequency climate variability (e.g. ENSO), and the role of climate forcing on fish growth (Lehodey et al. 2006, Black et al. 2014). Long-term growth responses derived from the otoliths of *Helicolenus* species from southern Australia and New Zealand revealed a collective, temporal growth signal, across 3000 km and parts of three ocean basins, despite the low synchrony in the individual *Helicolenus* populations (Chapter 4). At this geographic scale only very large-scale climatic drivers should be detectable (Morrongiello and Thresher 2015). My results indicated solar activity was the leading harmonizer, and growth declined with increased solar activity (Chapter 4, Fig.3). I also detected both synergistic and antagonistic effects of climate forcing within local environments on fish growth. Within my analyses, broad-scale climate variables typically caused greater change to growth than did local parameters. Broad scale climate patterns and weather can have synergistic/antagonistic effects on the environment that are amplified or dampened depending on the type of interaction (Stenseth et al. 2004, Brierley and Kingsford 2009, Travers-Trolet et al. 2014).

I compared fish growth across multiple regions, species and environmental parameters using univariate mixed-effects models to account for biological influences on growth. In this instance, a mixed-effects modelling approach was more effective for extracting environmentally driven growth variability in southern Australia and New Zealand (Morrongiello et al. 2012), rather than dendrochronological techniques as pioneered in the northeast Pacific region where strong climate signals prevail (e.g. Black et al. 2014). Because I used mixed-effects models, biological effects, such as age, could be partitioned to allow other sources of variability to be extracted from the growth record. Age accounted for the majority of growth variance in the fish (~ 70 to 80%), which was expected. Across the entire region, age-dependent growth of ocean perches varied among years, cohorts, locations and species. In each local region, different combinations of climatic/oceanographic variables affected species specific growth.

Annual growth synchrony varied between all individual regions and species, with the least synchrony seen in the *Helicolenus* species complex from west New Zealand (< 1%), whilst the *Helicolenus* species complex on the Chatham Rise east of New Zealand was most synchronous (15%). Growth synchrony reported in other marine fish populations is generally higher at around 50 to 80% (e.g. Black et al. 2008, Black et al. 2011, Gillanders et al. 2012). However, many species of fish have much lower levels of within-population growth synchrony (2 to 20%; Rountrey et al. 2014, Morrongiello and Thresher 2015, Nguyen et al. 2015). Lack of synchrony may reflect growth complacency in a species (i.e. low annual growth variation), an environment where climate signals are dampened (e.g. deep ocean depths), and/or variations in local microhabitat quality (i.e. food resources, habitat structure). Thus, variability in individual growth can increase, and subsequent integration into a population-level growth response adds unexplained variation and diminishes synchrony (Morrongiello and Thresher 2015).

Temporal magnitude and environmental directionality of growth responses differed substantially among the different *Helicolenus* populations. However, in all populations, growth increased through time. The annual growth rate of a deep dwelling species (*H. barathri*) was much lower compared to all other species; this may reflect the deeper depth at which the fish is living (Koslow et al. 2000), lower quality habitat (e.g. decreased food availability, sub-optimal temperature for growth; Arendt 1997) or a combination of the two.

Physiological and environmental influences on biogeochemical tracers in otoliths

Biogeochemical tracers found in the hard parts of organisms are frequently used to answer key ecological questions by linking the organism with the environment. However, biogenic structures are not always in direct contact with the environment and may be under some level of physiological control (e.g. otoliths are encapsulated in the fish's head, surrounded by endolymph). As physiological processes become more complex in higher organisms, the biogeochemical relationship between the environment and the biogenic structure becomes less predictable (Weiner and Dove 2003, Stanley 2006, Cusack and Freer 2008). Based on current research, I developed a conceptual model around element concentrations and

growth correlations within an otolith and among individual fish, and proposed that certain elements within otoliths are primarily under physiological control, environmental control or both (Chapter 5, Fig. 1a). I applied univariate and multivariate mixed-effects models to highly resolved element:Ca and growth profiles taken from *H. percoides* otoliths from an upwelling area of southern Australia. This provided a novel method to disentangle the effects of physiology and the environment on otolith chemistry and fish growth. My results showed otolith chemistry and fish growth displayed cyclic seasonal signals over a 17 year period in the marine system. Age-dependent relationships existed in the element:Ca and growth profiles, and responses to the environment differed as the fish aged. Temporal signals were correlated with seasonal upwelling events. Since elemental concentrations and growth were measured simultaneously within the otolith, direct comparisons between the otolith traits (i.e. element:Ca and growth profiles), both within and among individual fish, were made through time and revealed the strength and direction of relationships between element:Ca and growth. This tested the conceptual model hypothesising physiological-environmental controls on otolith chemistry. Physiologically regulated elements included Na:Ca and Sr:Ca, while Ba:Ca and Li:Ca were primarily controlled by environmental drivers. Fish growth and Mg:Ca concentrations were regulated by both physiology and the environment.

Temporal patterns among element:Ca and growth traits displayed distinct seasonal trends. Na:Ca and Sr:Ca were the most consistent through time and had the highest element:Ca synchrony, but displayed an inverse relationship. Seasonal sinusoidal patterns in otolith Sr:Ca over shorter time periods have been previously documented and are attributed to seasonal temperature changes aliased by reproductive physiology or other biological processes (Radtke and Targett 1984, Thorrold and Shuttleworth 2000, Hughes et al. 2015). Otolith Sr:Ca levels in plaice (*Pleuronectes platessa*) have been highly correlated with physiological processes, particularly reproduction (Sturrock et al. 2015). Ocean perch are live-bearing (Pavlov and Emel'yanova 2013) and have a winter reproductive period where fertilisation occurs in May/June, followed by gestation through the winter and parturition in October/November (Park 1993). The timing of increases in otolith Sr:Ca corresponds with gestation and parturition, and it is possible the seasonal environmental signal (i.e. upwelling) aliases the underlying cause of Sr:Ca fluctuation in ocean perch otoliths. The

Sr:Ca temporal signal and its association with reproduction should be thoroughly explored in the future, as this relationship has potential for use as a proxy to reconstruct reproductive histories. This would be especially useful when examining exploited populations for changes in reproductive characteristics through time (e.g. changes age-at-maturity, shifts in spawning season with climate variability).

The modelling results underpinned the conceptual model, which suggested Li:Ca and Ba:Ca were primarily controlled by environmental drivers as opposed to physiological processes. Previous studies have found Li:Ca and Ba:Ca were not related to reproduction (Sturrock et al. 2012, Sturrock et al. 2015), but Ba:Ca may be influenced to some extent by diet (Webb et al. 2012, Izzo et al. 2015). Seasonal upwelling is a key environmental driver of the local ecosystem, and has a 'cascading' effect where multiple changes occur in the environment due to increased wind stress, e.g. temperature, salinity decrease, primary production increases (Lewis 1981, Middleton et al. 2007). All elements and growth, except Li:Ca, were correlated with the upwelling index; Li:Ca was correlated with chlorophyll-a. Given this, otolith Li:Ca could be a potential indicator of productivity within the marine environment. Li:Ca has been linked to primary productivity in both molluscs (Thébault and Chauvaud 2013) and foraminifera (Vigier et al. 2015). Increased concentrations of Li:Ca in scallop shells were linked to Li-rich phytoplankton in their diet (Thébault and Chauvaud 2013), while a direct physiological response during test formation in foraminifera resulted in changes to Li:Ca concentrations (Vigier et al. 2015). Future research should investigate the mechanism of Li assimilation into otoliths.

Otolith Ba:Ca was negatively related to the Bonney upwelling index. This is the opposite relationship to that documented in carbonate records from other upwelling systems and potentially indicates upwelled water from the Flinders Current is not Ba enriched. I suggest that the water mass transported by the Flinders Current and upwelled along the Bonney Coast has had minimal contact with Ba enriched bottom waters/sediments and therefore, does not produce a 'typical' increased Ba:Ca upwelling signal in the otoliths (see Chapter 5 for further discussion on this point). Since Ba:Ca tracked Ba concentrations within the ambient water mass and because Ba:Ca was the only element:Ca to be correlated among individuals, this suggests that population-level fluctuations in ambient Ba are

simultaneously recorded by all individuals. This indicates that fluctuations in Ba:Ca likely represent broad-scale environmental change (as opposed to just individual based differences in assimilation due to physiology or movement) and has implications for population-level environmental reconstructions.

Future Directions:

Throughout this thesis, I focused on using otoliths as archives to detect environmental change in marine systems. Biogeochemical tracers (radiocarbon and trace elements) and growth chronologies derived from otoliths from a single fish genus formed the basis of my research. This approach demonstrated the usefulness of radiocarbon, trace elements and growth increments in fish otoliths for detecting environmental change, but further research is required around assumptions.

Otolith $\Delta^{14}C$ is a valuable alternative to $\Delta^{14}C$ from hermatypic corals, and should continue to be used to examine ocean circulation at higher latitudes or deeper waters where coral samples are not available. Moreover, since many species of fish are commercially harvested, samples of target species can be easily accessible. However, consideration should be given to the availability of ancillary data, such as depth and location of capture, to negate variability within the resultant $\Delta^{14}C$ record when trying to associate it with an explicit depth or water mass (Chapter 2; Grammer et al. 2015). Additionally, $\Delta^{14}C$ reference records constructed from the bomb $\Delta^{14}C$ decline will become more important through time as $\Delta^{14}C$ transport evolves; this is especially applicable for age validating in hard to age fish species. It is key for earlier otolith reference records (e.g. *Chrysophrys auratus*: Kalish 1993, *Centroberyx affinis*: Kalish 1995) to be extended to include the present $\Delta^{14}C$ decline.

Ocean perches of *Helicolenus* fit the profile of an 'ideal species', and my results showed these species were suitable as archives of ecological proxies for marine systems. Now that the groundwork has been laid, different species (i.e. genus/family) should be examined for species-specific responses to the environment. Then, proxies from all species could be combined to reconstruct histories of ecosystem and levels of change linked to climate variables. Additionally, research focusing on single species should continue to examine

broad-scale climate forcing to determine if the effects of climate forcing are amplified in systems exposed to large ocean basins and dynamic oceanographic processes. Also, research should focus on exploring long-term records of fish growth in climate 'hot spots' and discern if growth indirectly reflects increases in greenhouse gasses in the atmosphere.

Further research directions with otolith chemistry should include quantifying physiological (e.g. metabolism, reproductive condition) and environmental influences on element assimilation by focusing on all life history stages, since element assimilation is inherently linked with age-based growth. It is beneficial to continue with holistic approaches by including multiple elements and growth in analyses and examining the direction and magnitude of element assimilation and growth, when possible. It is also important to investigate the relationship between elements for assimilation interdependence, which has been explored to some extent (e.g. de Vries et al. 2005). The temporal signals of Sr:Ca, Li:Ca and Ba:Ca should be thoroughly examined to determine potential uses as proxies for reproduction, productivity and ambient water characteristics, respectively. Dietary and reproductive parameters should be added to mixed-effects models to further examine their effects on otolith chemistry.

Stable isotopes would be an excellent additional biogeochemical tracer to quantify past environmental conditions, diets, and/or metabolic rates (Kalish 1991a, Elsdon and Gillanders 2002, Gao and Beamish 2003). Using mixed-models to couple growth and trace element profiles with stable isotope data would create very strong proxies to reconstruct past ecological histories. To date, this has not been explored.

Specific Research Directions:

1. A complete Δ^4C curve that tracks the evolution of bomb ^{14}C in the environment from pre-bomb (ca. at least 1950) to the present should be produced from fish otolith carbonate for the Leeuwin Current on the west coast of Australia. The ^{14}C record presented in Chapter 3 for an upwelling region of the Great Australian Bight should be extended to the pre-bomb period. It is also of interest to produce bomb Δ^4C reference curves from otolith carbonate for freshwater areas of Australia. These records of bomb ^{14}C distribution in aquatic environments of Australia can be used in

various applications, e.g. tracing oceanic water masses, validating fish ages, and ocean-atmosphere carbon cycling.

2. Further research should focus on the relationship of Li:Ca in otoliths and primary productivity in the environment. This relationships needs to be both lab tested and further field tested. It should be examined in marine, estuarine, and freshwater systems in a variety of different fish species. Ba:Ca in marine fish otoliths along with ambient Ba should be further examined to determine Ba concentrations associated with the Flinders Current and other possible sources of Ba into the environment in the Bonney Upwelling area.

3. Research to incorporate growth chronologies and trace element profiles from fish otoliths with sediment cores from marine, estuarine and freshwater areas to examine connectivity and productivity of the ecosystem through time should be attempted. Time-resolved, trace element profiles from foraminiferal carbonate in the sediments can be compared with growth/trace element profiles of the fish to begin to establish multispecies responses to environmental change. This would be especially applicable around the mouth of the River Murray in southern Australia, where rainfall events have the potential to create large ecosystem disturbances. This is also an area where considerable change in freshwater input to oceans has occurred since river regulation occurred.

Conclusions:

Fish otoliths are excellent bioarchives from which a myriad of ecological proxies can be derived. For otoliths to be as useful and effective as possible, it is imperative to choose a species that fits within the criteria of the research question and physiological controls on the otolith be considered. The information gleaned from otoliths over the course of my research was as follows:

1. The application of fish otoliths to examine the bomb pulse of ^{14}C provided valuable insights into the timing of ^{14}C transport into depths approaching 1000 m in the

southwest Pacific Ocean and in a seasonal upwelling area of the southeast Indian Ocean;

2. Broad-scale climate patterns and weather have synergistic effects on the environment, and these interactions were seen within otolith growth increment records. Climate forcing was detected in multiple fish species over a broad region, and growth responses were related at different levels to ocean-atmosphere coupling.
3. Resolving element:Ca and growth profiles from otoliths to monthly increments over 17 years allowed an unprecedented level of detail to be compared through time, within an otolith, and among individual fish. Signals from marine systems were not temporally homogenous with respect to otolith chemistry or growth, and population level responses to the environment were evident in element:Ca concentrations and growth rates. Chronologies of otolith chemistry coupled with fish growth have the scope to be used as an ecological proxy, whereby temporal fluctuations in the physical environment can be directly correlated with changes in reproduction, diet or other biological parameters to reconstruct responses of past populations.

Consequently, after considering physiological processes and life history traits, biogeochemical tracers and sclerochronologies derived from *Helicolenus* otoliths have provided new data describing environmental change in marine systems of southern Australia and New Zealand. Otolith bioarchives are an accessible mechanism to detect and examine environmental change *in situ* in areas where it is too expensive or logistically difficult for rigorous instrumental data collection of physical or chemical parameters.

References

Andrews, A. H., J. M. Kalish, S. J. Newman, and J. M. Johnston. 2011. Bomb radiocarbon dating of three important reef-fish species using Indo-Pacific $\Delta^{14}C$ chronologies. Marine and Freshwater Research **62**:1259-1269.

Arendt, J. D. 1997. Adaptive intrinsic growth rates: an integration across taxa. The Quarterly Review of Biology **72**:149-177.

Attrill, M. J. and M. Power. 2002. Climatic influence on a marine fish assemblage. Nature **417**:275-278.

Black, B. A., R. J. Allman, I. D. Schroeder, and M. J. Schirripa. 2011. Multidecadal otolith growth histories for red and gray snapper (*Lutjanus* spp.) in the northern Gulf of Mexico, USA. Fisheries Oceanography **20**:347-356.

Black, B. A., G. W. Boehlert, and M. M. Yoklavich. 2008. Establishing climate-growth relationships for yelloweye rockfish (*Sebastes ruberrimus*) in the northeast Pacific using a dendrochronological approach. Fisheries Oceanography **17**:368-379.

Black, B. A., W. J. Sydeman, D. C. Frank, D. Griffin, D. W. Stahle, M. García-Reyes, R. R. Rykaczewski, S. J. Bograd, and W. T. Peterson. 2014. Six centuries of variability and extremes in a coupled marine-terrestrial ecosystem. Science **345**:1498-1502.

Brierley, A. S. and M. J. Kingsford. 2009. Impacts of climate change on marine organisms and ecosystems. Current Biology **19**:R602-R614.

Campana, S. E. 1997. Use of radiocarbon from nuclear fallout as a dated marker in the otoliths of haddock *Melanogrammus aeglefinus*. Marine Ecology Progress Series **150**:49-56.

Campana, S. E., J. M. Casselman, and C. M. Jones. 2008. Bomb radiocarbon chronologies in the Arctic, with implications for the age validation of lake trout (*Salvelinus namaycush*) and other Arctic species. Canadian Journal of Fisheries and Aquatic Sciences **65**:733-743.

Cusack, M. and A. Freer. 2008. Biomineralization: elemental and organic influence in carbonate systems. Chemical Reviews **108**:4433-4454.

de Vries, M. C., B. M. Gillanders, and T. S. Elsdon. 2005. Facilitation of barium uptake into fish otoliths: Influence of strontium concentration and salinity. Geochimica et Cosmochimica Acta **69**:4061-4072.

Elsdon, T. S. and B. M. Gillanders. 2002. Interactive effects of temperature and salinity on otolith chemistry: challenges for determining environmental histories of fish. Canadian Journal of Fisheries and Aquatic Sciences **59**:1796-1808.

Gao, Y. and R. J. Beamish. 2003. Stable isotope variations in otoliths of Pacific halibut (*Hippoglossus stenolepis*) and indications of the possible 1990 regime shift. Fisheries Research **60**:393-404.

Gillanders, B. M., B. A. Black, M. G. Meekan, and M. A. Morrison. 2012. Climatic effects on the growth of a temperate reef fish from the Southern Hemisphere: a biochronological approach. Marine Biology **159**:1327-1333.

Grammer, G. L., S. J. Fallon, C. Izzo, R. Wood, and B. M. Gillanders. 2015. Investigating bomb radiocarbon transport in the southern Pacific Ocean with otolith radiocarbon. Earth and Planetary Science Letters **424**:59-68.

Horn, P. L., H. L. Neil, L. J. Paul, and P. Marriott. 2010. Age validation and growth of bluenose *Hyperoglyphe antarctica* using the bomb chronometer method of radiocarbon ageing. Journal of Fish Biology **77**:1552-1563.

Horn, P. L., H. L. Neil, L. J. Paul, and P. J. McMillan. 2012. Age verification, growth and life history of rubyfish *Plagiogeneion rubiginosum*. New Zealand Journal of Marine and Freshwater Research **46**:353-368.

Hughes, J. M., J. Stewart, B. M. Gillanders, D. Collins, and I. M. Suthers. 2015. Relationship between otolith chemistry and age in a widespread pelagic teleost *Arripis trutta*: influence of adult movements on stock structure and implications for management. Marine and Freshwater Research: http://dx.doi.org/10.1071/MF14247.

Izzo, C., Z. A. Doubleday, A. G. Schultz, S. H. Woodcock, and B. M. Gillanders. 2015. Contribution of water chemistry and fish condition to otolith chemistry: comparisons across salinity environments. Journal of Fish Biology **86**:1680-1698.

Kalish, J. M. 1991a. ^{13}C and ^{18}O isotopic disequilibria in fish otoliths: metobolic and kinetic effects. Marine Ecology Progress Series **75**:191-203.

Kalish, J. M. 1991b. Oxygen and carbon stable isotopes in the otoliths of wild and laboratory-reared Australian salmon (*Arripis trutta*). Marine Biology **110**:37-47.

Kalish, J. M. 1993. Pre- and post-bomb radiocarbon in fish otoliths. Earth and Planetary Science Letters **114**:549-554.

Kalish, J. M. 1994. Investigating global change and fish biology with fish otolith radiocarbon. Nuclear Instruments and Methods in Physics Research Section B: Beam Interactions with Materials and Atoms **92**:421-425.

Kalish, J. M. 1995. Application of the bomb radiocarbon chronometer to the validation of redfish *Centroberyx affinis* age. Canadian Journal of Fisheries and Aquatic Sciences **52**:1399-1405.

Kalish, J. M., R. Nydal, K. H. Nedreaas, G. S. Burr, and G. L. Eine. 2001. A time history of pre- and post-bomb radiocarbon in the Barrents Sea derived from Arcto-Norwegian cod otoliths. Radiocarbon **43**:843-855.

Kerr, L. A., A. H. Andrews, K. Munk, K. H. Coale, B. R. Frantz, G. M. Cailliet, and T. A. Brown. 2005. Age validation of quillback rockfish (*Sebastes maliger*) using bomb radiocarbon. Fishery Bulletin **103**:97-107.

Koslow, J. A., G. W. Boehlert, J. D. M. Gordon, R. L. Haedrich, P. Lorance, and N. Parin. 2000. Continental slope and deep-sea fisheries: implications for a fragile ecosystem. ICES Journal of Marine Science: Journal du Conseil **57**:548-557.

Lehodey, P., J. Alheit, M. Barange, T. Baumgartner, G. Beaugrand, K. Drinkwater, J. M. Fromentin, S. R. Hare, G. Ottersen, R. I. Perry, C. Roy, C. D. van der Lingen, and F. Werner. 2006. Climate variability, fish, and fisheries. Journal of Climate **19**:5009-5030.

Lewis, R. 1981. Seasonal upwelling along the south-eastern coastline of South Australia. Marine and Freshwater Research **32**:843-854.

Middleton, J. F., C. Arthur, P. Van Ruth, T. M. Ward, J. L. McClean, M. E. Maltrud, P. Gill, A. Levings, and S. Middleton. 2007. El Nino effects and upwelling off South Australia. Journal of Physical Oceanography **37**:2458-2477.

Möllmann, C., G. Kornilovs, M. Fetter, and F. W. Köster. 2005. Climate, zooplankton, and pelagic fish growth in the central Baltic Sea. ICES Journal of Marine Science: Journal du Conseil **62**:1270-1280.

Morrongiello, J. R. and R. E. Thresher. 2015. A statistical framework to explore ontogenetic growth variation among individuals and populations: a marine fish example. Ecological Monographs **85**:93-115.

Morrongiello, J. R., R. E. Thresher, and D. C. Smith. 2012. Aquatic biochronologies and climate change. Nature Climate Change **2**:849-857.

Nguyen, H. M., A. N. Rountrey, J. J. Meeuwig, P. G. Coulson, M. Feng, S. J. Newman, A. M. Waite, C. B. Wakefield, and M. G. Meekan. 2015. Growth of a deep-water, predatory fish is influenced by the productivity of a boundary current system. Scientific Reports **5**:1-6.

Park, T. J. 1993. A comparison of the morphology, growth and reproductive biology of two colour forms of ocean perch (*Helicoleus percoides*), NSW, Australia. Masters. University of Sydney, Sydney, Australia.

Pavlov, D. A. and N. G. Emel'yanova. 2013. Transition to viviparity in the order Scorpaeniformes: Brief review. Journal of Ichthyology **53**:52-69.

Radtke, R. L. and T. E. Targett. 1984. Rhythmic structural and chemical patterns in otoliths of the Antarctic fish *Notothenia larseni*: Their application to age determination. Polar Biology **3**:203-210.

Rountrey, A. N., P. G. Coulson, J. J. Meeuwig, and M. Meekan. 2014. Water temperature and fish growth: otoliths predict growth patterns of a marine fish in a changing climate. Global Change Biology **20**:2450-2458.

Solomon, C. T., P. K. Weber, J. Cech, Joseph J, B. L. Ingram, M. E. Conrad, M. V. Machavaram, A. R. Pogodina, and R. L. Franklin. 2006. Experimental determination of the sources of otolith carbon and associated isotopic fractionation. Canadian Journal of Fisheries and Aquatic Sciences **63**:79-89.

Stanley, S. M. 2006. Influence of seawater chemistry on biomineralization throughout phanerozoic time: Paleontological and experimental evidence. Palaeogeography, Palaeoclimatology, Palaeoecology **232**:214-236.

Stenseth, N. C., G. Ottersen, J. W. Hurrell, and A. Belgrano. 2004. Marine ecosystems and climate variation. Oxford University Press, Oxford.

Sturrock, A. M., E. Hunter, J. A. Milton, E. Eimf, R. C. Johnson, C. P. Waring, and C. N. Trueman. 2015. Quantifying physiological influences on otolith microchemistry. Methods in Ecology and Evolution: doi: 10.1111/2041-1210X.12381.

Sturrock, A. M., C. N. Trueman, A. M. Darnaude, and E. Hunter. 2012. Can otolith elemental chemistry retrospectively track migrations in fully marine fishes? Journal of Fish Biology **81**:766-795.

Thébault, J. and L. Chauvaud. 2013. Li/Ca enrichments in great scallop shells (*Pecten maximus*) and their relationship with phytoplankton blooms. Palaeogeography, Palaeoclimatology, Palaeoecology **373**:108-122.

Thorrold, S. R. and S. Shuttleworth. 2000. In situ analysis of trace elements and isotope ratios in fish otoliths using laser ablation sector field inductively coupled plasma mass spectrometry. Canadian Journal of Fisheries and Aquatic Sciences **57**:1232-1242.

Thresher, R. E., J. A. Koslow, A. K. Morison, and D. C. Smith. 2007. Depth-mediated reversal of the effects of climate change on long-term growth rates of exploited marine fish. Proceedings of the National Academy of Sciences, USA **104**:7461-7465.

Travers-Trolet, M., Y.-J. Shin, L. J. Shannon, C. L. Moloney, and J. G. Field. 2014. Combined fishing and climate forcing in the southern Benguela upwelling ecosystem: an end-to-end modelling approach reveals dampened effects. PLoS ONE **9**:e94286.

Vigier, N., C. Rollion-Bard, Y. Levenson, and J. Erez. 2015. Lithium isotopes in foraminifera shells as a novel proxy for the ocean dissolved inorganic carbon (DIC). Comptes Rendus Geoscience **347**:43-51.

Webb, S. D., S. H. Woodcock, and B. M. Gillanders. 2012. Sources of otolith barium and strontium in estuarine fish and the influence of salinity and temperature. Marine Ecology Progress Series **453**:189-199.

Weiner, S. and P. M. Dove. 2003. An overview of biomineralization processes and the problem of the vital effect. Reviews in Mineralogy and Geochemistry **54**:1-29.

Appendix A: Permission for reproduction from publisher for Chapter 2

Title:	Investigating bomb radiocarbon transport in the southern Pacific Ocean with otolith radiocarbon
Author:	G.L. Grammer,S.J. Fallon,C. Izzo,R. Wood,B.M. Gillanders
Publication:	Earth and Planetary Science Letters
Publisher:	Elsevier
Date:	15 August 2015

Order Completed

Thank you very much for your order.

This is a License Agreement between Gretchen L Grammer ("You") and Elsevier ("Elsevier"). The license consists of your order details, the terms and conditions provided by Elsevier, and the payment terms and conditions.

Get the printable license.

License Number	3646801475355
License date	Jun 12, 2015
Licensed content publisher	Elsevier
Licensed content publication	Earth and Planetary Science Letters
Licensed content title	Investigating bomb radiocarbon transport in the southern Pacific Ocean with otolith radiocarbon
Licensed content author	G.L. Grammer,S.J. Fallon,C. Izzo,R. Wood,B.M. Gillanders
Licensed content date	15 August 2015
Licensed content volume number	424
Licensed content issue number	n/a
Number of pages	10
Type of Use	reuse in a thesis/dissertation
Portion	full article
Format	both print and electronic
Are you the author of this Elsevier article?	Yes
Will you be translating?	No
Title of your thesis/dissertation	Using biogeochemical tracers and sclerochronologies derived from fish otoliths to detect environmental change
Expected completion date	Jul 2015
Estimated size (number of pages)	200
Elsevier VAT number	GB 494 6272 12
Permissions price	0.00 AUD
VAT/Local Sales Tax	0.00 AUD / 0.00 GBP
Total	0.00 AUD